UNIVERSITY OF LIVERPOOL

An ontogenetic and comparative analysis of the bony semicircular canal form.

"Thesis submitted in accordance with the requirements of the University of Liverpool for the degree of Doctor in Philosophy by **Marcela Cárdenas-Serna**"

30 March 2023

Abstract

The semicircular canals – part of the vestibular system – are housed inside the petrous temporal bone. They detect angular acceleration of the head and are vital for gaze stabilisation and locomotion. The morphology of the semicircular canals is imperative for its function, given that alterations in variables such as length, circularity, position within the head or cross-section area can alter the sensitivity and the frequencies at which they can detect these accelerations. Given this tight association between form and function, the semicircular canal form must be highly regulated, as variation may give rise to functionally deleterious geometries. The unique morphology of a species' canals has been used extensively to infer function, particularly where agility and locomotion is concerned.

This work first investigates the semicircular canal form in humans to assess whether bone-remodelling dysregulation can lead to increased variation in form. Second, the ontogeny of the semicircular canal is evaluated to assess whether ossification is the limiting factor for canal form development. Lastly, the morphology of the canals across a set of mammalian species was evaluated to assess its relationship to the size of the perilymphatic space. A dataset of CT and microCT images that includes perinatal and adult humans, mice at several developmental stages, and a wider adult mammalian group was analysed using traditional morphometrics, geometric morphometrics and cross-section shape metrics.

In summary, this study shows that the overall shape and size of the human semicircular canals are established in utero and remain stable thereafter, although minute changes around the perimeter of the canals were observed, suggesting that regulation of the canal form continues until late adulthood regardless of any potential bone-remodelling dysregulation. In mice, canal form continued to develop postnatally until the point of ossification, after which the results are similar to those of the human. This suggests that ossification may be the limiting factor for mammalian canal development. Lastly, the cross-section shape of the bony canals seems

to vary with the size of the perilymphatic space, and it appears that it is possible to infer the size of the perilymphatic space using the cross-section aspect ratio.

Resumen

Los canales semicirculares, parte del sistema vestibular, se encuentran dentro de la porción petrosa del hueso temporal. Detectan la aceleración angular de la cabeza y son vitales para la estabilización de la mirada y la locomoción. La morfología de los canales semicirculares es imprescindible para su función, ya que alteraciones en variables como la longitud, la circularidad, la posición dentro de la cabeza o el área de la sección transversal pueden alterar la sensibilidad y las frecuencias a las que pueden detectar estas aceleraciones. Dada esta estrecha asociación entre forma y función, la forma del canal semicircular debe estar muy regulada, ya que la variación puede dar lugar a geometrías funcionalmente perjudiciales. La morfología única de los canales se ha utilizado ampliamente para inferir la función, particularmente en lo que respecta a la agilidad y la locomoción.

Este trabajo primero investiga la forma del canal semicircular en humanos para evaluar si la desregulación de la remodelación ósea puede conducir a una mayor variación en la forma. En segundo lugar, se evalúa la ontogenia del canal semicircular para investigar si la osificación es el factor limitante para el desarrollo de la forma del canal. Por último, se evaluó la morfología de los canales en un conjunto de especies de mamíferos para evaluar su relación con el tamaño del espacio perilinfático. Se analizó un conjunto de datos de imágenes de TC y microTC que incluye humanos perinatales y adultos, ratones en varias etapas de desarrollo y un grupo más amplio de mamíferos adultos, utilizando morfometría tradicional, morfometría geométrica y métrica de forma de sección transversal.

En resumen, este estudio muestra que la forma y el tamaño generales de los canales semicirculares humanos se establecen en el útero y permanecen estables a partir de entonces, aunque se observaron cambios mínimos alrededor del perímetro de los canales, lo que sugiere que la regulación de la forma del canal continúa hasta la edad adulta tardía, independientemente de cualquier posible desregulación del remodelado óseo. En ratones, la forma del canal continuó desarrollándose posnatal-

mente hasta el punto de osificación, después de lo cual los resultados son similares a los de los humanos. Esto sugiere que la osificación puede ser el factor limitante para el desarrollo del canal de los mamíferos. Por último, la forma de la sección transversal de los canales óseos parece variar con el tamaño del espacio perilinfático, y parece que es posible inferir el tamaño del espacio perilinfático utilizando la relación de aspecto de la sección transversal.

Acknowledgements

I would like to begin by thanking my supervisor, Professor Nathan Jeffery, who throughout my PhD was incredibly supportive, encouraging and patient with me, particularly in the face of COVID and major setbacks. Thank you for reading my (sometimes very rough) drafts, and for enduring my sense of humour: some things are more weird than funny. I would also like to thank the people at the Liverpool museum, at the Liverpool Small Animal teaching hospital, the staff at the William Henry Duncan Building and at University of Cambridge for their help with scanning specimens for this project. A special thanks goes out to people who have donated their body to research: this project would not have been possible without them.

I would also like to thank my colleagues at the EMB lab for the meetings, the chats, the journal clubs and the pints. Thank you for welcoming to the group with open arms and always lending a hand when I needed it. Then there is my Liverpool family: Mattia, Shauna, Cormac, Gina, Tom, Tai, Sarah, and Jonas. You have all been invaluable friends. Here I must make special mention of Kiran, who "encouraged" (read: threatened) me to do a PhD, who had to live with me through quarantine, who listened to my rants, who was a sounding board.

Finally, thank you to my family, who are my first and biggest supporters. Especially mum, dad, Daniel and Claudio, who have always believed in me no matter what I set out to do. I always strive to make you proud. Lastly, to my partner Rory, who' s been there for me through it all: I am so lucky to have you in my corner.

A mamá y papá.

Contents

List of abbreviations

CSF	Cerebrospinal fluid
CNS	Central nervous sytem
CT	Computed tomography
µCT	Micro computed tomography
µMRI	Micro magnetic resonance imaging
3D	Three-dimensional
A/P/L SCR	Radius of curvature of the anterior, posterior and lateral canals
AR	Aspect ratio
CI	Confidence interval
CS	Centroid size
CSA	Cross-section area
EDMA	Euclidean distance matrix analysis
FM	Foramen magnum
GMM	Geometric morophometrics
GPA	Generalised Procrustes alignment
HMH	Half maximum height
LO	Labyrinthitis ossificans
MRI	Magnetic resonace imaging
MT1-MMP	Membrane-type matrix metalloproteinase I
NF - kappaB	Nuclear factor kappaB
OPG	Osteoprotegerin
PC	Principal component
PCA	Principal components analysis
PD	Procrustes distance
PNS	Posterior nasal spine
RANKL	Receptor activator of nuclear factor kappaB ligand

RANK	Receptor activator of nuclear factor kappaB
SCC	semicircular canals
SCR	Semicircular canal radius of curvature
Sen. A/P/L	Sensitivity of anterior/posterior/lateral canals
SR-PCI	Synchotron radiation phase-contrast imaging
SSCD	Superior semicircular canal dehisence
Tcl	Tool-command language

Chapter 1

Introduction

1.1 Introduction

The inner ear consists of two functional parts: the cochlear portion, which contributes to the sense of hearing, and the vestibular portion, which is part of the organ of balance. The vestibular system is involved in the detection of head motion and orientation, both of which are essential for navigation, motor coordination, and spatial awareness. Altered vestibular function results in deficits in balance and can produce symptoms such as dizziness, disequilibrium, vertigo, nausea, pallor, diaphoresis, general malaise, and emesis [1].

1.2 Anatomy of the vestibular system

1.2.1 Gross anatomy

The inner ear is located at the base of the skull, inside the petrous temporal bone. It is referred to as the labyrinth, due to its complex morphology. Structurally, the labyrinth can be divided into two main components: an outer bony labyrinth and an inner membranous labyrinth. Morphologically, it is divided into three sections: the semicircular canals, the vestibule, and the cochlea. The first wo are part of the vestibular system, whilst the cochlea is part of the auditory system. The semicircular canals project superiorly from the vestibule. There are three canals: the anterior (also referred to as superior), the posterior, and the lateral (or horizontal). They are named accordingly to their general position in space. The anterior and posterior canals are oriented vertically, and the lateral canal is oriented horizontally. The

canals lie at approximately right angles from each other [2].

The bony labyrinth is the osseous casing of the inner ear. The lumen of the bony labyrinth is lined with periosteum and the cavity is filled with a liquid similar to cerebrospinal fluid (CSF) [3], the perilymph. The bony semicircular canals are – as the name suggests – semi toroidal in shape. They have a mostly smooth section, the slender portion, and a widening at one of the ends, where the canal meets the vestibule, the ampulla. The bony vestibule is a loosely oval-shaped structure, that lies between the canals and the cochlea. The cochlea projects antero-inferiorly from the vestibule (Figure 1.1).

Inside the lumen of the bony labyrinth, and surrounded by the perilymph, resides the membranous labyrinth Figure 1.1. It is a collection of epithelial tubes and sacs filled with fluid, the endolymph. The semicircular ducts follow a similar shape as the bony canals. In the bony ampulla, the membranous duct also widens, and inside it resides the end-organ of the canals. At the ampulla, a ridge covered in sensory cells – the crista ampullaris – protrudes from the wall. The entire lumen above the crista is obstructed by a gelatinous structure, the cupula. The hairs of the sensory cells are embedded into this structure.

The membranous ducts are continuous with the utricle, a membranous structure inside the bony vestibule. The membranous ducts are held in position inside the bony labyrinth by a fine connective tissue [5] and are suspended in place attached to the periosteum. These filaments anchor the membranous ducts to the bone so that the membranous and osseous canals move in a single, fluid movement. The membranous ducts open by five orifices into the utricle, one opening being common to the superior and posterior canals, the common crus. The saccule and the utricle do now follow the general shape of the bony vestibule, where they are contained. Instead, they are separated by a membranous structure – the membrana limitans – which divides the bony vestibule into a pars superior and a pars inferior [6].

These two structures detect linear acceleration of the head, and the semicircular canals detect angular acceleration. Their end organ, the macula, is located on one of the walls. It possesses a similar gelatinous structure to the cupula, but it does not obstruct the entire lumen of the saccule or utricle. Additionally, there are stones of calcium carbonate (the otoliths) embedded in this gelatinous membrane. From the postero-medial aspect of the vestibule and the base of the common crus, stems the endolymphatic duct, which connects these structures to the endolymphatic sac – a small collection of endolymph located in the cranial cavity that lies between the outer and inner dural membranes. The membranous labyrinth continues from the

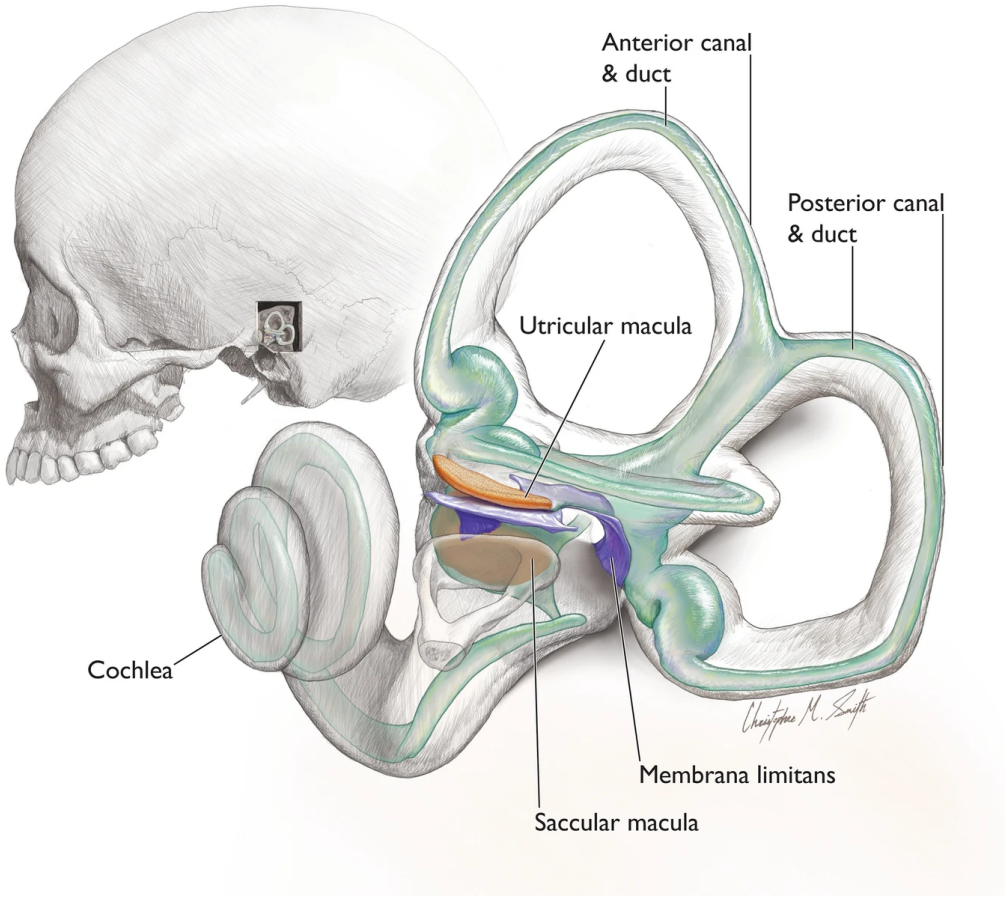

Figure 1.1: Schematic representation of the human labyrinth. The inner ear labyrinth is located inside the petrous temporal bone. The labyrinth is a series of cavities withing the bone, which are filled with perilymph. Inside this lumen, surrounded by perilymph, is the membranous labyrinth (shown in green), filled with endolymph. Figure sourced from Smith *et al.* [4].

saccule, where it forms the cochlear duct (scala media).

1.2.2 Function

The vestibular system detects acceleration of the head. This sense is vital for gaze stabilisation [7], postural control [8], navigation [9, 10], and locomotion [11–14]. This is achieved by sensing rotational acceleration by the semicircular canals and linear acceleration by the saccule and utricle.

The information from the vestibular system conveyed to the central nervous system via the vestibulochoclear nerve (VII) for processing. The vestibular afferents reach the superior, medial, ventral lateral and descending vestibular nuclei in the medulla. The medial and the dorsal nuclei receive most otolithic inputs. The vestibular nuclei receive other afferent information, such as spinal fibres that terminate in the caudal region of the dorsal and medial nuclei, projections from the reticular formation, the cerebellar floculus, nodulus and uvula, as well as cortical information from the vestibular cortex [15]. Information is also shared between the bilateral vestibular complex via commissural neurons, permitting the processing of bilateral vestibular inputs which in turn increases the sensitivity of second order neurons [16]. Efferent information from the vestibular complex is complicated, but it can be divided into five main pathways: vestibulo-ocular, vestibulo-spinal, vestibulo-cerebellar, vestibulo-autonomic, and vestibulo-thalamo-cortical. The ocular pathway, as its name suggests, is highly involved in the vestibulo-ocular reflex [17]. These neurons project to the oculomotor (III) and trochlear (IV), and abducens (VI) nuclei, via a complex system of ipsilateral and contralateral excitatory and inhibitory pathways. The vestibulo-spinal efferents are highly involved in neck muscle movement [18], as well as generalised postural control. These neurons travel via the medial and lateral vestibulo-spinal tracts, which terminate in the contrallateraly and ipsilaterally, respectively. The vestibulo-collic reflex is carried out by the vestibulo-spinal pathway [19] by innervating specific segments or in cases several segments of the spine, thus mediating postural control [15]. The cerebellar pathway not only receives afferents from the vestibular nuclei, but also directly from the vestibular nerve and nuclei of the paramedian tracts. Information from the vestibular nerve reaches the nodulus and uvula, whilst the vestibular nuclei afferents, mainly from the median, superior and descending nuclei, also terminate at the floccular complex. The paramedial tract cells receive information from many oculomotor premotor nuclei and project to the flocculus. The autonomic pathway relays information to

the nucleus tractus solitarius, the parabrachial complex, anteromedial and Edinger-Westphal nuclei, as well as the dorsal vagal nucleus and the nucleus ambiguous. This pathway is part of a more complex system that integrates sensory inputs, which regulate autonomic function. Lastly, the thalamo-cortical pathway: projections to this pathway synapse mainly at the ventral posterior lateral nucleus of the thalamus, which then are relayed to several areas in the cortex, including the prefrontal lobe, the temporo-parietal area, and the parietal cortex [20]. Given the wide range of connections to and from the vestibular system, it is no surprise that vestibular dysfunction can cause a wide range of symptoms. Vertigo, dizziness, visual and postural symptoms are characteristic of vestibular issues, but the connections via the autonomic pathway can cause symptoms such as nausea, pallor, diaphoresis and emesis. These symptoms are not pathognomonic of vestibular disorders but may accompany more classical vestibular symptoms, and may be so severe as to cause debilitating impact in quality of life.

Signal mechanotransduction occurs inside the membranous labyrinth, at the end organs: the cristae and the maculae. These organs contain two types of sensory cells, referred to as type I and type II. Type I cells are present in all mammals, birds and reptiles, whilst type II cells are common to all vertebrates and are thought to be older from an evolutionary perspective [21]. At the apical end of the sensory cells, a bundle of stereocilia protrudes 80 µm into the cupula (Figure 1.2). These cilia increase in length from one side to the other, culminating in a single, longer kinocilium. The tops of all cilia are connected by tip links, which in turn open sensory channels [22]. When the head accelerates, the endolymph inside the semicircular canals will lag behind the motion of the canal due to inertia. Therefore, relative to the canal, the endolymph moves in the opposite direction of the head. This applies a force parallel to the top of the cells (perpendicular to the cilia), which deflects the cilia towards the kinocilium, and opens potassium channels causing depolarization of the cells, activates the calcium channels in the basolateral membrane and ultimately leads to increased release of neurotransmitters, mainly glutamate [23, 24].

Then there is no relative flow of endolymph inside the canals, both type I and type II cells will have a baseline firing rate, which is higher for type I cells. This can occur in situations when the head is static or when there is constant velocity (i.e. no acceleration). Deflection of the cilia towards the kinocilium increases the baseline firing rate and vice versa, deflections away from the kinocilium will decrease the firing rate. The morphological organisation of the kinocilium and the cilia is different depending on the canal: in the lateral canal, the kinocilium is located towards the

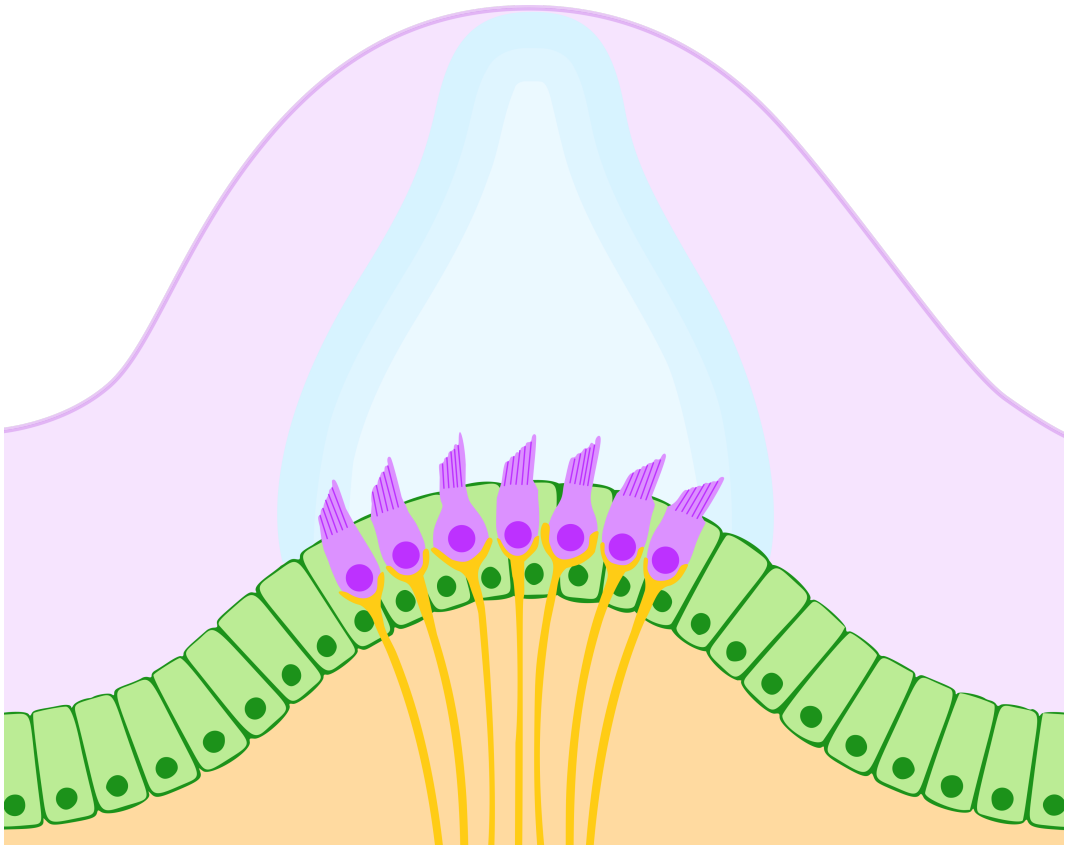

Figure 1.2: Schematic representation of the ampulla. Hair cells are depicted in purple, surrounded by support cells in green. The cilia of the hair cells protrude into the cupula (light blue). The light purple background represents the endolymph in the cupula. Afferent neurons of the vestibular nerve (CN VIII) in yellow.

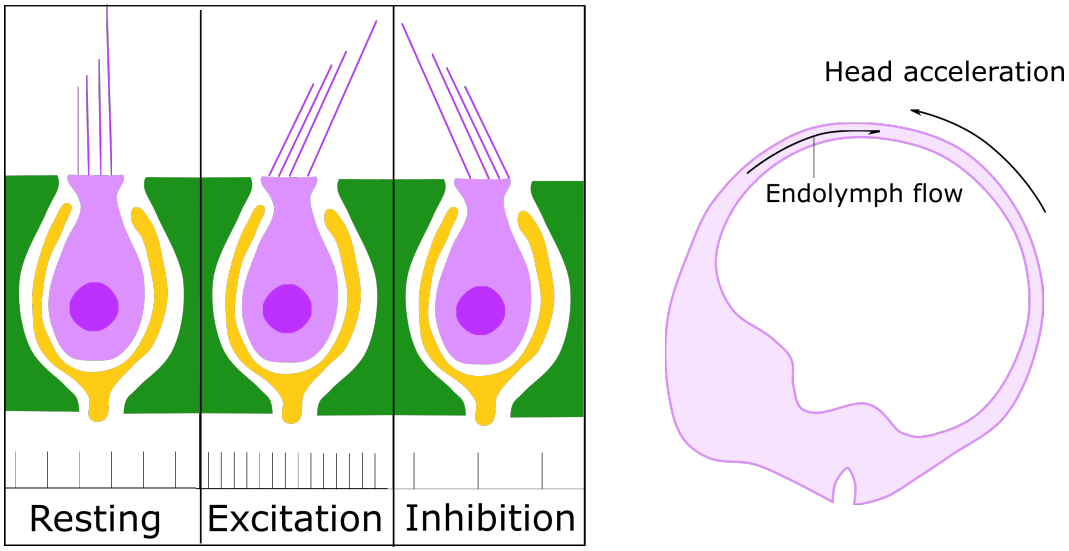

Figure 1.3: Direction of the endolymph flow is opposite to the direction of the head acceleration (right). Relative flow of the endolymph in the cupula deflects the cilia on hair cells. Deflection of the cilia towards the kinocilium increases neuronal firing, deflection away from the kinocilium decreases firing (left). Adapted from Bach-y-Rita [26].

vestibule, whereas in the posterior and anterior canal the kinocilium is towards the slender portion of the canal. This means that in the horizontal canal, firing rate will increase when the flow is towards the vestibule (ampullopetal) and decrease when it is directed towards the slender portion (ampullofugal) (see Figure 1.3). As expected, in the vertical canals, ampullopetal flow will decrease firing rate and ampullofugal will increase the firing rate [25].

Signal mechanotransduction works differently in the rest of the labyrinth. In the vestibule, it occurs on the macula, where the sensory epithelium for the saccule and utricle is located. The position of the otoconia on the surface of the otolithic membrane makes the membrane heavier than the endolymph that surrounds it. Linear movements of the head (horizontal and vertical for the utricle and saccule, respectively) will shift the surface of the membrane relative to the walls, which in turn displaces the hair cells in the macula, causing depolarisation and detection of the acceleration. [27]. The endolymph in the utricle is continuous with the semicircular canals via the openings of the common crus and the lateral canal. The membranous lumen is also continuous with the saccule via the ductus utriculosaccularis.

The sacule then connects to the cochlear duct via the ductus reuniens [28]. In the cochlea, for the hearing sense, the perilymphatic space plays a key role in signal mechanotransduction. The endolymphatic duct in this area – the cochlear duct – contains the end-organ: the organ of Corti. Vibrations of the stapes pass through the oval window and stimulate the perilymph. It is the interaction of the perilymph with the basilar membrane that generates a wave that travels through the cochlea, which will then generate movement in the endolymph that will stimulate the hair cells [29].

1.2.3 The lymphatic spaces

Perilymphatic space

The perilymphatic space is delimited by the bony labyrinth. This space is formed from the otic cyst, which arises from the otic placode. During development, mesenchymal cells surround the otic placode and fluid begins to collect between them. This collection of fluid will eventually form the perilymphatic space and the perilymph. This space, however, is not only filled with perilymph, but also by a cellular component. Fibroblasts with abundant processes are dispersed and form a web [30] with neighbouring cells (Figure 1.4). Additionally, sparse bundles of fibrils, most likely made up of type II collagen [31, 32], are dispersed throughout. The fibres appear to support the fibroblasts and provide a rigid scaffolding in the perilymphatic space, whilst still allowing free movement of the perilymph. The cavitation of the otic placode during development generates a loose mesh structure that eventually stretches out to become sparser. The fibroblast structure described above is most likely a remnant of that primordial structure [33].

Endolymphatic space

The endolymphatic space is delimited by the membranous labyrinth. It is filled with endolymph, a fluid rich in potassium ions. This space, just as the perilymphatic space, is continuous across the entire labyrinth. It is held in position by a direct attachment to the bony wall periostium, and the fibroblast structure in the perilymphatic space, which makes it move as one with the bony labyrinth. In the semicircular canals, the endolymphatic space is not entirely surrounded by perilymph, as its outer edge sits right on the wall of the bony labyrinth [35] (see Figure 1.4).

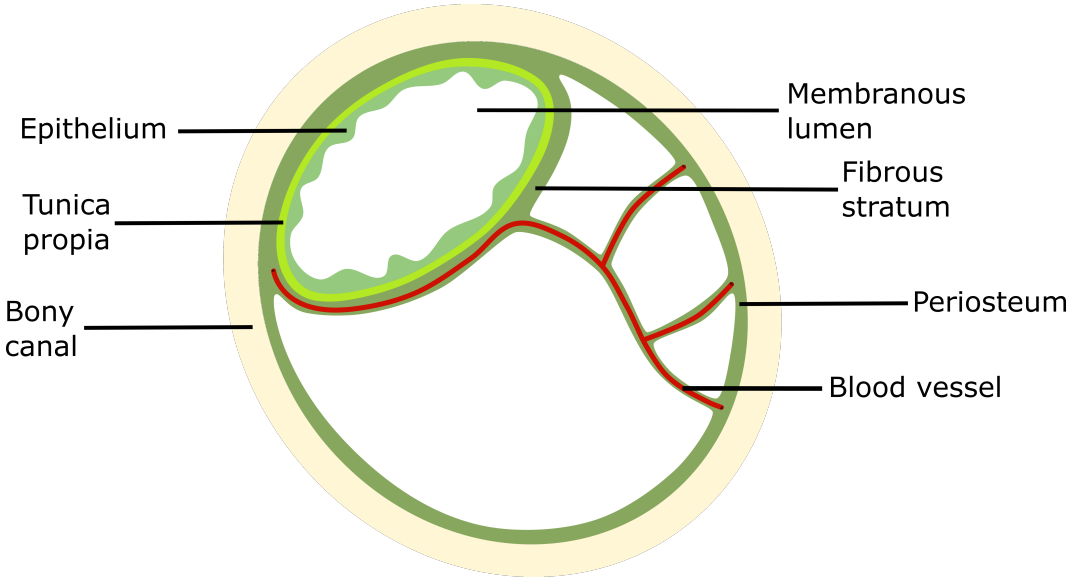

Figure 1.4: Cross-section of a human semicircular canal. In pale yellow is the bone of the petrous temporal bone. In dark green, the periopstium. Notice how the membranous canals (the endolymphatic space) occupy only a small portion of the total bony lumen. The portion of the bony lumen that is outside of the membranous ducts is the perilymphatic space. Based on Cunningham [34].

The labyrinthine fluids

Composition The labyrinthine fluids are a special form of extracellular fluids. The perilymph is more abundant by volume than the endolymph and its composition is similar to that of the cerebrospinal fluid (CSF). It is a liquid rich in Na^+ ions and deficient in K^+ ions. The ion concentration of the perilymph is Na^+ 0.15 mol L^{-1}, K^+ 0.005 mol L^{-1}, and Cl^- 0.11 mol L^{-1}. Oppositely, the endolymph is rich in K^+ and the exact ion concentrations have been shown to vary depending on the site they are collected from. A summary adapted from Sellick & Johnstone [3] is presented in Table 1.1.

Table 1.1: Endolymph ion concentration [3]

	$[Na^+]$mM	$[K^+]$mM	$[Cl^-]$mM	Resting potential	Equilibrium potential		
					Na^+	K^+	Cl^-
Cochlear duct	1	150	110	+80	+120	-86	0
Saccule	3	150	110	0	+99	-86	0
Utricle	12	140	110	0	+59	-83	0

Across higher vertebrates, the composition of the endolymph is high in K^+ and low in Na^+, whereas the composition of the perilymph is higher in Na^+ than K^+ [36]. In toadfish, the perilymph (in the saccule) follows the same trend, although reports show the composition of the endolymph to favours Na^+ as well, although with a much higher proportion of K^+ [36]. In the pigeon, the endolymph contains high amounts of K^+ in the scala media (140.6±27.3 $mmol/l$), and high amounts of Na^+ in the scala tympani and vestibuli (perilymph). In contrast, fish have relatively high Na^+ concentration in the endolymph when compared to mammals (139.43± 1.78$mmol/l$ versus 3–40 $mmol/l$) [37, 38]. Ion concentration is vital for appropriate function. The concentration of K^+ may be an energy-saving mechanism for hair cells, as influx of K^+ via the apical portion of the cells will leave passively via the basolateral channels, which are in contact with the lower-K^+ concentration in the perilymph [39]. Furthermore, the relatively low concentration of Na^+ means that there is less influx and therefore less need for pumping Na^+ out of the hair cells, which further enhances this low-energy advantage. In the case of the fish, which as described above has a much higher concentration of Na^+, carry higher metabolic costs for detection [39].

MECHANICAL PROPERTIES The endo- and the perilymph are compartmentalized inside the inner ear. This compartmentalisation serves two purposes. First, it allows an electrochemical gradient, which is necessary for the mechanotransduction into neural information [40]. Second, it minimises the effect of changes in atmospheric pressure on endolymph fluid dynamics [41]. Compartmentalisation is due to tight junctions at the apical surface of the membranous labyrinth cells, which results in their basolateral surface being exposed to the perilymph and their apical surface to endolymph.

The lymphatic fluids have a density similar to water ($\rho = 1.0 g/cm^2$) and a viscosity of 0.0085 $dyne/cm^2$. As viscosity in the endolymph was found to be independent of shear rate [42], it can be assumed that the endolymph has a Newtonian behaviour. The physical properties of labyrinthine fluids as described by Steer *et al.* [42] are summarized in Table Table 1.2. Additionally, Money *et al.* [43] assessed the physical properties of both fluids in pigeons and found that the mean viscosity of the perilymph was 0.76 cp $\pm$.03 (4.4 %, SD), and the mean viscosity of the endolymph was 1.19 cp $\pm$.057 (4.8 %, SD) [43]. It is important to note here that there is little information on the methods used for collection of the samples and the assessment of purity. The number of samples used or if they were pooled from several individuals is unknown. Although arguably, the density and viscosity of the labyrinthine fluids play a key role in the mechanotransduction of head movement, little research aside from the aforementioned studies has been conducted to assess those variables and they are usually considered constant across different species when deriving biomechanical models [44, 45].

Table 1.2: Physical properties of labyrinthine fluids. Adapted from Steer *et al.* [42].

	Human endolymph	Human perilymph	Cat perilymph	Measurement accuracies (%)	H_2O
Specific gravity	1.00	1.00	1.00	±2	1.00
Coefficient of expansion	$4.4x10^{-4}$/°C	$4.4x10^{-4}$/°C	$4.4x10^{-4}$/°C	±5	$4.0x10^{-4}$/°C
Viscosity (centipoise)	0.852	0.802	0.780	±2	0.7225
Specific viscosity ($\mathrm{Pa\,s^{-1}}$)	1.18	1.11	1.08		
Temperature coefficient of viscosity	−2.4%/°C		−2.5%/°C	±10	±2.0%/°C

1.2.4 Bony and membranous semicircular canal shape.

Overall, the general shape (semi-toroidal) and length of the membranous canals follows that of the bony labyrinth. Nonetheless, differences appear between the two. In humans, the membranous labyrinth is much smaller than the bony labyrinth. The endolymphatic space comprises 18.6% of the total volume of bony labyrinth lumen, and the perilymphatic space 81.4% [46]. Despite this difference in volume, the general shape of the membranous labyrinth follows that of the bony canals. The membranous canals have an oval cross-section, as does the bony canal [44]. When observing a perpendicular cross section of the canals, the long axis of the oval membranous canal lies perpendicular to the long axis of the bony canal [44, 47].

Other mammals, however, do not display the same morphology. As an example, cats show round bony canals with round membranous canals that occupy most of the cross-sectional area [44]. The guinea pig appears more oval (although not as markedly so as the humans) and so does the membranous canal, although their long axes are parallel. Rabbits, chinchillas and gerbils display canals shaped similarly to the cat and the guinea pig, but the squirrel monkey is remarkably similar to those of humans [45], and so may be the case for other primates [48]. Thus, studying the shape of the bony labyrinth to make inferences about the shape of the membranous canals, such as its cross-sectional area and volume is not reliable without specific information of that particular species anatomy, such as the ratio of bony to membranous labyrinth cross-sectional area.

1.3 Macroscopic form and function

The bony and membranous canals move as one with the head during any acceleration. When a rotational force is applied to the head, the endolymphatic fluid will move following Poiseuille flow: the fluid located closer to the membranous walls will move in unison with the acceleration due to friction, and the fluid closer to the centre of the lumen will lag behind due to inertia [49]. Relative to the cupula, the movement is the opposite: the fluid in the centre of the canal will move towards the cupula (and deflect it) and that closer to the walls will lag behind. These relative movement will deform the cupula, which in turn deflects the hair cilia, transducing the mechanical signal into a neural one [50]. As mentioned above (see subsection 1.2.2), ampullopetal flow will increase the firing rate in the lateral canal, but decrease firing rate in the vertical canals.

To describe the ability of a subject to perceive angular acceleration, several mathematical models have been proposed. In 1933, Steinhausen proposed a linear second order model for cupula dynamics [51]. This model was later refined by van Egmond *et al.* [52] who chose a torsion pendulum with a high degree of dampening as substitution for the model. In the torsion pendulum model, the cupula-endolymph system act as a solid mass that is opposed by three restraining forces:

1. K – Elastic force: due to the cupula's spring like properties
2. C – Viscous force: due to the viscosity of the cupula and endolymph. The magnitude of this force is proportional to the velocity of the displacement.
3. M – Inertial force: due to the fluid's mass. This force is proportional to the acceleration of the endolymph-cupula complex.

During normal movement of the head, the magnitude of the elastic and inertial forces is small, so that during any given acceleration, the endolymph-cupula complex is mostly opposed by the viscous drag of the cupula. Displacement of the cupula is therefore proportional to the velocity of head motion (see no. 3). In a given acceleration, the beginning of the movement will cause the endolymph in the centre of the lumen to lag behind relative to the head. A few seconds after, the forces will achieve balance, at which point the endolymph will move at one with the head. However, the endolymph will at this point have changed position relative to the cupula, which in turn would have been displaced a certain amount. The endolymph-cupula velocity and acceleration relative to the walls will be zero at this point, and there will be no viscous or inertial force, which means that cupula displacement will be dependent on the magnitude of the constant acceleration. Cupula displacement after an acceleration follows an exponential time course. Regardless of the magnitude, 63% of the total displacement will take place after a fixed delay, known as the long time constant or cupula time constant (T_c). This constant is governed by the viscous and elastic coefficients ($T_c = C/K$). In other words, it is directly proportional to the viscosity of the endolymph and inversely proportional to the cupula elasticity. The short time constant (viscous time constant) is governed by the inertial and viscous forces, such that $T_v = M/C$ [53], and it reflects the response speed of the system [54].

These time constants also govern the range of frequencies that the semicircular canals are able to detect. On the lower end, the minimum frequency that can be detected corresponds to $1/T_c$. Any slower accelerations will fail to deflect the cupula,

and there will be no perception of the acceleration. On the upper end, the range is limited by $1/T_v$ [29]. Higher frequency accelerations will cause excessive viscous force, such that there is no relative endolymph flow and the cupula is not stimulated.

Detection of angular acceleration is paramount to adequate posture and locomotion. Vestibular function must account for type of locomotion, visual acuity and ecology, which in turn translates to different patterns of head movement, and different functional requirements of the system that are species-dependent. These time constants, and therefore detection sensitivity, are highly influenced by canal morphology, which have adapted to cater to this vast array of functional needs. For example, in species such as the turtle, the cross-sectional area of the membranous ducts is large relative to the radius of curvature. This increase in area extends the bandwidth and sensitivity to angular acceleration, which is particularly important as turtles are more likely to have slower head movements. In mammals, especially those with faster head movements, the more slender canals are favoured to detect the higher frequency ranges [55]. It is important to note that not all adaptations to the system are morphological/mechanical bases, and that the signal transduction and processing plays a key role in the adaptations of the vestibular system. These include the presence and proportion of type I and type II cells [56] and the number of connections and projections of the vestibular afferents (see subsection 1.2.2). Nonetheless, morphological adaptation plays a key role in achieving the functional requirements of the system; some of the key morphological aspects are described below.

These time constants, and therefore detection sensitivity, are highly influenced by canal morphology. Some of the key morphological aspects are described below.

1.3.1 Geometry and function

The relationship between the semicircular canal geometry and sensitivity to angular acceleration has been subject of interest to researchers for over a century. Early anatomical studies have referenced a possible relationship between the size of the canals and an animal's agility. Based on his observations on the semicircular canal size of many species, Gray observed that those who were less agile, for example sloths, tended to have smaller canals and more agile species had larger canals [48]. Since then, many studies have focused on studying different morphological and morphometric characteristics of the semicircular canals, in the hopes to understand how it may alter the sensitivity of the system [57–59]. These characteristics have been

extrapolated to infer the agility and locomotor of extinct species [60–62].

1.3.2 Intraspecific and interspecific form variation

Canal size

The size of the semicircular canals its perhaps one of the most studied characteristics relating to sensitivity. The size can be described by linear measurements (such as the height and width of a particular canal, or the length of the entire labyrinth), or by conjugating several measurements into a ratio, more notably the radius of curvature. It has been noted, for example, that in birds species that are deemed "good fliers" have long, thin arcing canals [48]. More specifically, a canal with a greater length has been shown to translate to increased sensitivity to angular acceleration [40], and therefore improved performance. This relationship has proven true in interspecific differences of many species, such as rodents [63, 64], birds [43, 45], and many other mammals, including primates [61, 65], amongst others. Furthermore, this has also proven true in intraspecific comparisons in mice, where specimens with larger anterior canals (as measured by radius of curvature) showed higher sensitivity than those with smaller canals [63].

It is important to mention here that size of the semicircular canals is also correlated with mass. It has been shown across different mammalian species that there is a positive correlation between the radius of curvature and body mass [66], which has been corroborated on other mammalian species, including several primates [65]. That is, larger animals have larger canals, when compared with smaller species. More recently, studies using geometric morphometrics have shown similar conclusions, when using centroid size as a measure of size [67]. Most studies show a strong allometric component, so that relative to body size, smaller species have much larger canals compared to larger species [61, 62, 67, 68]. So, the relationship of size and agility is relative to body mass [61]. Jones & Spells [66] proposed that since larger animals usually have slower head movements they require large, sensitive canals to be able to detect the accelerations. Vice versa, small animals would display much faster head movements, which require smaller, less sensitive canals as to not be over-stimulated. In this instance, the frequency of the head movement (slow or fast) would be the determinant factor for canal size, providing the necessary adaptations to the time constants to adequately cover the range of expected frequencies (see section 1.3). Larger heads also carry the implication that there is increased sensitivity due to increased distance between contralateral labyrinths, which may also

contribute to a faster saturation of the canals. Nonetheless, when comparing similarly sized species, more agile animals tend to have larger radius of curvature than their slower counterparts [see, for example, 48]. This would then imply that species with higher agility require more sensitive canals as to detect smaller differences in acceleration. Aditionally, the shape and size of the bony labyrinth is influenced by ecology and phylogeny [68, 69]. In primates, particularly humans, the basicranium is flexed, likely due to enlargement of the brain [70]. This also comes with the coronal reorientation of the petrous bone. In humans, the shape of the bony labyrinth is correlated with the cranial base, although not necessarily with just the petrous bone, as there is no correlation between the labyrinth and the petrous bone size [71]. This infers that morphology is mainly influenced by functional constraints, although spatial constraints still play a role definitive role.

Orthogonality

The activation of the receptors in the ampulla of any given canal is determined in part by the relationship of the direction of the acceleration and the plane orientation of the canal. Assessment of the direction of the angular acceleration is achieved by consolidating information coming from both labyrinths. A single canal can provide some information about directionality by increasing or decreasing firing rate. However, both labyrinths are positioned in the head so that each canal lies roughly in the same plane as another contralateral canal: lateral canals are paired with each other, and anterior canals are paired with contralateral posterior canals. Angular acceleration of the head will activate the hair cells on one canal, and inhibit the cells in the contralateral canal (Figure 1.5, see subsection 1.2.2). Both the increase and decrease of the neuronal firing is then processed centrally, to deduce the direction and magnitude of the acceleration [72, 73].

In a labyrinth in which all three canals were of the same size, and they were perfectly orthogonal to the other two ipsilateral canals and perfectly parallel to their contralateral synergist, sensitivity to accelerations would be equal in all directions [72]. Although traditionally ipsilateral semicircular canals are described to lie perfectly orthogonal to each other and in the same plane as their contralateral pair, this is not always the case. Earlier studies showed great digression from orthogonality, with angles between ipsilateral canals deviating up to 11.76° [58, 74]. Nonetheless, sample sizes were incredibly small and the techniques used, which included bony dissection, stereotaxic measurements and bone casts are not as precise as more re-

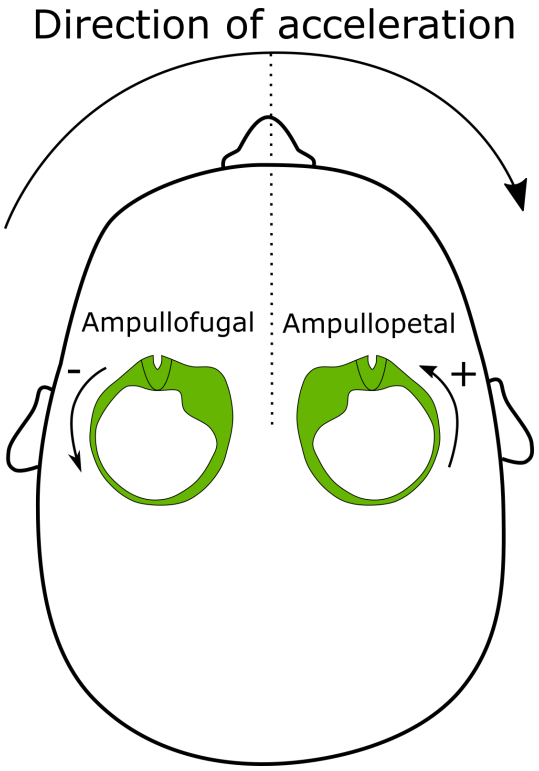

Figure 1.5: Schematic representation of an acceleration along the yaw axis. The lateral semicircular canals are depicted in green (not to scale). Contralateral canals will experience endolymph flow in opposite directions (one ampullofugal and one ampullopetal).

cent techniques. A study conducted on humans using computed tomography (CT) reported angles which were mostly orthogonal, with the greatest deviation being 4° between the anterior and posterior canals [75]. In a study of 39 mammalian species, angles between ipsilateral canals were found to range from 58.8° to 121.2° [76]. These deviations, however, do not take into account the possibility of intraspecific variation, which has been previously demonstrated in mice [77], opossums [78], primates [79], shrews [80] and sloths [81], although it is not as marked as interspecific variation.

Displacement of the endolymph inside a given canal is in part governed by the plane at which the canal lies in relationship to that of the acceleration. Maximal afferent response, however, is not at the exact plane of the anatomical plane, but shows interspecific variation [82–84]. However, this is not to say that only rotations on that plane will elicit a response. The "prime direction" of a canal is it's the rotation vector that only stimulates that canal [72].

In species where there is great deviation from orthogonality, an acceleration along a given axis is more likely to stimulate more than one ipsilateral canal. In these instances, the detection of the acceleration would be spread across more than one canal, which may increase sensitivity by means of having a wider range of detection for that particular direction, whilst having less sensitivity to other directions, as has been proposed for turtles [85]. This appears to be true for the guinea pig and rabbit [86], but it is not the case for the chinchilla, that has non-orthogonal canals, and yet it is almost equally sensitive in all directions [87].

Malinzak *et al.* [88] showed that deviation from orthogonality is strongly correlated with head rotation velocity independent of body size. They proposed that species that showed fast rotations on any axis have much less variation in canal orthogonality, while species with slow head movements have more variation. For example, sloths – a low moving species – have increased intraspecific variation in terms of orthogonality. This may be a result of relaxed selective pressure on the orthogonality of the canals, since there is no need for acute sensitivity to rotations [81]. This has been further demonstrated in primates [89]. In species with slow head movements, other functional pressures (e.g. subarcuate fossa size) may take precedent over orthogonality constraints, resulting in relaxed pressure and increased variation [90]. On the contrary, for agile species, information acquired by nearly orthogonal canals would not need to be corrected for directional variation which would mean that the processing in the central nervous system would be more efficient.

Circularity and plane torsion

Idealised representations of the semicircular canals usually show perfectly toroidal shape, this is not the case in reality. Oman *et al.* [49] established that the mechanical sensitivity of the cupula varies directly with the ratio of the area enclosed by the canal streamline to the streamline length. It follows that rounder canals would be favoured, as a stouter, more elliptical canal with similar length would decrease sensitivity [91]. Nonetheless, circularity of the canals cannot always be favoured when extreme spatial constraints of the petrous bone exist. This is true in squamates, where species with greater size constrains show higher ellipticity [92]. This correlation, however does not appear to hold true for mammals [93].

The length of the canal also increases when the streamline does not lie perfectly on a plane. Out-of-plane deviations have been reported before [94–96]. Increasing the torsion of the canals may be a means of lengthening the slender portion to allow for increased sensitivity in spatially-constrained petrous bones. Additionally, torsion of the canals may increase sensitivity by expanding the range of planes that may elicit endolymphatic flow and therefore generate a response [94, 95].

1.4 Semicircular canal ontogeny

1.4.1 Semicircular canal development

The inner ear develops from the pre-placodal region, and is composed of ectoderm. Around gestational week 4 (in humans), this region thickens to form the otic placode. The semicircular canals arise as two pouches which project vertically, to form the anterior and posterior canals, and laterally, to form the lateral canal. These pouches then fuse in the middle and the tissue is resorbed, which eventually forms the tubular canals [97]. The vestibular portion of the inner ear develops before the cochlea and grows at a faster rate. In humans, ossification centres start appearing in the periotic cartilage at week 16[98]. Meanwhile, the labyrinth inside the otic capsule continues to grow until it reaches adult size around weeks 17 to 19 [99].

The adult otic capsule composed of four distinct layers [100]. First, the endosteal layer that immediately surrounds the bony labyrinth. This layer is highly mineralised. Second, the endochondral layer. It surrounds the endosteal layer and it is also hyper mineralised, although there are chondral remnants scattered in the tissue. Third, the inner periosteal layer. This layer fills the space between the canals, but is not present in some regions, such as the arcuate eminence. It shows highly

mineralised vascular canals, with interspaces which are not as mineralised. Lastly, there is an outer periosteal layer, comprised of spongy and compact bone, which shows less mineralisation than the other three layers. Once these layers are ossified, primary bone in the perilabyrinthine zone appears to remain indefinitely, whilst the outer periosteal area is subject to remodelling [100, 101].

1.4.2 Perilabyrinthine bone

As mentioned above, it appears that the perilabyrinthine bone remains indefinitely. The normal turnover rate for bone (other than the otic capsule) is about 10% per year. A study conducted in mongrel dogs using sequential point labelling with calcein and tetracycline showed that bone turnover rate in perilabyrinthine bone is 2.1% per year [102]. It seems that the turnover rate increases in a centrifugal pattern, somewhat consistent with the notion that remodelling is limited to the outer periosteal area [101]. This pattern also suggests that since the areas closer to the canals are more highly protected, it may be due to local anti-remodelling factors. Three local factors are known to be the main regulators of bone turnover: Receptor activator of nuclear factor ($NF-kappaB$) ligand (RANKL), its cellular receptor, receptor activator of $NF-kappaB$ (RANK), and the decoy receptor osteoprotegerin (OPG) [103]. RANKL is necessary for osteoclast formation and activation, which in turn results in increased bone resorption. On the contrary, OPG is a neutralizer receptor that prevents RANKL binding to RANK, therefore decreasing bone resorption. It is possible that OPG could be responsible for the inhibition of bone remodelling in perilabyrinthine bone. A study in mice showed that expression of OPG: RANKL ratio in perilabyrinthine bone is 29:1, compared to 1:1 in the femur [104]. A quantification of the of OPG in the perilymph, serum, and CSF, which were found to be $972\,\mathrm{pg\,mL^{-1}}$, $131\,\mathrm{pg\,mL^{-1}}$, and $71\,\mathrm{pg\,mL^{-1}}$, respectively. Notably, after immunostaining, OPG was found to localise to the spiral ligament. An interesting finding from this study showed that the interface between the spiral ligament and the otic capsule showed no signs of membranes of any kind, which suggests that the lacunocanalicular system surrounding the cochlea is continuous with the spiral ligament and may be the main route for the diffusion of OPG to the surrounding bone. The high levels and specific localisation of OPG within the perilabyrinthine bone point towards OPG being the key inhibitor of bone remodelling. To further support this hypothesis, studies in OPG knockout mice showed significant remodelling of bone, characterised by focal hypercellular areas with bone resorption and

deposit [104].

Bone turnover conditions in the perilabyrinthine bone do not stay static throughout life. A comprehensive study of over 400 human petrous bones demonstrated a significant age-related biphasic loss of viable osteocytes within perilabyrinthine bone, most dramatically during the first few postnatal years of life (ages 2-4) but continuing into old age with a ~50% decrease between the 20 and 90 years of age [105]. The presence of viable osteocytes supports the inhibition of perilabyrinthine bone remodelling and thus help maintain the form-function integrity of the vestibular system. It follows that the reduction of viable osteocytes observed in later life may, therefore, lead to the shape of the bony labyrinth being more malleable compared to younger individuals. For example, the shape of the bony canals could more easily be influenced by forces travelling through the skull, for example, masticatory forces passing through the petrous portion of the temporal bone. Low bone remodelling may be the reason for increased accumulation of dead osteocytes. Additionally, a study has found osteoclastic activity in the otic capsule in patients of different ages, regardless of the presence of inflammation or other bone diseases [106]. As a consequence of the accumulation of osteocytes, there may be an increase in the occlusion of the lacunocanalicular network which will lead to a reduced amount of OPG permeation towards the outer areas of the perilabyrinthine bone. Ultimately, this could lead to increased bone remodelling in later life.

1.4.3 Evolution of the semicircular canals

The labyrinth has been present as early as cyclostomes [107]. The three-canal system described above, however, is specific to crown ganthostomes. Jawless stem gnathostomes (ostracoderms) possessed only two canals, homologous to the anterior and posterior canals in a three-canal system [108]. The lateral canal appears to be a more recent acquisition. Hagfish (agnatha) possess a singular torus-shaped canal, with two ampulla at either side [91, 109], whilst lamprey have two semicircular canals [110]. These two canals, however are not homologous to the anterior and posterior canal, such as described for stem gnathostomes, rather are two horizontal canals that appear to be unique to cyclostomes.

1.5 Methodological considerations

Morphometrics is the quantitative analysis of form. In this context, and throughout this work, form refers to both the shape and size of the specimen of interest. The study of the semicircular canal form has evolved throughout the years, and has encompassed many techniques. A brief summary is provided below.

In 1904, Gray published his comprehensive study of the labyrinth of animals [48]. Each petrous bone was fixed and dried using alcohol. For several weeks, it is dried in several solutions. After coating in paraffin, the specimen was then decalcified in an acid bath and carefully cleaned to isolate the labyrinth, which would then be made transparent using xylol. This allowed for photographs be taken, and stereoscopic images were generated. Gray offered a qualitative description and a detailed table of measurements of each labyrinth studied, where possible. Over the years, this technique was refined; petrous bones were dehydrated in a similar fashion, but latex paint was then injected into the labyrinth through the oval window, to allow for visualisation of the membranous labyrinth [111]. Both of these techniques allow for direct measurements of the labyrinth, be it in two-dimensional or three-dimensional space.

Given the small size of the labyrinth, the use of histological techniques allows for measurements similar as the ones described above. A similar decalcification and dehydration of the labyrinth is carried out for this process, but with the added step of staining the tissue to allow visualisation under the microscope. This technique, however, requires the sequential slicing of the tissue, for which a plane onto which the sections will be carried out needs to be chosen. This limits the measurements that can be taken, as the structure of interest (or at least the two points that encompass the measurement) need to be contained within a single slice, and the plane of sectioning may alter the results (see Figure 1.6). In the case of the semicircular canals, choosing an optimum plane for a particular canal will inevitably mean that the slicing will not be on the optimum plane for the other canals. Although it is possible to select smaller sections of tissue (e.g. one canal at a time), the smaller the pieces the less anatomical reference points are available for optimum selection of the plane. Nonetheless, it is possible to study the three-dimensional form of the canals (or any tissue) by digitising the serial slices, aligning them on the Z axis with a dedicated software, and generating as three-dimensional reconstruction of the labyrinth [112, 113]. This 3D reconstruction can then be visualised and measured. However, this technique is not infallible, as uneven staining, folds, wrinkles

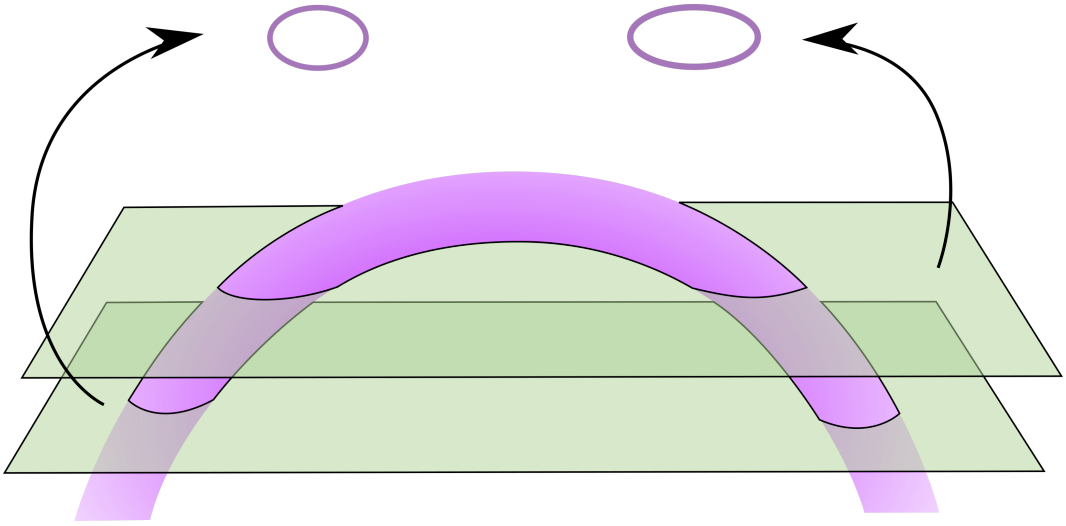

Figure 1.6: Two planes of section (green) on a hypothetical round canal. The lower plane is closer to a perpendicular plane of the canals, and therefore yields a rounder cross-section. The upper plane, much further from perpendicular, yields a more elliptical shape of the same canal.

or breakage when mounting the slides, distortion of the structures due to shrinkage, shear deformation caused by the microtome, etc may alter the final result, yielding inaccurate measurements. Yet, it seems, it is possible to achieve high accuracy with the reconstruction in this manner [114]. This leaves one problem: the destruction of the specimen. Because of its location, access to the petrous bone usually comes with severe damage to the skull, rendering the pieces useless for other research.

In more recent years, the use of computed tomography (CT) and magnetic resonance imaging (MRI), has allowed for visualisation of the bony labyrinth non-destructively and in three dimensions [11, 65, 115]. These imaging techniques also have the added advantage of being able to more readily study the labyrinth *in situ*, which in turn allows for more complex measurements, such as the relation to other cranial structures [116]. However, given the small sizes of the labyrinth, finer detail of the morphology is lost using these approaches. Advances in technology have given way to microCT (µCT) and microMRI (µMRI), which permits for greater resolution imaging ([for example, see 117–119]), although it may limit the size of the specimens that can be scanned. Although µMRI allows for high-resolution visualisation of the labyrinth and differentiation between fluid, nerves, and neuroepithelium, it is difficult to visualise bony structures, for which µCT is better suited. For this work, µCT was used for the study of form of the semicircular canals of humans, as disarticulated

petrous bones are small enough to be scanned, and mice, where the head is small enough to be scanned in its entirety. For Chapter 4, µCT was used where available, and strictly in smaller species where the whole head could be scanned, and regular CT was used for the rest of the sample.

Traditional morphometrics involves the use of linear measurements (e.g. length and width). Linear measurements, however, carry information related not only to shape, but also size. The problem with this approach is that linear measurements are overwhelmed by size. To diminish the influence of size, it is possible to generate ratios between the measurements, although this is not without its problems. Given that the semicircular canals appear to be a tightly regulated structure, it was necessary to select a technique that would allow capture of as much of the shape of the structure as possible, as to allow the discerning of more nuanced shape changes.

Several techniques can be used to study shape. Euclidean distance matrix analysis (EDMA) is a landmark-based approach that does not rely on coordinates [120], which has the advantage of avoiding coordinate covariation that occurs during superimposition [121]. However, this method disregards biologically homologous points, and gives equal weight to the entire structure. Other analyses are based on outline methods. One such is elliptical Fourier analysis. This method uses partial differential equations comprised of sine and cosine to describe an outline [121]. This approach is best used when studying a shape as an approximation of a continuous contour is sufficient. Geometric morphometrics (GMM) is a landmark-based technique for the study of form. In GMM, shape is defined as "[…] what is left when the differences which can be attributed to translations, rotations, and dilatations have been quotiented out." [122]. To achieve this, the shape to be studied is landmarked, and the collection of landmarks from one specimen is then treated as a unit, henceforth referred to as the *configuration*. The set of configurations in a sample are then processed through a method named Procrustes superimposition. The configuration is scaled, rotated and translated – keeping to Kendall's definition of shape. These operations are done cyclically, and several methods for optimisation exist. In this process, we have chosen minimum Procrustes distance: the sum of the square distances between the corresponding landmarks of all the configurations in the analysis [123].

The scaling that occurs during the superimposition, removes some of the size information from the configuration. It is possible still to measure size with GMM by employing centroid size. This is calculated as the square root of the sum of the squared distances of each landmark to the centre of the configuration. Centroid size,

therefore, is measured separately from shape and it is statistically uncorrelated with shape when all of the changes occur isometrically [124]. That is, it is not affected by scaling, but it is affected by allometry.

1.5.1 Landmarks

To carry out a GMM analysis, it was necessary to select landmarks. These are defined as discrete anatomical loci that can be recognised as the same loci in all specimens of the study [125]. The selection of landmarks for three-dimensional GMM analysis ideally needs to fulfil 4 criteria [124]:

1. Be homologous across specimens
2. Do not alter their topological position relative to other landmarks
3. Appropriately capture the morphology to study
4. Can be found reliably

Homology here refers to *correspondence* of landmarks. Depending on the characteristics to be studied, this can be interpreted in several ways. For example, landmarks can be biologically homologous, such that the structures that define a landmark are present in all specimens. However, biomechanic, developmental and evolutionary studies may require a different interpretation of homology, where biological homology can be disregarded in favour of other placements, for example, at the widest point of the skull.

Landmarks can also be classified into three types, as defined by Bookstein [126]. Type 1 landmarks are defined by the juxtaposition of several tissues and in terms of specific local features. Type 2 landmarks are defined by one geometric criterion, such as the tip of a bony process. Lastly, type 3 landmarks are not defined by any surrounding structures, rather by being at an extreme distance from another point, e.g. widest diameter or nadir of a concave structure. Type 1 landmarks are the easiest to identify and therefore the most reliable, and type 2 landmarks are the opposite.

Studying the semicircular canals creates a few challenges in terms of landmark selection, as anatomical landmarks are sparse. The surface of the bony labyrinth, for the entire length of the slender portion, has no distinct anatomical features. In this work, the approach used was placing landmarks along the centreline of the canal lumen (see chapter 2 for more details to this approach).

If only the loci mentioned above are selected, which somewhat fulfil the homology, topology and reliability criteria, the landmarks would still not quite capture the morphology of the canals. As mentioned in the Geometry section, the shape and size of the slender portion is functionally the most important. By using landmarks placed only at the ends, measures like the radius of curvature are left out. To solve this, some studies have added additional landmarks on the slender portion of the canal. Lebrun *et al.* [68] added two landmarks per canal on their slender portion, their references being to the absolute position of the labyrinth inside the head. In the anterior canal, landmarks 16 and 17 are described as the anterolateral-most point and the superior-most point, respectively [68]. In this instance, since only the labyrinth data was available, the planes had to be estimated from the labyrinth itself, not in relation to other cranial structures, or by alignment of the head to a given plane (such as Reid's baseline). This makes reliability for those landmarks worse, as it depends on the observer to be able to accurately define the plane, and accurately place the landmark relative to that plane. Even with absolute reliability of the observer, the loci are not truly homologous: if two identical canals were part of different labyrinths, each positioned on a different plane of the head, the "anterior-most" point would not be the same on both. Lastly, even with increased number of landmarks as implemented by Lebrun *et al.*, two landmarks on a rounded surface fail to appropriately characterise the arch defined by the slender portion. They leave out information about the circularity and the torsion of the canals, and in extreme instances, even the size.

To solve these issues, the analyses in chapters 2 and 3 include a mix of both traditional and sliding semi-landmarks. Sliding semi-landmarks can be placed along curves by dividing the length of the curve into equidistant segments where the landmark would be placed. These landmarks can then "slide" along a line tangent to the curve at that point. However, the actual curve is not known, so it is estimated as a line parallel to the line connecting the two adjacent landmarks. During the superimposition process, these landmarks will be optimised not by minimum bending energy [127], rather than Procrustes distance. Here it is important to note that an increased number of sliding landmarks makes the tangent line calculation more accurate, but will add the problem of increasing the role they will play on the superimposition. For this work, it was decided that 10 sliding semi-landmarks would be enough to fully capture the shape of the slender portion.

1.6 General structure of this work

Since the shape, size and function of the canals are closely correlated, it stands to reason that semicircular canal form is highly regulated, as variation may give way to geometries that are functionally deleterious. From an ontogenetic perspective, the limiting factor in semicircular canal form variation is ossification. Once the canals are ossified, bone remodelling in the periotic bone is incredibly low compared to other structures. Nonetheless, given the potential dysregulation of bone remodelling, is there a possibility for later life form changes? Some species, like humans, have fully ossified labyrinths by the time of birth, whilst others only ossify until early postnatal life. Does the postnatal semicircular canal form continue changing until the point of ossification, or is the shape already developed to adult morphology before ossification?

Primate semicircular canals are also unique amongst other mammals. Whilst in most species (with a few non-primate exceptions) the endolymphatic space encompasses almost the entire cross-section of the slender portion of the canals, primates – and particularly humans – have enlarged perilymphatic spaces with much smaller (in comparison) endolymphatic spaces. This poses two questions. First, when using bony labyrinth morphology to make inferences on canal function, how much of the bony labyrinth geometry actually represents the membranous duct shape? Second, why would some species favour larger perilymphatic spaces over smaller, more slender canals?

To address these questions, this work is divided into five chapters. Chapter 2 addresses the first aim: to assess the human postnatal semicircular canal ontogeny to address the question of whether later life dysregulation leads to increased variation in semicircular canal form, likely due to decreased physiological constraints. In chapter 3, the aim is to assess murine postnatal semicircular canal form, spanning both pre and post canal ossification stages and including late life. In chapter 4, a comparative study was carried out, to assess possible anatomical answers as to why some species have differently sized perilymphatic spaces, and what inferences can be made of the membranous labyrinth given the cross-sectional morphology of the canals. Lastly, all these questions are discussed in chapter 5.

References

1. Zalewski, C. K. *Aging of the Human Vestibular System* in *Seminars in Hearing* **36** (Thieme Medical Publishers, 2015), 175–196.
2. Blanks, R., Curthoys, I., Bennett, M. & Markham, C. Planar Relationships of the Semicircular Canals in Rhesus and Squirrel Monkeys. *Brain research* **340,** 315–324. ISSN: 0006-8993 (1985).
3. Sellick, P. M. & Johnstone, B. M. Production and Role of Inner Ear Fluid. *Progress in neurobiology* **5,** 337–362. ISSN: 0301-0082 (1975).
4. Smith, C. M., Curthoys, I. S. & Laitman, J. T. First Evidence of the Link between Internal and External Structure of the Human Inner Ear Otolith System Using 3D Morphometric Modeling. *Scientific Reports* **13,** 4840. ISSN: 2045-2322 (1 2023).
5. Gray, H. *Anatomy of the Human Body* (Lea & Febiger, 1878).
6. Smith, C. M., Curthoys, I. S., Mukherjee, P., Wong, C. & Laitman, J. T. Three-Dimensional Visualization of the Human Membranous Labyrinth –The Membrana Limitans and Its Role in Vestibular Form. *The Anatomical Record* **n/a.** ISSN: 1932-8494 (2021).
7. Waespe, W. & Henn, V. in *Reviews of Physiology, Biochemistry and Pharmacology, Volume 106: Volume: 106* 37–125 (Springer, Berlin, Heidelberg, 1987). ISBN: 978-3-540-47713-6.
8. Allum, J. H. J., Honegger, F. & Pfaltz, C. R. in *The Role of Stretch and Vestibulo-Spinal Reflexes in the Generation of Human Equilibriating Reactions* (eds Allum, J. H. J. & Hulliger, M.) *Afferent Control of Posture and Locomotion* Chapter 32 (Elsevier, 1989).
9. Fitzpatrick, R. C., Butler, J. E. & Day, B. L. Resolving Head Rotation for Human Bipedalism. *Current Biology* **16,** 1509–1514. ISSN: 0960-9822. pmid: 16890526 (2006).
10. Taube, J. S. The Head Direction Signal: Origins and Sensory-Motor Integration. *Annual Review of Neuroscience* **30,** 181–207. ISSN: 0147-006X. pmid: 17341158 (2007).
11. Spoor, F., Wood, B. & Zonneveld, F. Implications of Early Hominid Labyrinthine Morphology for Evolution of Human Bipedal Locomotion. *Nature* **369,** 645–648. ISSN: 1476-4687 (6482 1994).

12. Bent, L. R., McFadyen, B. J. & Inglis, J. T. Vestibular Contributions during Human Locomotor Tasks. *Exercise and Sport Sciences Reviews* **33,** 107–113. ISSN: 0091-6331 (2005).

13. Rossignol, S., Dubuc, R. & Gossard, J.-P. Dynamic Sensorimotor Interactions in Locomotion. *Physiological reviews* **86,** 89–154 (2006).

14. Pfaff, C., Martin, T. & Ruf, I. Bony Labyrinth Morphometry Indicates Locomotor Adaptations in the Squirrel-Related Clade (Rodentia, Mammalia). *Proceedings. Biological sciences* **282,** 20150744. ISSN: 1471-2954 0962-8452. pmid: 26019162 (2015).

15. Highstein, S. M. & Holstein, G. R. in *Progress in Brain Research* 157–203 (Elsevier, 2006). ISBN: 978-0-444-51696-1.

16. Kasahara, M. & Uchino, Y. Selective Mode of Commissural Inhibition Induced by Semicircular Canal Afferents on Secondary Vestibular Neurones in the Cat. *Brain Research* **34,** 366–369. ISSN: 0006-8993. pmid: 5143125 (1971).

17. Cohen, B., Suzuki, J.-I. & Bender, M. B. XVI Eye Movements from Semicircular Canal Nerve Stimulation in the Cat. *Annals of Otology, Rhinology & Laryngology* **73,** 153–169. ISSN: 0003-4894 (1964).

18. Goldberg, J. M. & Cullen, K. E. Vestibular Control of the Head: Possible Functions of the Vestibulocollic Reflex. *Experimental Brain Research* **210,** 331–345. ISSN: 1432-1106 (2011).

19. Flourens, P. *Recherches Expérimentales Sur Les Propriétés et Les Fonctions Du Système Nerveux Dans Les Animaux Vertébrés (2e Édition, Corrigée...) / Par P. Flourens | Gallica* (J.-B. Baillière (Paris), 1842).

20. de Waele, C., Baudonnière, P. M., Lepecq, J. C., Tran Ba Huy, P. & Vidal, P. P. Vestibular Projections in the Human Cortex. *Experimental Brain Research* **141,** 541–551. ISSN: 0014-4819. pmid: 11810147 (2001).

21. Mackowetzky, K., Yoon, K. H., Mackowetzky, E. J. & Waskiewicz, A. J. Development and Evolution of the Vestibular Apparatuses of the Inner Ear. *Journal of Anatomy* **n/a.** ISSN: 1469-7580 (2021).

22. Hudspeth, A. J. & Corey, D. P. Sensitivity, Polarity, and Conductance Change in the Response of Vertebrate Hair Cells to Controlled Mechanical Stimuli. *Proceedings of the National Academy of Sciences of the United States of America* **74,** 2407–2411. ISSN: 0027-8424. pmid: 329282 (1977).

23. Hudspeth, A. J. How the Ear's Works Work: Mechanoelectrical Transduction and Amplification by Hair Cells. *Comptes Rendus Biologies* **328,** 155–162. ISSN: 1631-0691. pmid: 15771001 (2005).

24. McPherson, D. R. Sensory Hair Cells: An Introduction to Structure and Physiology. *Integrative and Comparative Biology* **58,** 282–300. ISSN: 1540-7063. pmid: 29917041 (2018).

25. Hallpike, C. S. On the Case for Repeal of Ewald's Second Law Some Introductory Remarks. *Acta Oto-Laryngologica* **53,** 7–14. ISSN: 0001-6489, 1651-2251 (sup159 1961).

26. Bach-y-Rita, P. *The Control of Eye Movements* (Elsevier, 2012).

27. Purves, D. *et al.* in *Neuroscience. 2nd Edition* (Sinauer Associates, 2001).

28. Hensen, V. Zur Morphologie Der Schnecke Des Menschen Und Der Saugertiere. *Zeitschrift für wissenschartliche Zoologie* **13,** 481–512 (1863).

29. Obrist, D. Flow Phenomena in the Inner Ear. *Annual Review of Fluid Mechanics* **51,** 487–510 (2019).

30. Arimal, T., Shibata, Y. & Uemural, T. The Ultrastructure of the Supporting System in the Guinea Pig Semicircular Canal. *European Archives of Oto-Rhino-Laryngology* **247,** 256–260. ISSN: 1434-4726 (1990).

31. Tomoda, K., Yamashita, T., Kumazawa, T. & Yoo, T. J. Type Ii Collagen Distribution in the Middle and Inner Ear. *Ear Research Japan* **15,** 199–202 (1984).

32. Slepecky, N. B., Savage, J. E. & Yoo, T. J. Localization of Type II, IX and V Collagen in the Inner Ear. *Acta Oto-Laryngologica* **112,** 611–617. ISSN: 0001-6489 (1992).

33. Engström, H. Microscopic Anatomy of the Inner Ear. *Acta Oto-Laryngologica* **40,** 5–22. ISSN: 0001-6489, 1651-2251 (1951).

34. Cunningham, D. J. *Text-Book of Anatomy* 1427 pp. (W. Wood and company, New York, 1909).

35. Igarashi, M., O-Uchi, T. & Alford, B. R. Volumetric and Dimensional Measurements of Vestibular Structures in the Squirrel Monkey. *Acta Oto-Laryngologica* **91,** 437–444. ISSN: 0001-6489 (1981).

36. Ghanem, T. A., Breneman, K. D., Rabbitt, R. D. & Brown, H. M. Ionic Composition of Endolymph and Perilymph in the Inner Ear of the Oyster Toadfish, Opsanus Tau. *The Biological Bulletin* **214,** 83–90 (2008).

37. Mugiya, Y. & Takahashi, K. Chemical Properties of the Saccular Endolymph in the Rainbow Trout, Salmo Gairdneri. 北海道大學水産學部研究彙報 **36,** 57–63 (1985).

38. Sterkers, O., Ferrary, E. & Amiel, C. Production of Inner Ear Fluids. *Physiological Reviews* **68,** 1083–1128. ISSN: 0031-9333 (1988).

39. Köppl, C., Wilms, V., Russell, I. J. & Nothwang, H. G. Evolution of Endolymph Secretion and Endolymphatic Potential Generation in the Vertebrate Inner Ear. *Brain, Behavior and Evolution* **92,** 1–31. ISSN: 0006-8977, 1421-9743. pmid: 30415265 (2018).

40. Rabbitt, R. D., Damiano, E. R. & Grant, J. W. in *The Vestibular System* 153–201 (Springer, 2004).

41. Yamauchi, A., Rabbitt, R. D., Boyle, R. & Highstein, S. M. Relationship between Inner-Ear Fluid Pressure and Semicircular Canal Afferent Nerve Discharge. *JARO - Journal of the Association for Research in Otolaryngology* **3,** 26–44. ISSN: 1525-3961, 1438-7573 (2002).

42. Steer, R. W., Li, Y. T., Young, L. R. & Meiry, J. L. *Physical Properties of the Labyrinthine Fluids and Quantification of the Phenomenon of Caloric Stimulation* in. Third Symposium on the Role of Vestibular Organs in Space Exploration. Ames: NASA (1967), 409–420.

43. Money, K. *et al.* Physical Properties of Fluids and Structures of Vestibular Apparatus of the Pigeon. *American Journal of Physiology-Legacy Content* **220,** 140–147. ISSN: 0002-9513 (1971).

44. Curthoys, I. S., Markham, C. H. & Curthoys, E. J. Semicircular Duct and Ampulla Dimensions in Cat, Guinea Pig and Man. *Journal of Morphology* **151,** 17–34. ISSN: 0362-2525. pmid: 830956 (1977).

45. Ramprashad, F., Landolt, J. P., Money, K. E. & Laufer, J. Dimensional Analysis and Dynamic Response Characterization of Mammalian Peripheral Vestibular Structures. *American journal of anatomy* **169,** 295–313. ISSN: 0002-9106 (1984).

46. Igarashi, M., Ohashi, K. & Ishii, M. Morphometric Comparison of Endolymphatic and Perilymphatic Spaces in Human Temporal Bones. *Acta oto-laryngologica* **101,** 161–164 (1986).

47. Igarashi, M. *Dimensional Study of the Vestibular End Organ Apparatus* in *Second Symposium on the Role of the Vestibular Organs in Space Exploration, NASA Ames Research Center, Moffett Field, CA* (Citeseer, 1966), 47–54.

48. Gray, A. A. *The Labyrinth of Animals: Including Mammals, Birds, Reptiles and Amphibians* (J. & A. Churchill, 1908).

49. Oman, C. M., Marcus, E. N. & Curthoys, I. S. The Influence of Semicircular Canal Morphology on Endolymph Flow Dynamics: An Anatomically Descriptive Mathematical Model. *Acta oto-laryngologica* **103,** 1–13. ISSN: 0001-6489 (1987).

50. Rabbitt, R. D. *et al.* Dynamic Displacement of Normal and Detached Semicircular Canal Cupula. *Journal of the Association for Research in Otolaryngology* **10,** 497–509. ISSN: 1438-7573 (2009).

51. Steinhausen, W. Ueber Die Beobachtung Der Cupula in Den Bogengangsampullen Des Labyrinths Des Lebenden Hechts. [On the Observation of the Ampullary Crest in the Labyrinthic Canals of the Living Pike.] *Pflügers Archiv für die Gesamte Physiologie des Menschen und der Tiere* **232,** 500–512 (1933).

52. van Egmond, A. A. J., Groen, J. J. & Jongkees, L. B. W. The Mechanics of the Semicircular Canal. *The Journal of Physiology* **110,** 1–17. ISSN: 0022-3751. pmid: 15406377 (1949).

53. Baloh, R. W., Honrubia, V. & Kerber, K. A. *Baloh and Honrubia's Clinical Neurophysiology of the Vestibular System* ISBN: 978-0-19-932278-7 (Oxford University Press, 2011).

54. David, R., Stoessel, A., Berthoz, A., Spoor, F. & Bennequin, D. Assessing Morphology and Function of the Semicircular Duct System: Introducing New in-Situ Visualization and Software Toolbox. *Scientific Reports* **6.** ISSN: 2045-2322. pmid: 27604473 (2016).

55. Rabbitt, R. D. Semicircular Canal Biomechanics in Health and Disease. *Journal of Neurophysiology* **121,** 732–755. ISSN: 0022-3077 (2019).

56. Fritzsch, B. & Straka, H. Evolution of Vertebrate Mechanosensory Hair Cells and Inner Ears: Toward Identifying Stimuli That Select Mutation Driven Altered Morphologies. *Journal of comparative physiology. A, Neuroethology, sensory, neural, and behavioral physiology* **200,** 5–18. ISSN: 0340-7594. pmid: 24281353 (2014).

57. Oman, C. M. & Young, L. R. The Physiological Range of Pressure Difference and Cupula Deflections in the Human Semicircular Canal: Theoretical Considerations. *Acta oto-laryngologica* **74,** 324–331. ISSN: 0001-6489 (1972).

58. Curthoys, I. S., Blanks, R. H. I. & Markham, C. H. Semicircular Canal Functional Anatomy in Cat, Guinea Pig and Man. *Acta oto-laryngologica* **83,** 258–265 (1977).

59. Muller, M. Semicircular Duct Dimensions and Sensitivity of the Vertebrate Vestibular System. *Journal of Theoretical Biology* **167,** 239–256. ISSN: 0022-5193 (1994).

60. Spoor, F., Bajpai, S., Hussain, S. T., Kumar, K. & Thewissen, J. G. Vestibular Evidence for the Evolution of Aquatic Behaviour in Early Cetaceans. *Nature* **417,** 163. ISSN: 1476-4687 (2002).

61. Spoor, F. *et al.* The Primate Semicircular Canal System and Locomotion. *Proceedings of the National Academy of Sciences* **104,** 10808–10812. ISSN: 0027-8424. pmid: 17576932 (2007).

62. Walker, A., Ryan, T. M., Silcox, M. T., Simons, E. L. & Spoor, F. The Semicircular Canal System and Locomotion: The Case of Extinct Lemuroids and Lorisoids. *Evolutionary Anthropology: Issues, News, and Reviews: Issues, News, and Reviews* **17,** 135–145. ISSN: 1060-1538 (2008).

63. Yang, A. & Hullar, T. E. Relationship of Semicircular Canal Size to Vestibular-Nerve Afferent Sensitivity in Mammals. *Journal of neurophysiology* **98,** 3197–3205. ISSN: 0022-3077 (2007).

64. Bhagat, R., Bertrand, O. C. & Silcox, M. T. Evolution of Arboreality and Fossoriality in Squirrels and Aplodontid Rodents: Insights from the Semicircular Canals of Fossil Rodents. *Journal of Anatomy* **238,** 96–112. ISSN: 1469-7580 (2021).

65. Spoor, F. & Zonneveld, F. Comparative Review of the Human Bony Labyrinth. *American Journal of Physical Anthropology: The Official Publication of the American Association of Physical Anthropologists* **107,** 211–251. ISSN: 0002-9483 (1998).

66. Jones, G. M. & Spells, K. E. A Theoretical and Comparative Study of the Functional Dependence of the Semicircular Canal upon Its Physical Dimensions. *Proceedings of the Royal Society of London. Series B. Biological Sciences* **157,** 403–419. ISSN: 0080-4649 (1963).

67. Benson, R. B. J., Starmer-Jones, E., Close, R. A. & Walsh, S. A. Comparative Analysis of Vestibular Ecomorphology in Birds. *Journal of anatomy* **231,** 990–1018. ISSN: 1469-7580 0021-8782. pmid: 29156494 (2017).

68. Lebrun, R., de León, M. P., Tafforeau, P. & Zollikofer, C. Deep Evolutionary Roots of Strepsirrhine Primate Labyrinthine Morphology. *Journal of Anatomy* **216,** 368–380. ISSN: 0021-8782. pmid: 20039977 (2010).

69. Ekdale, E. G. Form and Function of the Mammalian Inner Ear. *Journal of Anatomy* **228,** 324–337. ISSN: 1469-7580 0021-8782. pmid: 25911945 (2016).

70. Ross, C. F. & Ravosa, M. J. Basicranial Flexion, Relative Brain Size, and Facial Kyphosis in Nonhuman Primates. *American Journal of Physical Anthropology* **91,** 305–324 (1993).

71. Le Maître, A. Role of Spatial Integration in the Morphology of the Bony Labyrinth in Modern Humans. *Bulletins et Mémoires de la Société d'Anthropologie de Paris* **31,** 34–42. ISSN: 0037-8984, 1777-5469 (2019).

72. Rabbitt, R. D. Directional Coding of Three-Dimensional Movements by the Vestibular Semicircular Canals. *Biological Cybernetics* **80,** 417–431. ISSN: 03401200 (1999).

73. Jones, S. M., Jones, T. A., Mills, K. N. & Gaines, G. C. Anatomical and Physiological Considerations in Vestibular Dysfunction and Compensation. *Seminars in hearing* **30,** 231–241. ISSN: 0734-0451. pmid: 21072129 (2009).

74. Blanks, R. H. I., Curthoys, I. S. & Markham, C. H. Planar Relationships of the Semicircular Canals in Man. *Acta oto-laryngologica* **80,** 185–196 (1975).

75. Della Santina, C. C., Potyagaylo, V., Migliaccio, A. A., Minor, L. B. & Carey, J. P. Orientation of Human Semicircular Canals Measured by Three-Dimensional Multiplanar CT Reconstruction. *Journal of the Association for Research in Otolaryngology* **6,** 191–206 (2005).

76. Berlin, J. C., Kirk, E. C. & Rowe, T. B. Functional Implications of Ubiquitous Semicircular Canal Non-Orthogonality in Mammals. *PLoS One* **8,** e79585. ISSN: 1932-6203 (2013).

77. Calabrese, D. R. & Hullar, T. E. Planar Relationships of the Semicircular Canals in Two Strains of Mice. *JARO: Journal of the Association for Research in Otolaryngology* **7,** 151–159. ISSN: 1525-3961. pmid: 16718609 (2006).

78. Ekdale, E. G. Ontogenetic Variation in the Bony Labyrinth of Monodelphis Domestica (Mammalia: Marsupialia) Following Ossification of the Inner Ear Cavities. *Anatomical Record (Hoboken, N.J.: 2007)* **293,** 1896–1912. ISSN: 1932-8494. pmid: 20730862 (2010).

79. Perier, A., Lebrun, R. & Marivaux, L. Different Level of Intraspecific Variation of the Bony Labyrinth Morphology in Slow- Versus Fast-Moving Primates. *Journal of Mammalian Evolution* **23,** 353–368. ISSN: 1573-7055 (2016).

80. Welker, K. L., Orkin, J. D. & Ryan, T. M. Analysis of Intraindividual and Intraspecific Variation in Semicircular Canal Dimensions Using High-Resolution x-Ray Computed Tomography. *Journal of Anatomy* **215,** 444–451. ISSN: 1469-7580 (2009).

81. Billet, G. *et al.* High Morphological Variation of Vestibular System Accompanies Slow and Infrequent Locomotion in Three-Toed Sloths. *Proceedings. Biological sciences* **279,** 3932–3939. ISSN: 1471-2954 0962-8452. pmid: 22859594 (2012).

82. Estes, M. S., Blanks, R. H. & Markham, C. H. Physiologic Characteristics of Vestibular First-Order Canal Neurons in the Cat. I. Response Plane Determination and Resting Discharge Characteristics. *Journal of Neurophysiology* **38,** 1232–1249. ISSN: 0022-3077 (1975).

83. Dickman, J. D. Spatial Orientation of Semicircular Canals and Afferent Sensitivity Vectors in Pigeons. *Experimental brain research* **111,** 8–20. ISSN: 0014-4819 0014-4819. pmid: 8891631 (1996).

84. Haque, A., Angelaki, D. E. & Dickman, J. D. Spatial Tuning and Dynamics of Vestibular Semicircular Canal Afferents in Rhesus Monkeys. *Experimental Brain Research* **155,** 81–90. ISSN: 0014-4819, 1432-1106 (2004).

85. Brichta, A. M., Acuña, D. L. & Peterson, E. H. Planar Relations of Semicircular Canals in Awake, Resting Turtles, Pseudemys Scripta. *Brain, Behavior and Evolution* **32,** 236–245. ISSN: 0006-8977, 1421-9743. pmid: 3266090 (1988).

86. Mazza, D. & Winterson, B. J. Semicircular Canal Orientation in the Adult Resting Rabbit. *Acta Oto-Laryngologica* **98,** 472–480. ISSN: 0001-6489. pmid: 6524343 (1984 Nov-Dec).

87. Hullar, T. E. & Williams, C. D. Geometry of the Semicircular Canals of the Chinchilla (Chinchilla Laniger). *Hearing Research* **213,** 17–24. ISSN: 0378-5955 (2006).

88. Malinzak, M. D., Kay, R. F. & Hullar, T. E. Locomotor Head Movements and Semicircular Canal Morphology in Primates. *Proceedings of the National Academy of Sciences* **109,** 17914–17919. ISSN: 0027-8424. pmid: 23045679 (2012).

89. Gonzales, L. A., Malinzak, M. D. & Kay, R. F. Intraspecific Variation in Semicircular Canal Morphology—A Missing Element in Adaptive Scenarios? *American Journal of Physical Anthropology* **168,** 10–24. ISSN: 1096-8644 (2019).

90. Jeffery, N., Ryan, T. M. & Spoor, F. The Primate Subarcuate Fossa and Its Relationship to the Semicircular Canals Part II: Adult Interspecific Variation. *Journal of Human Evolution* **55,** 326–339. ISSN: 0047-2484 (2008).

91. McVean, A. The Semicircular Canals of the Hagfish Myxine Glutinosa. *Journal of Zoology* **224,** 213–222. ISSN: 1469-7998 (1991).

92. Goyens, J. High Ellipticity Reduces Semi-Circular Canal Sensitivity in Squamates Compared to Mammals. *Scientific Reports* **9,** 16428. ISSN: 2045-2322 (1 2019).

93. Cox, P. G. & Jeffery, N. Semicircular Canals and Agility: The Influence of Size and Shape Measures. *Journal of Anatomy* **216,** 37–47. ISSN: 0021-8782 (2010).

94. Tremble, G. E. The Bony Labyrinth Of The New-born Infant And Of The Adult: A Comparative Study. *Archives of Otolaryngology - Head and Neck Surgery* **9,** 175–180. ISSN: 0886-4470 (1929).

95. Muren, C., Ruhn, G. & Wilbrand, H. Anatomic Variations of the Human Semicircular Canals: A Radioanatomic Investigation. *Acta Radiologica. Diagnosis* **27,** 157–163. ISSN: 0567-8056 (1986).

96. Sato, H., Sando, I., Takahashi, H. & Fujita, S. Torsion of the Human Semicircular Canals and Its Influence on Their Angular Relationships. *Acta Oto-Laryngologica* **113,** 171–175. ISSN: 0001-6489, 1651-2251 (1993).

97. Whitfield, T. T. Development of the Inner Ear. *Current Opinion in Genetics & Development. Developmental Mechanisms, Patterning and Organogenesis* **32,** 112–118. ISSN: 0959-437X (2015).

98. Som, P. & Naidich, T. Development of the Skull Base and Calvarium: An Overview of the Progression from Mesenchyme to Chondrification to Ossification. *Neurographics* **3,** 169–184 (2013).

99. Jeffery, N. & Spoor, F. Prenatal Growth and Development of the Modern Human Labyrinth. *Journal of anatomy* **204,** 71–92. ISSN: 0021-8782 0021-8782. pmid: 15032915 (2004).

100. Doden, E. & Halves, R. On the Functional Morphology of the Human Petrous Bone. *American Journal of Anatomy* **169,** 451–462. ISSN: 1553-0795 (1984).

101. Sølvsten Sørensen, M., Balslev Jørgensen, M. & Bretlau, P. Drift Barriers in the Postcartilaginous Development of the Mammalian Otic Capsule. *European Archives of Oto-Rhino-Laryngology* **249.** ISSN: 0937-4477, 1434-4726 (1992).

102. Frisch, T., Overgaard, S., Sørensen, M. S. & Bretlau, P. Estimation of Volume Referent Bone Turnover in the Otic Capsule after Sequential Point Labeling. *Annals of Otology, Rhinology & Laryngology* **109,** 33–39. ISSN: 0003-4894 (2000).

103. Hofbauer, L. C. & Heufelder, A. E. Role of Receptor Activator of Nuclear Factor-kB Ligand and Osteoprotegerin in Bone Cell Biology. *Journal of molecular medicine* **79,** 243–253. ISSN: 0946-2716 (2001).

104. Zehnder, A. F. *et al.* Osteoprotegrin Knockout Mice Demonstrate Abnormal Remodeling of the Otic Capsule and Progressive Hearing Loss. *The Laryngoscope* (2006).

105. Bloch, S. L., Kristensen, S. L. & Sørensen, M. S. The Viability of Perilabyrinthine Osteocytes: A Quantitative Study Using Bulk-Stained Undecalcified Human Temporal Bones. *The Anatomical Record* **295,** 1101–1108. ISSN: 1932-8486 (2012).

106. Kamakura, T. & Nadol Jr, J. B. Evidence of Osteoclastic Activity in the Human Temporal Bone. *Audiology and Neurotology* **22,** 218–225. ISSN: 1420-3030 (2017).

107. Wever, E. G. in *Auditory System: Anatomy Physiology (Ear)* (eds Ades, H. W. *et al.*) 423–454 (Springer, Berlin, Heidelberg, 1974). ISBN: 978-3-642-65829-7.

108. Higuchi, S. *et al.* Inner Ear Development in Cyclostomes and Evolution of the Vertebrate Semicircular Canals. *Nature* **565,** 347–350. ISSN: 1476-4687 (7739 2019).

109. Jørgensen, J. M., Shichiri, M. & Geneser, F. A. Morphology of the Hagfish Inner Ear. *Acta Zoologica* **79,** 251–256. ISSN: 1463-6395 (1998).

110. Maklad, A., Reed, C., Johnson, N. S. & Fritzsch, B. Anatomy of the Lamprey Ear: Morphological Evidence for Occurrence of Horizontal Semicircular Ducts in the Labyrinth of Petromyzon Marinus. *Journal of Anatomy* **224,** 432–446. ISSN: 1469-7580 (2014).

111. Martin, P. & Swanson, G. J. Descriptive and Experimental Analysis of the Epithelial Remodellings That Control Semicircular Canal Formation in the Developing Mouse Inner Ear. *Developmental biology* **159,** 549–558. ISSN: 0012-1606 0012-1606. pmid: 8405678 (1993).

112. Hashimoto, S., Naganuma, H., Tokumasu, K., Itoh, A. & Okamoto, M. Three-Dimensional Reconstruction of the Human Semicircular Canals and Measurement of Each Membranous Canal Plane Defined by Reid's Stereotactic Coordinates. *Annals of Otology, Rhinology & Laryngology* **114,** 934–938. ISSN: 0003-4894 (2005).

113. Pichat, J., Iglesias, J. E., Yousry, T., Ourselin, S. & Modat, M. A Survey of Methods for 3D Histology Reconstruction. *Medical Image Analysis* **46,** 73–105. ISSN: 1361-8415 (2018).

114. Rau, T. S., Würfel, W., Lenarz, T. & Majdani, O. Three-Dimensional Histological Specimen Preparation for Accurate Imaging and Spatial Reconstruction of the Middle and Inner Ear. *International Journal of Computer Assisted Radiology and Surgery* **8,** 481–509. ISSN: 1861-6429 (2013).

115. Luo, Z.-X., Ruf, I., Schultz, J. A. & Martin, T. Fossil Evidence on Evolution of Inner Ear Cochlea in Jurassic Mammals. *Proceedings of the Royal Society B: Biological Sciences* **278,** 28–34 (2011).

116. Cox, P. G. & Jeffery, N. Geometry of the Semicircular Canals and Extraocular Muscles in Rodents, Lagomorphs, Felids and Modern Humans. *Journal of Anatomy* **213,** 583–596 (2008).

117. Rook, L. *et al.* The Bony Labyrinth of Oreopithecus Bambolii. *Journal of Human Evolution* **46,** 347–354. ISSN: 0047-2484 (2004).

118. Silcox, M. T. *et al.* Semicircular Canal System in Early Primates. *Journal of Human Evolution* **56,** 315–327. ISSN: 0047-2484 (2009).

119. Ekdale, E. G. & Rowe, T. Morphology and Variation within the Bony Labyrinth of Zhelestids (Mammalia, Eutheria) and Other Therian Mammals. *Journal of Vertebrate Paleontology* **31,** 658–675. ISSN: 0272-4634 (2011).

120. Lele, S. & Richtsmeier, J. T. Euclidean Distance Matrix Analysis: A Coordinate-Free Approach for Comparing Biological Shapes Using Landmark Data. *American Journal of Physical Anthropology* **86,** 415–427. ISSN: 0002-9483, 1096-8644 (1991).

121. Caple, J., Byrd, J. & Stephan, C. N. Elliptical Fourier Analysis: Fundamentals, Applications, and Value for Forensic Anthropology. *International Journal of Legal Medicine* **131,** 1675–1690. ISSN: 1437-1596 (2017).

122. Kendall, D. G. Shape Manifolds, Procrustean Metrics, and Complex Projective Spaces. *Bulletin of the London Mathematical Society* **16,** 81–121. ISSN: 0024-6093 (1984).

123. Dryden, I. L. & Mardia, K. V. *Statistical Shape Analysis, with Applications in R. Second Edition.* (John Wiley and Sons, Chichester, 2016).

124. Zelditch, M. L., Swiderski, D. L. & Sheets, H. D. *Geometric Morphometrics for Biologists: A Primer* ISBN: 0-12-386904-8 (Academic Press, 2012).

125. Bookstein, F. L. *Morphometric Tools for Landmark Data: Geometry and Biology* (Cambridge University Press, 1991).

126. Bookstein, F. L. Biometrics, Biomathematics and the Morphometric Synthesis. *Bulletin of Mathematical Biology* **58,** 313–365. ISSN: 0092-8240, 1522-9602 (1996).

127. Perez, S. I., Bernal, V. & Gonzalez, P. N. Differences between Sliding Semi-Landmark Methods in Geometric Morphometrics, with an Application to Human Craniofacial and Dental Variation. *Journal of Anatomy* **208,** 769–784. ISSN: 0021-8782. pmid: 16761977 (2006).

Chapter 2

Human semicircular canal form ontogeny

A version of this chapter was published in the *Journal of Anatomy*:
Cárdenas-Serna, M. and Jeffery, N. (2022) Human semicircular canal form: Ontogenetic changes and variation of shape and size. *Journal of Anatomy*, 240, 541–555. https://doi.org/10.1111/joa.13576

Author contributions to this chapter:
Cárdenas-Serna, M: Data acquisition, data analysis, data interpretation and drafting of the manuscript.
Jeffery, N: Data acquisition

2.1 Introduction

The semicircular canals detect angular acceleration of the head. The signal is transduced into proprioceptive neuronal signals coded for time and motion of the head in three dimensions [1]. As discussed in the previous chapter (see subsection 1.2.1), the canals contain two main parts: an outer bony canal, filled with perilymph and an inner membranous canal filled with endolymph. Signal mechanotransduction occurs in the ampulla, inside the membranous labyrinth. There, the cilia of hair cells – embedded within the cupula – are mechanically deformed by inertial flow of the endolymph.

The sensitivity of the canals to a given angular acceleration depends largely on

the volume of fluid displaced by inertia, which is dependant on the length and cross-sectional area of the canal [see 2–5]. Nonetheless, if the volume displacement is maximised, the deflection limits of the cilia are reached sooner, which in turn reduces the frequency range over which the canals can operate effectively. Therefore, slender and longer canals are favoured over shorter and wider ones as an evolutionary compromise, possibly because narrowing of the canals has the advantage of diminishing viscous blocking and promoting Poiseuille flow [6]. These qualities have been observed in the empirically well-established relationship between canal length – as approximated by the radius of curvature of the canals – and postural behaviour. As early as 1908, Gray noted that the size of the semicircular canals appeared to correlate with the flying abilities of different species [7]. Since then, many studies have used the radius of curvature (or a variation) to infer the locomotor behaviour and agility of extant and extinct taxa [8–13], subject to adjustments for body size scaling effects [9, 14].

Canal sensitivity is also influenced by the vector as well as the volume of endolymphatic flow; it requires encoding of the afferent signals from all six canals to generate a complete picture of the acceleration [15] (see subsubsection 1.3.2 for a more comprehensive review). Therefore, the planar relationships of the canals to each other, to the principal axes of the eye and head motion influence how well the direction of the acceleration is detected [15–17]. In humans, ipsilateral canals are mostly orthogonal to each other [18] although they do not lie at exact right angles [19]. Pairs of contralateral canals are mostly parallel to each other, but with deviations up to 12° [18]. Additionally, the semicircular canals do not lie in a single plane, but rather exhibit out-of-plane deviations, or torsion, that are thought to increase the sensitivity of the canal by broadening the range of planes of angular acceleration that can stimulate endolymphatic flow [20, 21]. Notably, however, the anatomical plane of the canal and the plane of maximal response are not the same, differing on average by 10° [15]. Features such as ellipticity (or deviation from circularity) of the circuit are also considered important attributes, particularly in accommodating relatively longer, and therefore more sensitive, canals in smaller crania [22]. The development of the bony semicircular canals is precocious in terms of skull development [23]. The petrous temporal bone, for one, continues its rapid development after birth [24]. Additionally, it will experience a coronal reorientation with development [25, 26]. However, as mentioned above, semicircular canal orientation is paramount for adequate function. Despite the reorientation of the petrous bone, it appears that the position of the semicircular canals is in adult position at the time

of birth, although slight differences in the position of the vertical canals have been noted [27, 28]

Because canal form is so tightly correlated with sensitivity as well as operational range, the conservation of the canal form throughout life is likely critical to maintain adequate reflexes and functions – especially locomotion –and to avoid potentially phenotypic variants. The inner ear development is remarkably precocious. Unlike any other system, the adult shape and size of the canals are achieved in utero for a range of different mammals [29, 30, see also 31, 32]. Additionally, any subsequent adaptation of the perilabyrinthine bone is also inhibited [33], likely to prevent bone remodelling stimulated by mechanical forces that propagate through the petrous bone (e.g. masticatory forces). The mechanism behind this inhibition is most likely increased levels of osteoprotegerin (OPG) within the perilymph [34], which then enters the surrounding bone through the lacuno-canalicular system. The persistence and permeability of these canaliculi are entirely dependent on the presence of viable osteocytes to maintain the system. In early life, more viable osteocytes are located centripetally in the perilabyrinthine bone. Around 20% of viable osteocytes are lost during the first three years of life, with a much smaller decline of osteocytes in later years [35]. The remaining osteocytes slowly shift the distribution centrifugally [36], which may inhibit the diffusion of OPG radially (see subsection 1.4.2 for more details). This may cause a disinhibition of bone remodelling, or may be superfluous to maintaining sufficient inhibition. In this chapter, the hypothesis that remodelling is indeed disinhibited postnatally is tested by scrutinising morphological outcomes for evidence of 1) organised postnatal change, possibly allowing for functional refinements; 2) disorganised, stochastic, variation as part of a general entropic trend with age. Organised change predicts that perinatal canals are subtly different from adults in ways not previously captured by conventional metrics [e.g. 29] whereas disorganised change would be evidenced by canals that may be similar on average but less variable than those seen amongst adults. Additionally, the angles between the semicircular canals and key landmarks at the base of the skull are measured to test the possibility of canal orientation changes with ontogeny. These predictions are tested in this chapter using microCT (µCT) data representing adult and perinatal modern humans together with methods that can capture and analyse more detail than in previous studies, as well as MRI data for the visualisation of the canals within the skull.

2.2 Methods

2.2.1 General considerations and sample collection

For this study, there were two sets of analyses. First, a three-dimensional (3D) geometric morphometric analysis of shape with landmarks placed across all three canals. The totality of the shape represented by said landmarks will be referred to as configuration shape. Second, a cross-sectional morphometric analysis along the centrelines of each canal. For both analyses, endocasts of human semicircular canals (SCC) obtained from micro computed tomography (µCT) were used.

Samples were collected as follows. The young cohort was comprised of 51 perinatal unarticulated petrous temporal bones (Table 2.1). They were obtained from the University of Liverpool's MeCoMa collection, which consists of perinatal bone specimens collected from the Brownlow Hill workhouse in Liverpool, England, during the 19th century. Out of the 51 specimens, two were discarded due to fractures on the superior semicircular canal and one was left out due to having an abnormally small lateral canal. The adult cohort was comprised of 48 specimens, of which 17 were obtained from the bone collection at the Human Anatomy Resource Centre, the University of Liverpool (unknown gender and age , see Table 2.1). All specimens collected from the University of Liverpool were collected and analysed with approval of the Health and Life Sciences Research Ethics Committee (reference number 5504). An additional group of 16 adult specimens was collected from cadavers donated to the Anatomy department, the University of Cambridge. The latter dataset had an average age of 84.8 years (SD: 9.3, Median: 86). The remaining 15 specimens were obtained from an online repository [37]. Specimens collected at the University of Liverpool were µCT scanned using a SkyScan 1272 Micro-X-ray CT (Bruker) with an isotropic resolution of 13 microns (perinates: 60 kV; 166 µA; 0.25 mm; Al filter. adults: 100 kV; 100 µA; 0.11 mm Cu filter). The dataset from University of Cambridge were scanned at approximately 24 microns (125 kV; 120 µA; no filter). The specimens from the online repository were scanned at approximately 60 microns. Because of the nature of our samples, biometric data were limited. Although the specimens used were all accurately classified as perinates or adults, no data pertaining to sex nor exact chronological age or ethnicity were available, except for the age of the subset of adult samples from Cambridge. A summary of each dataset and the analyses they were included in can be seen in Table 2.1. Available biometric and image resolution details for each specimen are provided in the appendix (page 181,

Table 2.1: Samples details by group and dataset. Further information on each of the specimens is available as a supplementary table.

Group – dataset	Age (years)	Sex & N	Spatial resolution (µm)	Configuration analysis	Cross-section analysis
Perinates – Liverpool	<0.5	Female: 6 Male: 9 Unknown: 33	∼13	Yes	Yes
Adult – Liverpool	Unknown	Unknown: 17	∼13	Yes	Yes
Adult – Cambridge	68 to 98	Unknown: 16	∼25	Yes	Yes
Adult – Wimmer	Unknown	Unknown: 15	∼61	Yes	No

Table A.1).

2.2.2 Segmentation of endocasts

The acquired images were imported into ImageJ (1.53a v NIH, USA). For each stack, a plot profile was created and the threshold value was calculated by the half maximum height (HMH) technique [38] with reference to the bone and canal lumen values. Ten measurements were taken for each specimen at different locations throughout the stack. The stacks were then imported into Amira [39]. Segmentation of the canals was carried out by thresholding, using the mean HMH values previously calculated. The segmented area representing the lumen of the canals and the vestibule was then saved as a labelmap. A surface generated from the labelmap can be seen in Figure 2.1, A.

For subsequent analyses, the centrelines of each canal were computed. To find the centrelines, the labelmaps were down-sampled and the Distance-ordered thinner (Len of ends: 10) and the Trace line modules were used, which generated a line set. This resulting line set was edited using the Filament Editor, to remove unwanted branching lines (Figure 1, B). The Smooth lineset module was then used (smooth: 0.9; attach to data: 0.05; Number of iterations: 100). Lastly, the line set was trimmed at the point where the canals meet the vestibule (Figure 1, C). The centrelines were divided, so that one line segment was generated for each canal, and one for the common crus.

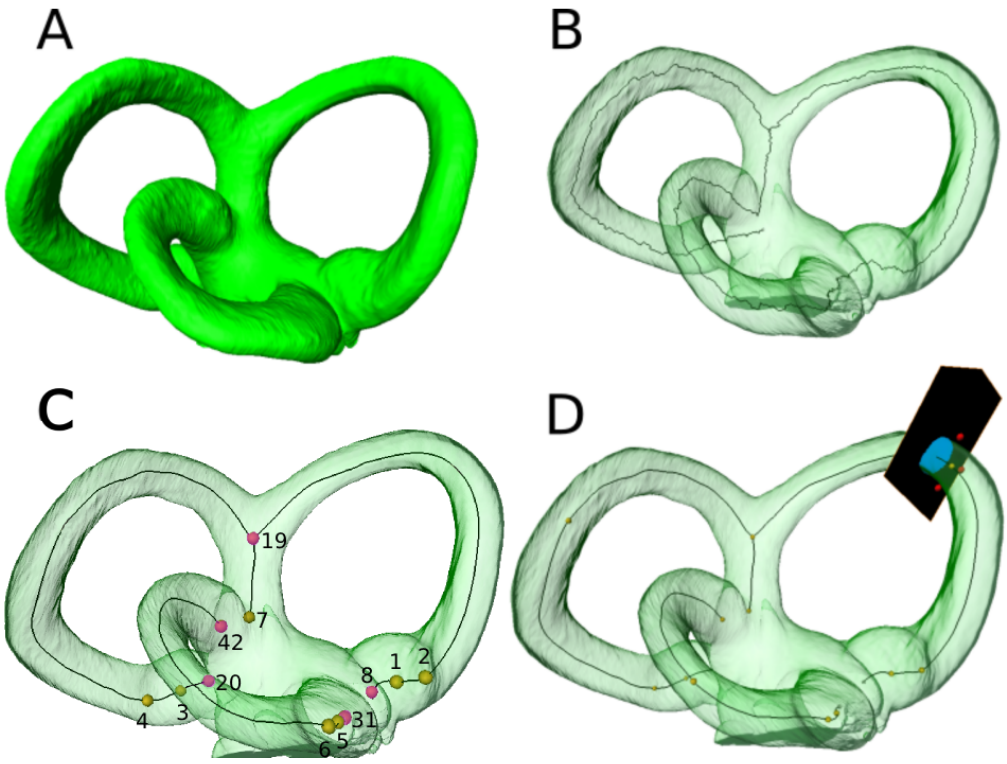

Figure 2.1: Segmentation of the bony semicircular canal endocasts to calculate centrelines. A: A surface map generated from a completed segmentation of the three canals and the superior portion of the vestibule. B: Centrelines calculated using the skeletonization procedure (distance ordered thinner and trace lines). C: Centrelines are smoothed and cropped at the points where the canals meet the vestibule. Landmarks are placed along the centreline of the canals. In yellow: fixed landmarks (1-7). In pink: fixed landmarks used as anchors for sliding landmarks (8, 19, 20, 31, 42). D: the centrelines are used to generate perpendicular slices along the length of the canals. Section in blue represents the segmented bony canal, which is then used for the analyses.

2.2.3 Geometric morphometric analysis

Shape configuration was analysed using a landmark-based 3D geometric morphometric (GMM) approach [40, 41]. This method is a quantitative way of analysing shape. In GMM, shape is defined as the geometric information remaining after removing scale, location and orientation [42], using a method called Procrustes superimposition. The landmarks are discrete anatomical loci, selected a priori, which represent a biological structure and are homologous across individuals [43]. The resulting shape configurations will therefore be aligned at the origin, standardised

to unit size, and rotated to the same orientation. However, fixed landmarks have the disadvantage of leaving out relevant information between landmarks, such as curvature. For this reason, sliding semi landmarks were used to analyse centrelines [40]. The semi landmarks are allowed to slide along a curve to match corresponding sliding semi landmarks in the reference configuration. For this study, bending energy between the reference and target specimen was used for optimisation of the sliding process. The GMM analysis was carried out in R [44], using the following packages: Geomorph (Version 3.1.3), Morpho (Version 2.7), and RVAideMemoire (Version 4.0.3) [45–47].

2.2.4 Landmarks

The landmarks for the SCC analysis were placed using the Amira Landmark module, on the centrelines of each canal. There were 7 landmarks placed on each specimen (2 on each canal, 1 on the common crus, see Figure 2.1). For a more accurate representation of slender portion of the canals, 10 sliding landmarks were placed along the centrelines of each canal. For this, the line sets representing the centrelines were exported as coordinates and down sampled to 10 equidistant points along the entire length of each canal, using the *digit.curves* function in Geomorph. A full description of the landmarks and sliding landmarks can be seen on Table 2.2 and Figure 2.1. C.

Table 2.2: SCC landmarks and description. All landmarks are placed on the centrelines generated by the skeletonization process.

Canal	No.	Landmark description	Landmark type
Anterior (ASC)	1	Centre of the ampulla of the ASC	Fixed
	2	Slender portion of the canal meets the ampulla	Fixed
Posterior (PSC)	3	Centre of the ampulla of the PSC	Fixed
	4	Slender portion of the canal meets the ampulla	Fixed
Lateral (LSC)	5	Centre of the ampulla of the LSC	Fixed
	6	Slender portion of the canal meets the ampulla	Fixed
Common crus (CC)	7	Common crus as it meets the vestibule	Fixed
	8	Anchor anterior (ampullated side meets vestibule)	Fixed
ASC	9-18	10 equidistant points across the canal.	Sliding
	19	Anchor anterior (common crus bifurcation)	Fixed
	20	Anchor posterior (ampullated side meets vestibule)	Fixed
PSC	21-30	10 equidistant points across the canal.	Sliding
	19	Anchor posterior (common crus bifurcation)	Fixed
	31	Anchor lateral (ampullated side meets vestibule)	Fixed
LSC	32-41	10 equidistant points across the canal.	Sliding
	42	Anchor lateral (non-ampullated side meets vestibule)	Fixed

Other studies have suggested the use of an additional set of landmarks on the outer surface of each canal, in an attempt to further characterise shape changes localised closer to the centreline of the membranous labyrinth [48]. It is worth noting that when evaluating measurement error, the authors found that by changing the thresholding values and the spatial resolution of the scans, the centrelines of the canals were not affected, whilst the landmarks placed on the outer surface experienced the most variation. Given that our adult cohort comprised three datasets acquired with slightly different parameters, the landmarks were placed along the centrelines of the canals, as to minimise potential shape changes due to differences in the scanning process. All three datasets had similar distribution in morphospace (see Appendix A for PC1 and 2 grouped by dataset [Figure A.1]).

2.2.5 Configuration size and shape variation

To assess the influence of size on shape, centroid size was used as a proxy. Centroid size is the square root of the sum of the squared distances between each landmark and the centroid (centre of the configuration), and it is the only measure of size that is mathematically independent of shape [49]. After testing for normality, centroid size means between adults and perinates were compared using a T test. The medians and variances were tested using a Mood test and an F test, respectively. Procrustes distance –the square root of the sum of squared distances between corresponding Procrustes-aligned points –was used to measure the distribution of the shape configurations across the morphospace. In this instance, a value of 0 represents a shape located exactly at the mean, and increasing values represent further distance from the mean. Additionally, Procrustes ANOVA was peformed to assess influence of size on shape [50] and added the residuals to the mean configuration to use as size-corrected shapes. Two models were created to assess whether each group had unique or common allometries. The common allometry model was used as null model, and a Procrustes ANOVA showed no differences between the two models ($p = 0.44$), meaning the groups had a common allometric component. Principal components analysis (PCA) was used to visualise the shape variables (Procrustes-aligned coordinates) in morphospace and canonical variates analysis (CVA) was used to find maximum shape differences between the two groups. CVA analysis was performed on the first 10 PC scores after size correction. Subsequently, cross-validation was performed using the leaving-one-out procedure. It is important to note that for our study, PCA was used to visualize shape changes in the GMM analysis, rather than

between-group PCA (bg-PCA). Although the use of bg-PCA would have perhaps better illustrated shape differences between both groups, the decision to use PCA was made considering that bg-PCA may lead to exaggerated differences between groups that are not representative of the actual differences in the samples [51].

2.2.6 Measurement error

To assess repeatability of the landmarking, the semicircular canal landmarks were repeated 4 times from 5 specimens selected at random. One specimen was landmarked at a time and was not repeated until the others were completed, allowing time to pass between each specimen repeat. The repeated sets of landmarks from each specimen were submitted to generalised Procrustes alignment (GPA) and to PCA along with the rest of the samples. The repeated measurements for each specimen clustered together on the first 4 principal components, indicating small errors compared to the overall variability of the sample. PC 1 to 4 can be seen in the appendix (Figure A.2, Figure A.3). Additionally, a Procrustes ANOVA was calculated using the individuals and repeats as categorical values. The results were then used to calculate an intraclass correlation coefficient as detailed by Fruciano [52] which was then used to calculate repeatability. Repeatability of the landmarking was 93.4%.

2.2.7 SCC cross-sections

For this analysis, only 33 adults and 45 perinates were included. During preliminary tests, it was found that convexity and solidity were sensitive to changes in resolution. The samples acquired at the University of Liverpool and the University of Cambridge had similar results across all metrics used for the analyses described below, whereas the Wimmer dataset fell in line with the other adults only for aspect ratio and cross-sectional area, but was an outlier for convexity and solidity (see Figure A.4, Figure A.5, Figure A.6, Figure A.7). The resolution of the Wimmer dataset (60 microns) was considerably poorer than the other two (13-26 microns) and was therefore not included in the following analyses, to minimise the possibility that observed differences would be due to spatial resolution differences.

The endocast labelmaps obtained from the segmentation process and the µCT images were then re-sliced as cross-sectional images that spanned the entire length of the canals. This was done in Amira following previous literature [53]. In short, the Slice module and the Trajectory module were connected to the labels and the

smoothed centreline, respectively. To iterate throughout all segments of the centreline, a tool command language (Tcl) script based on Johnson Chacko *et al.* [53] was implemented. Cross-sectional images were created using the centrelines as guidelines for the slicing (Figure 2.1, D). The images were extracted as 2D tiff files. Additionally, a spreadsheet containing the coordinates of each point and the voxel size for each slice was generated and used for area and length calculations.

2.2.8 Cross-section measurements and statistical analysis

The label cross-sections were imported into ImageJ and measured using Shape Descriptors in the Measure command (1.53a v NIH, USA), and the Convex Hull option in the Edit Selection menu. The aspect ratio, solidity, convexity and cross-sectional area were used for subsequent analyses.

Aspect ratio was calculated as

$$\frac{\text{Major axis}}{\text{Minor axis}}$$

such that 1 represents a perfect circle. Solidity and convexity are calculated by using the convex hull option in ImageJ. Solidity is calculated as

$$\frac{\text{Area}}{\text{Convex area}}$$

and convexity is calculated as

$$\frac{\text{Convex perimeter}}{\text{Perimeter}}$$

For both solidity and convexity, values less than 1 are indicative of cross-sections with more irregular perimeters. The aspect ratio was chosen to quantify form, solidity to morphological textural roughness, and convexity to quantify textural roughness, as defined by Liu *et al.* [54]. Although both solidity and convexity are affected by the perimeter of the shape, solidity is more sensitive to concavities in the shape (the cross-section), which translate to bony protrusions into the lumen. Convexity on the other hand is sensitive to roughness of the shape, in this case both concavities and convexities of the wall. Each specimen was analysed as a stack of slices throughout the length of the canal. To perform the measurements, a script was written to iterate through each slice in the stack, select the biggest masked region (the canal) and the measurements were then performed on the selection. The area was

calculated by taking the area measured in ImageJ (in pixels) and multiplied by the squared pixel size of each slice. Lastly, the lengths of the canals were calculated by summing the Euclidean distances between each point of the centrelines, as described by Johnson Chacko *et al.* [53]. A t test was performed to test for length differences between groups for each canal, Mood' s test was performed to test for differences in the length medians, and an F test was performed to assess differences in length variances.

Resulting data points were analysed using R. Subsequent analyses for the aspect ratio, area, solidity, and convexity were performed as follows. Slice positions were standardised to percentage length, where 0 represents the beginning of the ampullated side of the canal and 100 is the point where the canal meets the vestibule, in the case of the lateral canal, or where it meets the common crus, in the case of the anterior and posterior canals. The common crus was not included in the analyses as the cross-sections were heavily influenced by the vestibule and the slender portion of the anterior and posterior canals. Then, the slices were grouped into 50 bins, as this number of provides sufficient resolution to assess canal patterns in each group. To ensure that specimens with higher resolution (more slices per bin) would not unfairly contribute to either group, measurements were averaged so that each specimen would provide one value per measurement to each bin. A Mann-Whitney-U test was performed for each bin to test mean differences between groups. Additionally, a Mood' s test was performed to test for differences in the medians, as some of the regions (several bins) across all 4 variables (Aspect Ratio, Area, Convexity and Solidity), therefore both differences in means and medias were reported for all variables. Differences in variances were assessed using a Bartlett's test. A Bonferroni correction of the resulting p values was performed.

2.2.9 Semicircular canal position within the skull

Samples

For this part of the study, 30 adult and 30 perinatal specimens were analysed. T2 MRI data was sourced from publicly accessible repositories. The perinatal cohort was sourced from the Development Human Connectome Project [55]. The adult cohort was sourced from the IXI Dataset [56].

Measurements and satistical analyis

The MRI data was imported into Slicer 3D (version 4.10.2) [57] for landmarking. For a detailed list of the landmarks, see Table 2.3. In short, landmarks were placed along the base of the skull and the face, and 1 landmark on each semicircular canal, bilaterally. A further 5 equidistant landmarks were placed along the superior-most border of the petrous portion of the temporal bone, to be used as sliding landmarks. We performed a geometric morphometric analysis, using the same parameters as described in subsection 2.2.5. The landmarks were then imported into R [44] and analysed using the Geomorph package [Version 3.1.3] [45]. For the sliding landmarks, minimum-bending energy between the reference and the target was used for specimen for optimisation. The centroid size was used to assess the influence of size on shape.

To further assess rotation of the semicircular canals inside the petrous temporal bone and the skull, angles were calculated by creating a centerline vector from the posterior nasal spine to the sella, and a vector joining each canal landmark to the basion. The angle between these two vectors was then calculated. To assess the rotation of the petrous bone, the "anchor anterior" and "anchor posterior" landmarks were connected to the basion to create a vector, and then compared against the centreline vector.

Table 2.3: Skull and SCC landmark details

	Skull region	Landmark name	Description
1	Face	NASION	Nasion
2,3		OS	Superior-most point of orbit
4		SELLA	Centre of hypophyseal fossa
5,6	Base	EAM	External acoustic meatus, superior border
7,8		OC	Opening of the optic canals into the endocranial cavity
9		BASION	Basion
10,11	Canals	ANT	Point most distant from the vestibule - Anterior canal
12,13		POST	Point most distant from the vestibule - Posterior canal
14,15		LAT	Point most distant from the vestibule - Lateral canal
16,23	Base	ANC-A	Anchor - at cochlea level
17,24		Petrous crest	Sliding semi-landmark
18,25		Petrous crest	Sliding semi-landmark
19,26		Petrous crest	Sliding semi-landmark
20,27		Petrous crest	Sliding semi-landmark
21,28		Petrous crest	Sliding semi-landmark
22,29		ANC-P	Anchor - posterior canal

2.3 Results

2.3.1 Landmark analysis

Size

There was some difference in centroid sizes (Figure 2.2, A). Adults had slightly larger centroid sizes (mean, 29.10 mm; median 29.29 mm) compared with perinates (mean, 27.84 mm; median 28.96 mm). These differences were significant (t test p-value = 0.0000497; mood' s test p-value = 0.00763). There was no difference in the variance of centroid size (Figure 2.2, A) between the two groups (p = 0.739).

Shape

To visualise shape distribution in morphospace, a principal component analysis (PCA) was performed. The analysis produced 95 PCs, of which the first 25 accounted for 95% of the variance. PC 1 represents 19.01% of the variance. The distribution of the shapes between both groups overlaps on all PCs. Shape distribution along PC1 and PC2 can be seen in Figure 2.2, C, and the shape variation along PC1 is shown in Figure 2.3. Most of the variation across PC1 describes relative elongation of the posterior and lateral canals, with minimal changes to the anterior canal. Individuals with the highest PC1 scores had large lateral canals and small posterior canals, whereas individuals with lower PC1 scores had large posterior and small lateral canals. There was no clustering of Procrustes-aligned coordinates and both groups overlapped across all PCs.

The allometric component was found to be statistically significant (p-value: 0.001), although it only accounted for 3.1% of the variation. To assess difference in morphospace distribution after size correction, the residuals from regression were added to the mean Procrustes-aligned and a PCA was conducted on these allometry-free configurations. The results from PCs 1 and 2 can be seen in Figure 2.2, D. Unsurprisingly, the size corrected shape variables are nearly identically distributed on all major axes when compared to the original shapes.

The results for the CVA can be seen in Figure 2.2, E. Upon cross validation, adults were only correctly classified in 66.66% of the cases, and 64.58% for the perinates (Figure 2.2,E and F). Lastly, the Procrustes distance from each specimen to the configuration' s mean can be seen in Figure 2.2, B. The average Procrustes distance for group were 0.067 for the adults and 0.073 for the perinates. There was

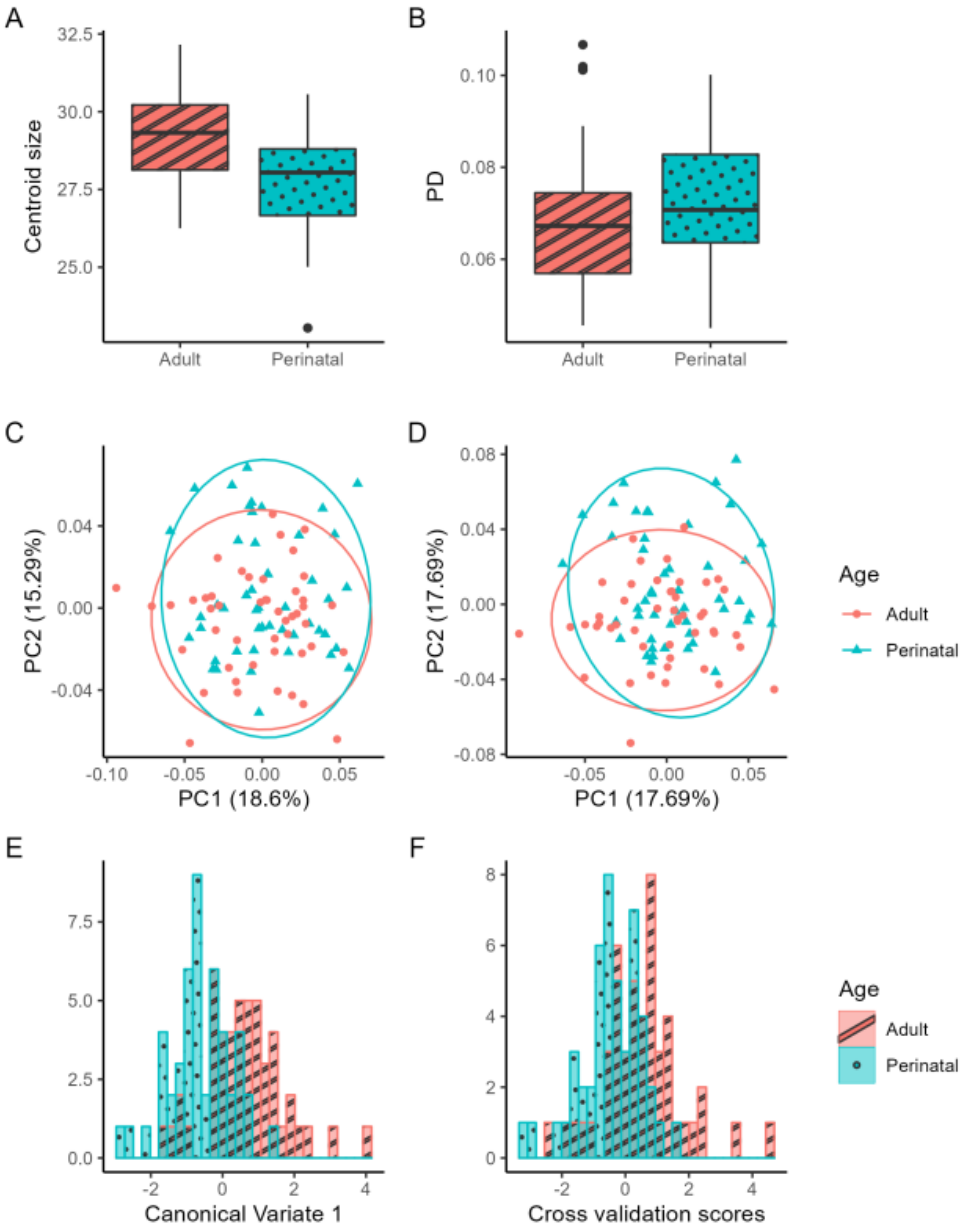

Figure 2.2: GMM analysis of SCC. A: Centroid size by age group (mm). B: Procrustes distance (PD) from shape configuration mean by group. C: PCA (PCs 1 and 2) from original shape variables. D: PCA (1 and 2) of allometry-corrected shapes. PCA plots show 90% confidence ellipses of population means. E: Canonical variate 1 by age group. F: Cross validation scores from CVA using leave-one-out procedure.

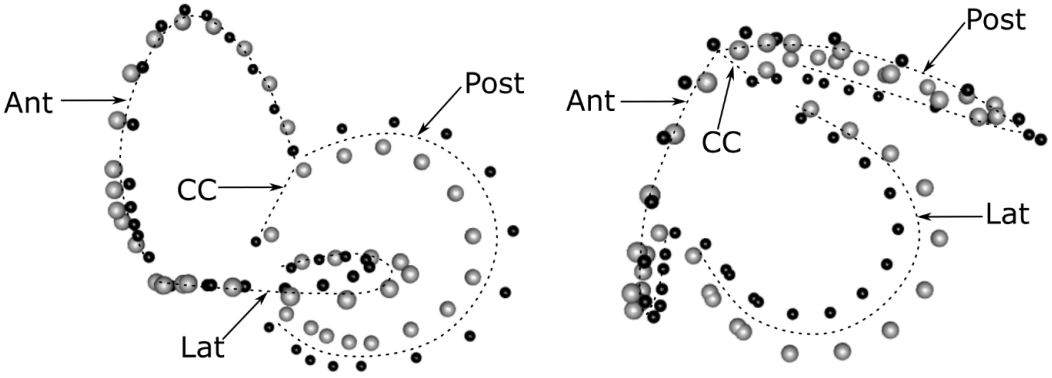

Figure 2.3: Shape changes along principal component 1. Black dots represent extreme values at PC1 min, and grey dots represent extreme values at PC1 max. Dotted lines illustrate general shape of the canals for ease of visualisation. The greatest changes are seen in the size of the posterior and lateral canals, with minimal changes to the anterior canal. NB these changes do not represent actual specimens, and neither group localised to a particular region of PC1.

no statistically significant difference between the two groups (p-value = 0.0762).

2.3.2 Centrelines and cross-sections

Length

The results of the length analyses can be seen in Figure 2.4. The posterior canal was the longest of the three for both the perinatal and the adult groups. The anterior canal was the second longest, and the lateral canal was the shortest. The only canal that showed any differences in means between groups was the anterior canal, where the adults had a mean length of 14.9 mm and the perinates 14.1 mm ($p = 0.000479$), and a Mood' s median test showed statistically significant differences ($p= 0.\ 0163$). Differences in variances were only statistically significant for the anterior canal ($p = 0.0259$), where perinates were more variable. The results for the other canals can be seen in Table 3.

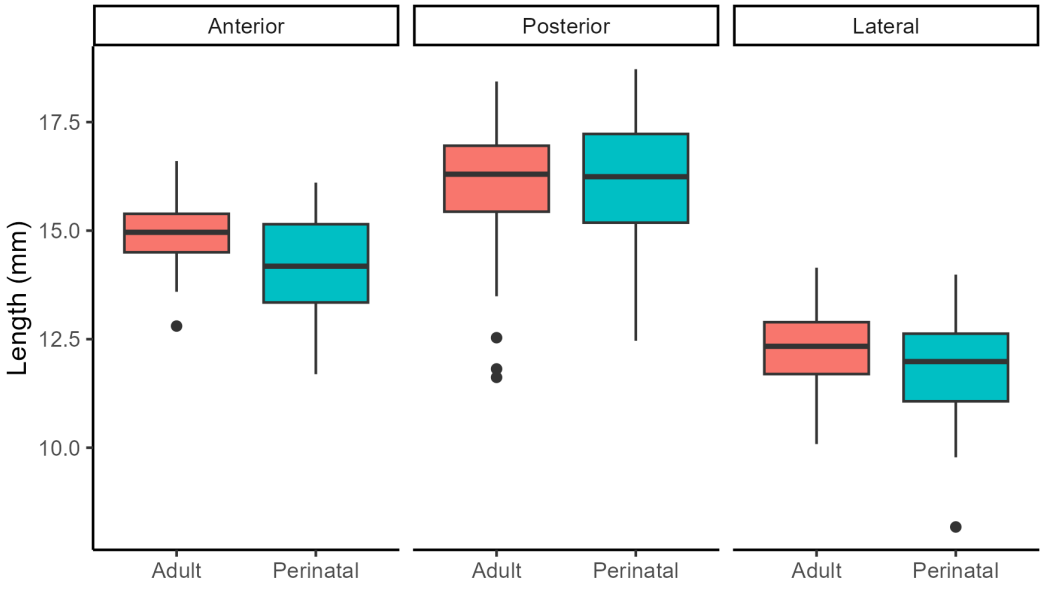

Figure 2.4: Centreline length. Lengths were calculated by computing Euclidean distances between each point in the centreline of the canals. Centrelines were trimmed at the point where each canal met the vestibule and/or the common crus. Only the anterior canal showed significant differences between group means and medians (Refer to Table 2.4).

Table 2.4: Semicircular canal length mean, median and coefficient of variation. Perinates and adults are compared using a t-test (difference of means), a Mood' s test (difference of medians), and an F test (difference in variation).

Canal	Mean (mm)			Median (mm)			Coefficient of variation		
	Adult	Perinate	P value	Adult	Perinate	P value	Adult	Perinate	P value
Anterior	14.867	14.107	0.000479	14.962	14.181	0.0163	0.0531	0.0804	0.0259
Posterior	16.025	16.182	0. 656	16.299	16.242	0.828	0.106	0.0912	0.361
Lateral	12.322	11.862	0.0518	12.335	11.984	0.050	0.080	0.0983	0.305

Aspect ratio

There were minimal differences in aspect ratio between the two groups (Figure 2.9). There were no statistically significant differences in the means of the slender portion of any of the three canals. Some differences were found in the ampullary region of the lateral canal. The adults showed with aspect ratios closer to 1. The variance was also similar between both groups, except for small portions of the central region of the slender posterior and lateral canals (bins 30-40). In general, the shape of the cross sections is elliptical in both groups, with the long axis of the cross-section being parallel to the radius of curvature of the canal (elongated radially), but gets rounder as it approaches the vestibule on the ampullary side.

Solidity

Solidity (Figure 2.5) differences were more marked in the anterior canal, where they are statistically significant along almost the entire length of the slender portion. The perinatal group has solidity values closer to one than adults do, although both groups follow a very similar pattern. Differences in the posterior canal are smaller; statistically significant regions are only at the non-ampullated end of the canal, although both groups also follow similar patterns. No differences were found in the lateral canal. Notably, the perinates had a solidity closer to one across the entire length of all three canals. In general, the lowest values are at the extremes. The variance was significantly different across different sections of all three canals, although localised to specific regions of the slender portion of the canals, and in general, adults had a larger variance than perinates. Extreme examples are shown in Figure 2.6.

Convexity

The differences in convexity (Figure 2.7) were statistically significant in all three canals. The perinatal group has convexity values closer to one across the entire length of all canals. Differences were present along the entirety of all three canals, except for a few bins at the beginning of the canal in the ampullary side. The pattern of convexity is very similar between groups in the posterior and lateral canals, but diverges in the slender portion of the anterior canals, where differences were the greatest. A small portion of the lateral canal showed differences in variances (adults showed greater variance). The rest of the canals had no statistically significant difference in the amount of the variance. Extreme examples are shown in Figure 2.8.

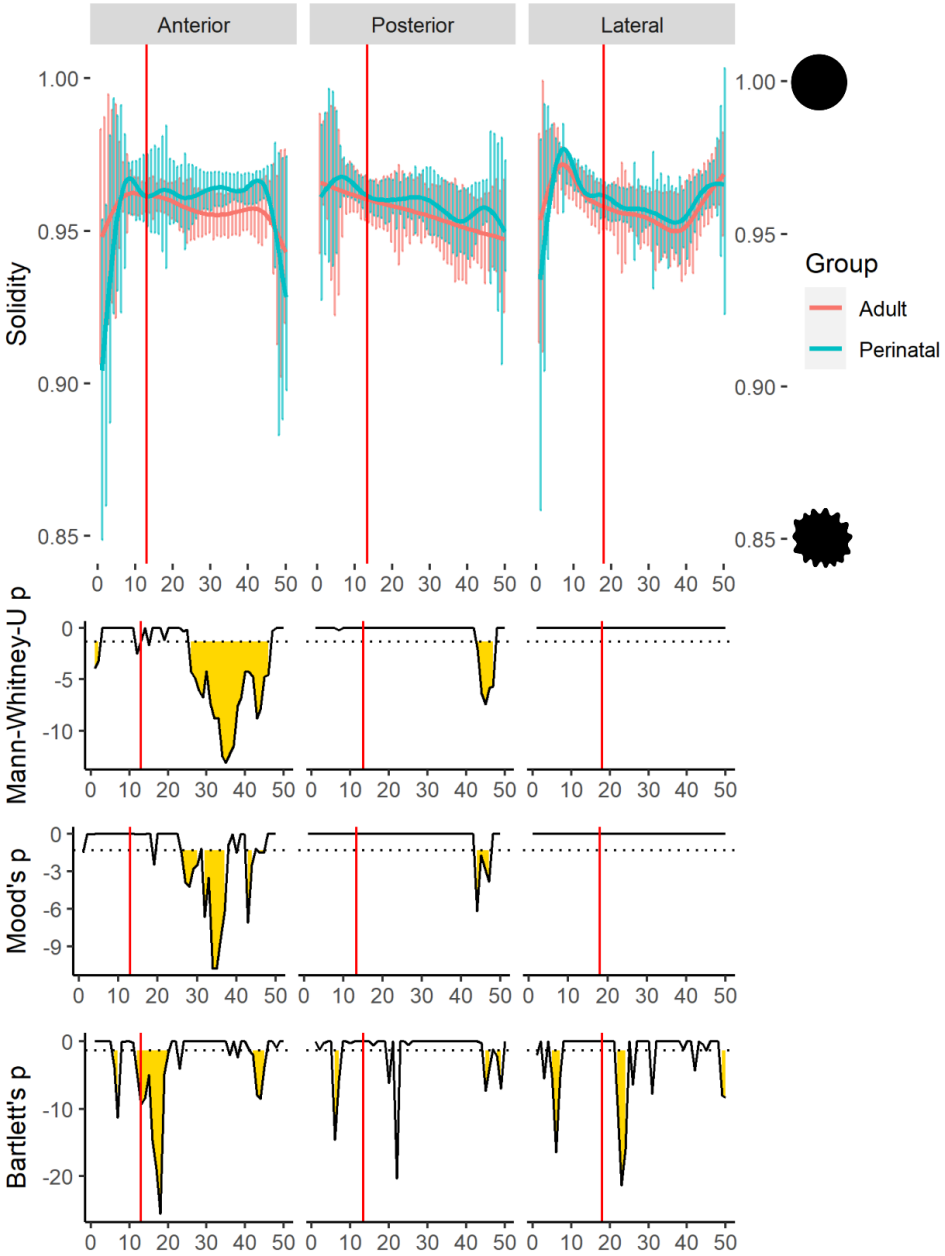

Figure 2.5: Solidity. Each canal represented by 50 bins, which span the length of the canal, from the ampulla to the vestibule or the common crus. Vertical red lines represent the average ampulla start. Top: Solid lines represent the smoothed mean for each group. Vertical coloured lines are the standard deviation for each group bin. Bottom: log p values for Mann-Whitney-U, Mood' s and Bartlett tests for differences between adult and perinate bin means, medians and variances, respectively. Horizontal dotted line represents log 0.05 and yellow area under the curve highlights bins with statistically significant differences ($p<0.05$).

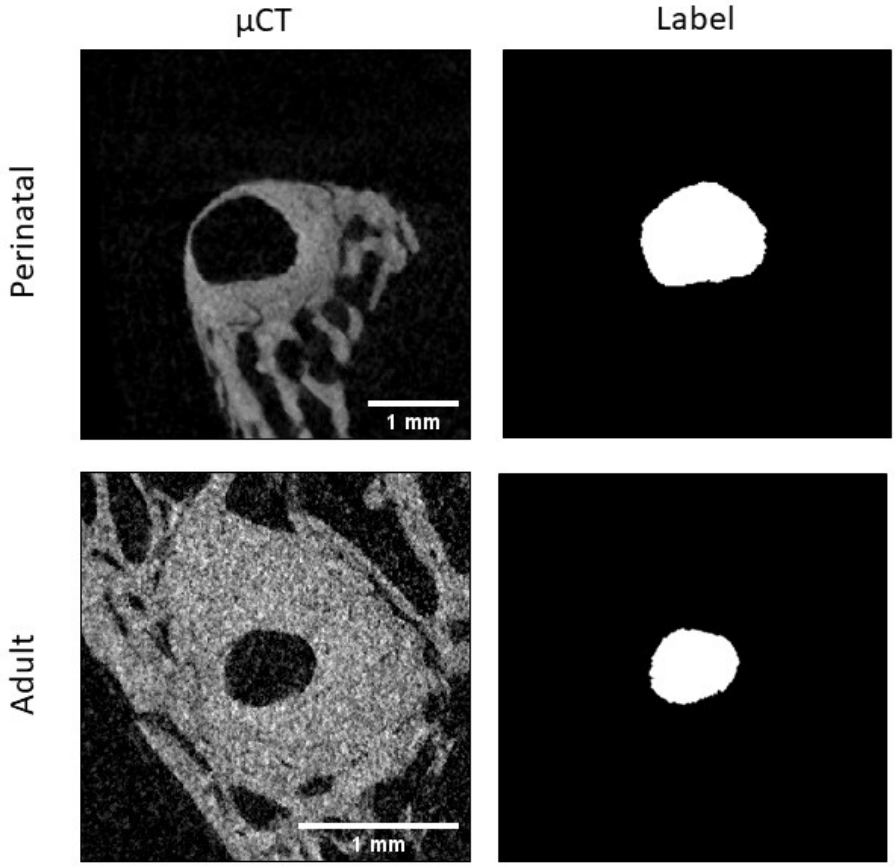

Figure 2.6: µCT and labelmap of an adult and perinatal specimen at bin 35 of the anterior canal. The solidity measures were 0.96 and 0.95 for the perinatal and adult, respectively.

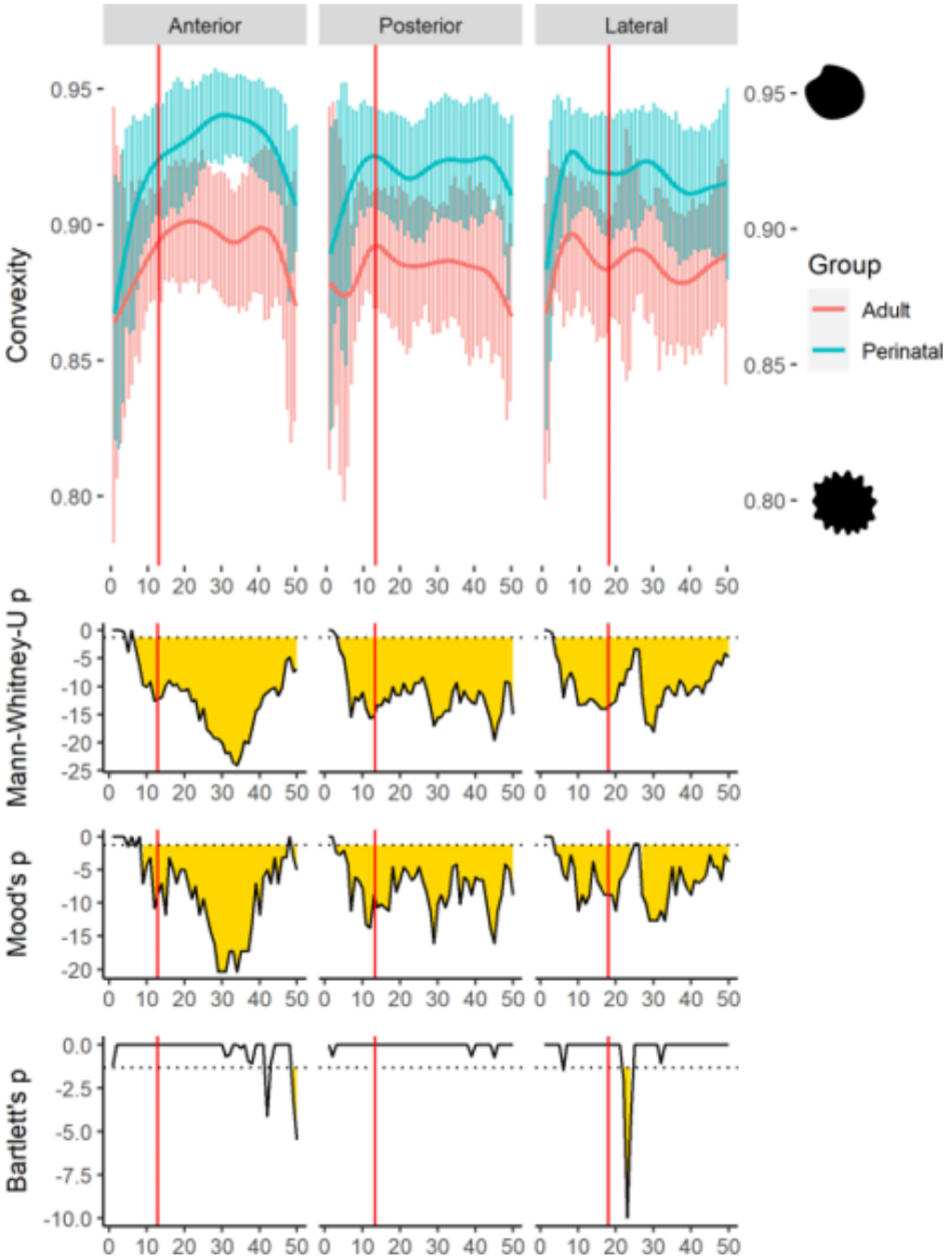

Figure 2.7: Convexity. Each canal represented by 50 bins, which span the length of the canal, from the ampulla to the vestibule or the common crus. Vertical red lines represent the average ampulla start. Top: Solid lines represent the smoothed mean for each group. Vertical coloured lines are the standard deviation each group bin. Bottom: log p values for Mann-Whitney-U, Mood' s and Bartlett tests for differences between adult and perinate bin means, medians and variances, respectively. Horizontal dotted line represents log 0.05 and yellow area under the curve highlights bins with statistically significant differences ($p<0.05$).

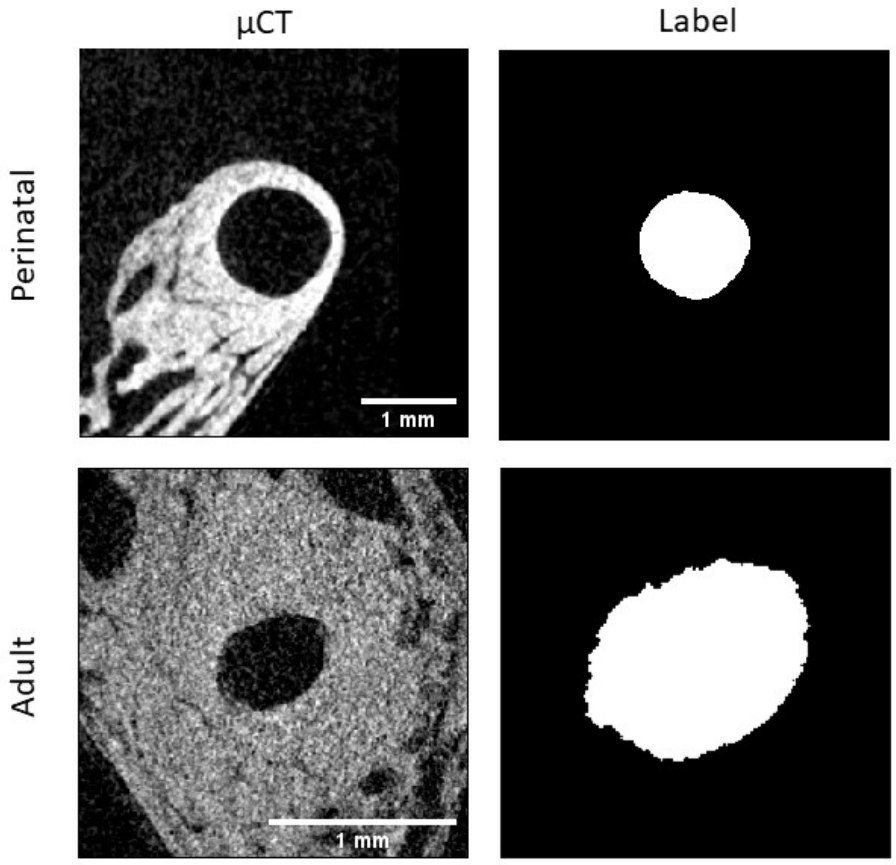

Figure 2.8: μCT and labelmap of an adult and perinatal specimen at bin 30 of the anterior canal. The convexity measures were 0.97 and 0.86 for the perinatal and adult, respectively.

Cross-section area

Lastly, no statistically significant differences were found for the cross-sectional area between groups in any of the canals (Figure 2.10). The general pattern of the area shows that the slender portion of the canal is the smallest in terms of cross-sectional area. The patterns for the anterior and lateral canals follow a parabolic shape where the area increases closer the vestibule in the ampullated and non-ampullated sides, whereas the posterior canal is mostly flat with some increase in area at both ends. In general, both groups follow an almost identical pattern. Variance between the groups is larger for the perinates across all three canals, except for two small sections in the posterior and lateral canal, where there were no differences.

2.3.3 SCC within the skull

GMM analysis

Centroid size (see Figure 2.11, A) was compared using Welch Two Sample t-test. Group means were 238.3361 and 137.0591, for the adults and perinates, respectively ($t = 53.687$, p-value $< 2.2e\text{-}16$, 95% CI: 97.49 105.06). Procrustes distance to the overall configuration mean is shown in Figure 2.11, B. The mean distances for each group were 0.085 for the adults and 0.095 for the perinates. No significant differences were found between the two groups (p-value = 0.025).

The results for PCs 1 and 2 can be seen in Figure 2.11, C. The groups are clearly clustered along the first PC, which accounts for 46.85% of the total variation. A common and a unique allometry model were compared (ANOVA), and no significant differences were found ($p = 0.15$), indicating that both had a common allometric component. This model was used to correct the shapes, which were then subjected to PCA again and no clustering was found (see Figure 2.11). After allometry correction, PC1 only accounts for 16.89% of the total variation.

Angles

The full list of results can be found in Table 2.5. All three angles (anterior, posterior and lateral) were found to be significantly different between adults and perinates. In all cases, the mean adult values were larger than the perinates. In terms of the petrous bone, both the anterior and posterior anchor angles were found to be significantly different. Just as with the rest of the angles, the adults showed a larger angle compared to the perinates. In terms of variability, no difference was found in

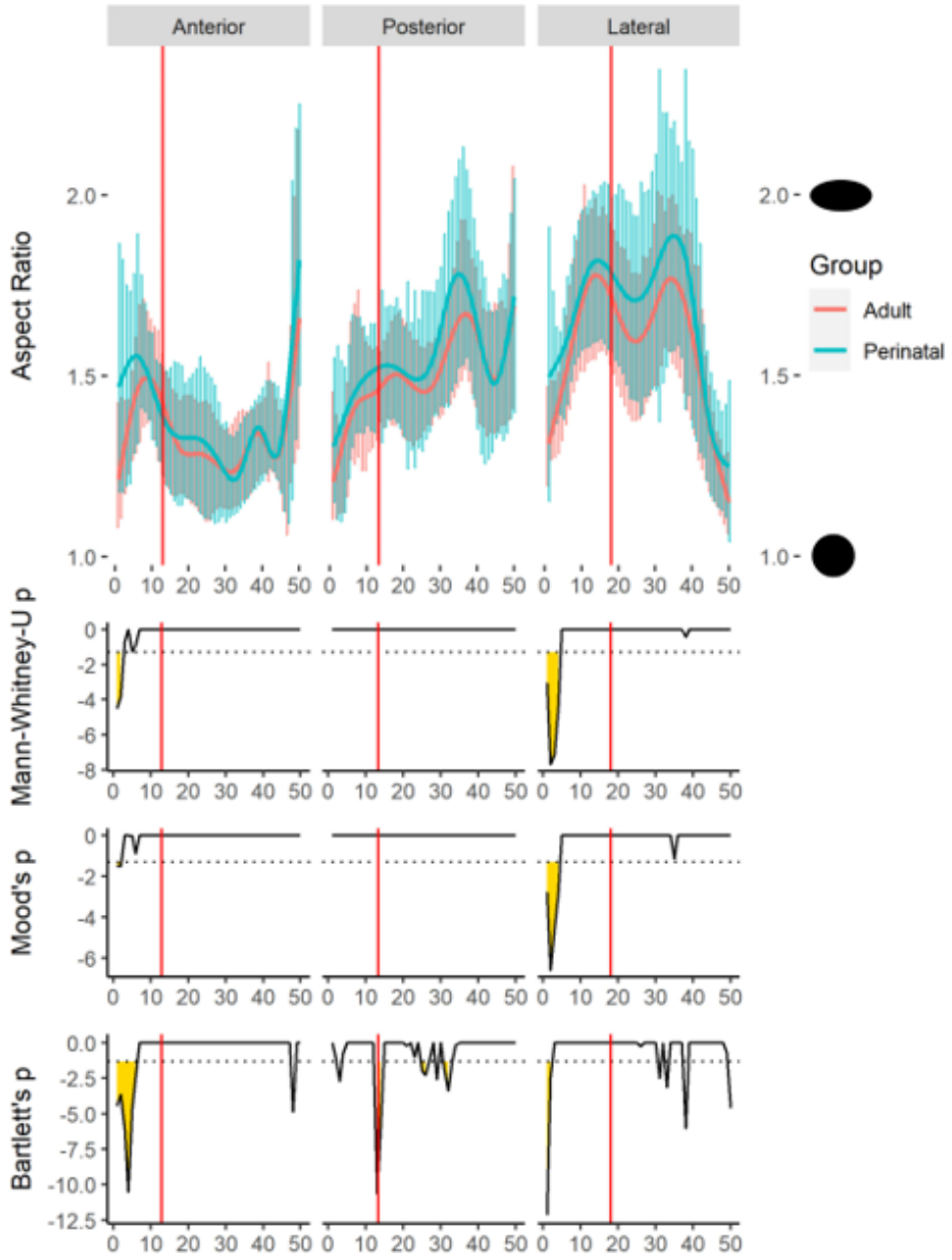

Figure 2.9: Aspect Ratio. Each canal represented by 50 bins, which span the length of the canal, from the ampulla to the vestibule or the common crus. Vertical red lines represent the average ampulla start. Top: Solid lines represent the smoothed mean for each group. Vertical coloured lines are the standard deviations each group bin. Bottom: log p values for Mann-Whitney-U, Mood' s and Bartlett tests for differences between adult and perinate bin means, medians and variances, respectively. Horizontal dotted line represents log 0.05 and yellow area under the curve highlights bins with statistically significant differences ($p<0.05$).

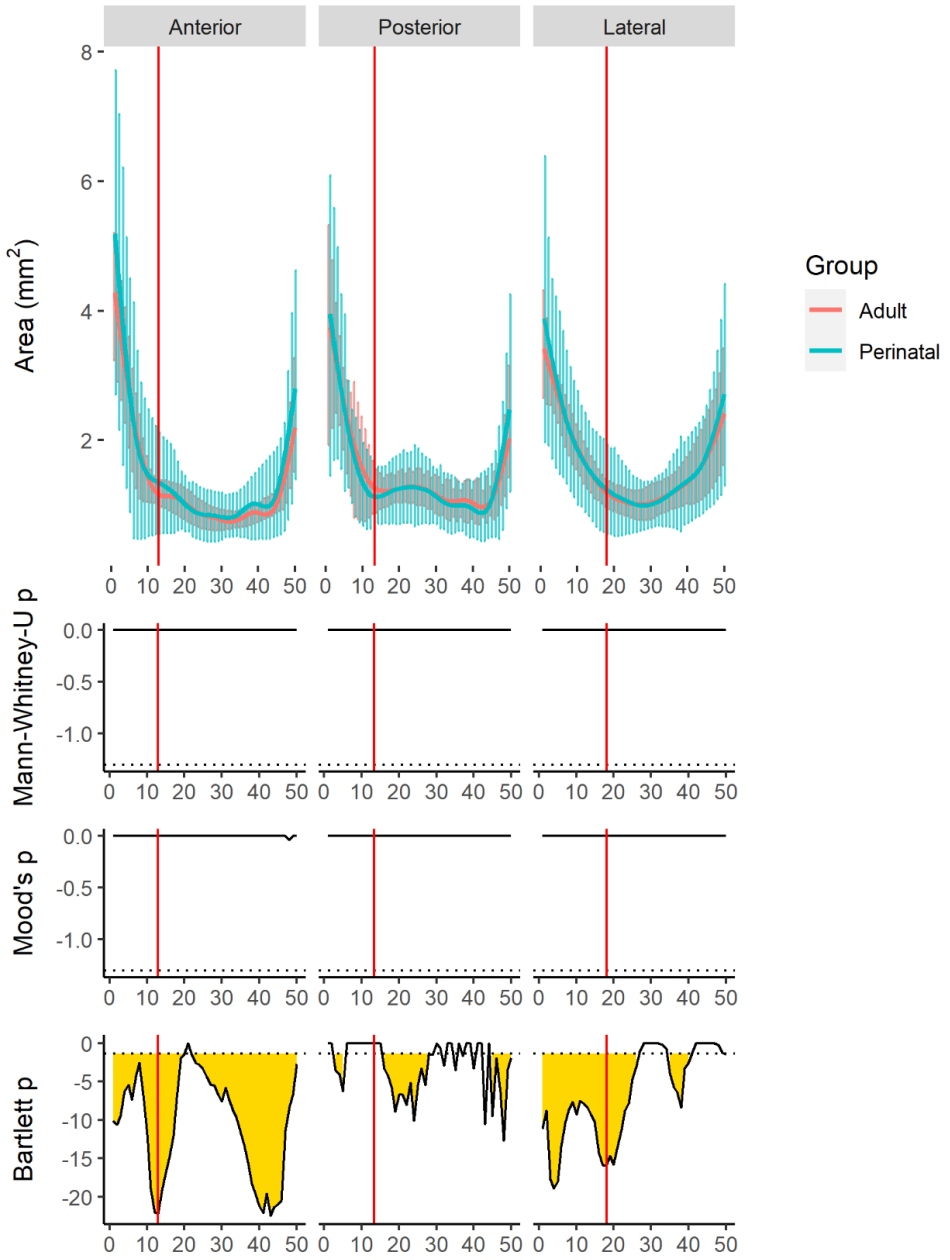

Figure 2.10: Cross-section area. Each canal is shown in 50 different bins, which represent the length of the canal, from the ampulla to the vestibule or the common crus. Vertical red lines represent the average ampulla start. Top: Solid lines represent the smoothed mean for each group. Vertical coloured lines are the standard deviation each group bin. Bottom: log p values for Mann-Whitney-U, Mood' s and Bartlett tests for differences between adult and perinate bin means, medians and variances, respectively. Horizontal dotted line represents log 0.05 and yellow area under the curve highlights bins with statistically significant differences ($p<0.05$).

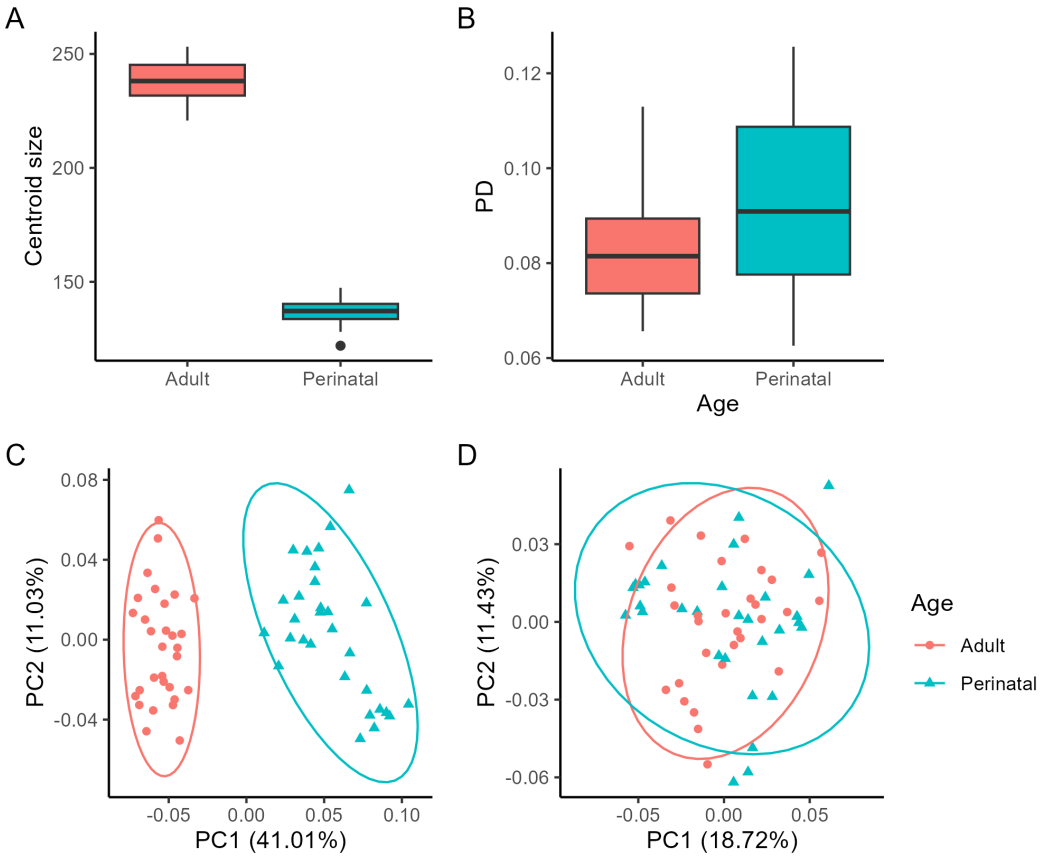

Figure 2.11: GMM results for skull shape. A: Centroid size by age group. B: Procrustes distance (PD) from configuration mean. C: Principal components analysis (PCs 1 and 2) with original shape variables. D: PCA (PCs 1 and 2) with allometry-corrected shape variables. PCA plots show 90% confidence ellipses of population means.

Table 2.5: Mean angles by group. W and p values from Wilcoxon signed-rank test.

Angle	Mean Adult	Mean perinate	W	P value	95 % CI
Anterior	250.7914	245.844	631	0.006969	1.210029-8.098531
Posterior	232.2852	220.6398	780	1.898e-07	5.798753-12.221847
Lateral	231.6618	213.3453	892	1.133e-15	14.81933-20.91694

any angles between the two groups.

In summary, adults were only found to marginally differ from perinates in the following respects: they had slightly larger centroid sizes and slightly longer anterior semicircular canals; cross-sections from the slender portions were more elliptical and had solidity and convexity values further from one. With respect to the variability, adults were more variable than perinates in terms of canal solidity and convexity. Surprisingly, the perinates were slightly more variable than the adults in terms of cross-sectional area and anterior canal length. In all other respects, adults were not different to perinates.

2.4 Discussion

For this study, the goal was to test the hypothesis that bone remodelling disinhibition in human perilabyrinthine bone can lead to changes and/or increased variation in the shape and size of the bony canals during postnatal life. The disinhibition of bone remodelling would allow for new bone formation and bone resorption on the wall of the bony labyrinth, which could be organised or stochastic. In the former, it is expected that there would be significant differences in the shape and size of the canals between perinates and adults, both in the overall canal configuration and in the anatomy of individual canals. Such changes could reflect functional shifts, possibly the maturation of obligatory bipedalism. For stochastic change, it is expected that size or shape may not differ, but that the adult cohort would exhibit greater variation than the perinates, following bone remodelling disinhibition.

Several metrics in this study showed directional change. One such change is in size. The size changes were evaluated by observing three different metrics: the centroid size of the landmark configuration shape, the length of the canals and finally, their cross-sectional area. The results supported the hypothesis that size of the canals is different between the two groups to a limited extent. The results show that adults have on average a larger centroid size and a longer anterior canal.

Differences, however, only represented around 4.4% change in centroid size and the lengthening of the anterior canal was only around 4.6%. To put this in context, the largest adult centroid size was 22.5% larger than the smallest adult centroid size. Additionally, there were almost no differences in cross-sectional area, aside from a small portion of the posterior canal. A previous study suggests that humans achieve adult semicircular canal size in utero, around the 18th week of gestational age [29]. Findings from the current study suggest there is a subtle size change after birth. The longer anterior canal corroborates other reports of differences in size due to lengthening of the canals with increases as much as 3 mm [20]. However, Daocai *et al.* [58] measured the length and width of each canal in young children (<7yrs) as well as adults and found no statistically significant differences. The authors used a single plane that most optimally displayed the entirety of the semicircular canal. It is possible, therefore, that measurements could have been skewed due to the torsion of semicircular canals that has been reported [see 59, 60]. It is also possible that Daocai *et al.* averaged out changes by aggregating findings from 9 months to 7 years in their young children category. The average area for the slender portion of the adult canals reported here was also similar to that for adult humans reported by Johnson Chacko *et al.* [53], both in terms of size at around 0.8 to 1.2 mm^2 and the pattern of variation along the canal. The parabolic distribution of the cross-sectional area is due to the widening of the canals at the ampulla and the transition from slender portion to the wider vestibule. It should be noted that determining centrelines seemed less reliable near the vestibule and the common crus, where the skeletonization process would have included parts of the vestibule as well as the canal, and probably exaggerated the corresponding aspect ratios and cross-sectional areas. In summary, there was limited evidence for small scale (<5%) size change after birth but we do not envisage these to be functionally significant. Moreover, we cannot discount sampling or measurement error biases with respect to such small margins. In terms of shape, organised changes were less consistent. Configuration shape, for example, was similar in perinates and adults. The trend across PC1 for both age groups described a relative lengthening of the posterior and lateral canals, with minimal changes to the anterior canal. These results seem to contradict the findings regarding lengthening of the anterior canal. This is because the lengths of the posterior and lateral canal were more variable overall compared to the anterior canal (see coefficients of variation in Table 2.4), but were more similarly distributed across both adults and perinates. By contrast, the overall range of variation smaller for the anterior canal, but the distribution (and the mean) was

different when comparing adults and perinates (see Figure 2.4). When considering the shape changes along PC1, it is also important to bear in mind that these were not representative of a single group, rather the variation across the entire sample (perinates and adults together). Shape measures representing the canal cross-section painted a slightly different picture. Aspect ratio, for example, showed differences between groups in the posterior and lateral canals. In both groups, nonetheless, the slender portion of the canals was elliptical, which is consistent with previous reports [60]. By contrast, the measures of solidity and convexity were generally further away from unity in adults, which is indicative of increased irregularity for the internal walls of the bony canals. Broadly, the results showed little organised difference of bony canal shape between perinates and adults. This would seem to support the notion of its functional imperativeness necessitating tighter genetic regulation of form, which in turn supports previous studies showing a close correspondence of form with, for example, population genetics [61].

Some evidence of heightened variation was also detected between both groups. Whilst there were no differences in the variability of the configuration size (centroid size), the results showed that perinates have a more variable anterior canal length compared to adults. This is not consistent with the hypothesis that postnatal disinhibition heralds disordered changes to the bony canal. Adults did have more variable convexity and solidity measures than perinates, especially in the anterior canal, and more variable aspect ratios in some sections of the slender portion as well. It is tempting to suggest that this proves the disinhibition of bone remodelling. However, it is important to note that solidity and convexity measures will have been sensitive to thresholding and interpolation artefacts. In addition, adult variability may also have been exaggerated by the inevitable limitations of the samples. Human material is scarce and therefore the adult group was drawn from several sources to achieve reasonable N values. Unfortunately, the metadata available for these different sources were patchy. The exact ages of the adult Liverpool and Wimmer dataset specimens, nor the gender of any of the adults are known. Consequently, the greater adult variation may be due in part to, for example, differences of ageing, in particular age and gender related oestrogen levels, and other environmental factors that cannot be attibuted given the paucity of biometric data available. By contrast, the perinatal cohort was geographically, ontogenetically and chronologically confined, and whilst the causes of premature death were unknown and could have included, for example, malnutrition, recent work on rats suggests that the inner ear remains relatively impervious such factors [62]. Thus, the data only implies and cannot prove that the

adult bony canals were disinhibited in comparison with perinates. Similarly, it is also possible that noise within the populations masked subtler size or shape differences consistent with co-ordinated bone remodelling. Further investigation is thus warranted using, for example, histological techniques to validate µCT data captured for more widely available non-human animal material.

In a similar fashion, the results from the MRI data do not provide a clear picture. Unsurprisingly, there were major differences in terms of centroid size between the adult and perinate skulls. In the PCA, it is evident that the clustering along PC1 was due to the size component, since it disappeared after allometry correction. In terms of Procrustes distance, the groups were indistinguishable. These results are at odds with the current literature, as it has been established that the human skull base goes through flexion and the petrous bone goes through coronal reorientation during ontogeny, likely due to encephalization [25, 26]. This may be due to the selection of landmarks within the skull, as only the sella, the optic canal opening and the basion are relatively close to the midline to show such changes. Likely, these landmarks were not enough to characterise the postnatal changes expected of the base of the skull. The petrous crest, in contrast, was very well characterised by 2 landmarks and 5 semi-landmarks, and yet, no significant differences were found between the groups. It is possible that the landmarks were not adequately placed, as the bony tissue is hard to discriminate in an MRI. As for the angles, the results showed a statistically significant increase from the perinates to the adults. An increase in angulation, however, would require the labyrinth to come closer to the sagittal plane, whilst a decrease would show direction towards the coronal plane. Nonetheless, especially in the anterior canal, the difference between groups is between 5 – 15°, which may be within the margin of error of the placement of the landmarks especially at the basion, where variance of the placement was larger than other landmarks. The MRI modality for this study was selected due to ease of accessibility (online repositories) and because it allows for visualisation of the canals when using T2 modality. However, the landmarks placed on the canals were type 2 landmarks (defined by a single geometric criterion; see subsection 1.5.1, and they were compared against a bony landmark, which is hard to place on MRI. Evidently, future projects that endeavour to assess the position and rotation of the labyrinth must use co-registered CT and MRI data, or a combination of regular and micro CT and MRI, although this may prove difficult due to the difficulty of access to specimens of this nature, especially for perinates.

Overall, the findings seem to suggest that the remaining osteocytes are suffi-

cient to suppress substantive postnatal size and shape change. This implies that functional changes linked to postural maturation and the transition to bipedalism, which is not completed until around 15 months of age, are predominantly, if not entirely, accommodated by postnatal adjustments of the underlying neurophysiological systems [63, 64] (see subsection 1.2.2). But if the early bony form is good enough that, for example, the vestibular pathways can be relied upon to adapt the signal encoding to accommodate a range of functions, why inhibit bone remodelling and constrain that bony form in the first place? A possible explanation is that the focus of this work is on the wrong place for the associated form changes. In this study, only the bony labyrinths could be examined. It is possible that postnatal functionally related adjustments are reflected more so in the morphology of the membranous labyrinth, where signal mechanotransduction occurs. The membranous part adheres to the outermost internal surface of the bony canal and the lengths should be closely correlated. It may therefore be the case that bony morphology is constrained to maintain the length of the membranous canals within certain tolerances. Indeed, the potential importance of the small but significant postnatal increase in the length of the bony, and presumably of the membranous, anterior semicircular canal, may have been understated, as it is particularly sensitive to movements in the vertical plane and its lengthening has been linked to the evolution of human bipedalism [65, 66]. In addition, there is scope for form-function modifications of the cross-section geometry of the membranous canal to go unnoticed since it occupies less than 10% of the bony canal lumen with the remaining space filled with perilymph and a fibroblast trabeculae [67]. In humans the space forms rapidly in-utero and lines the full length of each membranous canal by around 13 weeks in-utero [30]. Notably, the role of the perilymphatic space remains elusive, and it is clear that marked differences between primates and other taxa exist, and explanations regarding body size, locomotion and phylogeny do not paint a clear picture [7, 67]. In chapter 4, a comparative study is carried out to try and elucidate the potential driving forces for these differences. Additionally, this chapter has focused on human postnatal ontogeny, at which point the bony labyrinth is fully ossified. However, it is not clear if the semicircular canal form continues changing and is limited by ossification, or whether ossification occurs after form maturity. In the next chapter, the bony labyrinth of *Mus musculus* is investigated, as its postnatal ossification allows for further exploration of this question.

References

1. Berlin, J. C., Kirk, E. C. & Rowe, T. B. Functional Implications of Ubiquitous Semicircular Canal Non-Orthogonality in Mammals. *PLoS One* **8,** e79585. ISSN: 1932-6203 (2013).
2. Jones, G. M. & Spells, K. E. A Theoretical and Comparative Study of the Functional Dependence of the Semicircular Canal upon Its Physical Dimensions. *Proceedings of the Royal Society of London. Series B. Biological Sciences* **157,** 403–419. ISSN: 0080-4649 (1963).
3. Lambert, F. M., Beck, J. C., Baker, R. & Straka, H. Semicircular Canal Size Determines the Developmental Onset of Angular Vestibuloocular Reflexes in Larval Xenopus. *The Journal of Neuroscience* **28,** 8086–8095. ISSN: 0270-6474. pmid: 18685033 (2008).
4. Yang, A. & Hullar, T. E. Relationship of Semicircular Canal Size to Vestibular-Nerve Afferent Sensitivity in Mammals. *Journal of neurophysiology* **98,** 3197–3205. ISSN: 0022-3077 (2007).
5. Iversen, M. M. & Rabbitt, R. D. Wave Mechanics of the Vestibular Semicircular Canals. *Biophysical Journal* **113,** 1133–1149. ISSN: 0006-3495 (2017).
6. Obrist, D. Flow Phenomena in the Inner Ear. *Annual Review of Fluid Mechanics* **51,** 487–510 (2019).
7. Gray, A. A. *The Labyrinth of Animals: Including Mammals, Birds, Reptiles and Amphibians* (J. & A. Churchill, 1908).
8. Rabbitt, R. D., Damiano, E. R. & Grant, J. W. in *The Vestibular System* 153–201 (Springer, 2004).
9. Spoor, F. *et al.* The Primate Semicircular Canal System and Locomotion. *Proceedings of the National Academy of Sciences* **104,** 10808–10812. ISSN: 0027-8424. pmid: 17576932 (2007).
10. Walker, A., Ryan, T. M., Silcox, M. T., Simons, E. L. & Spoor, F. The Semicircular Canal System and Locomotion: The Case of Extinct Lemuroids and Lorisoids. *Evolutionary Anthropology: Issues, News, and Reviews: Issues, News, and Reviews* **17,** 135–145. ISSN: 1060-1538 (2008).
11. David, R. *et al.* Motion from the Past. A New Method to Infer Vestibular Capacities of Extinct Species. *Comptes Rendus Palevol. Imaging & 3D in Palaeontology and Palaeoanthropology* **9,** 397–410. ISSN: 1631-0683 (2010).

12. Ryan, T. M. *et al.* Evolution of Locomotion in Anthropoidea: The Semicircular Canal Evidence. *Proceedings of the Royal Society B: Biological Sciences* **279,** 3467–3475 (2012).

13. Le Maitre, A., Schuetz, P., Vignaud, P. & Brunet, M. New Data about Semicircular Canal Morphology and Locomotion in Modern Hominoids. *Journal of anatomy* **231,** 95–109. ISSN: 1469-7580 0021-8782. pmid: 28523740 (2017).

14. Spoor, F. & Zonneveld, F. Comparative Review of the Human Bony Labyrinth. *American Journal of Physical Anthropology: The Official Publication of the American Association of Physical Anthropologists* **107,** 211–251. ISSN: 0002-9483 (1998).

15. Rabbitt, R. D. Directional Coding of Three-Dimensional Movements by the Vestibular Semicircular Canals. *Biological Cybernetics* **80,** 417–431. ISSN: 03401200 (1999).

16. Van Buskirk, W. C. *The Biomechanics of the Semicircular Canals* in. Proceedings of the Annual International Conference of the IEEE Engineering in Medicine and Biology Society (IEEE, 1988), 1056–1057. ISBN: 0-7803-0785-2.

17. Cox, P. G. & Jeffery, N. Semicircular Canals and Agility: The Influence of Size and Shape Measures. *Journal of Anatomy* **216,** 37–47. ISSN: 0021-8782 (2010).

18. Blanks, R., Curthoys, I., Bennett, M. & Markham, C. Planar Relationships of the Semicircular Canals in Rhesus and Squirrel Monkeys. *Brain research* **340,** 315–324. ISSN: 0006-8993 (1985).

19. Lee, J.-Y. *et al.* A Morphometric Study of the Semicircular Canals Using Micro-CT Images in Three-Dimensional Reconstruction. *The Anatomical Record* **296,** 834–839. ISSN: 1932-8494 (2013).

20. Tremble, G. E. The Bony Labyrinth Of The New-born Infant And Of The Adult: A Comparative Study. *Archives of Otolaryngology - Head and Neck Surgery* **9,** 175–180. ISSN: 0886-4470 (1929).

21. Muren, C., Ruhn, G. & Wilbrand, H. Anatomic Variations of the Human Semicircular Canals: A Radioanatomic Investigation. *Acta Radiologica. Diagnosis* **27,** 157–163. ISSN: 0567-8056 (1986).

22. Goyens, J. High Ellipticity Reduces Semi-Circular Canal Sensitivity in Squamates Compared to Mammals. *Scientific Reports* **9,** 16428. ISSN: 2045-2322 (1 2019).

23. Bastir, M., Rosas, A. & O' Higgins, P. Craniofacial Levels and the Morphological Maturation of the Human Skull. *Journal of Anatomy* **209,** 637–654. ISSN: 0021-8782. pmid: 17062021 (2006).

24. Varvares, A. M., Mcnulty, M. A., Holmes, M. A. & Deleon, V. B. *Comparative Analysis of the Growth and Development of the TemporalBbone in Mice and Humans* in *AMERICAN JOURNAL OF PHYSICAL ANTHROPOLOGY* **159** (2016), 322–322.

25. Ross, C. F. & Ravosa, M. J. Basicranial Flexion, Relative Brain Size, and Facial Kyphosis in Nonhuman Primates. *American Journal of Physical Anthropology* **91,** 305–324 (1993).

26. Lieberman, D. E., Ross, C. F. & Ravosa, M. J. The Primate Cranial Base: Ontogeny, Function, and Integration. *American Journal of Physical Anthropology* **113,** 117–169. ISSN: 1096-8644 (2000).

27. Spoor, C. F. *The Comparative Morphology and Phylogeny of the Human Bony Labyrinth* (Utrecht University, Netherlands, 1993). 145 pp.

28. Lyu, H.-Y. *et al.* The Age-Related Orientational Changes of Human Semicircular Canals. *Clinical and Experimental Otorhinolaryngology* **9,** 109–115. ISSN: 1976-8710. pmid: 27090280 (2016).

29. Jeffery, N. & Spoor, F. Prenatal Growth and Development of the Modern Human Labyrinth. *Journal of anatomy* **204,** 71–92. ISSN: 0021-8782 0021-8782. pmid: 15032915 (2004).

30. Ishikawa, A. *et al.* Formation of the Periotic Space During the Early Fetal Period in Humans. *The Anatomical Record* **301,** 563–570. ISSN: 1932-8494. pmid: 29293291 (2018).

31. Hoyte, D. A. N. The Postnatal Growth of the Ear Capsule in the Rabbit. *American Journal of Anatomy* **108,** 1–16. ISSN: 0002-9106, 1553-0795 (1961).

32. Ekdale, E. G. Ontogenetic Variation in the Bony Labyrinth of Monodelphis Domestica (Mammalia: Marsupialia) Following Ossification of the Inner Ear Cavities. *Anatomical Record (Hoboken, N.J.: 2007)* **293,** 1896–1912. ISSN: 1932-8494. pmid: 20730862 (2010).

33. Frisch, T., Overgaard, S., Sørensen, M. S. & Bretlau, P. Estimation of Volume Referent Bone Turnover in the Otic Capsule after Sequential Point Labeling. *Annals of Otology, Rhinology & Laryngology* **109,** 33–39. ISSN: 0003-4894 (2000).

34. Zehnder, A. F. *et al.* Osteoprotegrin Knockout Mice Demonstrate Abnormal Remodeling of the Otic Capsule and Progressive Hearing Loss. *The Laryngoscope* (2006).

35. Bloch, S. L., Kristensen, S. L. & Sørensen, M. S. The Viability of Perilabyrinthine Osteocytes: A Quantitative Study Using Bulk-Stained Undecalcified Human Temporal Bones. *The Anatomical Record* **295,** 1101–1108. ISSN: 1932-8486 (2012).

36. Bloch, S. L. & Sørensen, M. S. The Viability and Spatial Distribution of Osteocytes in the Human Labyrinthine Capsule: A Quantitative Study Using Vector-Based Stereology. *Hearing Research* **270,** 65–70. ISSN: 0378-5955 (2010).

37. Wimmer, W. *et al.* Human Bony Labyrinth: Co-Registered CT and Micro-CT Images, Surface Models and Anatomical Landmarks (2019).

38. Spoor, F. & Zonneveld, F. Morphometry of the Primate Bony Labyrinth: A New Method Based on High-Resolution Computed Tomography. *Journal of Anatomy* **186,** 271–286. ISSN: 0021-8782. pmid: 7649826 (Pt 2 1995).

39. *Amira* version 6.0.0. Thermo Fisher Scientific.

40. Bookstein, F. L. *Morphometric Tools for Landmark Data: Geometry and Biology* (Cambridge University Press, 1991).

41. Bookstein, F. L. Biometrics, Biomathematics and the Morphometric Synthesis. *Bulletin of Mathematical Biology* **58,** 313–365. ISSN: 0092-8240, 1522-9602 (1996).

42. Kendall, D. G. The Diffusion of Shape. *Advances in Applied Probability* **9,** 428–430. ISSN: 0001-8678, 1475-6064 (1977).

43. Zelditch, M. L., Swiderski, D. L. & Sheets, H. D. *Geometric Morphometrics for Biologists: A Primer* ISBN: 0-12-386904-8 (Academic Press, 2012).

44. R Core Team. *R: A Language and Environment for Statistical Computing* manual (R Foundation for Statistical Computing, Vienna, Austria, 2022).

45. Adams, D., Collyer, M. & Kaliontzopoulou, A. Geomorph: Software for Geometric Morphometric Analyses. R Package Version 3.2.1. (2020).

46. Schlager, S. in *Statistical Shape and Deformation Analysis* (eds Zheng, G., Li, S. & Szekely, G.) 217–256 (Academic Press, 2017). ISBN: 978-0-12-810493-4.

47. Hervé, M. *RVAideMemoire: Testing and Plotting Procedures for Biostatistics* manual (2021).

48. Gunz, P., Ramsier, M., Kuhrig, M., Hublin, J.-J. & Spoor, F. The Mammalian Bony Labyrinth Reconsidered, Introducing a Comprehensive Geometric Morphometric Approach. *Journal of anatomy* **220,** 529–543. ISSN: 1469-7580 0021-8782. pmid: 22404255 (2012).

49. Klingenberg, C. P. Size, Shape, and Form: Concepts of Allometry in Geometric Morphometrics. *Development Genes and Evolution* **226,** 113–137. ISSN: 1432-041X (2016).

50. Goodall, C. Procrustes Methods in the Statistical Analysis of Shape. *Journal of the Royal Statistical Society. Series B (Methodological)* **53,** 285–339. JSTOR: 2345744 (1991).

51. Bookstein, F. L. Pathologies of Between-Groups Principal Components Analysis in Geometric Morphometrics. *Evolutionary Biology* **46,** 271–302. ISSN: 1934-2845 (2019).

52. Fruciano, C. Measurement Error in Geometric Morphometrics. *Development Genes and Evolution* **226,** 139–158. ISSN: 1432-041X (2016).

53. Johnson Chacko, L. *et al.* Analysis of Vestibular Labyrinthine Geometry and Variation in the Human Temporal Bone. *Frontiers in Neuroscience* **12.** ISSN: 1662-453X (2018).

54. Liu, E. J., Cashman, K. V. & Rust, A. C. Optimising Shape Analysis to Quantify Volcanic Ash Morphology. *GeoResJ* **8,** 14–30. ISSN: 2214-2428 (2015).

55. Cordero-Grande, L. *et al.* Sensitivity Encoding for Aligned Multishot Magnetic Resonance Reconstruction. *IEEE Transactions on Computational Imaging* **2,** 266–280. ISSN: 2573-0436 (2016).

56. Group, B. I. A. *IXI Dataset – Brain Development* Imperial College London, 2022.

57. Fedorov, A. *et al.* 3D Slicer as an Image Computing Platform for the Quantitative Imaging Network. *Magnetic Resonance Imaging. Quantitative Imaging in Cancer* **30,** 1323–1341. ISSN: 0730-725X (2012).

58. Daocai, W. *et al.* Size of the Semicircular Canals Measured by Multidetector Computed Tomography in Different Age Groups: *Journal of Computer Assisted Tomography* **38,** 196–199. ISSN: 0363-8715 (2014).

59. Sato, H., Sando, I., Takahashi, H. & Fujita, S. Torsion of the Human Semicircular Canals and Its Influence on Their Angular Relationships. *Acta Oto-Laryngologica* **113,** 171–175. ISSN: 0001-6489, 1651-2251 (1993).

60. Ifediba, M. A., Rajguru, S. M., Hullar, T. E. & Rabbitt, R. D. The Role of 3-Canal Biomechanics in Angular Motion Transduction by the Human Vestibular Labyrinth. *Annals of biomedical engineering* **35,** 1247–1263. ISSN: 0090-6964 0090-6964. pmid: 17377842 (2007).

61. Ponce de León, M. S. *et al.* Human Bony Labyrinth Is an Indicator of Population History and Dispersal from Africa. *Proceedings of the National Academy of Sciences* **115,** 4128–4133. ISSN: 0027-8424, 1091-6490. pmid: 29610337 (2018).

62. Ward, D. L. *et al.* Early Life Malnutrition and Fluctuating Asymmetry in the Rat Bony Labyrinth. *The Anatomical Record* **n/a.** ISSN: 1932-8494 (2021).

63. Ornitz, E. M., Atwell, C. W., Walter, D. O., Hartmann, E. E. & Kaplan, A. R. The Maturation of Vestibular Nystagmus in Infancy and Childhood. *Acta Oto-Laryngologica* **88,** 244–256. ISSN: 0001-6489, 1651-2251 (1979).

64. Dechesne, C. J. & Sans, A. Development of Vestibular Receptor Surfaces in Human Fetuses. *American Journal of Otolaryngology* **6,** 378–387. ISSN: 01960709 (1985).

65. Spoor, F., Wood, B. & Zonneveld, F. Implications of Early Hominid Labyrinthine Morphology for Evolution of Human Bipedal Locomotion. *Nature* **369,** 645–648. ISSN: 1476-4687 (6482 1994).

66. Fitzpatrick, R. C., Butler, J. E. & Day, B. L. Resolving Head Rotation for Human Bipedalism. *Current Biology* **16,** 1509–1514. ISSN: 0960-9822. pmid: 16890526 (2006).

67. Curthoys, I. S., Markham, C. H. & Curthoys, E. J. Semicircular Duct and Ampulla Dimensions in Cat, Guinea Pig and Man. *Journal of Morphology* **151,** 17–34. ISSN: 0362-2525. pmid: 830956 (1977).

Chapter 3

Murine bony semicircular canal form ontogeny

3.1 Introduction

From an ontogenetic perspective, the semicircular canal morphology is incredibly precocious. In humans, the semicircular canals attain adult size in utero [1], which is contemporaneous with the ossification of the bony labyrinth. As the results of the previous chapter showed, the bony semicircular canal morphology is attained before birth (see chapter 2). The overall morphology and the cross-sectional shape of the canals remains stable throughout life, barring some small changes to the walls of the lumen, likely due to bone remodelling disinhibition. The time-point of maturity for the bony labyrinth is interesting as it predates gait development and unassisted head support [2], although the vestibulo-ocular reflex is present since birth [3].

The precociousness of the semicircular canal maturity is not unique to humans. For many mammals, most of the canal maturation occurs prenatally. Pigs, for example, begin ossification prenatally [4], although it is unclear whether there is any maturation after the fact. Cetaceans begin ossification quite prematurely, at 32% of the gestation period, at which point the semicircular canal form has reached adult morphology [4]. Elephants on the other hand begin the ossification of the periotic capsule quite late in the gestation period compared to other mammals [5], but it ossifies prenatally nonetheless. This, however, is not necessarily a rule for all mammals. Rodents are born with unossified labyrinths [6, 7]. This is also true in some marsupials [8]. Specifically in mice, the bony labyrinth does not ossify in

utero, but it becomes ossified at around 8 days post-partum [9].

Due to the early ossification of the periotic capsule, mammalian remains of any post-natal ontogenetic stage are likely to have bony remains that are conserved enough for study. The bony labyrinth has been extensively used before for inferring many characteristics of extinct species, from head position to locomotion [10–15]. When studying extant species, determining the age of a specimen might not be too complicated, especially if postcranial material is available. In the case of extinct species, especially where remains are limited, it becomes more difficult to determine the age of the specimens. In some species, the relationship between form and function may be distorted by other ontogenetic constraints that are not exclusively represented in the canal form. Nonetheless, maturity of the canals at the time of ossification has been noted in other taxa aside from humans, such as lagomorphs [16], marsupials [17], bovids [18], orycteropodids [19] and cetaceans [20]. Yet, it is still a possibility for the morphology of the semicircular canals to vary depending on the ontogenetic stage, even after ossification, and consideration must be given to this point as it would make morphological studies less reliable.

Mice are great model species for studying ontogeny. They can be accessed with relative ease, in adequate numbers for statistical significance and can be studied at many different time-points. Additionally, they can be monitored and kept in well-regulated conditions, which removes any potential outside factors from changing the morphology, although the labyrinth morphology appears to be especially impervious to environmental influence, [see 21], and using only male specimens remove any change due to sexual dimorphism [22]. Additionally, several murine lines with vestibular phenotypes have been characterised before ([see 23, for a comprehensive review]. Mice also are highly sensitive to vestibular abnormalities, displaying behavioural changes, which makes the phenotype easy to screen [24]. For example, Kiernan *et al.* [25] tested 7 different lines identified due to circling behaviour. All seven lines showed truncation of the lateral semicircular canal, with more variable structural changes to the anterior and posterior canals, although changes ranged from smaller ampullae to complete absence of a particular canal. Similar results have been found in other knockout litters, and the defects are also mapped to chromosome 4 [26], likely showing allelic homogeneity. The structural changes occur at the time of fusion of the canals (between E12.5 and E13.5), and the area where the canals are malformed causes irregular thickening of the bone. However, no details are available regarding the timing of ossification of the canals in these mutant mice, which makes it difficult to ascertain whether these structural changes may be affect-

ing the phenotype due to altered ossification patterns. Mice are also an interesting species to study as they do not begin locomotion until around 14 days post-partum [27]. Regarding the auditory system, it appears that they can be conditioned to auditory cues from day 4, which suggests, at least functionally, the cochlear portion of the capsule may have reached maturity by then. Early postnatal behaviour, and the relative lateness of the otic capsule ossification suggest there might be a brief window of phenotypic adjustment of the canal form. In the present study, murine semicircular canals were investigated, and it was hypothesised that the canal shape and size change significantly from birth until the otic capsule fully ossifies, at which point the variations substantially diminish through adulthood, including old age, notwithstanding the possibility for small appositional changes such as the ones described in chapter 2.

3.2 Methods

3.2.1 Sample and imaging

A total of 43 mouse heads (C57BL/6J WT *Mus musculus*) were used for this study. The sample included 6 specimens each at 1, 7, 14, 28 and 48 days, and 13 specimens at 26 months post-natal age. Mice aged 1 to 48 days were reared and culled at the University of Michigan in accordance with Institutional Animal Care & Use Committee approval (PRO6079). The 26-month-old specimens were reared and culled at the University of Liverpool, and were biowaste from other projects. All specimens were collected immediately after culling, and placed in phosphate-buffered formalin until scanned. All mice were first imaged with standard microCT using a SkyScan 1272 (Bruker Ltd) with 50 kV, 200 µA and a 0.25 mm aluminium filter. After initial scanning, mice aged 1,7 and 14 days had areas in the petrous bone that were not fully ossified, therefore they were stained with I_2KI (9% w/v) and scanned as described above. After evaluation of the otic capsule ossification, and with reference to Bryant *et al.* [9], the contrast enhanced scans were used for the P1 and P7 groups, and the standard scans were used for the remaining groups. After imaging, each ear was processed separately, giving a total biological sample of 86. Details on the ages, staining, acquisition details and analyses are described in Table 3.1.

Table 3.1: Sample details. P1-14: Postnatal days 1-14. M1-26: posntal months 1-26. The oldest 3 groups are described in terms of months for ease of comparison.

Group	n	Age	Sex	Resolution (cubic voxels)
P1	12	1 day	Male	9 µm
P7	12	7 days	Male	12 µm
P14	12	14 days	Male	12 µm
M1	12	28 days	Male	12 µm
M2	12	48 days	Male	12 µm
M26	26	26 months	Male	13 µm

3.2.2 Endocast segmentation and centrelines

For the analyses described in this chapter, it was necessary to calculate a line along the centre of each canal, which represents the streamline of the canal. This starts at the ampullated side and ends at the point where the canal meets the vestibule or the common crus. The centrelines described here are calculated as described in chapter 2. In short, each bony labyrinth was segmented, and the lines calculated using the *Distance-ordered thinner* and *Trace lines* modules in Amira [28].

3.2.3 Geometric morphometric analysis

Canal shape was investigated using a geometric morphometric (GMM) analysis using a landmark-based approach [29] to compare the form of the semicircular canals. For this process, a total of 37 landmarks (7 fixed and 30 sliding semi-landmarks) were used as described in the previous chapter (see subsection 1.5.1). All the landmarks were placed on the centrelines. The regular landmarks were placed using the Landmark module in Amira, and the sliding semi landmarks were set by down sampling the centrelines to 10 equidistant points, using the *digit.curves()* function in the Geomorph package [30]. The GMM analysis was carried out in R [31], using the Geomorph package.

Intra-observer error

One specimen from each group was selected at random for repeated landmarking. The procedure was as follows: one specimen was landmarked at a time and would not be repeated until all the selected specimens were landmarked. One day was allowed to pass between each repeated landmarking. These repeated sets of landmarks were then aligned using a generalised Procrustes superimposition, and the resulting con-

figurations were visualised using principal components analysis (PCA). A Procrustes ANOVA was then performed [32] using the individuals and the repeat number as predictors. The results were used to calculate an intraclass correlation coefficient, which was then converted into a repeatability measure [33]. The repeatability of the landmarking was 98.08%.

Configuration shape and size

The configuration size was assessed using centroid size, which is the square root of the sum of the squared distances between each landmark and the centroid (centre of the configuration) [34]. The means for each group were compared using ANOVA and pairwise t tests. PCA was used to visualise the shape variables across morphospace. A Procrustes ANOVA was performed to assess the influence of size. The residuals were then added to the overall sample mean, and used as allometry-free shape variables. We used Procrustes distance to the overall mean and to the group mean to assess the shape distribution across morphospace and the variation within each group, respectively. This is calculated as the square root of the sum of the squared distances between corresponding Procrustes-aligned points.

3.2.4 Canal cross-sections and lengths

For the cross-sections and length measurements, the procedure was identical to that described in chapter 2. In short, the centrelines were used to align perpendicular planes for the *slice* module in Amira. The extracted images were then imported to ImageJ (1.53a v NIH, USA) where we used the Shape Descriptors to measure area (in pixels) and aspect ratio. The latter was calculated as

$$\frac{\text{Major axis}}{\text{Minor axis}}$$

such that 1 represents a circle and values increase from 1 the more elongated the shape. The area was calculated in millimetres by multiplying the squared pixel size by the number of pixels calculated by ImageJ. The lengths of the canals were calculated by adding the Euclidean distances between each point in the centreline. For all three measurements, we used ANOVA and pairwise t tests in R to compare means between all six groups.

3.2.5 Contrasted / non-contrasted comparisons

For all the analyses mentioned above, it was necessary to determine whether any potential significant differences that appeared between the ossified and non-ossified groups were due to differences in the scanning (contrast versus no contrast). For this purpose, all above analyses were repeated for the P14 group using both the contrasted and non-contrasted scans, and they were compared against each other using t tests.

3.2.6 Pixel value normalisation

To visualise the ossification of the bony labyrinth, the non-contrasted scans of one specimen from each group were standardised. This was done in ImageJ (Version 1.53e, NIH) using the *Enhance contrast* module in the *Process* menu with the following parameters: Saturated pixels: 0.3%,"Normalise","Process all slices", and "use stack histogram". This allowed for visual comparison of the level of ossification of the canals. No statistical analyses were applied to this process.

3.3 Results

3.3.1 Ossification

At day 1 post-partum, there was no bone deposition around the canals, although there was some deposition in other areas of the petrous temporal bone (Figure 3.1). At 7 days, there was a thin layer of bone that completely surrounds all three canals, including the common crus, although the limits between the slender portion of the posterior and lateral canals were not fully delimited, with both canals appearing to share a common lumen at that point. Over the next seven days, this layer of bone thickened and became denser and the process continued centrifugally until 28 days (M1). No differences were observed in the following months.

3.3.2 Methodological comparisons and intra-observer repeatability

In the geometric morphometric analysis, it was found that the contrast enhanced (P14-c) and standard datasets overlapped on all principal components. The results for the first 6 components are shown on Figure 3.2. There were no differences of length (Figure 3.3) for the anterior ($p = 0.827$), posterior ($p = 0.231$) or lateral

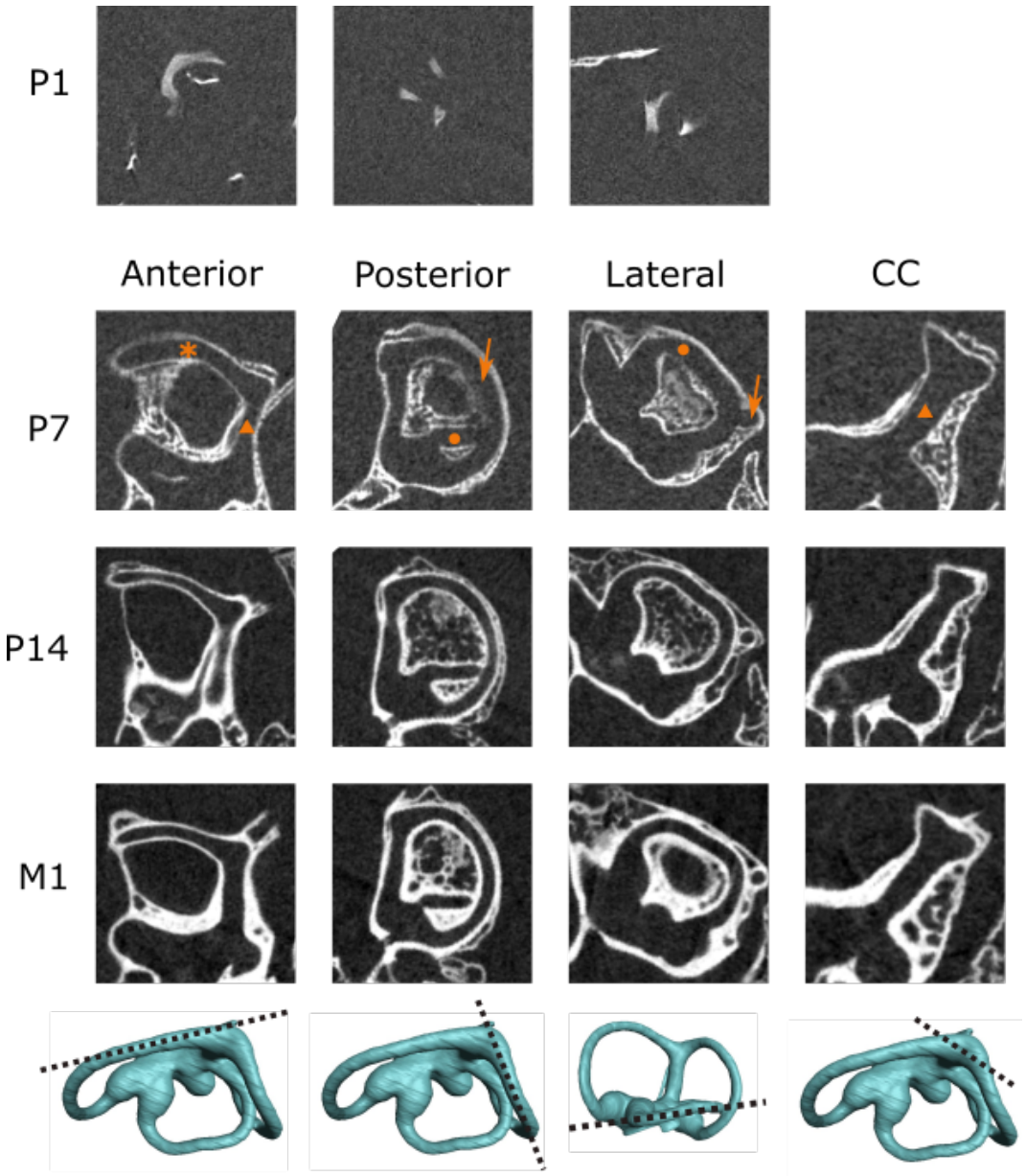

Figure 3.1: Image sections of non-contrasted scans showing the anterior, posterior, and lateral canals, as well as the common crus. CT histograms have been normalized across age groups. In the P1 sections, the plane is approximated to match the planes of the others. CC: Common crus. Bottom row: planes of sectioning for each column. Anterior canal is marked with a star, posterior canal with an arrow, lateral canal with a circle, and common crus with a triangle.

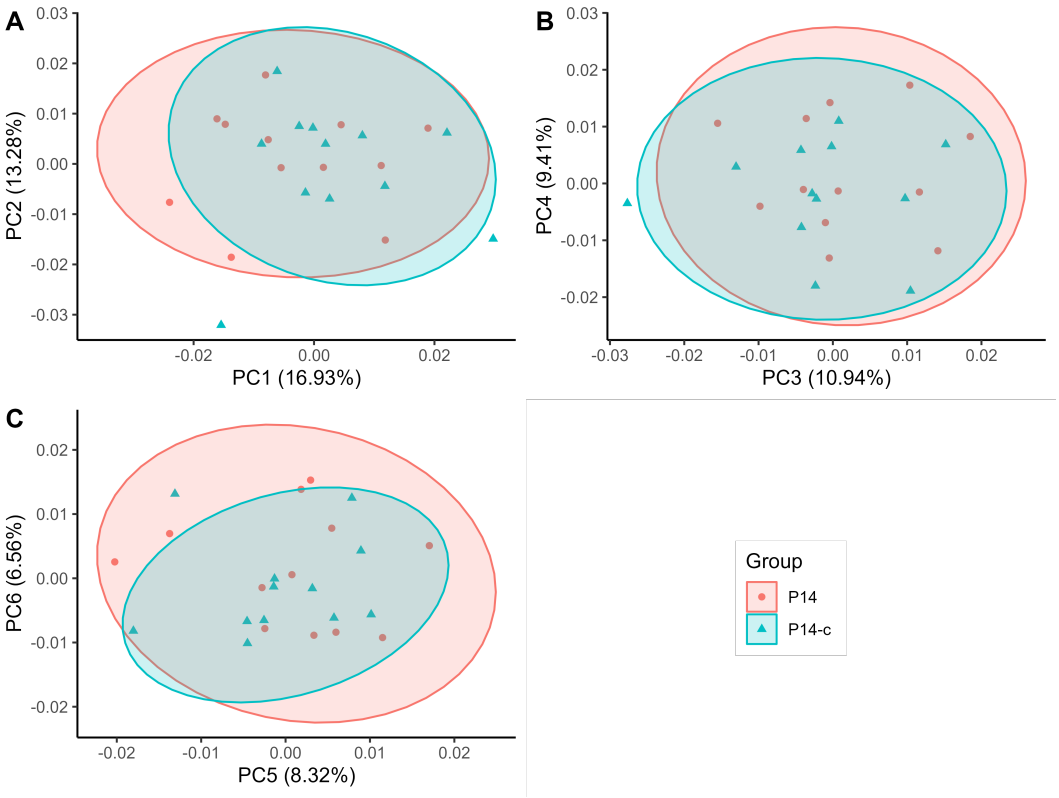

Figure 3.2: PC1-6 for the contrasted versus regular scans. A: PC1 versus PC2, B: PC3 versus PC4, C: PC5 versus PC6. Notice both groups overlap on all depicted PCs.

canal (p = 0.671). Similarly, in terms of cross-sectional area, there were no statistically significant differences across the length of all three canals, except for a few bins in the slender portion of the anterior canal (Figure 3.4). The aspect ratio (Figure 3.5), however, showed statistically significant differences along large sections of the slender portion of all three canals, although more pronounced in the lateral canal. Additionally, it seems that contrasted scans have a much higher variation in aspect ratio when compared to the non-contrasted scans. Upon inspection, it seems that the surface of the contrasted endocasts have a much rougher or uneven surface when compared to the smoother non-contrasted scans (Figure 3.6).

3.3.3 Configuration shape analysis

The first 18 components encompassed 95% of the variation in the overall sample. The first principal component represented 64% of the overall variance; the second

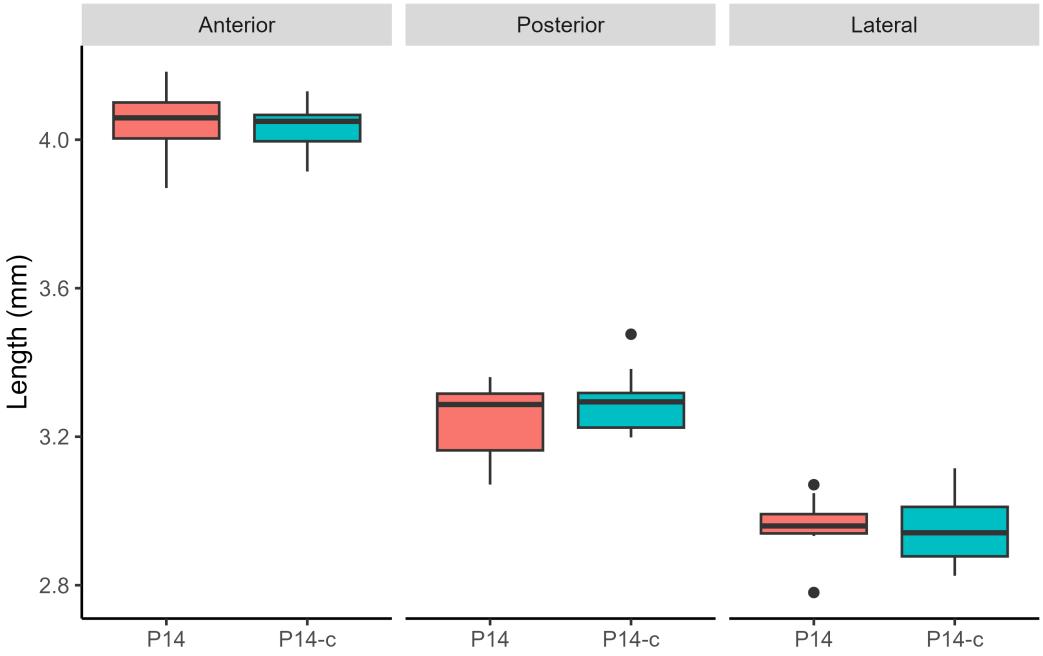

Figure 3.3: Length in mm for the contrasted versus regular scan. No differences were found between groups for any of the three canals.

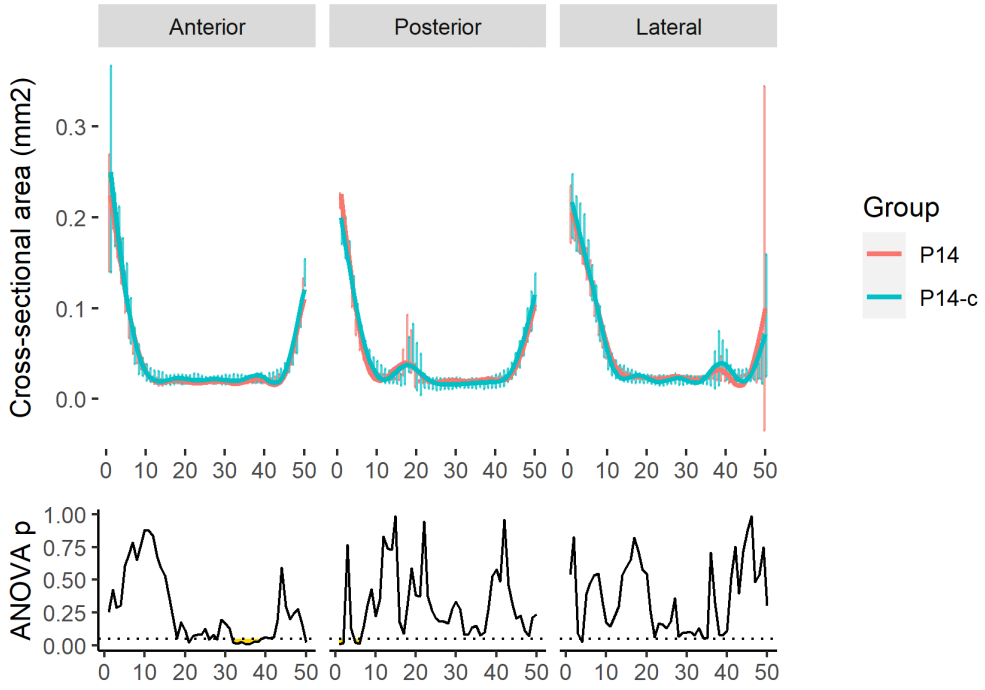

Figure 3.4: Cross-section area comparison between contrasted and non-contrasted scans. Above: average area by group. Below: ANOVA p values. Areas highlighted in yellow are statistically significant ($p < 0.05$).

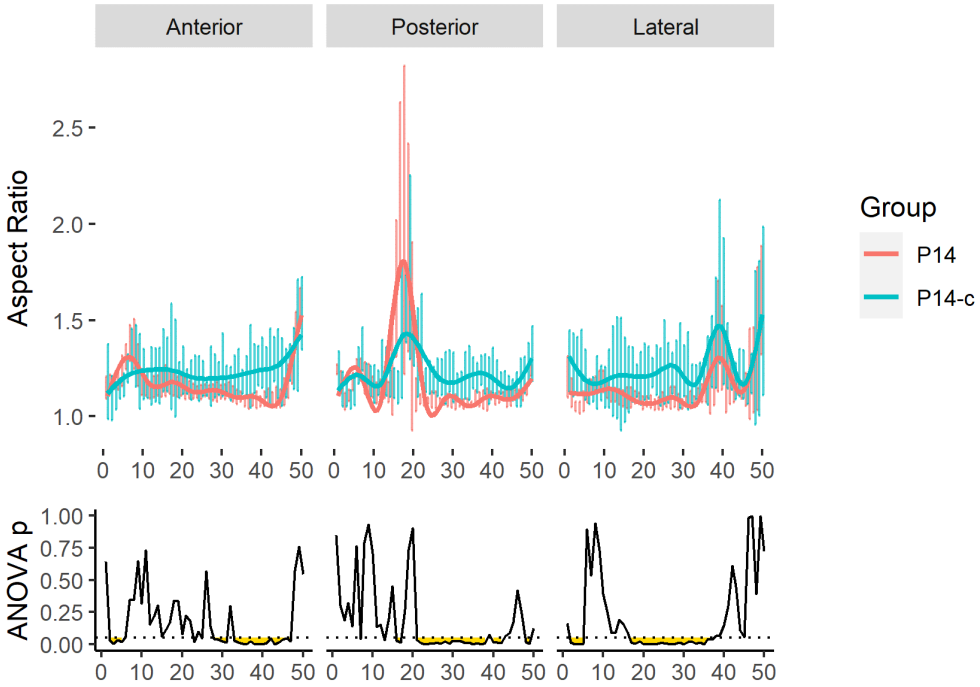

Figure 3.5: Cross-section aspect ratio of contrasted versus non contrasted P14 specimens. Above: average aspect ratio by group. Below: ANOVA p values. Areas highlighted in yellow are statistically significant ($p < 0.05$).

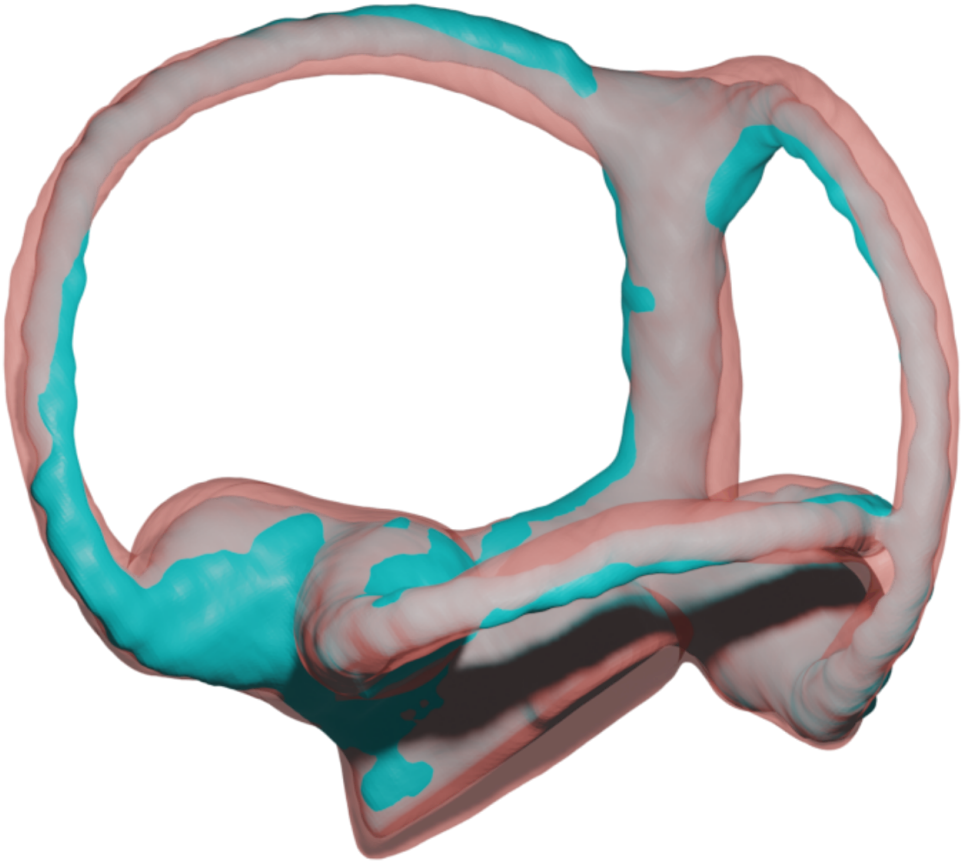

Figure 3.6: Superimposed meshes of the endocasts of the same P14 specimen. The endocast derieved from the contrast-enhanced scan is depicted in solid blue. In transparend red is the endocast for the non-contrasted scan.

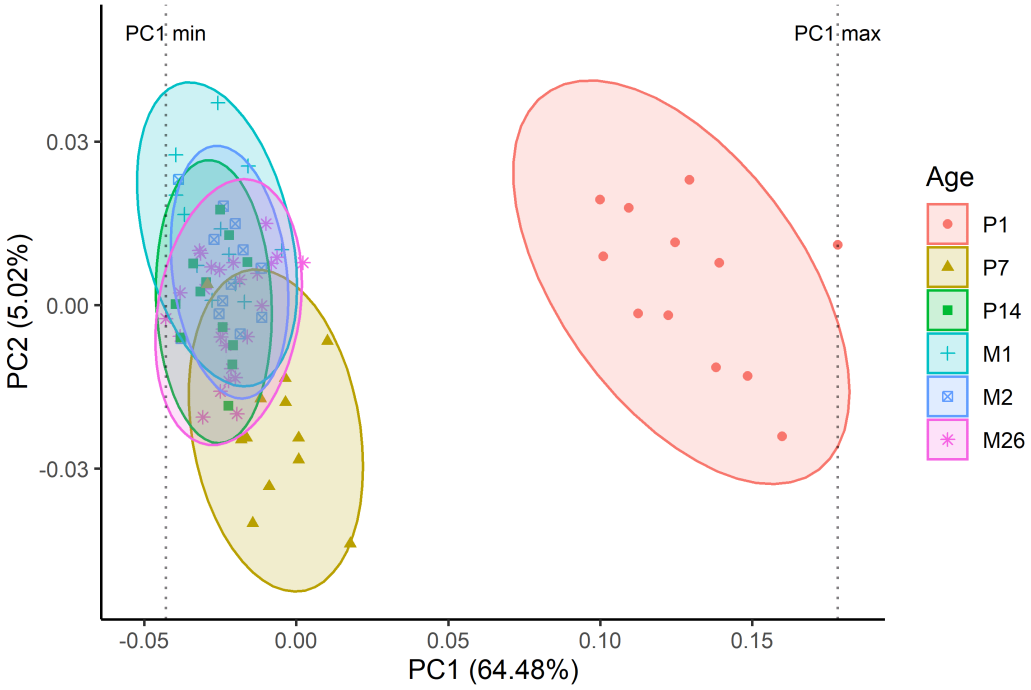

Figure 3.7: PC 1 and 2. The ellipses show the 95% confidence interval (CI). Vertical lines show PC1 maximum (max) and minimum (min) values. Notice all groups overlap on PC1 except the P1 group. Most specimens overlap along PC2, with the exception of some of the P7 group.

component represented only 5%. Along PC1 (Figure 3.7), the P1 group is separate from the others, whereas the rest of the groups overlap each other. To visualise the shape changes across PC1, meshes were warped to the PC1 max (0.178) and PC1 min (-0.0429) values (Figure 3.8). These changes are most evident on the anterior canal, which has a very elliptical, flat shape on PC1 max. In PC1 max, which most closely resembles the shape of the average P1 specimen, the anterior canal forms almost a right angle with the common crus, whereas the shape of PC1 min (closer to the rest of the specimens) it describes a more rounded circuit. Similar changes appear on the posterior and lateral canals, where PC1 max canals describe sharper angles and flatter canals. Additionally, out of plane deviations are more marked on the PC1 min shape, where the anterior canal is much more medially angled on the superior portion. In looking at the rest of the principal components, there was no separation of the groups across any of them.

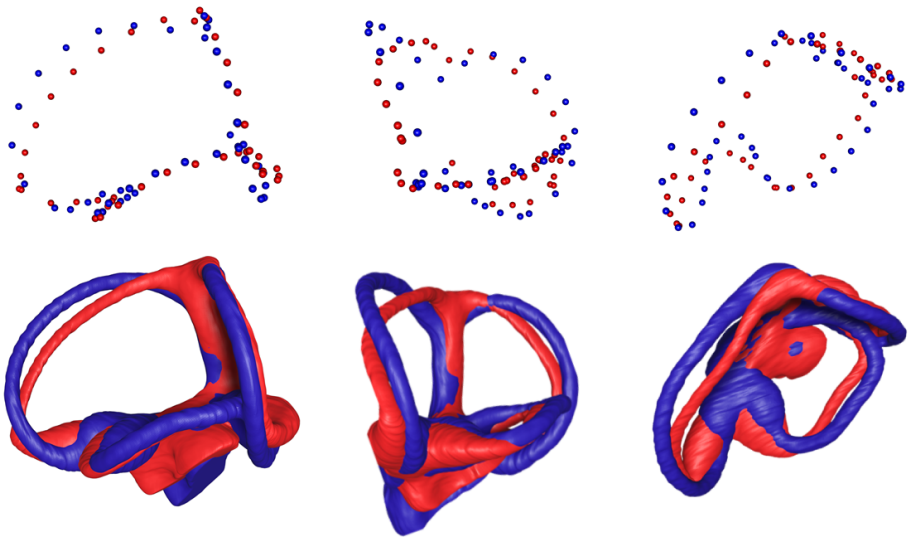

Figure 3.8: PC1 shape changes. PC1 max represented in red, PC1 min represented in blue. Above, the landmark configuration. Below, average mesh warped to the landmark configuration.

Table 3.2: Centroid size pairwise t test p values

	P1	P7	P14	M1	M2
P7	<0.0001	-	-	-	-
P14	<0.0001	<0.0001	-	-	-
M1	<0.0001	<0.0001	0.0310981	-	-
M2	<0.0001	<0.0001	0.6841995	0.1318133	-
M26	<0.0001	<0.0001	0.0919844	0.6841995	0.352066

Centroid size

An ANOVA showed that centroid size mean was significantly different between groups (Figure 3.9). The p values from the pairwise t tests are detailed on Table 3.2. Overall, P1 and P7 were significantly smaller when compared to the rest of the groups. The biggest growth was between P1 and P7 where the shape configuration nearly doubles in size. There is still some statistically significant growth between P7 and P14, although it only accounts for a 11% growth.

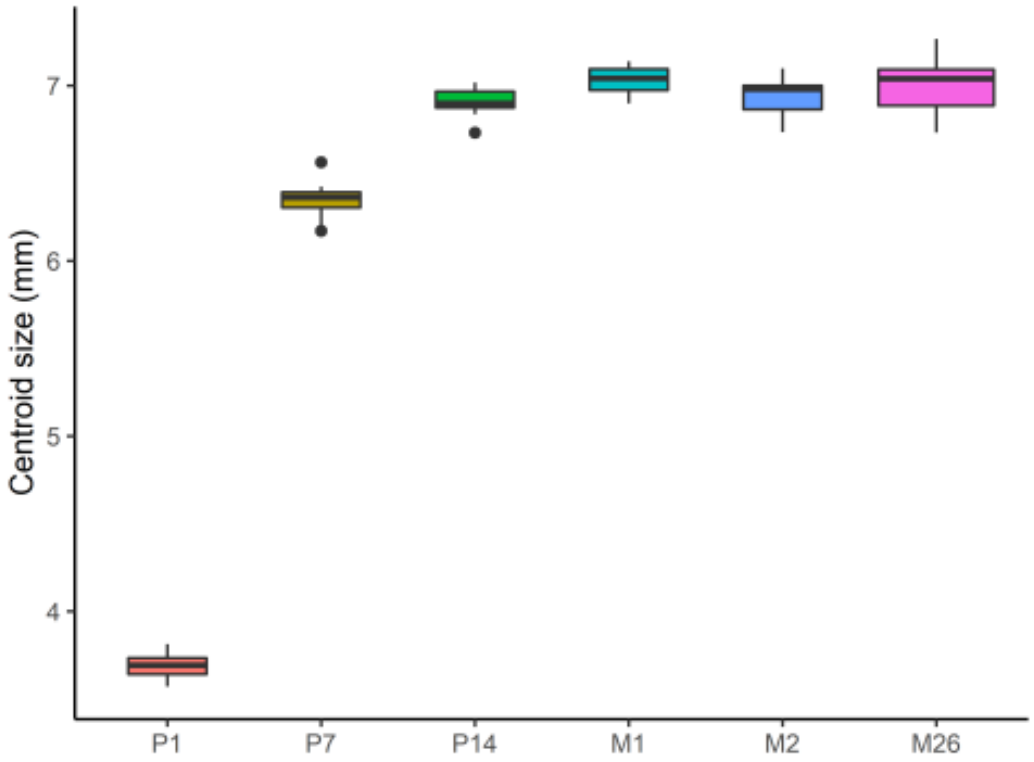

Figure 3.9: Centroid size (in mm) by age group. The greatest differences were found between the P1 group and the rest of the groups. There were significant but smaller differences between P7 and The other groups.

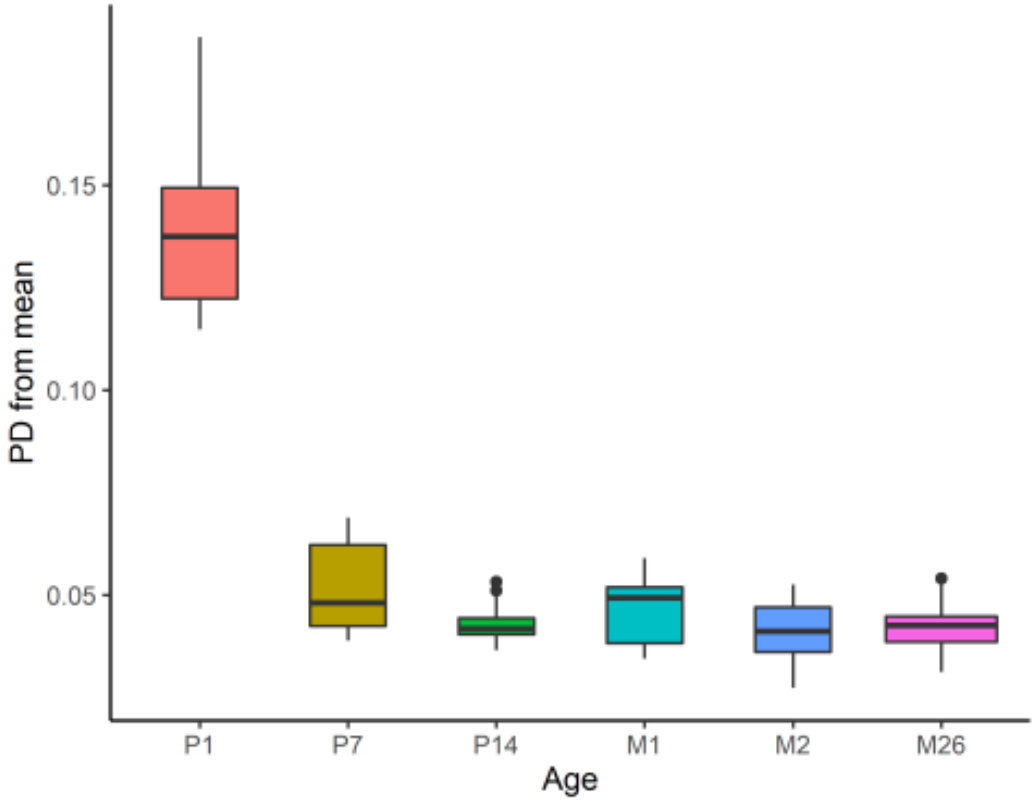

Figure 3.10: Procrustes distance to overall mean by age group. No significant differences except with P1 when compared to the rest of the groups.

Procrustes distance

The Procrustes distance was calculated to the overall sample mean (Figure 3.10). The P1 group had the highest Procrustes distance, followed by the P7. An ANOVA showed a statistically significant difference ($p < 0.001$) between groups, and pairwise t tests (Table 3.3) corroborate that P1 is statistically different from all other groups, but there are no differences between the rest. The same procedure was calculated for the Procrustes distance to the group mean (Figure 3.11). The ANOVA showed statistically significant differences between groups. The p values from the pairwise t test are detailed in Table 3.4. In this instance, the P7 group was also found to be significantly different from all other groups.

Table 3.3: Procrustes distance to overall mean: t test p values.

	P1	P7	P14	M1	M2
P7	<0.0001	-	-	-	-
P14	<0.0001	0.6679756	-	-	-
M1	<0.0001	1.0000000	1.0000000	-	-
M2	<0.0001	0.2198732	1.0000000	1.0000000	-
M26	<0.0001	0.2224048	1.0000000	1.0000000	1.0000000

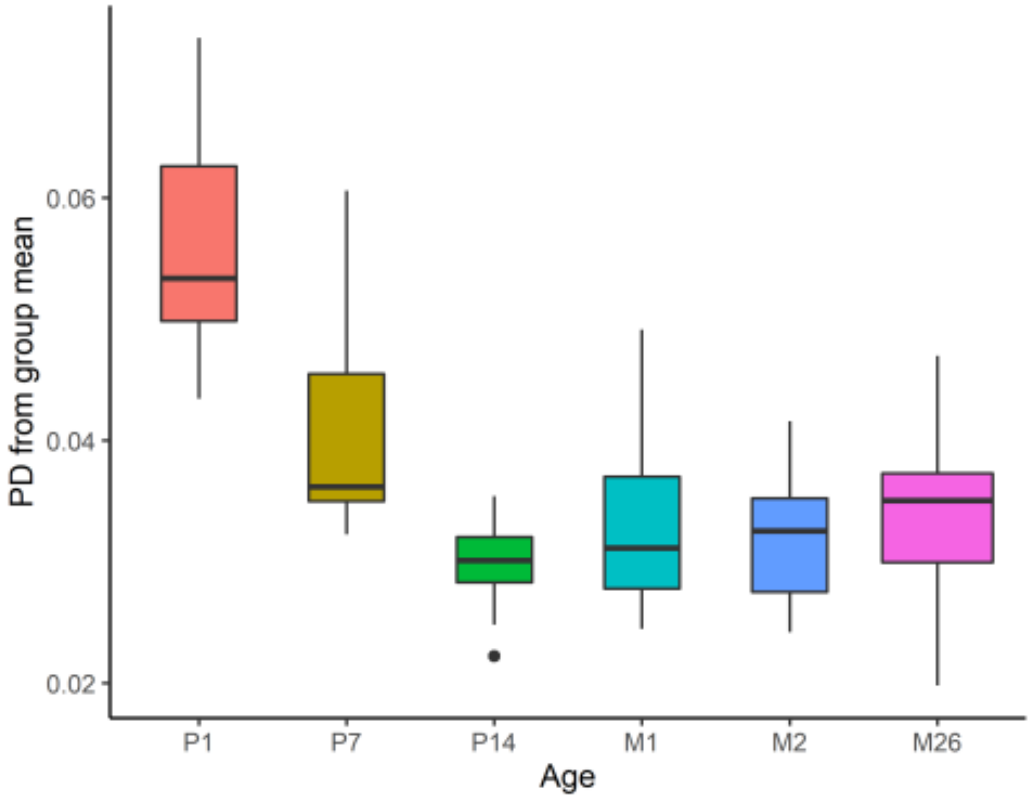

Figure 3.11: Procrustes distance to the group mean by age group. Significant differences were found between P1 and all other groups and between P7 and some groups (see Table 3.4)

Table 3.4: Procrustes distance to group mean: t test p values.

	P1	P7	P14	M1	M2
P7	0.0000138	-	-	-	-
P14	0.0000000	0.0015315	-	-	-
M1	0.0000000	0.0511380	1.0000000	-	-
M2	0.0000000	0.0175909	1.0000000	1.0000000	-
M26	0.0000000	0.0511380	0.4083283	1.0000000	1.0000000

Allometry

A Procrustes ANOVA showed that the allometric component was statistically significant ($p = 0.001$) and it accounted for 61.21% of the overall shape variation. Age was also a significant model effect ($p = 0.001$), but only accounted for 6.94% of the variation. Comparison between the common allometry and unique allometry models ($p = 0.06$) indicated that there is a common allometric component between all groups. The allometry corrected shapes were subjected to PCA. There was overlap of all groups along PC1, which accounted for 14.33% of the total variation (Figure 3.12). On PC2, however, it appears as if the P7 group is somewhat separated from the rest of the sample, although major overlap between the groups persists. No separation was seen in the rest of the principal components. Shape variation along PC2 appears to be mostly due to slight shortening of the canals, with no other major shape differences described. Nonetheless, after correction, age is still a significant effect, explaining 15.84% of the variation ($p=0.001$).

3.3.4 Canal length and cross-sections

Length

The P1 group had the shortest lengths across all three canals, followed by P7 (Figure 3.13). ANOVAs were significant in all three canals ($p<0.001$). The anterior canal was the longest across all groups, followed by the posterior and then the lateral canal. It appears that the canals continue to lengthen significantly postnatally. All three canals nearly doubled in size between P1 and P7. There was a smaller, yet statistically significant lengthening of all canals, but especially of the anterior canal. Some other statistically significant differences were found between specific groups (e.g. between P14 and M25 but not M1 or M2 in the lateral canal), but the differences were usually small and do not follow a particular pattern. Overall, the

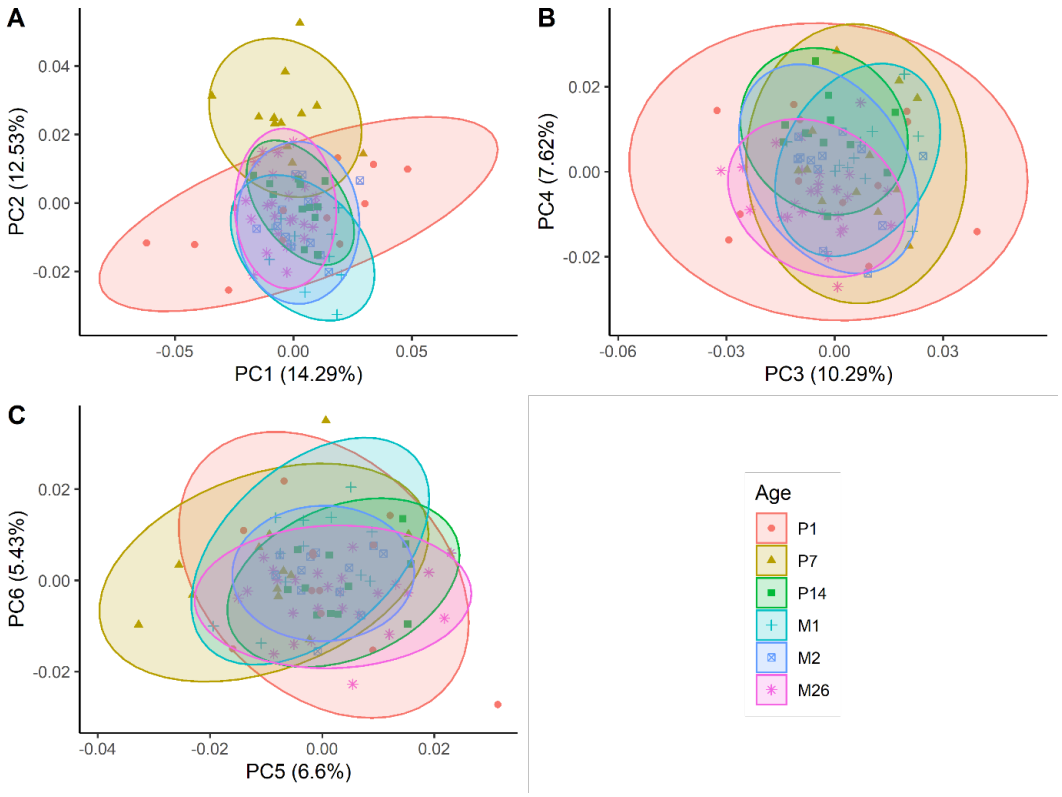

Figure 3.12: PCs 1-6 of allometry-corrected shapes. Notice there is overlap of all groups in all major PCs, with the exception of some of the P7 along PC2.

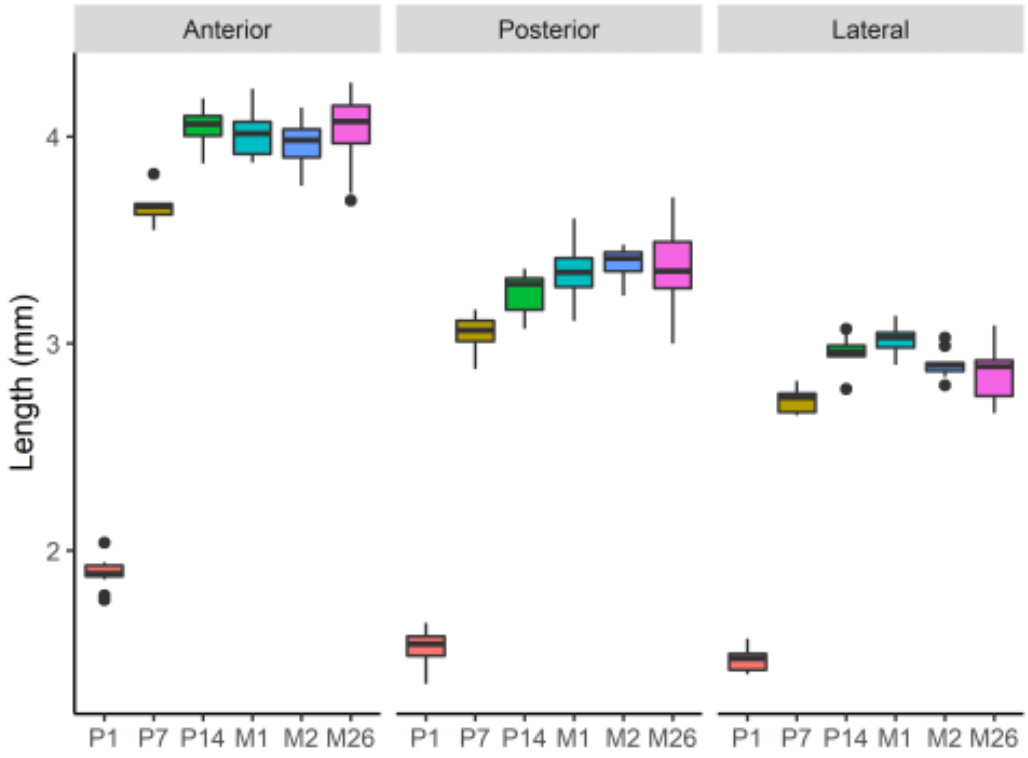

Figure 3.13: Canal length (mm) by age group per canal. Largest differences observed between P1 and all other groups, across all three canals.

trend was very similar across all groups and all three canals.

Cross-sectional area

The cross-sectional area (CSA) was shown to be significantly different between groups along almost the entirety of all three canals, except for a small region of the posterior canal and the lateral canal (Figure 3.14). The biggest differences are in the posterior canal, at the midpoint of the slender portion, where the P1 group has the highest CSA ($\sim$0.04 mm^2) and P14 and M26 have the smallest (0.02 mm^2). A lot of this difference may be due to the influence of the communicating portion between the posterior and lateral canal, as the difference between these groups diminishes towards the other regions of the slender portion. Additionally, in the anterior canal (where there is no communication with other canals), the difference between the largest (P1) and the smallest (P7 vs. M26) is much less, at around 0.007 mm^2.

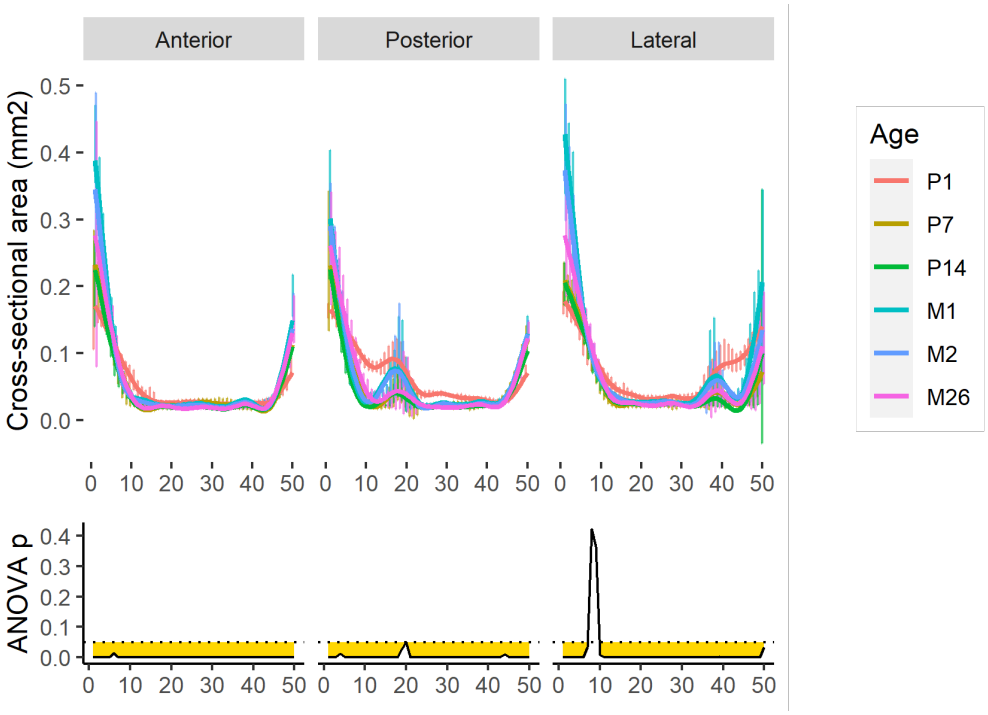

Figure 3.14: Cross-sectional area (mm^2) by canal. Below: ANOVA p values. Regions highlighted in yellow are statistically significant ($p < 0.05$).

There were no differences between the rest of the groups.

Aspect ratio

The cross-section aspect ratio of the canal was found to be significantly different between groups (ANOVA p <0.05) (Figure 3.15). P1 and P7 had the highest aspect ratio across all three canals, at around 1.3 for the lateral canal. All other four groups had very similar aspect ratios, around 1.12. The aspect ratio followed a somewhat similar pattern across the canals, with the highest values at the ends where the canals meet the vestibule. There were significant increases in aspect ratio of the posterior and lateral canal, which coincide with the section of the canals where the lumen is continuous between the two. Upon visual inspection, the shape of the canals at that portion is mostly rounded, and the bony lumens merge to form a figure of eight shaped cross section.

In summary, findings show that as reported before, the murine labyrinth becomes encased in a thin layer of bone between days 1 and 7. It is during this period that the canals grow substantially, and the biggest change in postnatal configuration shape

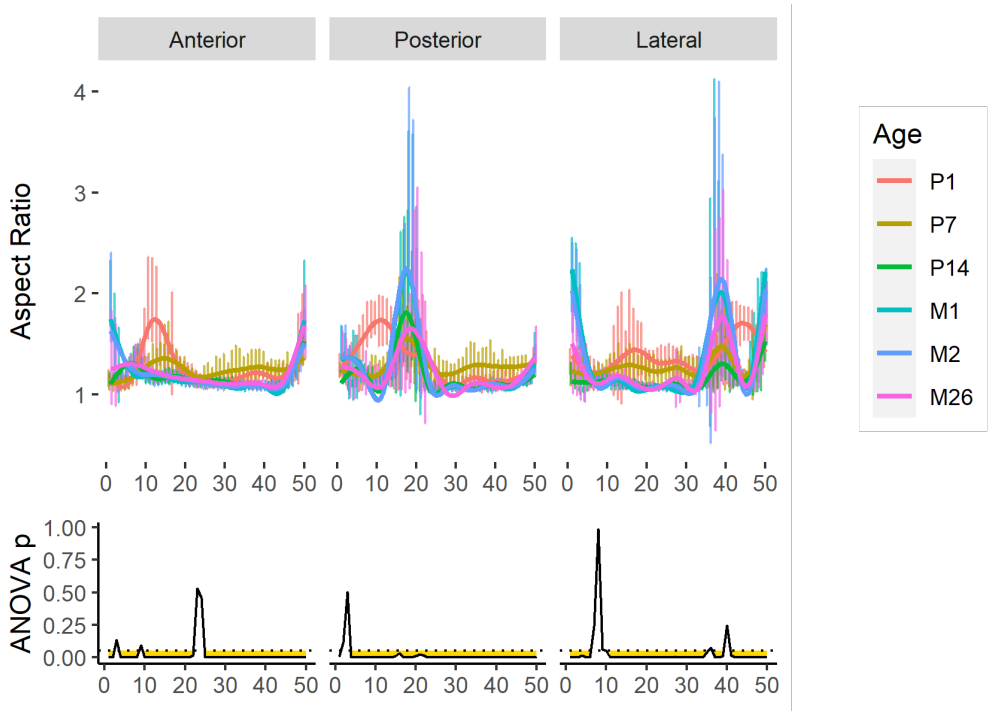

Figure 3.15: Cross-section aspect ratio by canal. Below: ANOVA p values. Regions highlighted in yellow are statistically significant ($p < 0.05$).

occurs. In support of the hypothesis, the growth and shape changed plateaued after this period, concurrently with the timepoint where there is a thin layer of bone around all three canals. Nonetheless, there was a small increase in size in the next seven days (P7 to P14), at which point the bone continued to thicken. There was no significant changes of shape or size after this time point. There was no evidence of change in the cross-sectional area or aspect ratio, suggesting these characteristics attain maturity even sooner, although the mixed imaging strategy might have obscured some changes at a smaller scale.

3.4 Discussion

Substantial growth occurred during the first seven days (P1 to P7), This was reflected both in the length of each individual canal, as well as increase in centroid size when assessing the configuration shape. At the first time point (P1) the anterior canal was found to be the longest, followed by the posterior and the lateral canals. This is consistent with the trend displayed by most mammals [35]. For the next time point, there was still a statistically significant increase in length, although not as large as the one observed between P1 and P7. This was true of all three canals. Interestingly, this secondary lengthening occurred after there was already a layer of bone around all three canals, suggesting that there may still be some small refinements to canal morphology. As the canals continued to ossify, that is the bone layer became thicker, no changes in length were observed. The relative length of the canals to each other remained the same through all time-points, with the anterior canal being the longest and the lateral the smallest. The geometric morphometric analysis told a similar story. Centroid size measures the size of the entire configuration, so assessment of individual canal growth was not possible with this approach. The centroid size showed the largest increase between P1 and P7, and in similar fashion to the length, there was a small but statistically significant increase in centroid size between P7 and P14, which corroborates the previous finding. When assessing size and growth, the length of the canals does not provide any information on the canal shape, namely the ellipticity or deviation of circularity. The centroid size, on the other hand, is more influenced by the shape of the canals, namely planarity, which can alter the position of the landmarks, the position of the centroid, and consequently the centroid size. Nonetheless, it is evident that centroid size and canal streamline length are intricately related, as the findings for both follow a markedly similar pattern.

Traditionally, the size of the semicircular canals has been measured by the radius of curvature [for example 36–40]. It is evident from this study, however, that the length of the canal streamline (centreline) is invariably related to the radius of curvature. The findings in this study are markedly similar to those reported in regards to radius of curvature, where the anterior canal is the largest, followed by the posterior and the lateral [41], as this is the pattern that was observed by measuring the centreline lengths. Therefore, inferences can be made regarding sensitivity with the findings presented here. Canal size has been shown to be correlated to sensitivity, both in inter- and intra-specific comparisons [39]. Species with relatively longer canals are more agile [38, 42], likely due in part to increased canal sensitivity [43, 44]. Consequently, such a massive increase in size during the first postnatal week is likely to bring about a substantial increase in murine vestibular sensitivity. Mice do not begin locomotion until the second postnatal week [45], however mature locomotion is not achieved until around P23. No detailed studies have been conducted on mouse locomotive behaviour before P7. During this time frame, rats double the percentage of head elevation off the ground, and go from no movement to "pivoting" where they can move around with the pelvis on the floor by pushing off with the forelimbs [46]. The transition from P7 to P14 sees rats go from crawling to walking [46], which is concomitant with the stage of mouse canal maturation (and when all three canals have a complete layer of bone surrounding them) described here. It is likely that the pattern in mice is very similar, and the maturation of gait is simultaneous with semicircular canal maturity.

In terms of shape, there was a significant change of the shape of the canals, as assessed by geometric morphometrics, when comparing P1 to the rest of the groups. The changes were similar across all three canals, but are more easily observed in the anterior canal. The main difference was that P1 canal shape was markedly elliptical, whereas the rest of the age groups showed a more rounded streamline. Note that in the changes illustrated above, the extreme values of PC1, which more or less correspond with the P1 group (PC1max) and the rest of the groups (PC1min). Nonetheless, these shapes are somewhat exaggerated by the fact that the mesh used to represent the figures is the endocast of the mean specimen of the sample, which is a P14. The actual shape of the P1 group (Figure 3.16) is very similar to PC1 max Figure 3.8, with the caveat that the angle between the ampulla and the slender portion is not as sharp as the one depicted for PC1 max Figure 3.8.

Oman *et al.* [43] established that the mechanical sensitivity of the cupula varies directly with the ratio of the area enclosed by the canal streamline to the streamline

Figure 3.16: Mean specimen from each group. Above, from left to right: P1, P7 and P14. Below, from left to right: M1, M2, M26. Specimens are depicted to scale. The greatest shape differences were observed between P1 and the other groups.

length. Considering that, a more elliptical shape for the same perimeter would decrease sensitivity [47], in which case rounder canals would be favoured. Nonetheless, previous research has shown that in squamates, higher ellipticity is correlated with size constraints in the skull, so that species with less dorso-ventral skull space will favour it over circularity, as it allows for larger, and particularly longer canals [48]. This would be beneficial for stages where the petrous bone has not reached mature size. In a study conducted in mice, it appears that the petrous bone does not grow during the first postnatal week [49], although it must be noted that these measurements were taken on microCT scans, so only the ossified portions of the bone could be measured. It is possible that there is rapid cartilaginous growth during this period, and when adequate size has been achieved, bone deposition rapidly increases. At this point (∼P7), as stated in the results of this study, the semicircular canals have also begun ossification, and have in fact attain a thin layer of bone around virtually of the lumen. It is possible that this level of bone deposition does not restrict further growth, rather that ossification only begins when maturity of the structure is achieved. Endochondral ossification, like that of the petrous bone, involves induction of mature osteoblasts by the Indian Hedgehog (*Ihh*) pathway [50]. In the mouse basioccipital bone, *Ihh* begins expression as early as E12, and it continues un-

til the postnatal stages. Whether the basioccipital undergoes cartilaginous growth after this stage is unclear, as studies have relied on microCT imaging for measuring postnatal growth [51]. Timing of expression in the otic capsule, however, is not known. Nonetheless, favouring ellipticity to increase length does not appear to the norm for mammals, where there is no correlation between skull size and ellipticity of the canals [42]. It is relevant to note that this is true of mammalian canals that have reached shape maturity and it may well be the case that during developmental stages mammals exhibit a much more elliptic shape, prioritising growth in other areas of the skull, or even of the brain and specifically the temporal lobe or the petrosal lobule of the parafloculus [52], over that of the petrous bone. Although it is more likely that this would have a bigger impact on the rotation and orientation of the canals, which were not measured for this study. Nonetheless, it is unlikely, based on the GMM results, that mice exhibit any significant changes in terms of angles between ipsilateral canals. Any such changes would have been evident even after Procrustes superimposition, as landmarks within a single configuration are only allowed to change in unison (ratio of distribution between landmarks is maintained). The changes observed here are mostly accounted by size and out-of-plane deviations. However, there is still possibility for the labyrinth to rotate within the skull, as these rotations are eliminated during superimposition.

Additionally, there were increased out-of-plane deviations when comparing the P1 group to the rest of the sample. These deviations were particularly evident in the anterior canal, where in the P7 onwards the superior portion (closer to the common crus) moves antero-medially, and the anterior-most portion (closer to the ampulla) is positioned more laterally. In comparison, the P1 anterior canal is not as curved, projecting more laterally from the superior portion and describing a flatter trajectory towards the ampulla. It is possible that just like with the increase of circularity, these deviations also increases sensitivity of the canals by expanding the range of planes that may stimulate endolymphatic flow and therefore elicit a response [53, 54]. In two similarly sized canals, out of plane deviations would also increase the streamline length of the canals, which would therefore increase sensitivity as explained above. However, the potential for sensitivity increase described here is purely due to the increased range of planes that can elicit responses, and the potential lengthening due to this curvature is negligible when compared to the length increases described before.

When assessing cross-sectional shape, the picture was less clear. The cross-sectional area, for one, seems to be similar throughout all timepoints studied. No

major differences between the groups, aside from a few bins, although the pattern seems to imply stable area. Decreases in the cross-sectional area of the canals increase the viscous damping which in turn extends the range of frequencies that can be detected [55]. It appears then that cross-sectional area maturity is achieved *in utero*, and does not change throughout life. This is before they attain overall canal shape and at least a week before bone deposition around the canals begins. It is possible then that any further optimisation that can be achieved through changes to the lumen area are minimal, and that other morphological adjustments are favoured. For the aspect ratio, the results were not as clear. Whilst an ANOVA showed statistically significant differences, these appear to be driven by the P1 and P7 groups, whereas the rest of the groups were extremely similar to each other. The differences, however, were small, and overall the cross-sectional shape was mostly rounded. Most likely, the differences found were driven by the differences in imaging, given that the P1 and P7 groups included in the cross-sectional analysis were contrast-enhanced.

When the contrasted versus non-contrasted scans were compared in terms of aspect ratio it became apparent that the inclusion of the contrasting technique significantly alters the surface of the canals after segmentation Figure 3.6. The contrast-enhanced images make soft tissues visible, meaning that there is a possibility that the periosteum in the P14 specimens has been highlighted, making it impossible to differentiate from the bone, thus explaining some of the differences seen in Figure 3.6. Notably, the cross-sectional area was not as sensitive to the technique, although some of the differences seen in some select regions are likely due to the imaging. In contrast, the configuration shape did not show any differences. This is probably due to the fact that it is based on the centreline of the canal, which is more impervious to small changes in the surface [56], especially when compared with the cross-section form metrics, which are heavily dependent on the surface of the canals. Iodine-contrasted scans are helpful for visualising the non-ossified canals, and centreline-based geometric morphometrics proves robust enough for adequate statistical comparison. Nonetheless, metrics such as convexity which rely heavily on the perimeter of the shape (in this case the walls of the bony canals), should be interpreted carefully, as the periosteum may be highlighted leading to inaccurate results.

Whilst there is some bone deposition in the petrous temporal bone (see Figure 3.1, P1), there is no deposition directly around the semicircular canals. By the next time-point, P7, the canals appeared to be fully lined by bone, although there was only a very thin layer, and there seem to be small gaps in certain areas, partic-

ularly where the posterior and lateral canals meet. It seems that M1 is the point where the layer of bone is the thickest, indicating there may still be mineralisation of the surrounding areas up until this point. Other rodents, namely hamsters, also ossify postnatally [6], although it is unclear at which point the otic capsule is fully ossified, and whether there are any postnatal changes to canal form. Notably, the configuration shape studied here attained adult morphology at P7, which would be consistent with the notion that the adult shape is attained at the point of complete ossification. No meaningful changes of shape were observed afterwards, including in the elderly 26M specimens.

In terms of size, there is a small but statistically significant lengthening of all three canals between P7 and P14, indicating that growth is still possible after the first thin layer of bone surrounds the labyrinth. It may be that the differences we observed are due to inaccurate trimming of the centrelines. Consistency with the increase in centroid size somewhat reassures that this is not the case, although as mentioned before, having placed landmarks on the centreline, centroid size in invariably overwhelmed by the length of the centrelines.

Skull maturity in mice, both in terms of shape and size, is not attained until around 60 days postnatally [51]. Mice are altricial animals and do not open their eyes until around postnatal days 11-13, and only begin locomotion around day 14 onwards [27]. Therefore, there may be no need for a fully developed bony labyrinth at the time of birth, and the timing of attainment of a complete layer of bone around the canals correlates well with the timing of eye opening and the point at which adult shape is attained. Humans, which are also altricial, are born with fully developed and ossified canals [1] and there does not seem to be any correlation with the beginning of locomotion. Whether this pattern is the norm for most altricial animals, rodents, or due to other characteristic remains unknown.

References

1. Jeffery, N. & Spoor, F. Prenatal Growth and Development of the Modern Human Labyrinth. *Journal of anatomy* **204,** 71–92. ISSN: 0021-8782 0021-8782. pmid: 15032915 (2004).

2. Zubler, J. M. *et al.* Evidence-Informed Milestones for Developmental Surveillance Tools. *Pediatrics* **149,** e2021052138. ISSN: 0031-4005 (2022).

3. Ornitz, E. M., Kaplan, A. R. & Westlake, J. R. Development of the Vestibulo-ocular Reflex from Infancy to Adulthood. *Acta Oto-Laryngologica* **100,** 180–193. ISSN: 0001-6489, 1651-2251 (1985).

4. Hodges, P. C. Ossification in the Fetal Pig. A Radiographic Study. *The Anatomical Record* **116,** 315–325. ISSN: 0003-276X, 1097-0185 (1953).

5. Hautier, L., Stansfield, F. J., Allen, W. R. T. & Asher, R. J. Skeletal Development in the African Elephant and Ossification Timing in Placental Mammals. *Proceedings of the Royal Society B: Biological Sciences* **279,** 2188–2195 (2012).

6. Van Arsdel III, W. C. The Ossification of the Middle and Internal Ear of the Golden Hamster (Cricetus Auratus) (1951).

7. Sølvsten Sørensen, M., Balslev Jørgensen, M. & Bretlau, P. Drift Barriers in the Postcartilaginous Development of the Mammalian Otic Capsule. *European Archives of Oto-Rhino-Laryngology* **249.** ISSN: 0937-4477, 1434-4726 (1992).

8. Clark, C. T. & Smith, K. K. Cranial Osteogenesis in Monodelphis Domestica (Didelphidae) and Macropus Eugenii (Macropodidae). *Journal of Morphology* **215,** 119–149. ISSN: 1097-4687 (1993).

9. Bryant, J.-P. *et al.* Multimodal Atlas of the Murine Inner Ear: From Embryo to Adult. *Frontiers in Neurology* **12,** 1204. ISSN: 1664-2295 (2021).

10. Walker, A., Ryan, T. M., Silcox, M. T., Simons, E. L. & Spoor, F. The Semicircular Canal System and Locomotion: The Case of Extinct Lemuroids and Lorisoids. *Evolutionary Anthropology: Issues, News, and Reviews: Issues, News, and Reviews* **17,** 135–145. ISSN: 1060-1538 (2008).

11. David, R. *et al.* Motion from the Past. A New Method to Infer Vestibular Capacities of Extinct Species. *Comptes Rendus Palevol. Imaging & 3D in Palaeontology and Palaeoanthropology* **9,** 397–410. ISSN: 1631-0683 (2010).

12. Orliac, M. J., Benoit, J. & O'Leary, M. A. The Inner Ear of Diacodexis, the Oldest Artiodactyl Mammal. *Journal of anatomy* **221,** 417–426. ISSN: 1469-7580 0021-8782. pmid: 22938073 (2012).

13. Ryan, T. M. *et al.* Evolution of Locomotion in Anthropoidea: The Semicircular Canal Evidence. *Proceedings of the Royal Society B: Biological Sciences* **279,** 3467–3475 (2012).

14. Bernardi, M. & Couette, S. Eocene Paleoecology of Adapis Parisiensis (Primate, Adapidae): From Inner Ear to Lifestyle. *Anatomical record (Hoboken, N.J. : 2007)* **300,** 1576–1588. ISSN: 1932-8494 1932-8486. pmid: 28452186 (2017).

15. Beaudet, A. The Inner Ear of the Paranthropus Specimen DNH 22 from Drimolen, South Africa. *American journal of physical anthropology.* ISSN: 1096-8644 0002-9483. pmid: 31290572 (2019).

16. Hoyte, D. A. N. The Postnatal Growth of the Ear Capsule in the Rabbit. *American Journal of Anatomy* **108,** 1–16. ISSN: 0002-9106, 1553-0795 (1961).

17. Ekdale, E. G. Ontogenetic Variation in the Bony Labyrinth of Monodelphis Domestica (Mammalia: Marsupialia) Following Ossification of the Inner Ear Cavities. *Anatomical Record (Hoboken, N.J.: 2007)* **293,** 1896–1912. ISSN: 1932-8494. pmid: 20730862 (2010).

18. Costeur, L., Mennecart, B., Müller, B. & Schulz, G. Prenatal Growth Stages Show the Development of the Ruminant Bony Labyrinth and Petrosal Bone. *Journal of Anatomy* **230,** 347–353. ISSN: 1469-7580 (2017).

19. Berlioz, E., Cornette, R., Lenoir, N., Santin, M. D. & Lehmann, T. Exploring the Ontogenetic Development of the Inner Ear in Aardvarks. *Journal of Anatomy* **238.** ISSN: 1469-7580 (2020).

20. Thean, T., Kardjilov, N. & Asher, R. J. Inner Ear Development in Cetaceans. *Journal of anatomy* **230,** 249–261. ISSN: 1469-7580 0021-8782. pmid: 27995620 (2017).

21. Ward, D. L. *et al.* Early Life Malnutrition and Fluctuating Asymmetry in the Rat Bony Labyrinth. *The Anatomical Record* **n/a.** ISSN: 1932-8494 (2021).

22. Osipov, B. *et al.* Sexual Dimorphism of the Bony Labyrinth: A New Age-Independent Method. *American journal of physical anthropology* **151,** 290–301. ISSN: 1096-8644 0002-9483. pmid: 23640711 (2013).

23. Jones, S. M. *et al.* A Comparison of Vestibular and Auditory Phenotypes in Inbred Mouse Strains. *Brain research* **1091,** 40–46. ISSN: 0006-8993. pmid: 16499890 (2006).

24. Hardisty-Hughes, R. E., Parker, A. & Brown, S. D. M. A Hearing and Vestibular Phenotyping Pipeline to Identify Mouse Mutants with Hearing Impairment. *Nature Protocols* **5,** 177–190. ISSN: 1750-2799 (1 2010).

25. Kiernan, A. E. *et al.* ENU Mutagenesis Reveals a Highly Mutable Locus on Mouse Chromosome 4 That Affects Ear Morphogenesis. *Mammalian Genome* **13,** 142–148. ISSN: 0938-8990, 1432-1777 (2002).

26. Hawker, K., Fuchs, H., Angelis, M. H. & Steel, K. P. Two New Mouse Mutants with Vestibular Defects That Map to the Highly Mutable Locus on Chromosome 4 Dos Nuevos Ratones Mutantes Con Defectos Vestibulares Hallados En El Altamente Mutable Locus Del Cromosoma 4. *International Journal of Audiology* **44,** 171–177. ISSN: 1499-2027. pmid: 15916118 (2005).

27. Brust, V., Schindler, P. M. & Lewejohann, L. Lifetime Development of Behavioural Phenotype in the House Mouse (Mus Musculus). *Frontiers in Zoology* **12,** S17. ISSN: 1742-9994 (2015).

28. *Amira* version 6.0.0. Thermo Fisher Scientific.

29. Bookstein, F. L. Biometrics, Biomathematics and the Morphometric Synthesis. *Bulletin of Mathematical Biology* **58,** 313–365. ISSN: 0092-8240, 1522-9602 (1996).

30. Adams, D., Collyer, M. & Kaliontzopoulou, A. Geomorph: Software for Geometric Morphometric Analyses. R Package Version 3.2.1. (2020).

31. R Core Team. *R: A Language and Environment for Statistical Computing* manual (R Foundation for Statistical Computing, Vienna, Austria, 2022).

32. Goodall, C. Procrustes Methods in the Statistical Analysis of Shape. *Journal of the Royal Statistical Society. Series B (Methodological)* **53,** 285–339. JSTOR: 2345744 (1991).

33. Fruciano, C. Measurement Error in Geometric Morphometrics. *Development Genes and Evolution* **226,** 139–158. ISSN: 1432-041X (2016).

34. Klingenberg, C. P. Size, Shape, and Form: Concepts of Allometry in Geometric Morphometrics. *Development Genes and Evolution* **226,** 113–137. ISSN: 1432-041X (2016).

35. Ekdale, E. G. Comparative Anatomy of the Bony Labyrinth (Inner Ear) of Placental Mammals. *PLOS ONE* **8,** e66624. ISSN: 1932-6203 (2013).

36. van Egmond, A. A. J., Groen, J. J. & Jongkees, L. B. W. The Mechanics of the Semicircular Canal. *The Journal of Physiology* **110,** 1–17. ISSN: 0022-3751. pmid: 15406377 (1949).

37. Curthoys, I. S., Blanks, R. H. I. & Markham, C. H. Semicircular Canal Radii of Curvature (R) in Cat, Guinea Pig and Man. *Journal of Morphology* **151,** 1–15. ISSN: 0362-2525 (1977).

38. Spoor, F. *et al.* The Primate Semicircular Canal System and Locomotion. *Proceedings of the National Academy of Sciences* **104,** 10808–10812. ISSN: 0027-8424. pmid: 17576932 (2007).

39. Yang, A. & Hullar, T. E. Relationship of Semicircular Canal Size to Vestibular-Nerve Afferent Sensitivity in Mammals. *Journal of neurophysiology* **98,** 3197–3205. ISSN: 0022-3077 (2007).

40. Welker, K. L., Orkin, J. D. & Ryan, T. M. Analysis of Intraindividual and Intraspecific Variation in Semicircular Canal Dimensions Using High-Resolution x-Ray Computed Tomography. *Journal of Anatomy* **215,** 444–451. ISSN: 1469-7580 (2009).

41. Calabrese, D. R. & Hullar, T. E. Planar Relationships of the Semicircular Canals in Two Strains of Mice. *JARO: Journal of the Association for Research in Otolaryngology* **7,** 151–159. ISSN: 1525-3961. pmid: 16718609 (2006).

42. Cox, P. G. & Jeffery, N. Semicircular Canals and Agility: The Influence of Size and Shape Measures. *Journal of Anatomy* **216,** 37–47. ISSN: 0021-8782 (2010).

43. Oman, C. M., Marcus, E. N. & Curthoys, I. S. The Influence of Semicircular Canal Morphology on Endolymph Flow Dynamics: An Anatomically Descriptive Mathematical Model. *Acta oto-laryngologica* **103,** 1–13. ISSN: 0001-6489 (1987).

44. Rabbitt, R. D., Damiano, E. R. & Grant, J. W. in *The Vestibular System* 153–201 (Springer, 2004).

45. Clarke, K. & Still, J. Development and Consistency of Gait in the Mouse. *Physiology & Behavior* **73,** 159–164. ISSN: 00319384 (2001).

46. Altman, J. & Sudarshan, K. Postnatal Development of Locomotion in the Laboratory Rat. *Animal Behaviour* **23,** 896–920. ISSN: 00033472 (1975).

47. McVean, A. The Semicircular Canals of the Hagfish Myxine Glutinosa. *Journal of Zoology* **224,** 213–222. ISSN: 1469-7998 (1991).

48. Goyens, J. High Ellipticity Reduces Semi-Circular Canal Sensitivity in Squamates Compared to Mammals. *Scientific Reports* **9,** 16428. ISSN: 2045-2322 (1 2019).

49. Varvares, A. M., Mcnulty, M. A., Holmes, M. A. & Deleon, V. B. *Comparative Analysis of the Growth and Development of the TemporalBbone in Mice and Humans* in *AMERICAN JOURNAL OF PHYSICAL ANTHROPOLOGY* **159** (2016), 322–322.

50. Karaplis, A. C. in *Principles of Bone Biology* 53–84 (Elsevier, 2008). ISBN: 978-0-12-373884-4.

51. Maga, A. M. Postnatal Development of the Craniofacial Skeleton in Male C57BL/6J Mice. *Journal of the American Association for Laboratory Animal Science* **55,** 131–136 (2016).

52. Jeffery, N. & Spoor, F. The Primate Subarcuate Fossa and Its Relationship to the Semicircular Canals Part I: Prenatal Growth. *Journal of Human Evolution* **51,** 537–549. ISSN: 00472484 (2006).

53. Tremble, G. E. The Bony Labyrinth Of The New-born Infant And Of The Adult: A Comparative Study. *Archives of Otolaryngology - Head and Neck Surgery* **9,** 175–180. ISSN: 0886-4470 (1929).

54. Muren, C., Ruhn, G. & Wilbrand, H. Anatomic Variations of the Human Semicircular Canals: A Radioanatomic Investigation. *Acta Radiologica. Diagnosis* **27,** 157–163. ISSN: 0567-8056 (1986).

55. Obrist, D. Flow Phenomena in the Inner Ear. *Annual Review of Fluid Mechanics* **51,** 487–510 (2019).

56. Gunz, P., Ramsier, M., Kuhrig, M., Hublin, J.-J. & Spoor, F. The Mammalian Bony Labyrinth Reconsidered, Introducing a Comprehensive Geometric Morphometric Approach. *Journal of anatomy* **220,** 529–543. ISSN: 1469-7580 0021-8782. pmid: 22404255 (2012).

Chapter 4

The bony semiciruclar canals and the perilymphatic space

4.1 Introduction

The semicircular canals are surrounded by a thick layer of bone, the otic capsule. This area inside the petrous temporal bone is incredibly dense. In humans, the 0.2 mm of bone surrounding the semicircular canals are highly mineralised and show a circular course of collagen fibres [1]. Because of the structural organisation of the inner and outer layers and its position within the skull, the bony labyrinth is well preserved in fossil specimens [see for example 2]. However, the position within the skull limits the accessibility to the bony labyrinth for direct measurement, as isolation of the petrous bone would inevitably damage the surrounding tissues. Nonetheless, the use of CT and µCT has allowed for full visualisation of the bony labyrinth without any damage to the specimens. Newer advances to CT technology have increased the quality and resolution at which the specimens can be scanned, and have made the study of bony labyrinth form more precise. Because of this, there has been a rapid increase in the study and understanding of the bony labyrinth morphology as it relates to evolution. Examples include extinct rodents [3], lizards [4], lemurs [5], and primates [6, 7]. Specimens dating as far back as the Triassic Period have been preserved well enough that accurate 3D models of the bony labyrinth can be generated from scans [2]. These models can be readily compared with extant species to make inferences of evolution and ecology based on the morphology.

From an ontogenetic perspective, the semicircular canal morphology is incredi-

bly precocious. A notable example is humans, where the semicircular canals attain adult size *in utero* [8]. This is particularly interesting as it predates postural control of the head [9] and gait, by several months to a year. The attainment of adult semicircular canal shape and size in humans is also contemporaneous with ossification of the labyrinth. As was discussed in chapter 3, mice –whose canals are not fully developed at the time of parturition –also attain adult morphology at the time of ossification. This is likely a trend across most species, as it has been previously noted in other mammals [10–13]. When studying fossilised remains of extinct species, a big limitation is the age or point of ontogenetic maturity of the specimen. Assessment of a specimen' s development often includes inferring body size, skeletal maturity, dentition, or other characteristics [see 14, for a comprehensive review], which usually would require postcranial evidence to be assessed. In some species, such as mice, sexual maturity, size maturity and osteological maturity are not particularly aligned. If one is interested in a specific ontogenetic end-point, it is important to control for such possible differences in maturity, as skeletal remains may not paint a full picture. For the study of the semicircular canals, however, this is not a concern; as long as the structure is fully ossified, it can safely be assumed that the shape and size can be extrapolated to any post-ossification ontogenetic stage (see chapter 2 and chapter 3).

The morphology of the bony labyrinth, and in particular the semicircular canals, has proven useful for inferential analyses of extinct taxa, especially when comparing the findings to extant taxa [5, 7, 15–18]. These studies rely on different morphological characteristics to make functional inferences such as agility and locomotion, and have also been proven useful to evaluate evolutionary trends. The most common measurement used is radius of curvature of a particular semicircular canal (or the average of the three). Spoor *et al.* [19] studied the radius of curvature of early hominids, and they propose that increased radius of curvature of the anterior and posterior canals is linked to bipedal locomotion, as they are needed for detecting motion in the vertical plane. Similarly, Spoor *et al.* [20] demonstrated a correlation between agility and semicircular canal radius of curvature in a large sample spanning 210 mammalian species, including 91 primates. Walker *et al.* [5] demonstrated this principle in lemurs and lorises. Billet *et al.* [21] later used this principle to infer the agility of Megatherium, which helped elucidate some evolutionary trends in sloths. Likewise, radius of curvature has helped understand the evolutionary point of "no return" for cetacean independence from life on land [22]. The conclusions behind these studies are based on the fact that increased radius of curvature correlates with

increased sensitivity of the canals to rotational acceleration. Yet, Hullar [23] showed that radius of curvature and lumen radius do not appear to correlate with sensitivity in the pidgeon and the squirrel monkey, although they did in the cat. Alternatively, some studies have characterised the bony labyrinth morphology by using geometric morphometric analyses: Lebrun *et al.* [24] found that in primates, canal morphology can distinguish between locomotor abilities, but Bronzati *et al.* [2] concluded that in archosaurs increased sensitivity was not correlated with flight, and proposed that it was linked to increased visual acuity. Presumably, the ability to distinguish between locomotor behaviours using canal morphology is only possible for certain locomotive patters, or it may also be that the phylogenetic signal is stronger in some taxa but not in others. Still, it raises the question of whether using metrics such as radius of curvature, radius of the lumen, or canal size (as approximated by centroid size) would yield accurate enough results to infer ecological characteristics.

It is important to recall that signal mechanotransduction occurs inside the membranous ducts and not in the bony labyrinth (which surrounds the perilymphatic space). Given that the membranous ducts are the relevant structure functionally, the best approximations, especially when inferring the behaviours of extinct specimens, would be those based on membranous duct data. High-quality imaging of the membranous ducts can be achieved using contrast enhanced CT [25] and synchrotron radiation phase-contrast imaging (SR-PCI) [26]. However, this requires access to fresh specimens, which are difficult to come by for extant species but impossible for extinct species. For this reason, the bony labyrinth has been used as a proxy for the membranous labyrinth in these studies. For some cases, this may not be an issue, as it has been shown that the general form of the membranous duct closely follows that of the bony labyrinth [27]. However, this is not true of all species. In species such as the gerbil (see Figure 4.1), the cat, and the guinea pig measurements of the planarity and torsion of the bony canal would result in virtually identical results to those of the bony labyrinth, as the planarity and torsion of the membranous ducts would be similar to that of the bony labyrinth [28]. However, if using the radius of curvature, discrepancies may arise: the centreline of the bony canal (as defined in chapter 2) does not match the centreline of the membranous duct (see Figure 4.2). This is because the membranous ducts are not located in the centre of the bony canal cross-section [28–30]. Discrepancies would be even larger if using the cross-section area of the bony canals as the area of the membranous duct. As mentioned above, species such as the cat have membranous ducts that encompass almost the entirety of the bony canal, whilst human [28] and other primate ducts (note the baboon in

Walker *et al.* [5]) only encompass a small portion of the cross section, which would yield varying levels of inaccuracy depending on the degree of discrepancy. Some models of canal function rely on the squared radius (r) to assess sensitivity [31, 32] and some using r^4 [33–35]. Evidently, large discrepancies between the bony and membranous canals would be greatly compounded by raising them to the power of 2 or 4.

To accurately use the bony labyrinth morphology as a proxy for membranous duct morphology, the relationship between the two needs to be elucidated. The above-mentioned differences in duct and bony cross-sectional area have previously been recorded for some species (see section 4.2), but are not known for the vast majority of species. Moreover, a link between the ratio of perilymphatic to endolymphatic cross-sectional area and other phenotypical characteristics has not been made. Consideration must be given to the possible functional significance of an enlarged perilymphatic space, that is the area surrounding the membranous ducts contained within the bony canals. It has been hypothesised before that the size of the perilymphatic space (not necessarily the bony canals) may be directly related to the overall mass of a species [36] but no functional link has been proposed. This relationship to mass may be due to a more nuanced increase in size, that is the size of the head and by proxy the distance between the two contralateral labyrinths. Distance from the centre of rotation has a direct influence on the stimulation of the canals, such that rotations further from the axis more strongly stimulate the cupula [37]. Two contralateral canals that are further apart would experience higher stimulation during a normal head movement, and it is possible that increased perilymphatic space may have a buffering influence on the stimulus. In terms of functional implications, one potential benefit for enlarged perilymphatic spaces could be temperature regulation. As has been demonstrated with caloric testing, rapid temperature changes in the middle ear can cause increased or decreased neuronal firing when the temperature rises or lowers, respectively [38]. An increased perilymphatic space would protect the endolymph from sudden temperature changes as the perilymph –with a bigger mass than the endolymph in the canals –would buffer the quick changes. Another possibility is that increased perilymphatic space may act as sound insulation. Tullio' s phenomenon is the pathognomonic symptom for patients with superior semicircular canal dehiscence (SSCD). The phenomenon refers to sound-induced vertical nystagmus and is usually accompanied by vertigo, dizziness and nausea [39]. In SSCD, the opening to the cranial cavity acts as a third window that allows for a pulsatile flow between the oval window and the third pathological window. This wave moves the

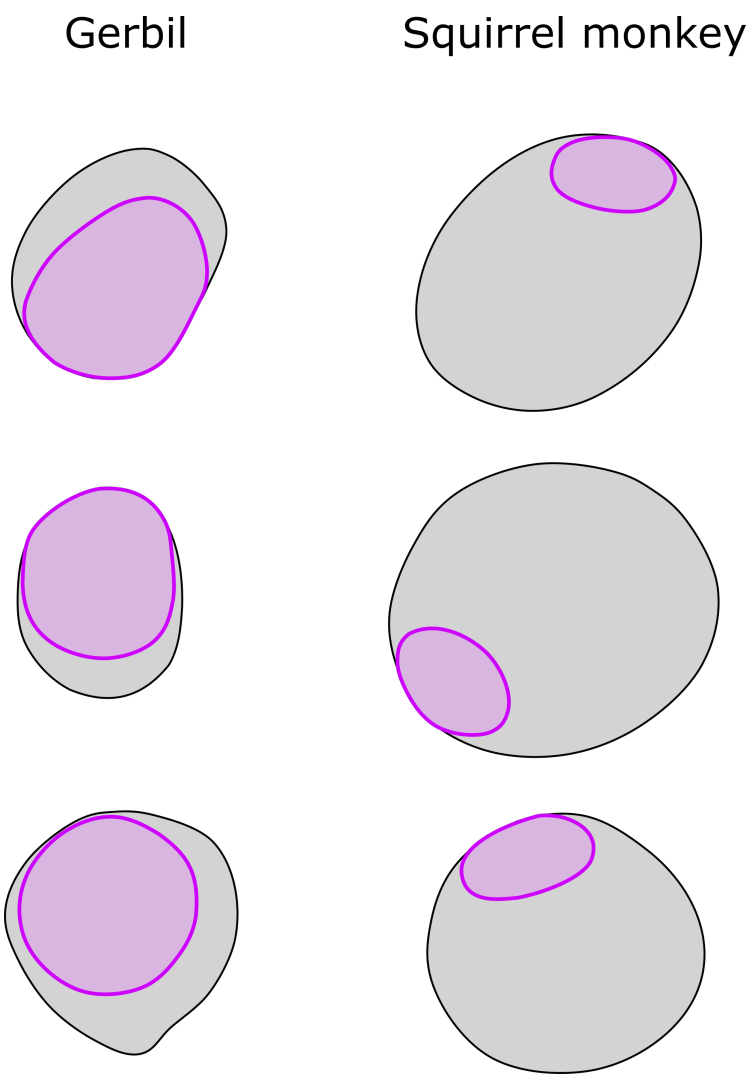

Figure 4.1: Example cross sections from the gerbil and squirrel monkey. From top to bottom: anterior, lateral and posterior canals. The outline of the bony canal cross-section is depicted in black and the perilymphatic space in grey. The pink outlines represent the membranous ducts. Notice how the membranous ducts of the gerbil encompass the majority of the cross-sectional area of the bony canal, whilst the ducts of the squirrel monkey are quite small compared to the bony canal cross-section. Adapted from Ramprashad *et al.* [27]

membranous ducts, causing endolymph flow which in turn stimulates the cupula [40, 41]. Masticatory noise travelling through the petrous bone could also potentially elicit an abnormal response. The presence of a larger perilymphatic space, especially one with a rich fibroblast network, may help dampening the pressure

Figure 4.2: Ideslised human semicircular canal. The bony labyrinth and perilymphatic space are depicted in green. The membranous ducts are depicted in blue. The white dotted line represents the centreline of the membranous ducts; the black dotted line the centreline of the bony labyrinth. Notice the discrepancy between the two lines.

waves. The presence of an enlarged perilymphatic space may also be functionally advantageous from the "roller-pump" hypothesis perspective. First described by Steer Jr [42], this hypothesis proposes that a flexible membranous duct, that is immersed and surrounded by incompressible fluids will be pumped against the cupula (which encompasses the entirety of the bony cross-section) and displace it, by creating a pressure differential. Anliker & Buskirk [43] later showed that it is mainly the perilymph that causes deflection of the cupula. In this scenario, an increased perilymphatic space would yield increased sensitivity to angular accelerations.

On the other hand, it is possible that enlarged perilymphatic spaces are mostly due to phylogenetic signal. From the current, albeit limited literature, it is clear that some primates have particularly large perilymphatic spaces. Although some other non-primate mammals also exhibit enlarged perilymphatic spaces (e.g. the seal), there likely is a strong phylogenetic component to the presence or absence

of the perilymphatic space in the semicircular canals. It is also possible that more than one of the proposed functional or phylogenetic hypothesis are at play. In this chapter, morphological characteristics of different mammalian species' skulls are measured to try to elucidate the relationship between the position of the labyrinth to the other skull structures among adults. Additionally, the cross-sectional shape of the semicircular canals is investigated, to try to infer the relative size of the perilymphatic space and thus help the functional inferences about extinct taxa.

4.2 Methods

4.2.1 General considerations

Two analyses were carried out: a study of the canals within the framework of the skull using linear measurements and a bony semicircular canal cross-section shape analysis. For both analyses, species were categorised into three different groups depending on the relative size of the perilymphatic space in the canals: Small, Medium and Large. Categorisation of each species was based on the description and photographs of the perilymphatic space of Gray [44], and on the measurements taken by Jones & Spells [32]. Species were allocated to the Small perilymphatic group if there was little to no visible perilymphatic space in the slender portion of the canal, regardless of visibility in the ampulla. Species were categorised into the Large perilymphatic space if the size of the space was at least double the size of the endolymphatic duct. All other species were allocated to the Medium group. Throughout this work, mentions "perilymphatic space size" refer to the ratio of perilymphatic to endolymphatic space in a cross-section (relative size of the perilymphatic space compared to the endolymphatic space) of the slender portion of the canals. All the phylogenetic data was sourced from the mammalian phylogeny tree published by Bininda-Emonds *et al.* [45], which was used for visualisation purposes (see Figure 4.3). To demonstrate the potential application of the extant comparative cross-sectional analysis, two extinct mammalian species were also included in the cross-section shape analysis: *Diplobune minor* [46] and *Megatherium americanum* [21]. These two species were not categorised into perilymphatic groups, as no data was available on their membranous duct morphology.

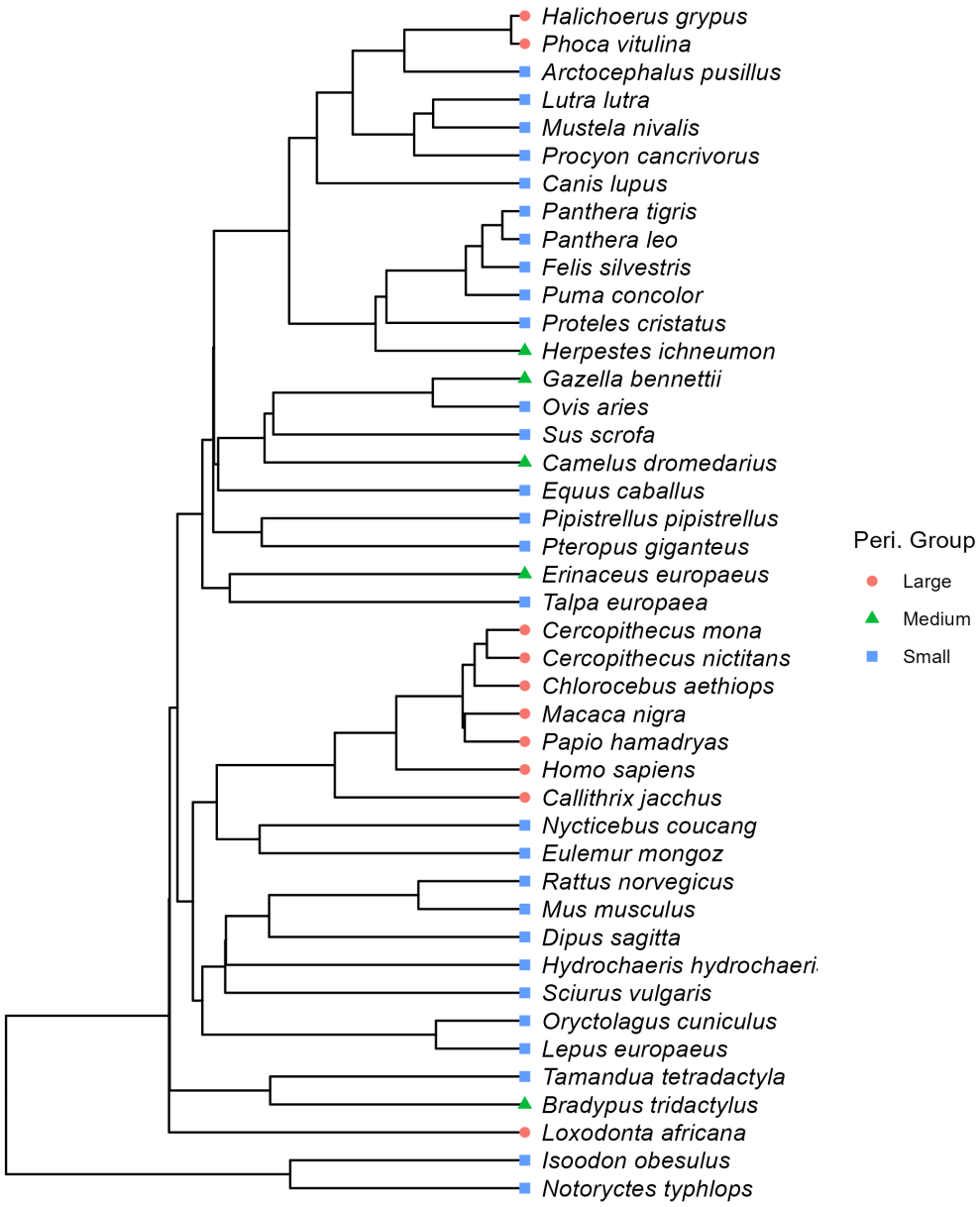

Figure 4.3: Phylogenetic tree of species used in both analyses, categorised by perilymphatic group. Phylogenetic data was sourced from the mammalian phylogeny tree published by Bininda-Emonds *et al.* [45].

4.2.2 Skull measurements

For the skull measurements, CT images from 40 different mammalian species (one specimen per species) were sourced (see Appendix B, Table B.1). The mammalian species were selected to cover a wide range of mammals and a sufficient sample of specimens per perilymphatic group. The species had to be selected from a reduced pool of mammals for which both the membranous morphology data was available and the CT data was available (or could be obtained to an adequate resolution). The details on the species, image source, and image resolution can be found in Appendix B. For species where the perilymphatic group or imaging data was not available, the closest related species of equivalent body size available was used.

CT data was imported into 3D Slicer (Version 4.11.20200930) [47]. Using 3D Slicer' s *Markup* function, the images were landmarked. The resulting landmarks were imported into R studio. Five measurements were then generated by calculating the Euclidean distance between the two relevant landmarks; the average measurement was used for *condyle distance* as this is a bilateral measurement. The landmarks and measurements selected characterise the size of the head, the relative position of the canals within the head, and their distance to one of the axes of rotation: the occipital condyles. The landmarks and resulting measurements are detailed on Table 4.1. Additionally, data regarding semicircular canal radius of curvature, mass and agility were sourced from the data published by Spoor *et al.* [20].

Table 4.1: Skull landmarks and measurements.

Measurement	Description	Landmark placement
Canal distance	Distance between the two contralateral bony canals	Common crus bifurcation (bilateral)
Head width	Distance between the two contralateral external acoustic meatuses	Superior border of external acoustic meatus (bilateral)
Head Length	Distance between the posterior nasal spine (PNS) and foramen magnum (FM).	Posterior-most border of PNS and ventral-most edge of FM
Condyle distance	Distance between bony canals and ipsilateral occipital condyle; averaged from each side.	Common crus bifurcation and centre of ipsilateral occipital condyle

4.2.3 Cross-section aspect ratio

For the cross-section shape analysis, a total of 24 species were included (see Appendix B, Table B.2). Similarly to the skull measurements, the species were selected based on the availability of membranous data, as well as CT data or access to specimens for scanning. Where CT images were available, the analysis was similar to that described in chapter chapter 2. In short, the images were imported into Amira (Version 6.0.0, Thermo Fisher Scientific), and endocasts of the bony labyrinth were generated using thresholding at the HMH value between the bone and the air in the canal lumen. The resulting endocasts were visually inspected and manually adjusted where necessary. The endocasts were thinned until the centrelines for each canal were generated. The centrelines were then used to calculate perpendicular cross-sections of the canals, as described by Johnson Chacko *et al.* [48]. Where endocasts were available (see Table B.2), the endocast meshes were imported into Amira, and using the *Surface-to-volume* module they were converted into segmentations. The endocast segmentations were then treated as described above to generate the cross-sections.

The cross-sections were then imported to imageJ (1.53a v NIH, USA), and measured using the Shape Descriptors in the Measure command. For this analysis, only the aspect ratio was used. It was calculated as follows:

$$\frac{\text{Major axis}}{\text{Minor axis}}$$

Values closer to 1 represent a perfect circle and values greater than one represent increasingly oblong shapes. Since the major axis is always used as a numerator, there are no values lower than 1.

4.2.4 Statistical analyses

All statistical analyses described below were conducted in R version 4.1.3 [49].

For the skull analysis, the agility score and radius of curvature data was not available for two species *Arctocephalus pusillus* and *Tamandua tetradactyla*. These two species were excluded from the linear discriminant analysis, but otherwise used in all other analyses. Body mass was converted to base 10 logarithmic scale. A correlation matrix including all variables described above was calculated. The perilymphatic group (Large, Medium or Small) was computed as a number (3, 2, 1, respectively) for the correlation matrix and subsequent analyses. Afterwards, all variables were

subjected to linear regression with mass as the dependent variable and the residuals were then used to generate a size-corrected correlation matrix. A linear model with the significant variables was created by regressing all variables to the *Canal distance* as the dependent variable. A second linear model was then generated after selecting the relevant variables based on their estimates and p values. This second model included mass, radius of curvature and head length as the independent variables and *canal distance* as the dependent variable.

To assess whether it was possible to predict the perilymphatic group using the variables selected for the second linear model, a discriminant analysis with the perilymphatic groups as a categorical variable was carried out. The two species with missing values were omitted from this analysis. Cross-validation was performed using the leaving-one-out procedure. The results were then plotted for visualisation.

For the cross-section analysis, the measured aspect ratio was normalized to canal length on a scale of 1 to 100% and then subdivided into 50 bins, representing the ampullated side (bin 1) to the non-ampullated side (bin 50). All slices for each canal allocated to a particular bin were then averaged, so that each specimen contributed a single value from each bin. To more accurately represent the slender portion of the canal, only bins 20 to 30 were included in the following analysis. An ANOVA and pair-wise t test were performed, and the analyses were then repeated for each canal separately (anterior, posterior and lateral). To assess whether it was possible to predict the perilymphatic group from the aspect ratio, a linear discriminant analysis was performed, and cross-validation was carried out using leaving-one-out procedure.

4.3 Results

A total of 9 species were included in the Large perilymphatic group, 6 in the Medium group and 23 in the Small group.

The correlation values from the original data (not size corrected) are shown in Figure 4.4. Agility scores did not show significant correlation with any of the variables studied. The perilymphatic group showed significant correlation with body mass (0.37), SCR (0.49), canal distance (0.38) and head width (0.4). All other variables were correlated with each other (>0.85) and were found to be statistically significant. The size variables against body mass can be seen on Figure 4.5.

After size correction for mass, there was no change in terms of significant variables but, unsurprisingly, correlation decreased for most of the size-dependent variables (Figure 4.6). The highest scores were canal distance to head width (0.94), SCR

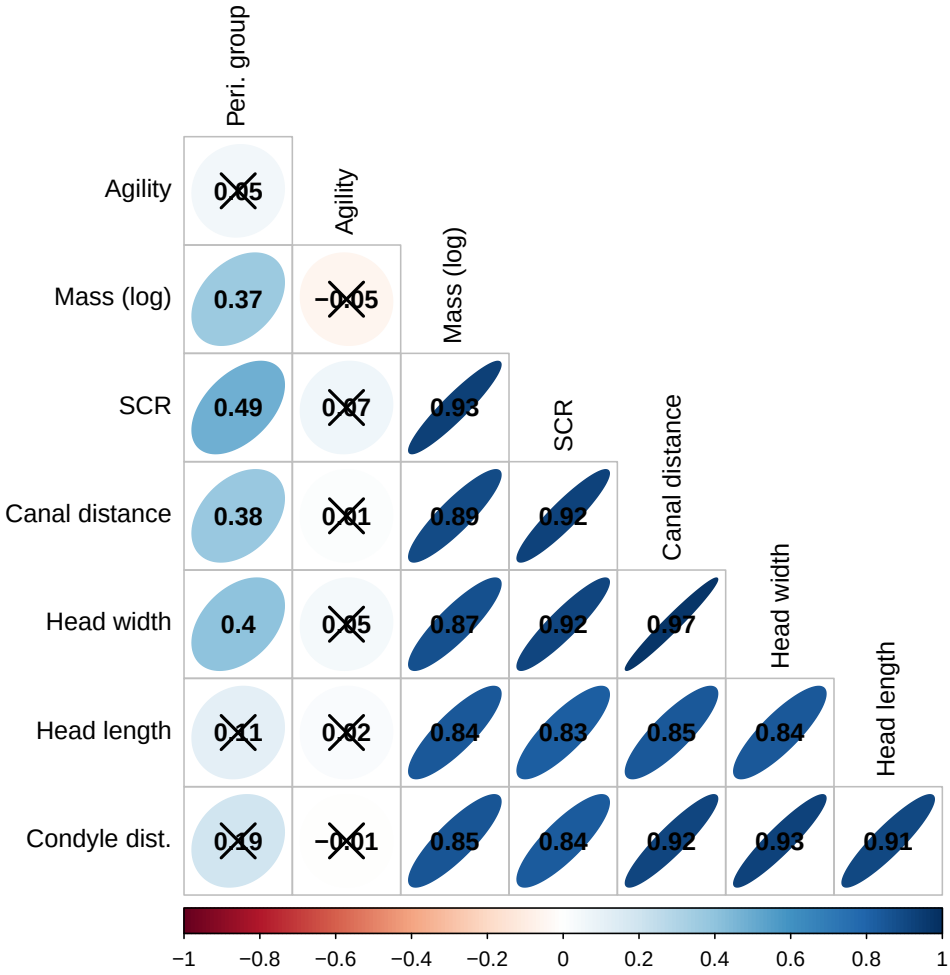

Figure 4.4: Correlation matrix for original data. Correlation values are displayed. Squares with crosses over the correlation are non-significant ($p > 0.05$).

(0.85) and head width to SCR (0.84). Perilymphatic group scores remained mostly unchanged, indicating low size influence.

The results of the linear model are detailed in Table 4.2. SCR had the highest estimate, but was not found to be statistically significant. Only mass, with an estimate of 0.169 was found to be statistically significant ($p = 0.008$).

The discriminant analysis showed an accuracy of 89.47% (accuracy over no information p value: <0.001). The Large perilymphatic group was always correctly classified, followed by the Small group, with one misclassification, and the Medium group,

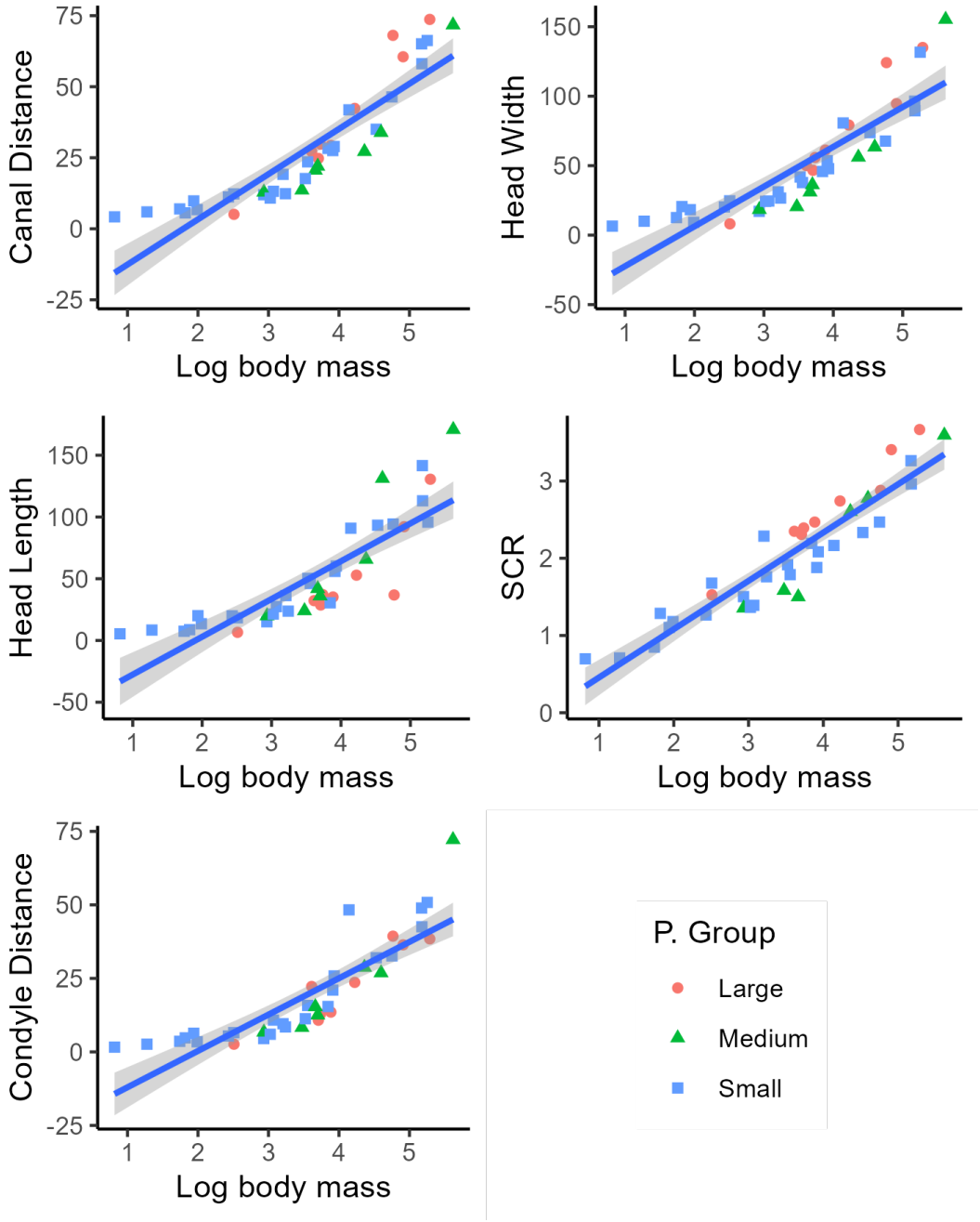

Figure 4.5: Regression plots against log body mass. All other variables are in mm. Data points are colour-coded for perilymphatic group (P. Group).

with 50% chance of correct classification. After leaving-one-out cross-validation, the accuracy lowered to 65.79% (p=0.312). The confusion matrix for the cross-validation

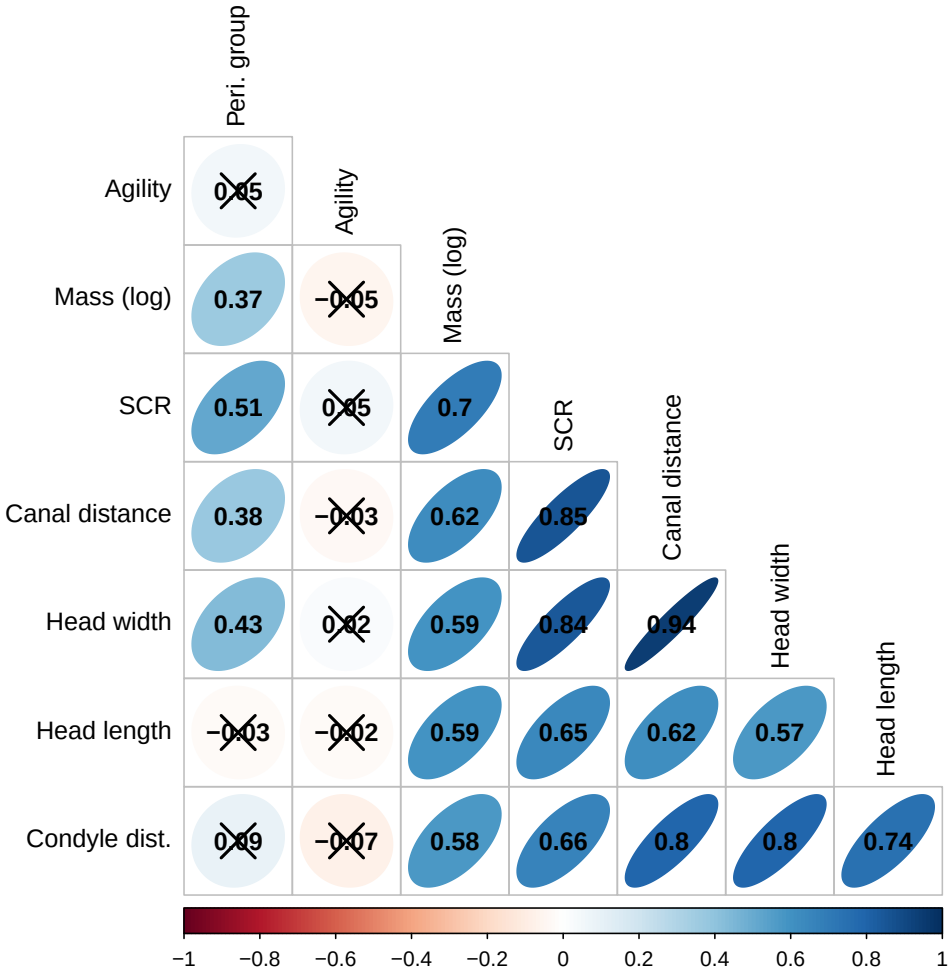

Figure 4.6: Correlation matrix for body mass-corrected data. Correlation values are displayed. Squares with crosses over the correlation are non-significant ($p > 0.05$).

Table 4.2: Linear model results.

	Estimate	SE	T statistic	P value
Intercept	0.284	0.092	3.078	0.004
Head length	0.223	0.114	1.963	0.058
SCR	0.324	0.272	1.189	0.243
Mass	0.169	0.060	2.820	0.008

is detailed in Table 4.3.

Table 4.3: Cross-validated confusion matrix.

	Observed		
Predicted	Large	Medium	Small
Large	7	0	4
Medium	1	1	2
Small	1	5	17

4.3.1 Cross-section measurements

A total of 5 species for the Large, 3 for the Medium and 15 for the Small group were included in this analysis. The combined canal analysis showed that the Large group had the highest aspect ratio (mean 1.425; median: 1.332), followed by the Medium group (mean: 1.231, median: 1.220) and the Small group (mean: 1.165, median: 1.148). An ANOVA showed the groups to be significantly different ($p < 0.001$), and pairwise test showed significant differences between all three groups (Figure 4.7).

When assessing the canals separately, the same pattern was observed: the Large group had the highest aspect ratio, followed by the Medium and the Small for all three canals. Notably, there was no difference for the anterior canal between the Large and Medium group, but both were significantly different from the Small group (Figure 4.8). For the posterior and lateral canal, the Medium and Small groups were not significantly different from each other ($p > 0.05$), but they were both significantly different from the Large group. Overall, when looking at specific canals the differences were not consistent across groups, but the Large perilymphatic group was always significantly different from the Small group.

The linear discriminant analysis showed aspect ratio (AR) had a coefficient of 4.771. It had an accuracy of 68.46% (accuracy over no information p value: <0.001). The results did not change after cross-validation. Running a separate analysis per canal did not increase the accuracy of the model. The Large group was correctly classified in 50.98% of the cases, the Medium in 0% of the cases and the Small group in 91.47% of the cases. The confusion matrix is detailed in Table 4.4.

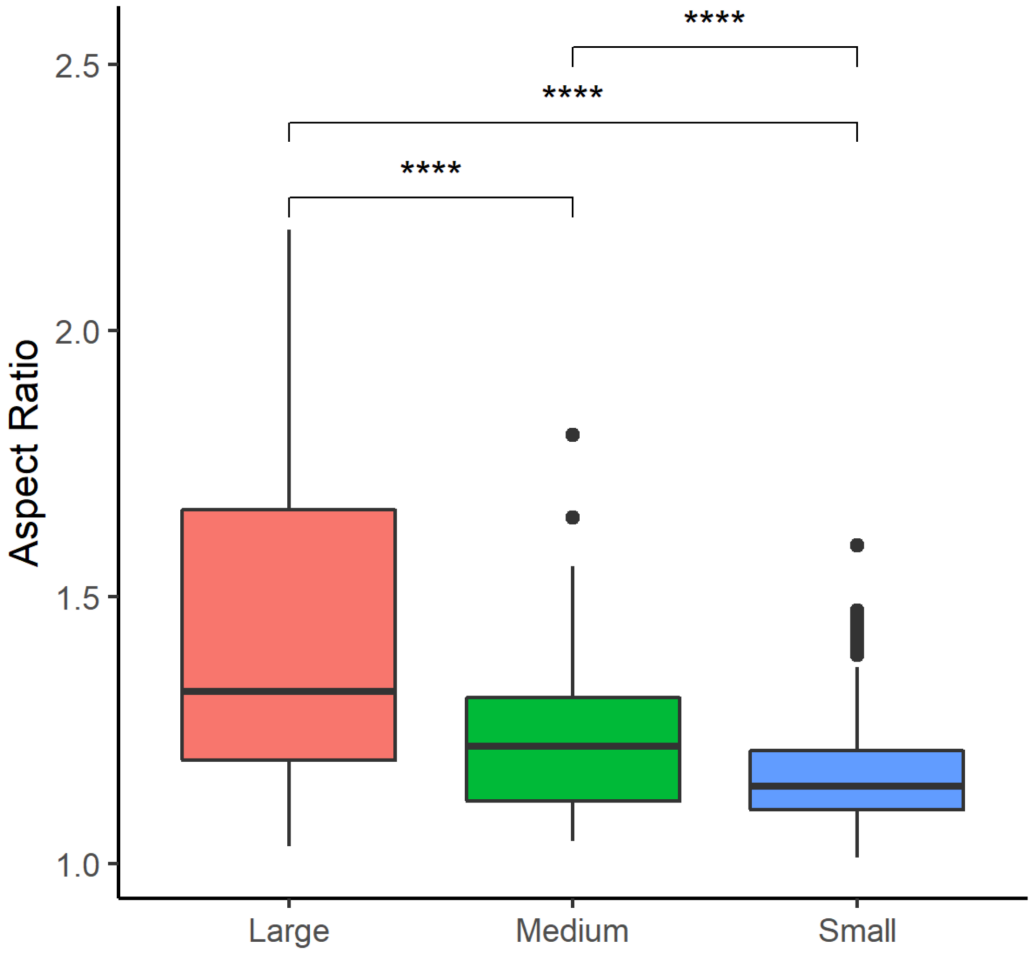

Figure 4.7: Aspect ratio by perilymphatic group. All three canals are shown for each group. ANOVA p was <0.001. P values from pairwise t tests. There were significant differences between all three groups.

Table 4.4: Cross-validated confusion matrix for aspect ratio discriminant analysis. On the columns are the observed values and on the rows the predicted values.

	Observed		
Predicted	Large	Medium	Small
Large	1147	56	202
Medium	0	0	0
Small	1103	202	2245

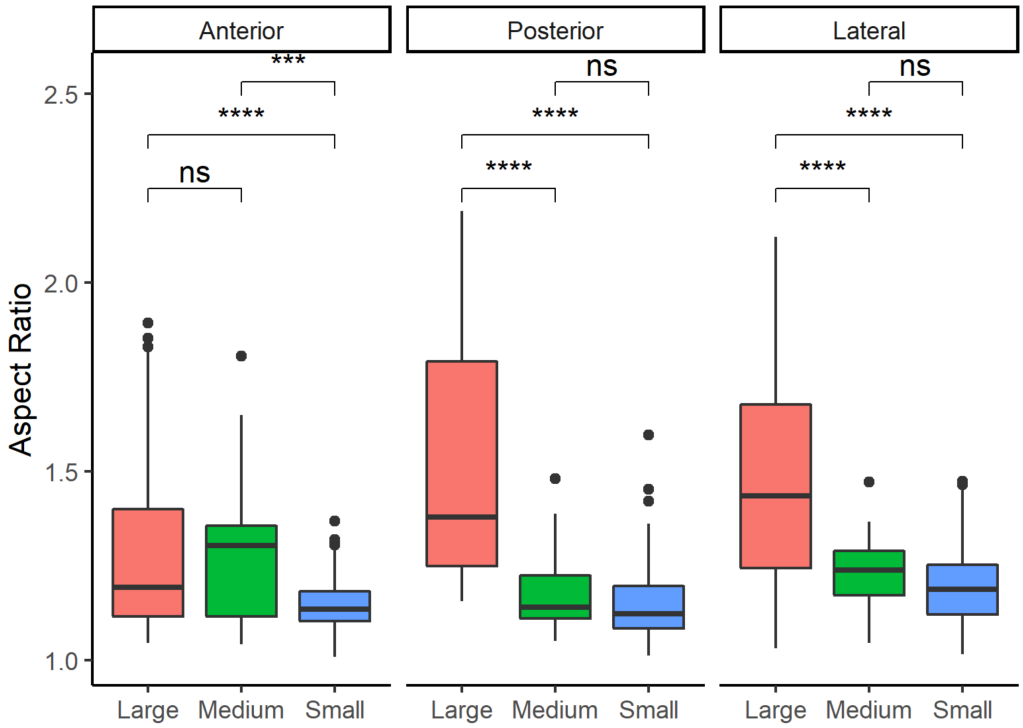

Figure 4.8: Cross-section aspect ratio by group. Each canal was treated separately for each group's for statistical analyses. ANOVA p was <0.001. P values from pairwise t tests. ns = non-significant.

4.3.2 Fossil specimens

Both *Diplobuine* and *Megatherium* were significantly different from the Large group ($p < 0.001$). No significant differences were observed between either species and the Medium or Small groups (Figure 4.9).

In short, the results show that the distance between the two contralateral labyrinths is highly correlated with the overall size of the head, as demonstrated by its correlation with head width, head length and distance to ipsilateral condyle. It also highly correlated with mass and SCR. When the variables were corrected for size, canal distance was still highly correlated with head size, although to a lesser extent. Interestingly, the linear model shows head length and mass as the only significant predictors of canal distance. The perilymphatic group was correlated with canal distance, SCR, head width, and mass. Prediction for perilymphatic group was low using the skull measurements. For the aspect ratio, it appears that the Large perilymphatic group has the highest aspect ratio, suggesting that cross-sections of the

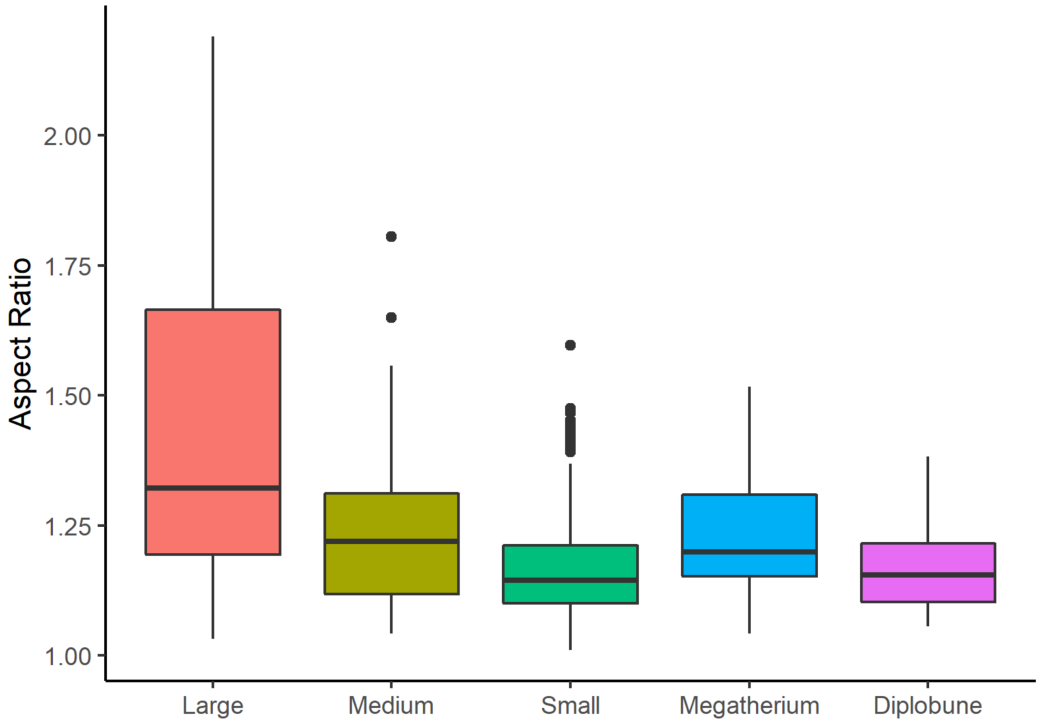

Figure 4.9: Aspect ratio of extant and extinct species. Extant species are plotted in their respective groups. The two extinct species, *Megatherium* and *Diplobune*, are plotted as separate groups to allow for comparison.

bony canals of species with larger perilymphatic spaces are much more elliptical in shape. As suggested by the discriminant analyses, the Medium group is difficult to classify, but it is possible, to an extent, to discriminate between the Large and the Small groups.

4.4 Discussion

It is evident from these results that mass is highly correlated with most of the variables studied. The metrics that assess the size of the head, for example, are highly correlated with mass, such that larger species tend to have larger heads (see Figure 4.5). It has previously been established that the size of the semicircular canals, as measured by radius of curvature, is correlated with mass, so that larger species have larger SRC [32, 50]. This may be due to the fact that larger species exhibit slower head movements [32] and thus these species have increased canal size

to lower the frequencies that can be detected [51]. It must be noted here that the relationship between SCR and mass (or head size in this case) is high, but still species with similar body mass may have differently sized canals, which appear to be correlated with agility [20], so that more agile species will exhibit larger SCR when compared to a less agile species of the same mass.

Also correlated with mass is the canal distance, which measures the distance between the contralateral labyrinths. This metric is also highly correlated with head width, length, and ipsilateral condyle distance. This suggests that while heads increase in size with mass, the position of the canals within the head appears to remain stable: the ratio of canal distance and head width remains the same. Increased distance between contralateral labyrinths during rotations of the head about an axis increases cupula stimulation [37]. It follows that species with larger heads would experience higher stimulation during a given head acceleration, assuming that the centre of rotation is positioned inside the head. This occurs, for example, when looking up, where the body would remain static and the head would rotate upwards. Additionally, it is possible for the axis of rotation to be outside the head, such as when turning a sharp corner. In this situation, the canal closer to the centre of rotation would experience lower stimulation than the contralateral canal, which would be further from the rotation [37]. Given that larger heads have greater distance between contralateral canals, larger species would have greater "interaural" difference when compared to smaller species, which would translate to greater ability to identify the centre of rotation.

The perilymphatic group (that is, the size of the perilymphatic space) was also correlated with mass, and other size variables such as canal distance and head width. Although the correlation was statistically significant, it was a weak correlation (see Figure 4.4). This is not surprising as each perilymphatic group included species of vastly different masses. For example, the Small perilymphatic group includes both *Pipistrellus pipistrellus* and *Equus caballus*; differences in mass were not as extreme in the Large perilymphatic group. Interestingly, whilst head width had a significant correlation, perilymphatic group was not correlated with head length nor condyle distance, further disproving the relationship between perilymphatic group and size.

Perilymphatic group, however, appears to be related to the cross-sectional shape of the canals. When assessing aspect ratio of the cross-sections, the results showed a significant difference between all three perilymphatic groups when all canals were considered. The Small perilymphatic group had the lowest aspect ratio, which implies a cross-section shape closer to a circle. The differences between the Small and

Medium perilymphatic groups are small, although they are statistically significant. In contrast, the Large perilymphatic group showed the highest aspect ratio, which represents a more elliptical shape. Interestingly, the differences were much larger in the posterior and lateral canal, and in the anterior canal the Medium and Large groups were not statistically different. Curthoys *et al.* [28] previously described the cross-section measurements of human bony labyrinths, and from their report the aspect ratio is 1.51. That is well within the range reported here and in chapter 2 for humans, and fall within the range of the Large perilymphatic group. Similarly, the cat values reported in their study (1.25) lie in the range of the Small group, which is the group into which cat was categorised as for this study. The small differences between the Medium and Small groups may be due to some ambiguity in the categorisation of the species. Whilst the L group was very evident from looking at photographs, the distinction between the S and M groups was less clear, and it is possible that some specimens could potentially be miscategorised, particularly when the photographs did not offer a clear image. Ideally, categorisation should be based on more exact metrics, such as histological cross-sections (although this may distort the membranous duct morphology) or on contrast-enhanced microCT images.

As is evident from Figure 4.7 and Figure 4.8 (and chapter 2), there is a wide range of cross-section aspect ratios within each group. It is possible that this wide range can be due to technical issues. The most important detail when sectioning the canals is to ensure that the section is perpendicular to the canal. The procedure for finding the plane of section uses the previous and following points in the centerline to calculate a perpendicular angle. Although the lines are smoothed and visually inspected before the sectioning process, small misalignments can change the angle of the cross-section, which in turn can return higher or smaller values than expected. This is similar to the results reported by Johnson Chacko *et al.* [48], where the cross-section area they report ranges from $0.6\,\mathrm{mm}^2$ to $2.1\,\mathrm{mm}^2$ in the same region. This, however, is only a portion of the variance seen here as it only accounts for intra-specimen variation. Another source of variation is due to the inclusion of several species with different aspect ratios in the same group, and each species is represented by n=1.

The shape of the bony cross-section does not tell the whole story. As has been mentioned in chapter 1 and the introduction to this chapter, the membranous labyrinth is positioned to the outer edge of the bony labyrinth, where its outer-most edge is in direct contact with the bony wall and its inner-most edge is in contact with the perilymphatic space. The exact morphology of the membranous labyrinth

cross-section, however, cannot necessarily be inferred by the bony aspect ratio. For species with Medium and Small perilymphatic spaces, the membranous labyrinth is mostly rounded, similar to the bony wall as it encompasses most of the cross-section. But species with large perilymphatic spaces pose a much more complicated problem. In humans, the cross-section shape of the membranous labyrinth is also elliptical, but the major axis of the membranous cross-section lies perpendicular to the major axis of the bony cross-section [52, 53]. Similarly, the squirrel monkey shows a cross-section that is very close to that of the human [27]. Yet, the pidgeon, which would be classified in the present study as having a large perilymphatic space (Large group), appears to show the opposite, with the major axes of both cross-sections parallel to each other [54]. Furthermore, the portion of the membranous wall that is in contact with the bony labyrinth is much smaller when compared to humans. It must be noted that these assumptions are based on histological sections, so it is possible that the aspect ratio may have been exaggerated by a sectioning plane that is not perpendicular to the canal at that point. Tissue shrinkage may also add to this problem, by changing the shape of the membranous duct. Nonetheless, based on the images presented by Ramprashad *et al.* [27] this does not appear to be the case. As an example, the sections shown for the rabbit present three very different angles: the shape of the bony wall ranges from circular to elliptical and the membranous shape seems to closely follow that of the bony canal. And yet, in all three angles, the portion of the membranous wall that is in contact with the wall remains the same. With the squirrel monkey, the sectioning angles are not as extreme as the rabbit, but they show a decent range of aspect ratios. In this case, the proportion of the membranous wall in contact with the bony wall also remains constant, at a much higher ratio.

The differences in membranous duct morphology appear to be species-dependent. This means that for two species with similar bony cross-section area, the membranous cross-section area can be significantly different. Aves, for example, are species with relatively large perilymphatic spaces [44], as the endolymphatic ducts make up a small portion of the bony lumen. This means that their bony morphology is not necessarily an accurate representation of their membranous ducts. Following the position of the membranous ducts in the outer edges of the canals, the measurement of length of a membranous duct would be larger than the length of the centerline of the bony canal. This difference can skew values for both length and SCR to an extent. But more importantly, measurement of the cross-section area of the bony canals of a given species is not representative of the cross-section area of the membranous

canals.

The purpose of an enlarged perilymphatic space remains unclear. As mentioned in the introduction, some earlier work suggested that the perilymph was responsible for deflection of the cupula, we know this not to be the case [54], mainly due to similar sensitivity across species with differently sized perilymphatic spaces. Nonetheless, it is key here that in species such as the human, the membranous ducts are not necessarily rigid structures. Since one side of the wall is firmly attached to the periosteum and lays against it, this wall would function as a rigid wall. But the opposite side, attached by the fibroblast network has the capacity to expand (more likely than contract, depending on the elasticity of this network), functioning essentially as a flexible wall. During accelerations where the axis of rotation is not about the axis of a given semicircular canal, the pressure differential is increased with the highest pressure against the "back wall" of the canal [see 37], and could potentially compress the membranous duct and therefore increasing cupula stimulation.

Another possibility is that increased perilymphatic space may help with dampening of sound waves traveling through the ear, mainly due to masticatory noises. Increased perilymphatic space, especially with a rich fibroblast network (unlike the perilymphatic space of the cochlea) could potentially dampen waves traveling through the semicircular canals. However, this seems unlikely to be the reason, as Tullio' s phenomenon is due to the third window effect when there is dehiscence of the superior canal [40]. In cases where there is no third window, the sound waves travel through the cochlea and out the round window, without disturbing the semicircular canals.

In terms of mass, the results herein do not support the hypothesis that species with larger mass have larger perilymphatic spaces. Nonetheless, the size (SCR) of the canals is correlated with mass, such that larger species have longer canals. However, an increased perilymphatic space does not necessarily increase the size of the canals, as ultimately the outer edge of the bony canal is the most important measure in determining membranous canal size. It is possible for two species to have different perilymphatic space sizes with virtually the same radius of curvature for the membranous canal, which functionally would not yield different sensitivity calculations (discounting the membranous duct cross-section area). The limiting factor for canal size is the outer edge size of the bony canal, which in turn seems to be limited by the space available in the head [55], although this does not appear to be a major factor in mammalian semicircular canal size [56].

Lastly, it is possible that the presence of an enlarged perilymphatic space has

a phylogenetic origin rather than a functional one. When looking at the species included in the Large perilymphatic group, it is evident that the group is heavily skewed towards primates (see Figure 4.3). The sample included here is not extensive and was heavily limited by the available membranous data, and there may be non-primate species with large perilymphatic spaces that have not been included that would paint a different picture. Nonetheless, there are three notable exceptions in the Large perilymphatic group: *Loxodonta*, *Halichoerus* and *Phoca*. It is likely that the phylogenetic component drives most of the variation in terms of perilymphatic space size, and the functional signal is secondary to phylogeny.

Independent of the reason for the presence of an enlarged perilymphatic space, it is clear that species with an elliptical cross-section are more likely to have a large perilymphatic space. This is also supported by the discriminant analysis carried out here, as it appears that is possible to an extent to distinguish between Large and Small perilymphatic groups, although the procedure is much more specific for the Small perilymphatic group. Due to the soft-tissue nature of the membranous ducts, data on its morphology can only be recovered from fresh specimens. Evidently, this is impossible for extinct species. The two extinct species studied here appear to lie within the ranges of the Small and Medium perilymphatic groups, meaning that differences between the membranous and bony canals are small. However, this is not the case for all species. Aves, for example, have enlarged perilymphatic spaces [44] and 3D reconstructions of non-avian dinosaurs appear to show an elliptic semicircular canal, although aspect ratio was not measured [see for example 57–60]. Calculations of semicircular canal sensitivity based on the bony labyrinth should therefore be done with caution, particularly where the cross-section area is involved.

For studies where the dimensions of the membranous labyrinth are unknown but highly relevant, it would be prudent to assess the cross-section shape of the bony canals, to establish how much the bony canal morphology can be extrapolated to the membranous ducts. If the cross-section is found to be mostly circular, the differences between morphologies are likely to be minimal. However, for species with elliptical sections, more consideration needs to be taken before proceeding.

References

1. Doden, E. & Halves, R. On the Functional Morphology of the Human Petrous Bone. *American Journal of Anatomy* **169,** 451–462. ISSN: 1553-0795 (1984).
2. Bronzati, M. *et al.* Deep Evolutionary Diversification of Semicircular Canals in Archosaurs. *Current Biology* **31,** 2520–2529.e6. ISSN: 0960-9822 (2021).
3. Bhagat, R., Bertrand, O. C. & Silcox, M. T. Evolution of Arboreality and Fossoriality in Squirrels and Aplodontid Rodents: Insights from the Semicircular Canals of Fossil Rodents. *Journal of Anatomy* **238,** 96–112. ISSN: 1469-7580 (2021).
4. Dickson, B. V., Sherratt, E., Losos, J. B. & Pierce, S. E. Semicircular Canals in Anolis Lizards: Ecomorphological Convergence and Ecomorph Affinities of Fossil Species. *Royal Society open science* **4,** 170058. ISSN: 2054-5703 2054-5703. pmid: 29134056 (2017).
5. Walker, A., Ryan, T. M., Silcox, M. T., Simons, E. L. & Spoor, F. The Semicircular Canal System and Locomotion: The Case of Extinct Lemuroids and Lorisoids. *Evolutionary Anthropology: Issues, News, and Reviews: Issues, News, and Reviews* **17,** 135–145. ISSN: 1060-1538 (2008).
6. Silcox, M. T. *et al.* Semicircular Canal System in Early Primates. *Journal of Human Evolution* **56,** 315–327. ISSN: 0047-2484 (2009).
7. Ryan, T. M. *et al.* Evolution of Locomotion in Anthropoidea: The Semicircular Canal Evidence. *Proceedings of the Royal Society B: Biological Sciences* **279,** 3467–3475 (2012).
8. Jeffery, N. & Spoor, F. Prenatal Growth and Development of the Modern Human Labyrinth. *Journal of anatomy* **204,** 71–92. ISSN: 0021-8782 0021-8782. pmid: 15032915 (2004).
9. Pineda, R. G. *et al.* Head Lag in Infancy: What Is It Telling Us? *The American Journal of Occupational Therapy* **70,** 7001220010p1–7001220010p8. ISSN: 0272-9490. pmid: 26709421 (2016).
10. Hoyte, D. A. N. The Postnatal Growth of the Ear Capsule in the Rabbit. *American Journal of Anatomy* **108,** 1–16. ISSN: 0002-9106, 1553-0795 (1961).

11. Ekdale, E. G. Ontogenetic Variation in the Bony Labyrinth of Monodelphis Domestica (Mammalia: Marsupialia) Following Ossification of the Inner Ear Cavities. *Anatomical Record (Hoboken, N.J.: 2007)* **293,** 1896–1912. ISSN: 1932-8494. pmid: 20730862 (2010).

12. Costeur, L., Mennecart, B., Müller, B. & Schulz, G. Prenatal Growth Stages Show the Development of the Ruminant Bony Labyrinth and Petrosal Bone. *Journal of Anatomy* **230,** 347–353. ISSN: 1469-7580 (2017).

13. Thean, T., Kardjilov, N. & Asher, R. J. Inner Ear Development in Cetaceans. *Journal of anatomy* **230,** 249–261. ISSN: 1469-7580 0021-8782. pmid: 27995620 (2017).

14. Hone, D. W. E., Farke, A. A. & Wedel, M. J. Ontogeny and the Fossil Record: What, If Anything, Is an Adult Dinosaur? *Biology Letters* **12,** 20150947 (2016).

15. David, R. *et al.* Motion from the Past. A New Method to Infer Vestibular Capacities of Extinct Species. *Comptes Rendus Palevol. Imaging & 3D in Palaeontology and Palaeoanthropology* **9,** 397–410. ISSN: 1631-0683 (2010).

16. Orliac, M. J., Benoit, J. & O'Leary, M. A. The Inner Ear of Diacodexis, the Oldest Artiodactyl Mammal. *Journal of anatomy* **221,** 417–426. ISSN: 1469-7580 0021-8782. pmid: 22938073 (2012).

17. Bernardi, M. & Couette, S. Eocene Paleoecology of Adapis Parisiensis (Primate, Adapidae): From Inner Ear to Lifestyle. *Anatomical record (Hoboken, N.J. : 2007)* **300,** 1576–1588. ISSN: 1932-8494 1932-8486. pmid: 28452186 (2017).

18. Beaudet, A. The Inner Ear of the Paranthropus Specimen DNH 22 from Drimolen, South Africa. *American journal of physical anthropology.* ISSN: 1096-8644 0002-9483. pmid: 31290572 (2019).

19. Spoor, F., Wood, B. & Zonneveld, F. Implications of Early Hominid Labyrinthine Morphology for Evolution of Human Bipedal Locomotion. *Nature* **369,** 645–648. ISSN: 1476-4687 (6482 1994).

20. Spoor, F. *et al.* The Primate Semicircular Canal System and Locomotion. *Proceedings of the National Academy of Sciences* **104,** 10808–10812. ISSN: 0027-8424. pmid: 17576932 (2007).

21. Billet, G., Germain, D., Ruf, I., de Muizon, C. & Hautier, L. The Inner Ear of Megatherium and the Evolution of the Vestibular System in Sloths. *Journal of anatomy* **223,** 557–567. ISSN: 1469-7580 0021-8782. pmid: 24111879 (2013).

22. Spoor, F., Bajpai, S., Hussain, S. T., Kumar, K. & Thewissen, J. G. Vestibular Evidence for the Evolution of Aquatic Behaviour in Early Cetaceans. *Nature* **417,** 163. ISSN: 1476-4687 (2002).

23. Hullar, T. E. Semicircular Canal Geometry, Afferent Sensitivity, and Animal Behavior. *The Anatomical Record Part A: Discoveries in Molecular, Cellular, and Evolutionary Biology: An Official Publication of the American Association of Anatomists* **288,** 466–472. ISSN: 1552-4884 (2006).

24. Lebrun, R., de León, M. P., Tafforeau, P. & Zollikofer, C. Deep Evolutionary Roots of Strepsirrhine Primate Labyrinthine Morphology. *Journal of Anatomy* **216,** 368–380. ISSN: 0021-8782. pmid: 20039977 (2010).

25. Glueckert, R. *et al.* Visualization of the Membranous Labyrinth and Nerve Fiber Pathways in Human and Animal Inner Ears Using MicroCT Imaging. *Frontiers in Neuroscience* **12.** ISSN: 1662-453X (2018).

26. Li, H. *et al.* Vestibular Organ and Cochlear Implantation–A Synchrotron and Micro-CT Study. *Frontiers in Neurology* **12.** ISSN: 1664-2295 (2021).

27. Ramprashad, F., Landolt, J. P., Money, K. E. & Laufer, J. Dimensional Analysis and Dynamic Response Characterization of Mammalian Peripheral Vestibular Structures. *American journal of anatomy* **169,** 295–313. ISSN: 0002-9106 (1984).

28. Curthoys, I. S., Blanks, R. H. I. & Markham, C. H. Semicircular Canal Radii of Curvature (R) in Cat, Guinea Pig and Man. *Journal of Morphology* **151,** 1–15. ISSN: 0362-2525 (1977).

29. Blanks, R. H. I., Curthoys, I. S. & Markham, C. H. Planar Relationships of the Semicircular Canals in Man. *Acta oto-laryngologica* **80,** 185–196 (1975).

30. Curthoys, I. S. & Oman, C. M. Dimensions of the Horizontal Semicircular Duct, Ampulla and Utricle in Rat and Guinea Pig. *Acta oto-laryngologica* **101,** 1–10. ISSN: 0001-6489 0001-6489. pmid: 3515839 (1986 Jan-Feb).

31. Peterka, R. & Tomko, D. Differences between Cats in Response Properties of Horizontal Semicircular Canal Primary Afferents. *Experimental Brain Research* **56.** ISSN: 0014-4819, 1432-1106 (1984).

32. Jones, G. M. & Spells, K. E. A Theoretical and Comparative Study of the Functional Dependence of the Semicircular Canal upon Its Physical Dimensions. *Proceedings of the Royal Society of London. Series B. Biological Sciences* **157,** 403–419. ISSN: 0080-4649 (1963).

33. Rabbitt, R. D., Damiano, E. R. & Grant, J. W. in *The Vestibular System* 153–201 (Springer, 2004).

34. Ten Kate, J. H. The Mechanics of the Growing Semicircular Canal. *Journal of Experimental Biology* **58,** 351–366. ISSN: 0022-0949 (1973).

35. Squires, T. M. Optimizing the Vertebrate Vestibular Semicircular Canal: Could We Balance Any Better? *Physical Review Letters* **93,** 198106 (2004).

36. Urciuoli, A. *The Evolution of Semicircular Canals in Anthropoid Primates: Phylogenetic Implications for Miocene Catarrhines* (Universitat Autònoma de Barcelona, Barcelona, 2021). 246 pp.

37. Goyens, J. Modelling Shows That Stimulation of the Semicircular Canals Depends on the Rotation Centre. *Hearing Research* **396,** 108071. ISSN: 0378-5955 (2020).

38. Kassemi, M., Deserranno, D. & Oas, J. G. Effect of Gravity on the Caloric Stimulation of the Inner Ear. *Annals of the New York Academy of Sciences* **1027,** 360–370. ISSN: 00778923, 17496632 (2004).

39. Basura, G. J., Cronin, S. J. & Heidenreich, K. D. Tullio Phenomenon in Superior Semicircular Canal Dehiscence Syndrome. *Neurology* **82,** 1010–1010. ISSN: 0028-3878, 1526-632X. pmid: 24638216 (2014).

40. Obrist, D. Flow Phenomena in the Inner Ear. *Annual Review of Fluid Mechanics* **51,** 487–510 (2019).

41. Grieser, B. J., Kleiser, L. & Obrist, D. Identifying Mechanisms Behind the Tullio Phenomenon: A Computational Study Based on First Principles. *JARO: Journal of the Association for Research in Otolaryngology* **17,** 103–118. ISSN: 1525-3961. pmid: 26883248 (2016).

42. Steer Jr, R. W. *The Influence of Angular and Linear Acceleration and Thermal Stimulation on the Human Semicircular Canal.* (Massachusetts Institute of Technology, 1967).

43. Anliker, M. & Buskirk, W. V. The Role of Perilymph in the Response of the Semicircular Canals to Angular Acceleration. *Acta Oto-Laryngologica* **72,** 93–100. ISSN: 0001-6489 (1971).

44. Gray, A. A. *The Labyrinth of Animals: Including Mammals, Birds, Reptiles and Amphibians* (J. & A. Churchill, 1908).

45. Bininda-Emonds, O. R. P. *et al.* The Delayed Rise of Present-Day Mammals. *Nature* **446,** 507–512. ISSN: 1476-4687 (7135 2007).

46. Orliac, M. J., Araújo, R. & Lihoreau, F. The Petrosal and Bony Labyrinth of Diplobune Minor, an Enigmatic Artiodactyla from the Oligocene of Western Europe. *Journal of Morphology* **278,** 1168–1184. ISSN: 1097-4687 (2017).

47. Fedorov, A. *et al.* 3D Slicer as an Image Computing Platform for the Quantitative Imaging Network. *Magnetic Resonance Imaging. Quantitative Imaging in Cancer* **30,** 1323–1341. ISSN: 0730-725X (2012).

48. Johnson Chacko, L. *et al.* Analysis of Vestibular Labyrinthine Geometry and Variation in the Human Temporal Bone. *Frontiers in Neuroscience* **12.** ISSN: 1662-453X (2018).

49. R Core Team. *R: A Language and Environment for Statistical Computing* manual (R Foundation for Statistical Computing, Vienna, Austria, 2022).

50. Spoor, F. & Zonneveld, F. Comparative Review of the Human Bony Labyrinth. *American Journal of Physical Anthropology: The Official Publication of the American Association of Physical Anthropologists* **107,** 211–251. ISSN: 0002-9483 (1998).

51. Howland, H. C. & Masci, J. The Phylogenetic Allometry of the Semicircular Canals of Small Fishes. *Zeitschrift für Morphologie der Tiere* **75,** 283–296. ISSN: 0044-3131 (1973).

52. Igarashi, M., Ohashi, K. & Ishii, M. Morphometric Comparison of Endolymphatic and Perilymphatic Spaces in Human Temporal Bones. *Acta oto-laryngologica* **101,** 161–164 (1986).

53. Curthoys, I. S., Markham, C. H. & Curthoys, E. J. Semicircular Duct and Ampulla Dimensions in Cat, Guinea Pig and Man. *Journal of Morphology* **151,** 17–34. ISSN: 0362-2525. pmid: 830956 (1977).

54. Dohlman, G. F. & Kuehn, L. A. The Role Of The Perilymph In Semicircular Canal Stimulation. *Acta Oto-Laryngologica* **75,** 396–404. ISSN: 0001-6489, 1651-2251 (1973).

55. Goyens, J. High Ellipticity Reduces Semi-Circular Canal Sensitivity in Squamates Compared to Mammals. *Scientific Reports* **9,** 16428. ISSN: 2045-2322 (1 2019).

56. Jeffery, N. & Cox, P. G. Do Agility and Skull Architecture Influence the Geometry of the Mammalian Vestibulo-Ocular Reflex? *Journal of Anatomy* **216,** 496–509. ISSN: 0021-8782. pmid: 20210819 (2010).

57. Neenan, J. M., Chapelle, K. E. J., Fernandez, V. & Choiniere, J. N. Ontogeny of the Massospondylus Labyrinth: Implications for Locomotory Shifts in a Basal Sauropodomorph Dinosaur. *Palaeontology* **62,** 255–265. ISSN: 1475-4983 (2019).

58. Sipla, J. S. *The Semicircular Canals of Birds and Non-Avian Theropod Dinosaurs* (The Graduate School, Stony Brook University: Stony Brook, NY., 2007).

59. Andrzejewski, K. A., Polcyn, M. J., Winkler, D. A., Chindebvu, E. G. & Jacobs, L. L. The Braincase of Malawisaurus Dixeyi (Sauropoda: Titanosauria): A 3D Reconstruction of the Brain Endocast and Inner Ear. *PLOS ONE* **14,** e0211423. ISSN: 1932-6203 (2019).

60. Knoll, F., Witmer, L. M., Ortega, F., Ridgely, R. C. & Schwarz-Wings, D. The Braincase of the Basal Sauropod Dinosaur Spinophorosaurus and 3D Reconstructions of the Cranial Endocast and Inner Ear. *PLOS ONE* **7,** e30060. ISSN: 1932-6203 (2012).

Chapter 5

Discussion

5.1 Summary of results

Form maturity after at birth in humans After studying the overall and the cross-section shape of the human bony semicircular canals, it appears that they are extremely conserved structures. There appears to be minimal changes to the form of the bony canals after birth. In chapter 2, I detailed the results of a postnatal ontogenetic comparison of the bony semicircular canal form. The analyses using geometric morphometrics did not detect any significant changes of shape in the semicircular canals after birth. It suggests that the shape and size were established in utero and remained stable thereafter. With respect to the variability, adults were more variable than perinates in terms of canal solidity and convexity, both measures that test the surface texture of the bony canals. Additionally, there was a statistically significant increase in size, both measured by length and centroid size, but the increase only amounts to <5% of the total length and less than 7% of centroid size. The key finding from these results is that the overall shape of the bony canals is preserved throughout postnatal life. Although studies had shown a significant loss in osteocytes that would point towards a bone remodelling disinhibition, it appears that the remaining amount is more than sufficient to suppress any significant changes to the bony canal form.

Form maturity after ossification in mice. In chapter chapter 3, the bony canal postnatal development was assessed. In contrast to humans, *Mus musculus* semicircular canals do not ossify prenatally, which allowed for assessment of postnatal morphology both in the pre- and post-ossification stages. Bone deposition in

the petrous bone is visible in the P1 stage, although no bone deposition can be seen around the semicircular canals. By P7 there is a thin layer of bone completely surrounding the semicircular canals, which continues to thicken up to P28 (M1 group in this study). The results showed that the murine labyrinth continues growth from days 1 to 14, with the highest growth rate between days 1 and 7. After day 7, development plateaus, aside from a small increase in size between days 7 and 14. There are some shape changes during the first postnatal week, including increased torsion of the anterior canal and rounding of all three canals. After this point, no significant changes in shape or size were observed, although bone deposition around the canals continued until around 28 days. In both humans and mice, no functionally significant shape changes were observed after ossification is completed, which would imply that inhibition of shape and size changes is linked to ossification of the canals in mice (and possibly other, if not all, mammals).

Cross-sectional shape can predict perilymphatic space size. In chapter 4, the size of the perilymphatic space was categorised into three groups, ranging from small to large. The results showed that there was a statistically significant correlation between the perilymphatic space size (perilymphatic group), canal distance, radius of curvature, mass and head width. Additionally, it appears that it is possible to predict for perilymphatic group using the cross-sectional shape of the bony semicircular canals, as measured by aspect ratio. This analysis showed that species with large perilymphatic spaces tended to show a more elliptic cross-section shape, whereas species with small perilymphatic spaces were more rounded. It is harder, however, to classify species that fall in the middle of the range (medium group). These findings raise the prospect of inferring the size of the perilymphatic space using the cross-section's aspect ratio for species where no membranous duct morphological data is available.

5.2 Limitations

One of the main limitations of this thesis is the nature of the samples used. For the human chapter the data was sourced from 3 different collections (see chapter 2). The first issue that arises is the age of the samples. For the perinatal group, the exact age of all the specimens was known, and all specimens included in the sample were of perinatal age. For the adults, only the Cambridge dataset had ages recorded for the specimens (average age was 84.8 years). The rest of the sample were recorded as

adult, but could have contained young adult individuals. This though seems unlikely, as the specimens used were donors to Anatomy departments, and the average age of body donation is around 60-70 years [1]. The perinatal group was more constrained in terms of age when compared to the adult group. This could have increased the variation seen in the adult dataset, as this variation could be a function of age. Nonetheless, both groups were of fully ossified canals, which as has been shown throughout this work, limits the potential for shape and size changes. Furthermore, the two groups had similar sample sizes, which limits this as a source of variation. Additionally, no significant variation was found in terms of shape and size. As for the other metrics (convexity and solidity), the changes and increased variation observed there are unlikely to be heavily influenced by a wider spread of age. If any, it was expected that increased variation would be a function of increased age, so that the inclusion of a more varied sample, which could potentially include younger adult specimens, would decrease that variation. Another issue with the sample was the lack of sex information. For some of the perinatal samples, sex was known, but this information was not available for all specimens, nor for any of the adult specimens. This made it impossible to sex match the groups. Potentially, this could create a problem where one particular sex is overrepresented in one or both groups, so that differences observed could be due to sexual dimorphism. Osipov *et al.* [2] found that males have larger semicircular canals (height and width) when compared to females. They were able to accurately classify the specimens 80% of the time. Nonetheless, in the current study, only slight differences in size were observed (<5% increase for the adults). There are 6 known females in the perinatal sample; it is possible that the adult sample is entirely comprised of males, making the differences seen here due to sexual dimorphism in human semicircular canal size. Notably, Osipov *et al.* [2] only found differences of shape in the lateral canal, whilst no shape differences were observed here. However, it is also possible that the small changes observed are due to intra-specific variation. This variation may be more constrained in the perinatal sample due to all specimens undergoing the same scanning procedure, whislts the adults were scanned with similar but not identical protocols. On the other hand, body donors across the UK are relatively homogenous [1], whilst the perinatal sample may have included a broader demographic, given the origin of the samples (19th century workhouse in Liverpool).

Sourcing image data was the most complex for chapter 4. Samples were obtained from online repositories and some were scanned specifically for this project. All of the imaging studies used had different acquisition protocols and resolution. Nonethe-

less, sourcing was also difficult for the human ontogenetic study (chapter 2. The cross-sectional study (chapter 4) of the semicircular canals requires a high-resolution view of the bony labyrinth, which further lowered the available data. To scan the petrous temporal bone, it must be dissected to achieve a smaller field of view (and higher resolution). This is a destructive process, and these specimens can then no longer be used for other cranial base research or for anatomical instruction. The scarcity of cadaveric material, and the need to maximise the data collected from these samples makes it difficult to acquire a larger sample. Furthermore, live specimens (or patients) cannot be scanned, as the increased field of view would not allow for high enough resolution. Not to mention the ethical problem of subjecting specimens to high levels of radiation required for imaging without indication. Also, patients who require temporal bone imaging are likely to have some pathology that would disqualify them for the study. Using MRI as an alternative would not be feasible, as this modaliry would not yield sufficient resolution, since most MRI scanners have a pixel size around 0.5 - 1.5 mm (more than ten times the size used to scan the human samples in this study). Additionally, live specimens have higher chances of leading to motion artefacts, particularly of structures as small as the semicircular canals. The scarcity of cadaveric material, and the need to maximise the data collected from these samples makes it difficult to acquire a larger sample. Furthermore, a big challenge of chapter 4 was the availability of membranous labyrinth data. Mammals could only be included in the study if there was previous data or either the cross-section area of the membranous duct (in comparison to the cross-section area of the bony canal), histological or even photographic evidence of the bony to membranous ratio.

In terms of imaging, there were some issues that arose during the experimental process for chapter 2 in regards to the cross-section metrics. The convexity and the solidity metrics use Image J' s convex hull protocol to calculate these metrics. Convexity uses the perimeter of the selection and the convex hull perimeter, whilst solidity uses the selection area and convex hull area (see Appendix C). Due to this reliance on the convex hull, the question arose of whether the position of the selected area (in this case the masked cross-section of the segmentation) would have an impact on the convex hull. This is because when rotating the same image, a voxel (or pixel in the 2D sections) could become part of the selection (or drop out of the selection) depending on the position of the image. During the cross-sectioning protocol, the plane for cross-section is calculated at every cross-section, using the previous and the following points to calculate a perpendicular angle. The

orientation (rotation) of the plane of section cannot be modified in this process. Whilst no apparent differences in orientation from one slice to the next were visible, it is possible that some rotational differences may have increased or decreased these metrics (see Appendix C. Changes between groups were mostly in terms of convexity, and the differences seem large enough so that it is unlikely it is due to rotational changes (see chapter 2). Nonetheless, it was decided that the cross-section solidity and convexity would not be used for chapter 3.

The current study used microCT and contrast-enhanced microCT for visualisation of the semicircular canals. With the resolution achieved using this technique, the convexity and solidity measures were not reliable. Imaging studies with newer techniques, such as synchrotron radiation phase contrast imaging (SR-PCI) [3–5], can be used to visualise the bony labyrinth at a greater resolution and with better definition of the tissue boundaries. This would mean that many more voxels would characterise a small portion of the bony wall, making the perimeter measurements more reliable and less sensitive to rotational artefacts.

The original direction of this project included collecting endolymph and perilymph samples both from a human and animal model to study the mechanical properties of these fluids. Then, these results would inform an anatomically-accurate model of the human bony semicircular canal and membranous duct, which would include both the endolymphatic and perilymphatic spaces. However, due to COVID-19, donations of human cadaveric material were stopped, and it became impossible to find samples for this study. Therefore, the project had to be adapted to account for these circumstances, and those areas of study were dropped. Further work is still needed to appropriately characterise the fluids and to implement that data in biomechanical models of the canals that account for both the mechanical properties of the fluids.

5.3 Implications on semicircular canal form stabilisation

OPG and osteocyte viability As was outlined in chapter 1, bone turnover in the otic capsule is significantly lower than any other cranial or postcranial bones [6]. Likely, the inhibitor of bone remodelling in the perilabyrinthine bone is osteoprotegerin (OPG). OPG is a local factor that decreases bone resorption, as it works as a decoy receptor, preventing RANKL binding to RANK (for a more detailed descrip-

tion, see subsection 1.4.2). OPG is found in increased levels in the otic capsule when compared to other bones [7]. Anatomical studies suggest that a canaliculi mesh in the periotic bone allows for flow of OPG from the perilymphatic space. Osteocytes maintain the permeability of the canaliculi, so that the loss of osteocytes may decrease permeability, leading to increased remodelling. The results from chapter 2 indicate that indeed, some remodelling may be occurring in later life, as shown by the increased variation of convexity and solidity. Nonetheless, overall shape and size of the semicircular canals is maintained throughout life. Two possibilities arise to explain this phenomenon. First that indeed the loss in osteocytes does decrease permeability of the canaliculi, but not to the extent to allow for generalised bone resorption. Given that the changes observed in adult humans were only minute resorption or deposition (as measured by increased perimeter), it is possible that these are the results of small tissue islands with no permeable canaliculi. Second, that the canaliculi-OPG pathway is not responsible for bone resorption inhibition in the periotic bone. Evidence to this is the normal levels of OPG and osteocytes in perilabyrinthine bone of specimens with labyrinthitis ossificans (LO). LO is the pathological ossification of the labyrinth following an "insult" to the inner ear, usually of inflammatory nature [8]. This bone deposition would naturally occlude the path between the perilymphatic space and the canaliculi, leading to decreased OPG in the surrounding bone, decreased number of viable osteocytes and, subsequently, increased bone resorption. However, studies in the gerbil show that there is no difference in number of viable osteocytes between LO and control, suggesting an alternate route for OPG diffusion [9]. Interestingly, it seems that in most gerbils with LO, the periosteum remained intact. In the cases where the periosteum was destroyed, there was increased bone resorption and remodelling, which progressed in a centrifugal fashion. This could indicate that the periosteum plays a bigger role in the maintenance of semicircular canal form, perhaps even being the source of OPG or other signalling cytokines.

Osteogenic response to strain The petrous temporal bone, where the bony labyrinth is housed, is not a load-bearing bone, but it is subjected to other forces travelling through the skull. This includes masticatory forces, and forces that may be directly applied to the petrous bone through dural attachments or that may travel from the occipital condyles from head movement. In load-bearing bones, the microstructure of the bone continues to change until it meets the loading requirements of said bone [10]. A femur, for example, may develop until it is fully ossified

and continue to adapt its tissue structure in response to activity that applies load in a particular direction. Usually, increased mechanical forces will change the remodelling balance to favour osteoblastic rather than osteoclastic activity [11], resulting in a net increase in bone deposit. Although the overall bone shape may not be altered, localised bone deposition may cause minute changes that may become functionally relevant, especially in a structure as small as the semicircular canals. And yet, this does not appear to be the case for the petrous bone. It is unlikely that changes due to normal daily activity could generate any significant forces travelling through the skull base. Nonetheless, the skull is subject to masticatory forces, although most of the strain is on the face [12], and it can lead to considerable deformation of the facial skeleton [13, 14]. In humans, the forces in the glenoid fossa act on the petrotympanic fissure and cause a small diastasis, which may act as a stress breaker to transmit the forces around the tympanic ring, although some attenuated force will still act upon the facial canal, which in turn may be directed towards the vestibule. These forces are considerable enough to cause microfractures in the inner ear [15]. The attachment of the dural tentorium cerebelli on the upper border of the petrous bone may transfer forces from head movements, especially during traumatic injuries. The falx cerebri and tentorium play a role in adjacent nervous tissue injury, as they restrict the movement of the brain [16]. Whilst the role of these structures in conducting forces through the skull has not been studied, it is likely that the sites of attachment experience greater strain than other cranial areas. Calcification of the tentorium is a common age-related finding in radiology, and usually not considered pathological [17]. The exact cause of calcification is unknown, but it may be due to the increased strain it undergoes. Since the tentorium attaches anteriorly at the superior border of the petrous bone, these forces may indeed be strong enough to cause microstructural changes to the bone. The posterior canal, especially near the apex, would be particularly affected. However, changes in otic capsule microstructure may not necessarily translate to shape changes, unless the bone apposition occurs on the canal surface. This is because the bony canals are not a bone per se, but rather a cavity inside the petrous bone. For significant changes of shape to occur, forces would need to be exerted from the structures within, i.e. the membranous labyrinth.

Although in a fully ossified skull the forces traveling through the skull may have little influence on semicircular canal or petrous bone form, in a developing skull this may not be the case. As mentioned above, the major osteocyte drop in humans happens around 3 years of age [18]. This decrease may be due to the ossified state of the cranium at that point. Mechanical stress applied to the cartilage –in particular

tensile stress –may lead to deformation of the petrous bone and subsequently the semicircular canals. The ossification of the canals changes the material properties, therefore making the labyrinth more resistant to form changes. Once the surrounding structures have undergone quick growth, there may be less forces acting upon the petrous bone and therefore less need to maintain that osseous protection. In other species, such as the mouse, ossification does not occur until postnatal life. In these cases, the unossified structures would be more susceptible to mechanical forces until full ossification occurs. However, the small size of the head (and the overall mass) of the mouse imply that the forces the petrous bone is experiencing are much smaller than that of the human. The (at that point) cartilaginous labyrinth has the same material properties of that of the human, whilst resisting much smaller forces, which translates to less potential for shape changes. The urgent need to "stabilise" the labyrinth form via ossification may not be as relevant in smaller species.

5.4 Mouse as a model for human semicircular canals

Semicircular canal size One of the first factors to consider when comparing two species' semicircular canals is size. In most mammals, the anterior semicircular canal is the longest of the three, and has the largest radius of curvature [19]. In both humans and mice, the anterior semicircular canal is the longest, followed by the posterior canal and the lateral canal (see chapter 2 and chapter 3). These differences in size translate to differences in canal sensitivity. For example, Yang & Hullar [20] found that in mice, there is a significant difference between the mean sensitivity of the anterior and horizontal canals. Although the rankings of canal length between humans and mice are the same, it does not necessarily mean that the proportion of SCR between one particular canal and the other two are conserved. Data published by Spoor *et al.* [21] shows that the ratio of the radius of curvature between the canals in each species is somewhat similar, with the biggest difference being the ratio between the anterior and posterior canals (Table 5.1). However, the problem compounds when speaking in terms of sensitivity. Yang & Hullar [20] found that the sensitivity of the regular afferents is related to the radius of curvature as per the following formula:

$Sensitivity = 0.23R - 0.09$

Where R is the radius of curvature and sensitivity is expressed in $spike \cdot s^{-1}/deg \cdot s^{-1}$. Using data from Spoor *et al.* [21] for the radius of curvature, the ratio of sensitivity between one canal and another per species are much greater than when

Table 5.1: Semicircular canal radius of curvature and sensitivity for mice and humans. A/P/L SCR: Radius of curvature of the anterior, posterior and lateral canals. Sen. A/P/L: Sensitivity of anterior/posterior/lateral canals. Sensitivity is expressed in $spike \cdot s^{-1}/deg \cdot s^{-1}$. Data from Spoor *et al.* [21]

	Mice	Humans
ASCR (mm)	0.858	3.266
PSCR (mm)	0.716	3.152
LSCR (mm)	0.553	2.218
Sen. A	0.107	0.661
Sen. P	0.075	0.635
Sen. L	0.037	0.420
ASCR/PSCR	1.036	1.198
PSCR/LSCR	1.421	1.295
ASCR/LSCR	1.472	1.551
SenA/SenP	1.437	1.042
SenP/SenL	2.007	1.511
SenA/SenL	2.883	1.574

comparing the SCR by themselves (Table 5.1).

This problem is even greater when comparing size between the two species directly and not proportionally. When comparing mass, humans are three orders of magnitude larger than the mouse. As semicircular canal radius of curvature is correlated to mass, it is expected that the mice would exhibit absolutely smaller semicircular canals. However, radius of curvature exhibits negative allometry [21], meaning that the mouse has proportionally larger canals compared to humans. In absolute terms, the canals of the mouse are much smaller, with an average SCR of 0.7 mm compared to 2.8 mm in humans [21]. In terms of absolute sensitivity, the mouse semicircular canals are less sensitive than human canals (see Table 5.1). However, functionally, the distinction is not as clear. Differences in the velocity of head movement, for example, may mean that the detection of head rotational acceleration between the two species is similar. Evidently, comparisons between the two species need to consider the differences in canal radius and its implications on sensitivity of the canals.

Semicircular canal shape Aside from the aforementioned differences in size (and its implications on sensitivity), there are significant differences of shape between

the species. First, human semicircular canals are closer to orthogonality than mouse canals. In studies using CT, the highest deviation from orthogonality was reported to be around 4° between the anterior and posterior canals [22]. In mice, however, these deviations can be as large as 12° [23]. Deviations from orthogonality are negatively correlated with vestibular sensitivity [23], which would imply that the mouse semicircular canals are less sensitive than human canals, in addition to the previously discussed loss in sensitivity due to size.

In terms of planarity, the human semicircular canals exhibit greater out-of-plane deviations than mice. This is particularly apparent in the posterior semicircular canal. Out-of-plane deviations have been previously demonstrated in humans [24–26], and the results from chapter 2 seem to agree, although this is only a visual observation as planarity was not measured for either species. Deviation from planarity has been associated with increased range of planes that can elicit flow in a particular canal [24, 25]. Therefore, comparisons between the two labyrinths must consider these out-of-plane deviations (or lack thereof) when comparing responses to a given acceleration.

In humans, the anterior and posterior canals are connected via the common crus, whilst the lateral canal is completely isolated from the other two. In mice, the lateral and posterior canal do not share a proper secondary common crus like other mammals [27], but the bony canals do share a lumen up to at least P7. The slender portion of the bony posterior and lateral canal ar not yet defined as there is no deposition of bone separating the two cavities (see **??**, Figure 3.1, in the posterior an lateral columns for P7 compared to P14). Other species, such as the dog, have a bony secondary common crus without sharing a membranous duct [28]. Nonetheless, between P7 and P14 continued bone deposition clearly divides the canals into two distinct non-communicating cavities. Since the presence of the common crus has a definite impact on the function of the anterior and posterior canals [29], a secondary common crus would therefore alter the biomechanics of fluid flow in the posterior and lateral canals. Nonetheless, this potential influence of a common crus has been studied from a membranous-only perspective. The functional implications of a bony-only secondary common crus are unclear. In the mouse, this problem is lessened as there is no common canal, rather a small communication between the two which is then closed by the time of maturity.

Lastly, the greatest difference between the two species is the shape of the cross-section of the bony canals. The results from chapter 2 show that humans have oval cross sections (as measured by the aspect ratio), whilst mice have round cross-

sections (see chapter 3). Furthermore, mice have small perilymphatic spaces, whilst humans are one of the mammalian species with large perilymphatic spaces (see chapter 4), and the membranous duct encompasses almost the entirety of the bony canal. Functional implications of these differences are discussed in a subsequent section (see section 5.6).

Labyrinth ontogeny In terms of ontogeny, it is clear that the timing of development and ossification between humans and mice is not the same. However, there are other factors at play in terms of development of the canals. One of these is the petrosal lobule of the parafloculus. It occupies the space of the subarcuate fossa and the anterior canal wraps around the opening of the fossa. It is possible that the presence and development of a subarcuate fossa could directly impact the growth of the canals. The petrosal lobule could "push" into the subarcuate fossa, forcing outwards expansion of the canals, particularly that of the anterior canal. However, adult humans do not have a distinct petrosal lobule, whilst mice do. Phylogeny and ecology appear to be significant determinants of petrosal lobules scaling [30]. Nonetheless, the presence of the subarcuate fossa has been shown to be independent from the formation of the petrosal lobule [31], so development of the fossa may still influence canal development. In humans, the subarcuate fossa is present at birth, but rapidly decreases in size after that point [32]. Nonetheless, whether it is present in adults is less relevant than whether it is present during development of the canals. Looking at the data in Table 5.1, it seems that humans have proportionally smaller anterior canals than mice, although not by a big margin. It is possible that these small differences are due to the lack of petrosal lobule, but most likely other factors, such as timing of ossification. Overall, it does not appear that the lack of petrosal lobule would impede comparisons between humans and mice.

Aside from growth of the canals themselves, it is unclear whether the growth and ossification of the petrous portion of the temporal bone is similar in both species. No peer-reviewed studies yet have compared or extensively characterised the development of the petrous bone in either species. Data from a preliminary study suggests that petrous length growth in mice is significant after the labyrinth has mostly completed ossification (by the P7 stage). The growth rate appears to stabilise at around P14, which is contemporaneous to stabilisation of the semicircular canal size. The width on the other hand seems to be stable from P1, meaning it has reached its final width at the time of birth [33]. In humans, petrous bone growth (both width and length) continues postnatally, well after complete ossification of the bony labyrinth.

Table 5.2: Developmental stage length for *Homo sapiens* and *Mus musculus*. Based on Dutta & Sengupta [36]

Developmental stage	Human	Mouse	Human days:mouse days
Weaning	180	28	6.43:1
Prepuberty	4198	42	99.5:1
Adulthood onset	7300	70	104.3:1
Reproductive senecence	18615	450	41.37:1
Post-senescence phase	10585	60	176.4:1

Lifespan and developmental stages Another major difference between humans and mice is the lifespan and timing of life stages. The average lifespan of *Mus musculus* is around 24 months [34] and the human (global) life expectancy is 73 years [35]. Overall, 40 human days would be equivalent to 1 mouse day, but the developmental stages do not correlate 40:1 throughout their entire life. For example, looking at the weaning period, the ratio is 6.43 human days to 1 mouse day (P28 in mice to 180 days in humans) [36]. The relative duration of each life stage can be seen on Table 5.2. It must be noted that not only every stage may have different day ratios, but the definition for each stage changes by species. In the mouse, for example, adulthood onset is based on sexual maturity, whereas in humans it is determined by the growth plate closure. Furthermore, other stages, such as time of onset of locomotion are not the same in both species, and still have great relevance when assessing semicircular canal ontogeny and function.

Overall, researchers should exercise caution when using mouse as a model species for studying human bony labyrinth development, as the differeces outlined above may influence the results, particularly in terms of developmental milestones and direct functional extrapolations.

5.5 Implications on timing of ossification

The timing of ossification of the bony labyrinth is different across mammals. Early onset of overall cranial ossification has been observed in slow-growing species, and it is likely a function of gestation time [37]. Basicranial timing of ossification also appears to be the most labile in terms of timing in inter-species comparisons. Slow-growing species are also usually larger, as gestation time is correlated with mass at birth, but it is even more highly correlated with brain mass at birth [38]. Therefore, species that are larger, have longer gestation periods and bigger brain mass are more

likely to begin cranial ossification earlier.

As discussed in a previous section, it is possible that early ossification of the cranial bones is a way to prevent potential deleterious shape changes that can occur during development (particularly rapid growth) of adjacent tissues. For example, growth in the cranial midline can exert stress on the petrous bone, which if unossified, could lead to strain in the In chapter chapter 3, the bony canal postnatal development was assessed. In contrast to humans, *Mus musculus* semicircular canals do not ossify prenatally, which allowed for assessment of post-natal morphology both in the pre- and post-ossification stages. Bone deposition in the petrous bone is visible in the P1 stage, although no bone deposition can be seen around the semicircular canals. By P7 there is a thin layer of bone completely surrounding the semicircular canals, which continues to thicken up to P28 (M1 group in this study). The results showed that the murine labyrinth continues growth from days 1 to 14, with the highest growth rate between days 1 and 7. After day 7, development plateaus, aside from a small increase in size between days 7 and 14. There are some shape changes during the first postnatal week, including increased torsion of the anterior canal and rounding of all three canals. After this point, no significant changes in shape or size were observed, although bone deposition around the canals continued until around 28 days. In both humans and mice, no functionally significant shape changes were observed after ossification, which would imply that inhibition of shape and size changes is linked to ossification of the canals in mice (and possibly other, if not all, mammals)., causing a form change. The timing of ossification between different cranial bones, therefore, could be key determinant of shape and size outcomes. Structures that ossify later are more labile to outside forces than those already ossified, due to the differences in material properties between hyaline cartilage and bone. This could be the explanation for early ossification of the bony labyrinth in humans. Human otic capsule ossification occurs prenatally, with the earliest ossification centres appearing around gestational week 16 [39]. In contrast, ossification in mice occurs postnatally, around P7, although bone deposition continues centrifugally until around P28 (M1 group in this study, see chapter 3). Since humans have larger crania and proportionally smaller canals, the stress exerted on the bony labyrinth due to cranial growth and development is much larger. In contrast, mice have very large canals in proportion to head size, and the stress exerted on them is much smaller.

Both mice and humans achieve near adult form at the time of ossification, although there are some negligible changes of size after this timepoint. In both

species, ossification is the limiting factor for semicircular canal form development. Whether this can be extrapolated to all mammals is uncertain. Reports show that in cetaceans, radius of curvature was at least 51% of the adult size, and the largest specimen studied had reached only 66% adult size at the time of ossification [40]. One of the possible explanations for this phenomenon is that perhaps the specimens measured would not have reached adult size at all, and it is more difficult to create an accurate timeline as the specimens included in the study lacked age data and were characterised by body length and other morphological data. Nonetheless, cetaceans exhibit smaller semicircular canals than terrestrial mammals and early ossification, even before reaching adult size, could be due to the need to protect the shape via ossification. This would prevent the stress from growing adjacent tissues to form a potentially deleterious shape.

Body mass and gestation periods are also related to maturity at birth. Precocial mammals, for example, produce larger neonates. They also usually undergo longer gestation periods and reach adult size at a slower rate than altricial mammals [41]. It follows that precocial mammals, with their longer gestation periods would begin ossification of the labyrinth earlier than altricial mammals, which would be advantageous in regards to their locomotor abilities at the time of birth. Overall, there is little information in regards to timing of ossification of the bony labyrinth specifically, but it is known for some species. *Ornythorincus, Echidna,* and *Oryctolagus* [42], *Mesocricetus* [43], *Monodelphis* and *Macropus* [44], and *Canis* [42] –all altricial species –begin ossification of the bony labyrinth postnatally. In contrast, *Sus* [42], *Cetacea* [40], and *Homo* all begin ossification of the labyrinth prenatally. It must be noted here that humans are altricial in terms of locomotion, unlike *Sus* and *Cetacea*, whist all of them have early onset of ossification. In humans, gestation length has been positively correlated with bone mineral density [45]. However, this does not appear to be the case in pigs, as shortened gestation periods did not have a significant effect on bone strength [46], suggesting that the early development of the skeleton is impervious to gestation length. In both of these instances, the focus was on the appendicular skeleton and included long bones, which still undergo extensive development after birth. Whether ossified portions of the cranium exhibit the same outcomes remains to be seen. Furthermore, lengthening of appendicular bones is accompanied by lengthening of the surrounding structures, which biomechanically would only cause strain in the desired direction. Most likely, the early ossification of the bony labyrinth is indeed related to the quick growth of the cranium, where stress is applied in several directions.

Other factors driving onset of ossificaton Other factors may also be involved in the early ossification of the bony labyrinth. Given its relationship with the visual system via the vestibulo-ocular reflex, it is possible that achievement of semicircular canal maturity is somewhat correlated to onset of vision in a given species. Mice open their eyes at around 12 days postnatally [47], 5 days later than ossification of the bony labyrinth, but at similar time to when shape and size have stopped development. In contrast, humans open their eyes at the time of birth, but visual acuity is very low at this point, and continues developing during the first year of life. At this time point, however, the semicircular canals are fully ossified, so it appears that time to visual onset is not the driving force for ossification in humans. Indeed, in both species studied here, maturity of the semicircular canals is reached before visual onset, although the ossification of the human canals seems extremely precocious in this sense.

Locomotion is another important factor related to the semicircular canals. Onset of locomotion in mice appears early, as they begin crawling between P0 and P5. Full transition to walking does not occur until P5-P10 [48]. Timing of the onset of locomotion is contemporaneous to the beginning of ossification of the canals, and it appears that transition to walking is also in time with the canals achieving full size. Contrastingly, in humans locomotion onset is not until around 1 year postnatally, whereas the canals are fully ossified.

Overall, the timing of ossification of the semicircular canals in mice appears to be related to the onset of vision and locomotion, all off which occur between P7 and P14. Early ossification of human semicircular canals must be driven by other forces.

It must also be considered that not only the semicircular canals ossify prenatally: the entire bony labyrinth –including the cochlea –ossifies prenatally. It is possible that although the related systems and functional pressure for the vestibular apparatus (vision, holding the head up, locomotion, etc) are not developed until later in postnatal life, other functional pressures are. In humans, hearing onset occurs as early as 19 weeks in utero [49]. The cochlea ossifies at the same time as the semicircular canals [50]. It is possible that there is no functional drive behind the ossification of the semicircular canals at such an early stage, rather that ossification of the entire bony labyrinth may be driven by the ossification of the cochlea. It must be noted here that the auditory responsiveness is not fully mature at this point, but the continued development is most likely due to further development of the ventral cochlear nucleus and other soft tissue structures.

Early development of the vestibular system may be beneficial for motor control.

Although mice do not open their eyes until around P14, but vestibular afferents and central neurons already display some functionality in rats before this stage [51]. The early development of the vestibular apparatus seems to precede eye maturation, but may reduce the time for the VOR development once the eyes mature and calibration of the reflex can be made. Nonetheless, it is important to note that the VOR will not fully develop until vision onset, as vision impairment leads to VOR impairment [52]. Similarly, postural control requires a functional vestibular system, as well as muscle maturation and a wide range of neuronal connections and projections. Evidently, early maturation of the vestibular apparatus is beneficial for development of these reflexes, as rats that experienced weightlessness during development have been shown to have abnormal responses to stimuli and decreased branching of afferent neurons[53].

5.6 Cross-section shape and perilymphatic space

As has been established in chapter 4, it appears that the cross-section shape of the canals can be indicative of the ratio of endolymphatic to perilymphatic spaces. Rounder bony canals are indicative of a small perilymphatic space, whereas an oval cross-section is indicative of a large perilymphatic space. More importantly, the aspect ratio of the cross-section can be used to differentiate between small and large perilymphatic groups.

Phylogeny plays an important role in the presence or absence of the perilymphatic space. Primates have larger perilymphatic spaces, especially when compared to other clades. Humans, however, have markedly larger perilymphatic spaces, even when compared to other primates. Other mammalian species do not appear to have a defined perilymphatic space, with the notable exceptions of *Loxodonta*, *Halichoerus* and *Phoca*. Likely, the phylogenetic signal is the main determinant, and the remaining variation may be driven by functional factors, perhaps even by increased sensitivity.

One of the main implications of a species having an enlarged perilymphatic space is that the endolymphatic space does not encompass the entirety or the majority of the bony canal lumen. In species with little to no perilymphatic space, the membranous canals are in contact with the bony canal walls, and any potential expansion is stalled by the wall. However, it appears that in species with an enlarged perilymphatic space the membranous ducts do not sit in the centre of the canal, rather they lie against the outer wall (see chapter 1 and chapter 4). In this instance,

one of the membranous walls functions as a rigid wall and the wall in contact with the perilymphatic space has the capacity to expand due to changes in pressure gradients.

During a given acceleration, a pressure gradient is formed across the canals. The greater the pressure gradient is, the larger the strain is on the cupula, which translates to increased sensitivity [54]. The pressure gradient increases with increases in distance to the centre of rotation, but this is only true of rigid systems. Biomechanical models used to describe semicircular canal function usually follow the assumption of a rigid membranous wall [see for example 55–57]. These models do not account for membranous duct wall elasticity, and therefore may not be as applicable to species with large perilymphatic spaces. Steer Jr [58] described a model more akin to the human semicircular canal morphology, and explained that a flexible membranous duct attached on the outer wall to the bony canal would be constricted (reduce cross-section area) at the point where the acceleration pushes against the bony wall, and would expand where the acceleration pushes it away. How much constriction of the cross-section area may be dependent on the biomechanical properties of the fibroblast mesh surrounding the canals, although expansion is possible regardless of these properties. Rabbitt *et al.* [59] developed a 1 dimensional model of a lateral semicircular canal that included the perilymph and bony labyrinth, as well as a flexible membranous duct. They found that this model predicted flow of the perilymph that could displace the cupula at high frequencies (>5 Hz) by deforming the membranous duct. This deformation extends the bandwidth of potential frequencies that can be detected. Evidently, the same biomechanical models, with enlarged perilymphatic spaces, may not be applicable to species such as the mouse, with a small – almost negligible – perilymphatic space. Canals with large perilymphatic spaces are more likely to expand and contract in response to a given acceleration. Models that are tested under conditions where the accelerations occur about the axis of the canal may not highlight these differences as starkly, especially given the fact that accelerations with the axis of rotation outside the axis of the canal are more representative of naturally-occurring accelerations.

Studies regarding the evolution of locomotion have focused on measurements of the semicircular canals, usually of the radius of curvature by measuring the height and width of the canals [60], or using geometric morphometrics [61]. However, these studies fail to account for the possibility of the presence of an enlarged perilymphatic space. In measuring the radius of curvature, whether the measurement is taken from the centroid of the canal or the outer edge could alter the results, as in species with larger perilymphatic spaces the distance from the centroid of the

bony canal to the centroid of the membranous canal would be different. Similarly, using geometric morphometrics would have similar problems, as the landmarks are usually placed in the centroid of the bony canal. Evidently, in extinct species it is impossible to determine the exact position and cross-section area of the membranous ducts, but fossils that display oval cross-sections are more likely to have enlarged perilymphatic spaces. When studying inter-specific variation, it is important to take this into account, as it may artificially skew the results of the study. This is not as big a problem when studying intra-specific variation, as the error would be even throughout the sample, but it may carry more weight when comparing inter-specific differences or when extrapolating function from the geometry.

Cross-section duct area plays a key role on semicircular canal sensitivity. Larger cross-section area of the membranous duct reduces the viscous flow and alters the operating range of the canals, and these parameters are also dependent on the viscosity of the lymphatic fluids [62]. Aside from inferring sensitivity or tracking locomotor or agility trends, this principle has been used to study other traits, such as the origins of mammalian endothermy [63]. In this case, the authors argue that changes in body temperature alter the viscosity of the endo- and perilymph, and therefore the morphology of the semicircular membranous ducts would have to adapt in order to account for these changes in viscosity, to keep function stable. As per the results in chapter 4, the presence of an enlarged perilymphatic space makes the morphology of the semicircular ducts different from that of the bony canal. In this particular study, the species included in the extant mammalian sample would mostly fall within the category of a small perilymphatic space (and therefore would exhibit high correspondence between bony and membranous morphology). However, many of the species included, especially aves, do not follow this assumption. Furthermore, it is difficult to ascertain where the extinct sample would fall in terms of perilymphatic space size. Phylogenetic regressions that use the radius of curvature without any membranous data (n.b. this is the minority of the species used) could potentially lead to skewed results, as the radius could be slightly larger in species with large perilymphatic spaces. However, potential probelms could arise when using the bony cross-section area as a proxy for memrbanous cross-section area, in particular for species with large perilymphatic spaces, where the differences can be up to 5 times larger.

Overall, the use of the bony labyrinth morphology as a proxy for membranous duct data should be done with caution, particularly in terms of cross-section area, and the results need to consider the possibility of an enlarged perilymphatic space altering the results in terms of sensitivity, locomotion, agility, morphology variation

between closely related species and other functional implications.

5.7 Implications on semicircular canal form and function

Semicircular canal size (either radius of curvature or centroid size) is correlated with mass, with negative allometry. When comparing different species with similar mass, it appears that proportionally larger canals are linked with agility, such that more agile species have larger canals [21]. However, the present study did not find a significant correlation between agility and mass, although the sample studied here was a much smaller group of mammalian species. Nonetheless, it is possible that the explanation in the variance of radius of curvature is not necessarily due to agility per se, but rather to agility-related factors, such as gaze-stabilisation. A study conducted in 104 mammalian species found that after controlling for mass and phylogeny, eye size and visual acuity account for a significant proportion of the radius of curvature variation [64]. More importantly, agility did not explain this variation when body mas and eye size were controlled for. Nonetheless, mass still accounts for most of the interspecific variation in radius of curvature. The relationship with agility is not as clear, but factors such as eye size and visual acuity are inextricably related to agility, so that the variation is already accounted for. Yet, it is still possible that agility per se may explain some of the variation, but perhaps the method for characterising agility has not considered factors such as angular head acceleration, which would more directly relate to semicircular canal function.

It appears that the relationship between agility and SCR is conserved throughout vertebrates. In birds, semicircular canal centroid size is correlated with mass [65]. Secondary to mass, wing kinematics explain some of the variance in canal size, which again supports the notion for agility-driven selection of larger canal size, although indirectly. In contrast, ecology appears to be correlated with labyrinth size in turtles, with terrestrial turtles having relatively smaller canals [66]. Interestingly, although ecology appears to play a role, agility does not seem to explain this variation, as the relative canal size of turtles is greater than mammals whilst being usually less agile.

It is possible that the main limiting factor for semicircular canal size is the spatial constraints of the braincase across species, although some seem to be more affected than others. Head shape, particularly in species with flat heads (small vertical space) have limited space for semicircular canal expansion, which would lead to

smaller or potentially longer but more elliptical canals. In mammals, there appears to be no correlation [67], but it is the case with squamates [68]. Increased length at the expense of circularity appears to decrease sensitivity in extreme cases (high ellipticity) [56, 68], whilst in non-extreme cases the increased radius of curvature compensates for the loss in sensitivity due to ellipticity by increasing endolymph displacement. In a much more extreme case, the Saddleback toad (*Brachycephalus*) exhibits incredibly small semicircular canals [69], where the main concern is the lumen radius, as the small size increases resistance and reduces flow [70]. This, evidently, is due to the small available space in the head, although compensations in terms of ellipticity do not alter the flow issue. Potentially, when space is available, agility-related factors may play a bigger role in canal size, allowing for functional pressures to refine the system, whereas head size and braincase size may play a limiting role.

5.8 Future work

It has been made clear that in both humans and mice (and possibly other species with ossified labyrinths) ossification is the limiting factor for canal form variation, regardless of other developmental stages, functional forces or environmental factors that may occur afterwards. When the canals are still in their cartilaginous stage, however, size and shape can change rapidly. To test this hypothesis further, it would be relevant to study a species, namely a cartilaginous fish. In these species, the "bony" canals never ossify, therefore is there a limiting factor at all in these species? Is there a potential for shape and size of the canals to continue to change and adapt to different locomotive or visual requirements? Would the canals continue to develop and change throughout life? Would a single species dwelling in different environments be able to adapt to different functional requirements?

These questions could also be tested by using a mouse model, such as the Membrane-type matrix metalloproteinase I (MT1-MMP)-deficient mice, to elucidate the relationship between form maturity and complete ossification. Most mice with delayed ossification die hours after birth, but this particular model has been shown to live around 3 weeks [71], longer than the canals take to reach maturity. Delayed ossification leave the potential for more form changes, particularly growth, unless factors other than ossification are at play for the continued expansion of the canals.

To continue the research regarding the presence or absence of the perilymphatic

space, it would be important to continue to accurately characterise the membranous duct morphology, as the current data is based on histological 2D measurements and estimations from labyrinth photographs. Acquiring fresh specimens and using imaging techniques that do not disrupt the duct morphology would further our understanding of the relationship between the endolymphatic and perilymphatic spaces. Ideally, this would include the species already in this study, as well as a wider array of species. This could help to more accurately define the relationship between the cross-section shape of the bony canals with the perilymphatic space.

Most importantly, the morphology of the perilymphatic space should be taken into consideration to inform biomechanical models of semicircular canal function. The inclusion of a large perilymphatic space could change the behaviour of the membranous ducts and the endolymph and perilymph movement throughout the canals. Additionally, the position of the membranous ducts should be appropriately characterised as well: one rigid wall and one elastic wall, which most likely would perform differently to rotational accelerations than a model with a single lymphatic space and rigid walls. Furthermore, the presence of the perilymphatic fibroblast mesh could be included, as to model the potential expansion or compression of the endolymphatic ducts.

5.9 Conclusions

The first aim of this study was to investigate whether ossification was the limiting factor for human bony semicircular canal bone form development, and whether there was a possibility for post-ossification form changes. This was the first study to assess the postnatal form of the human semicircular canals. No other studies have focus on ontogenetically driven intra-specific variations in the human semicircular canals. A key strength of this study was the inclusion of the perinatal samples. These types of samples are particularly difficult to source, but were necessary as they allowed for a comprehensive look at the potential changes that can occur in postnatal life. It is especially important in humans to look at the perinatal specimens since many developmental stages related to the function of the semicircular canals, such as visual acuity, holding the head upright and transition to bipedalism, occur after this stage. This study confirmed that there are negligible changes to the semicircular canal form in postnatal life, and those small changes are unlikely to bring any functional differences. These findings suggest that, in humans, timing of form and function of the semicircular canals have diverged, although the function is still dependent on

the geometry of the canals. Bony canals ossify in prenatal life, whilst the functional paradigm continues to change both massively and rapidly, especially in the first year of life. The prenatal maturation and ossification of the canals must be driven by other factors.

Supporting the findings in humans, the results from the murine study showed that the bony canals undergo negligible form changes after complete ossification, with the exception of a modest increase in size. These results confirm that ossification is the limiting factor for semicircular canal form development, and adult shape and size will be determined by the shape and size at the time of completeion of ossification.

The murine bony labyrinth, however, has significant differences from that of the humans from an ontogenetic perspective. The late ossification (in postnatal life) being one of the main ones. Crucially, development of the semicircular canals, in particular in terms of growth, is incredibly rapid after birth (first two weeks postnatally). This study has raised important questions about the use of mice as a model species for the human vestibular apparatus. Mice are not good models for studying functional-developmental relationships of the human semicircular canals. Studies focusing on developmental-functional implications of the human canals should not use mice as a model species. Clearly, prenatal interventions or factors have the potential to alter development in both species, but the murine model will be much more susceptible to environmental factors in postnatal life. Furthermore, the wildly different early postnatal stages between these two species make it nearly impossible to match morphological and functional development, which would make comparisons difficult.

The last aim of this study was to assess several cranial and cross-section variables to elucidate whether it was possible to infer the presence or absence of an enlarged perilymphatic space. This study was the first to investigate the cross-section shape of the semicircular canals across several mammalian species. Despite its exploratory nature, this study offers some insights into the potential functional implications of an enlarged perilymphatic space, in particular as to the rigid or elastic nature of the membranous wall. The evidence from this study suggest that the membranous duct morphology cannot be inferred from the bony labyrinth. The insights gained from this study may be of assistance to researchers investigating extinct species in particular, as caution is necessary when extrapolating bony labyrinth data to functional implications.

References

1. Smith, C. F. *et al.* Understanding Beliefs, Preferences and Actions amongst Potential Body Donors. *Anatomical Sciences Education* **16,** 224–236. ISSN: 1935-9780 (2023).
2. Osipov, B. *et al.* Sexual Dimorphism of the Bony Labyrinth: A New Age-Independent Method. *American journal of physical anthropology* **151,** 290–301. ISSN: 1096-8644 0002-9483. pmid: 23640711 (2013).
3. Li, H. *et al.* Vestibular Organ and Cochlear Implantation–A Synchrotron and Micro-CT Study. *Frontiers in Neurology* **12.** ISSN: 1664-2295 (2021).
4. Elfarnawany, M. *et al.* Micro-CT versus synchrotron radiation phase contrast imaging of human cochlea. *Journal of Microscopy* **265,** 349–357. ISSN: 1365-2818 (2017).
5. Iyer, J. S. *et al.* Visualizing the 3D Cytoarchitecture of the Human Cochlea in an Intact Temporal Bone Using Synchrotron Radiation Phase Contrast Imaging. *Biomedical Optics Express* **9,** 3757–3767. ISSN: 2156-7085 (2018).
6. Frisch, T., Overgaard, S., Sørensen, M. S. & Bretlau, P. Estimation of Volume Referent Bone Turnover in the Otic Capsule after Sequential Point Labeling. *Annals of Otology, Rhinology & Laryngology* **109,** 33–39. ISSN: 0003-4894 (2000).
7. Zehnder, A. F. *et al.* Osteoprotegrin Knockout Mice Demonstrate Abnormal Remodeling of the Otic Capsule and Progressive Hearing Loss. *The Laryngoscope* (2006).
8. Taxak, P. & Ram, C. Labyrinthitis and Labyrinthitis Ossificans - A Case Report and Review of the Literature. *Journal of Radiology Case Reports* **14,** 1–6. ISSN: 1943-0922. pmid: 33082921 (2020).
9. Bloch, S. L., McKenna, M. J., Adams, J. & Friis, M. Labyrinthitis Ossificans: On the Mechanism of Perilabyrinthine Bone Remodeling. *Annals of Otology, Rhinology & Laryngology* **124,** 649–654. ISSN: 0003-4894 (2015).
10. Duncan, R. L. & Turner, C. H. Mechanotransduction and the Functional Response of Bone to Mechanical Strain. *Calcified Tissue International* **57,** 344–358. ISSN: 0171-967X. pmid: 8564797 (1995).

11. Morse, A. *et al.* Mechanical Load Increases in Bone Formation via a Sclerostin-Independent Pathway. *Journal of Bone and Mineral Research* **29,** 2456–2467 (2014).

12. Toro-Ibacache, V., Zapata Muñoz, V. & O' Higgins, P. The Relationship between Skull Morphology, Masticatory Muscle Force and Cranial Skeletal Deformation during Biting. *Annals of Anatomy - Anatomischer Anzeiger. SI: Dental Morphology Research - Past Meets Present* **203,** 59–68. ISSN: 0940-9602 (2016).

13. Endo, B. Analysis of Stresses around the Orbit Due to Masseter and Temporalis Muscles Respectively. *Journal of the Anthropological Society of Nippon* **78,** 251–266 (1970).

14. Kragt, G., Ten Bosch, J. & Borsboom, P. Measurement of Bone Displacement in a Macerated Human Skull Induced by Orthodontic Forces; A Holographic Study. *Journal of Biomechanics* **12,** 905–910. ISSN: 00219290 (1979).

15. Proops, D. W., Hawke, W. M. & Berger, G. Microfractures of the Otic Capsule: The Possible Role of Masticatory Stress. *The Journal of Laryngology & Otology* **100,** 749–758. ISSN: 0022-2151, 1748-5460 (1986).

16. Ho, J., Zhou, Z., Li, X. & Kleiven, S. The Peculiar Properties of the Falx and Tentorium in Brain Injury Biomechanics. *Journal of Biomechanics* **60,** 243–247. ISSN: 0021-9290 (2017).

17. Kiroglu, Y., Calli, C., Karabulut, N. & Cagatay, O. Intracranial Calcifications on Computed Tomography: Pictorial Essay. *Diagnostic and Interventional Radiology.* ISSN: 1305-3825 (2009).

18. Bloch, S. L. & Sørensen, M. S. The Viability and Spatial Distribution of Osteocytes in the Human Labyrinthine Capsule: A Quantitative Study Using Vector-Based Stereology. *Hearing Research* **270,** 65–70. ISSN: 0378-5955 (2010).

19. Ekdale, E. G. Comparative Anatomy of the Bony Labyrinth (Inner Ear) of Placental Mammals. *PLOS ONE* **8,** e66624. ISSN: 1932-6203 (2013).

20. Yang, A. & Hullar, T. E. Relationship of Semicircular Canal Size to Vestibular-Nerve Afferent Sensitivity in Mammals. *Journal of neurophysiology* **98,** 3197–3205. ISSN: 0022-3077 (2007).

21. Spoor, F. *et al.* The Primate Semicircular Canal System and Locomotion. *Proceedings of the National Academy of Sciences* **104,** 10808–10812. ISSN: 0027-8424. pmid: 17576932 (2007).

22. Della Santina, C. C., Potyagaylo, V., Migliaccio, A. A., Minor, L. B. & Carey, J. P. Orientation of Human Semicircular Canals Measured by Three-Dimensional Multiplanar CT Reconstruction. *Journal of the Association for Research in Otolaryngology* **6,** 191–206 (2005).

23. Berlin, J. C., Kirk, E. C. & Rowe, T. B. Functional Implications of Ubiquitous Semicircular Canal Non-Orthogonality in Mammals. *PLoS One* **8,** e79585. ISSN: 1932-6203 (2013).

24. Tremble, G. E. The Bony Labyrinth Of The New-born Infant And Of The Adult: A Comparative Study. *Archives of Otolaryngology - Head and Neck Surgery* **9,** 175–180. ISSN: 0886-4470 (1929).

25. Muren, C., Ruhn, G. & Wilbrand, H. Anatomic Variations of the Human Semicircular Canals: A Radioanatomic Investigation. *Acta Radiologica. Diagnosis* **27,** 157–163. ISSN: 0567-8056 (1986).

26. Sato, H., Sando, I., Takahashi, H. & Fujita, S. Torsion of the Human Semicircular Canals and Its Influence on Their Angular Relationships. *Acta Oto-Laryngologica* **113,** 171–175. ISSN: 0001-6489, 1651-2251 (1993).

27. Gray, A. A. *The Labyrinth of Animals: Including Mammals, Birds, Reptiles and Amphibians* (J. & A. Churchill, 1908).

28. Ekdale, E. G. & Rowe, T. Morphology and Variation within the Bony Labyrinth of Zhelestids (Mammalia, Eutheria) and Other Therian Mammals. *Journal of Vertebrate Paleontology* **31,** 658–675. ISSN: 0272-4634 (2011).

29. Muller, M. & Verhagen, J. H. G. Optimization of the Mechanical Performance of a Two-duct Semicircular Duct System—Part 1: Dynamics and Duct Dimensions. *Journal of Theoretical Biology* **216,** 409–424. ISSN: 0022-5193 (2002).

30. Lang, M. M. *et al.* Scaling Patterns of Cerebellar Petrosal Lobules in Euarchontoglires: Impacts of Ecology and Phylogeny. *The Anatomical Record,* ar.24929. ISSN: 1932-8486, 1932-8494 (2022).

31. Jeffery, N., Ryan, T. M. & Spoor, F. The Primate Subarcuate Fossa and Its Relationship to the Semicircular Canals Part II: Adult Interspecific Variation. *Journal of Human Evolution* **55,** 326–339. ISSN: 0047-2484 (2008).

32. Carayon, D., Vaysse, F., Tramini, P., Dumoncel, J. & Esclassan, R. The Age-Related Maturational Pattern of the Human Subarcuate Fossa (Petromastoid Canal). Preliminary Results from the Application of a New Three-Dimensional Analytical Approach. *Comptes Rendus Palevol* **14,** 139–145. ISSN: 1631-0683 (2015).

33. Varvares, A. M., Mcnulty, M. A., Holmes, M. A. & Deleon, V. B. *Comparative Analysis of the Growth and Development of the TemporalBbone in Mice and Humans* in *AMERICAN JOURNAL OF PHYSICAL ANTHROPOLOGY* **159** (2016), 322–322.

34. Wilkinson, J. E. *et al.* Rapamycin Slows Aging in Mice. *Aging Cell* **11,** 675–682. ISSN: 1474-9726 (2012).

35. *Life Expectancy at Birth (Years)* World Health Organisation. `https://www.who.int/data/gho/data/indicators/indicator-details/GHO/life-expectancy-at-birth-(years)` (2022).

36. Dutta, S. & Sengupta, P. Men and Mice: Relating Their Ages. *Life Sciences* **152,** 244–248. ISSN: 0024-3205 (2016).

37. Sánchez-Villagra, M. R., Goswami, A., Weisbecker, V., Mock, O. & Kuratani, S. Conserved Relative Timing of Cranial Ossification Patterns in Early Mammalian Evolution. *Evolution & Development* **10,** 519–530. ISSN: 1525-142X (2008).

38. Sacher, G. A. & Staffeldt, E. F. Relation of Gestation Time to Brain Weight for Placental Mammals: Implications for the Theory of Vertebrate Growth. *The American Naturalist* **108,** 593–615. ISSN: 0003-0147, 1537-5323 (1974).

39. Som, P. & Naidich, T. Development of the Skull Base and Calvarium: An Overview of the Progression from Mesenchyme to Chondrification to Ossification. *Neurographics* **3,** 169–184 (2013).

40. Thean, T., Kardjilov, N. & Asher, R. J. Inner Ear Development in Cetaceans. *Journal of anatomy* **230,** 249–261. ISSN: 1469-7580 0021-8782. pmid: 27995620 (2017).

41. Derrickson, E. M. Comparative Reproductive Strategies of Altricial and Precocial Eutherian Mammals. *Functional Ecology* **6,** 57. ISSN: 02698463. JSTOR: 2389771 (1992).

42. De Beer, G. *The Development of the Vertebrate Skull.* Reprint. 546 pp. (Clarendon Press, Oxford, 1937).

43. Van Arsdel III, W. C. The Ossification of the Middle and Internal Ear of the Golden Hamster (Cricetus Auratus) (1951).

44. Clark, C. T. & Smith, K. K. Cranial Osteogenesis in Monodelphis Domestica (Didelphidae) and Macropus Eugenii (Macropodidae). *Journal of Morphology* **215,** 119–149. ISSN: 1097-4687 (1993).

45. Longhi, S. *et al.* Prematurity and Low Birth Weight Lead to Altered Bone Geometry, Strength, and Quality in Children. *Journal of Endocrinological Investigation* **38,** 563–568. ISSN: 1720-8386 (2015).

46. Magrini, S. H., Mossor, A. M., German, R. Z. & Young, J. W. Developmental Factors Influencing Bone Strength in Precocial Mammals: An Infant Pig Model. *Journal of Anatomy* **n/a.** ISSN: 1469-7580.

47. Fox, W. M. Reflex-Ontogeny and Behavioural Development of the Mouse. *Animal Behaviour* **13,** 234–IN5. ISSN: 0003-3472 (1965).

48. Williams, E. & Scott, J. P. The Development of Social Behavior Patterns in the Mouse, in Relation To Natural Periods 1). *Behaviour* **6,** 35–64. ISSN: 0005-7959, 1568-539X (1954).

49. Hepper, P. G. & Shahidullah, B. S. Development of Fetal Hearing. *Archives of Disease in Childhood Fetal and Neonatal edition* **71,** F81–F87. ISSN: 1359-2998. pmid: 7979483 (1994).

50. Richard, C. *et al.* Inner Ear Ossification and Mineralization Kinetics in Human Embryonic Development - Microtomographic and Histomorphological Study. *Scientific Reports* **7,** 4825. ISSN: 2045-2322 (1 2017).

51. Curthoys, I. S. Postnatal Developmental Changes in the Response of Rat Primary Horizontal Semicircular Canal Neurons to Sinusoidal Angular Accelerations. *Experimental Brain Research* **47,** 295–300 (1982).

52. Sherman, K. R. & Keller, E. L. Vestibulo-Ocular Reflexes of Adventitiously and Congenitally Blind Adults. *Investigative ophthalmology & visual science* **27,** 1154–1159 (1986).

53. Ronca, A., Fritzsch, B., Bruce, L. L. & Alberts, J. R. Orbital Spaceflight during Pregnancy Shapes Function of Mammalian Vestibular System. *Behavioral neuroscience* **122,** 224 (2008).

54. Goyens, J. Modelling Shows That Stimulation of the Semicircular Canals Depends on the Rotation Centre. *Hearing Research* **396,** 108071. ISSN: 0378-5955 (2020).

55. Van Buskirk, W. C., Watts, R. G. & Liu, Y. K. The Fluid Mechanics of the Semicircular Canals. *Journal of Fluid Mechanics* **78,** 87–98. ISSN: 1469-7645 (1976).

56. Oman, C. M., Marcus, E. N. & Curthoys, I. S. The Influence of Semicircular Canal Morphology on Endolymph Flow Dynamics: An Anatomically Descriptive Mathematical Model. *Acta oto-laryngologica* **103,** 1–13. ISSN: 0001-6489 (1987).

57. Damiano, E. R. & Rabbitt, R. D. A Singular Perturbation Model of Fluid Dynamics in the Vestibular Semicircular Canal and Ampulla. *Journal of Fluid Mechanics* **307,** 333–372. ISSN: 0022-1120, 1469-7645 (1996).

58. Steer Jr, R. W. *The Influence of Angular and Linear Acceleration and Thermal Stimulation on the Human Semicircular Canal.* (Massachusetts Institute of Technology, 1967).

59. Rabbitt, R. D., Damiano, E. R. & Grant, J. W. in *The Vestibular System* 153–201 (Springer, 2004).

60. Spoor, F., Wood, B. & Zonneveld, F. Implications of Early Hominid Labyrinthine Morphology for Evolution of Human Bipedal Locomotion. *Nature* **369,** 645–648. ISSN: 1476-4687 (6482 1994).

61. Le Maitre, A., Schuetz, P., Vignaud, P. & Brunet, M. New Data about Semicircular Canal Morphology and Locomotion in Modern Hominoids. *Journal of anatomy* **231,** 95–109. ISSN: 1469-7580 0021-8782. pmid: 28523740 (2017).

62. Obrist, D. Flow Phenomena in the Inner Ear. *Annual Review of Fluid Mechanics* **51,** 487–510 (2019).

63. Araújo, R. *et al.* Inner Ear Biomechanics Reveals a Late Triassic Origin for Mammalian Endothermy. *Nature* **607,** 726–731. ISSN: 1476-4687 (7920 2022).

64. Kemp, A. D. & Kirk, E. C. Eye Size and Visual Acuity Influence Vestibular Anatomy in Mammals. *The Anatomical Record* **297,** 781–790. ISSN: 1932-8494 (2014).

65. Benson, R. B. J., Starmer-Jones, E., Close, R. A. & Walsh, S. A. Comparative Analysis of Vestibular Ecomorphology in Birds. *Journal of anatomy* **231,** 990–1018. ISSN: 1469-7580 0021-8782. pmid: 29156494 (2017).

66. Evers, S. W. *et al.* Independent Origin of Large Labyrinth Size in Turtles. *Nature Communications* **13,** 5807. ISSN: 2041-1723 (1 2022).

67. Cox, P. G. & Jeffery, N. Semicircular Canals and Agility: The Influence of Size and Shape Measures. *Journal of Anatomy* **216,** 37–47. ISSN: 0021-8782 (2010).

68. Goyens, J. High Ellipticity Reduces Semi-Circular Canal Sensitivity in Squamates Compared to Mammals. *Scientific Reports* **9,** 16428. ISSN: 2045-2322 (1 2019).

69. Essner, R. L. *et al.* Semicircular Canal Size Constrains Vestibular Function in Miniaturized Frogs. *Science Advances* **8,** eabn1104 (2022).

70. Muller, M. Size Limitations in Semicircular Duct Systems. *Journal of Theoretical Biology* **198,** 405–437. ISSN: 0022-5193 (1999).

71. Zhou, Z. *et al.* Impaired Endochondral Ossification and Angiogenesis in Mice Deficient in Membrane-Type Matrix Metalloproteinase I. *Proceedings of the National Academy of Sciences* **97,** 4052–4057 (2000).

Appendix A

Supplementary material for chapter 2

A.1 Tables

Table A.1: Available biometric and image resolution details for each specimen used in chapter 2. Ages marked as Adult are unknown, but likely to be over 60 years of age

Specimen	Age	Sex	Source/Dataset	Voxel size (mm)	Group
Y18-L	9m	Unknown	Liverpool	0.0133396	Perinate
Y18-R	9m	Unknown	Liverpool	0.0133401	Perinate
YA5-R	9m	Unknown	Liverpool	0.0133389	Perinate
YA22-R	9m	Unknown	Liverpool	0.0133384	Perinate
YA37-L	9m	Unknown	Liverpool	0.0133408	Perinate
YA37-R	9m	Unknown	Liverpool	0.0133408	Perinate
YA55-L	9m	Unknown	Liverpool	0.01334	Perinate
YA55-R	9m	Unknown	Liverpool	0.01334	Perinate
YA56-L	9m	Unknown	Liverpool	0.0133384	Perinate
YA56-R	9m	Unknown	Liverpool	0.0133398	Perinate
YA74-L	9m	Unknown	Liverpool	0.0133384	Perinate
YA74-R	9m	Unknown	Liverpool	0.0133384	Perinate

continued on next page

Table A.1: (Continued)

Specimen	Age	Sex	Source/Dataset	Voxel size (mm)	Group
YA82-L	9m	Male	Liverpool	0.01333837	Perinate
YA86-L	9m	Male	Liverpool	0.0133384	Perinate
YA86-R	9m	Male	Liverpool	0.0133384	Perinate
YA88-L	9m	Unknown	Liverpool	0.0133384	Perinate
YA90-L	9m	Female	Liverpool	0.0133389	Perinate
YA90-R	9m	Female	Liverpool	0.0133384	Perinate
YA143-R	9m	Unknown	Liverpool	0.0133405	Perinate
YA153-L	9m	Male	Liverpool	0.0133374	Perinate
YA153-R	9m	Unknown	Liverpool	0.0133367	Perinate
YA166-L	9m	Unknown	Liverpool	0.0133362	Perinate
YA166-R	9m	Unknown	Liverpool	0.0133367	Perinate
YA175-L	9m	Female	Liverpool	0.0133391	Perinate
YA175-R	9m	Female	Liverpool	0.01334	Perinate
YA176-L	9m	Female	Liverpool	0.0133384	Perinate
YA190-L	9m	Unknown	Liverpool	0.01334	Perinate
YA190-R	9m	Unknown	Liverpool	0.01334	Perinate
YA199-L	9m	Male	Liverpool	0.01334	Perinate
YA199-R	9m	Male	Liverpool	0.01334	Perinate
YA230-L	9m	Unknown	Liverpool	0.0133408	Perinate
YA230-R	9m	Unknown	Liverpool	0.01334	Perinate
YA237-L	9m	Male	Liverpool	0.0133384	Perinate
YA267-L	9m	Male	Liverpool	0.0133389	Perinate
YA267-R	9m	Male	Liverpool	0.0133384	Perinate
YA272-R	9m	Female	Liverpool	0.01334	Perinate
YC2-L	9m	Unknown	Liverpool	0.0133401	Perinate
YD-L	9m	Unknown	Liverpool	0.0133408	Perinate
YD-R	9m	Unknown	Liverpool	0.0133408	Perinate
YK-L	9m	Unknown	Liverpool	0.0133396	Perinate
YK-R	9m	Unknown	Liverpool	0.0133401	Perinate
O11688	Adult	Unknown	Liverpool	0.0151997	Adult
O14097	Adult	Unknown	Liverpool	0.0151997	Adult

continued on next page

Table A.1: (Continued)

Specimen	Age	Sex	Source/Dataset	Voxel size (mm)	Group
O14128	Adult	Unknown	Liverpool	0.0151997	Adult
O14129	Adult	Unknown	Liverpool	0.0151997	Adult
O122571	Adult	Unknown	Liverpool	0.0152	Adult
YA165-R	9m	Unknown	Liverpool	0.01334	Perinate
YL6-R	9m	Unknown	Liverpool	0.0133384	Perinate
YL7-L	9m	Unknown	Liverpool	0.0133396	Perinate
YL7-R	9m	Unknown	Liverpool	0.0133396	Perinate
YS14-L	9m	Unknown	Liverpool	0.0133401	Perinate
YS31-R	9m	Unknown	Liverpool	0.0133401	Perinate
YS68-L	9m	Unknown	Liverpool	0.0133396	Perinate
O1M	Adult	Unknown	Liverpool	0.013201	Adult
O7M	Adult	Unknown	Liverpool	0.0132008	Adult
O8M	Adult	Unknown	Liverpool	0.0132008	Adult
O10M	Adult	Unknown	Liverpool	0.0132108	Adult
O11M	Adult	Unknown	Liverpool	0.0132008	Adult
O13M	Adult	Unknown	Liverpool	0.01320078	Adult
O15M	Adult	Unknown	Liverpool	0.0132008	Adult
O14M	Adult	Unknown	Liverpool	0.01321	Adult
O17M	Adult	Unknown	Liverpool	0.01321	Adult
O18M	Adult	Unknown	Liverpool	0.01321	Adult
O19M	Adult	Unknown	Liverpool	0.01321	Adult
O4M	Adult	Unknown	Liverpool	0.01321	Adult
Hum1	87	Unknown	Cambridge	0.024881848	Adult
Hum2	82	Unknown	Cambridge	0.022268293	Adult
Hum3	68	Unknown	Cambridge	0.025248964	Adult
Hum4	81	Unknown	Cambridge	0.025248964	Adult
Hum5	70	Unknown	Cambridge	0.024305935	Adult
Hum6	85	Unknown	Cambridge	0.02421683	Adult
Hum7	98	Unknown	Cambridge	0.025626692	Adult
Hum8	90	Unknown	Cambridge	0.026627563	Adult
Hum9	89	Unknown	Cambridge	0.024994765	Adult

continued on next page

Table A.1: (Continued)

Specimen	Age	Sex	Source/Dataset	Voxel size (mm)	Group
Hum10	94	Unknown	Cambridge	0.025006896	Adult
Hum11	80	Unknown	Cambridge	0.025006896	Adult
Hum12	96	Unknown	Cambridge	0.024439339	Adult
Hum13	92	Unknown	Cambridge	0.022870633	Adult
Hum14	70	Unknown	Cambridge	0.026211904	Adult
Hum15	92	Unknown	Cambridge	0.024535134	Adult
Hum16	83	Unknown	Cambridge	0.023036253	Adult
F01	Adult	Unknown	Wimmer et al.	0.0606996	Adult
F02	Adult	Unknown	Wimmer et al.	0.0606996	Adult
F03	Adult	Unknown	Wimmer et al.	0.0606996	Adult
F04	Adult	Unknown	Wimmer et al.	0.0606996	Adult
F05	Adult	Unknown	Wimmer et al.	0.0606996	Adult
F06	Adult	Unknown	Wimmer et al.	0.0606996	Adult
F07	Adult	Unknown	Wimmer et al.	0.0606996	Adult
F08	Adult	Unknown	Wimmer et al.	0.0606996	Adult
F09	Adult	Unknown	Wimmer et al.	0.0606996	Adult
F10	Adult	Unknown	Wimmer et al.	0.0606996	Adult
F11	Adult	Unknown	Wimmer et al.	0.0606996	Adult
F12	Adult	Unknown	Wimmer et al.	0.0606996	Adult
F13	Adult	Unknown	Wimmer et al.	0.0606996	Adult
F14	Adult	Unknown	Wimmer et al.	0.0606996	Adult
F15	Adult	Unknown	Wimmer et al.	0.0606996	Adult

A.2 Figures

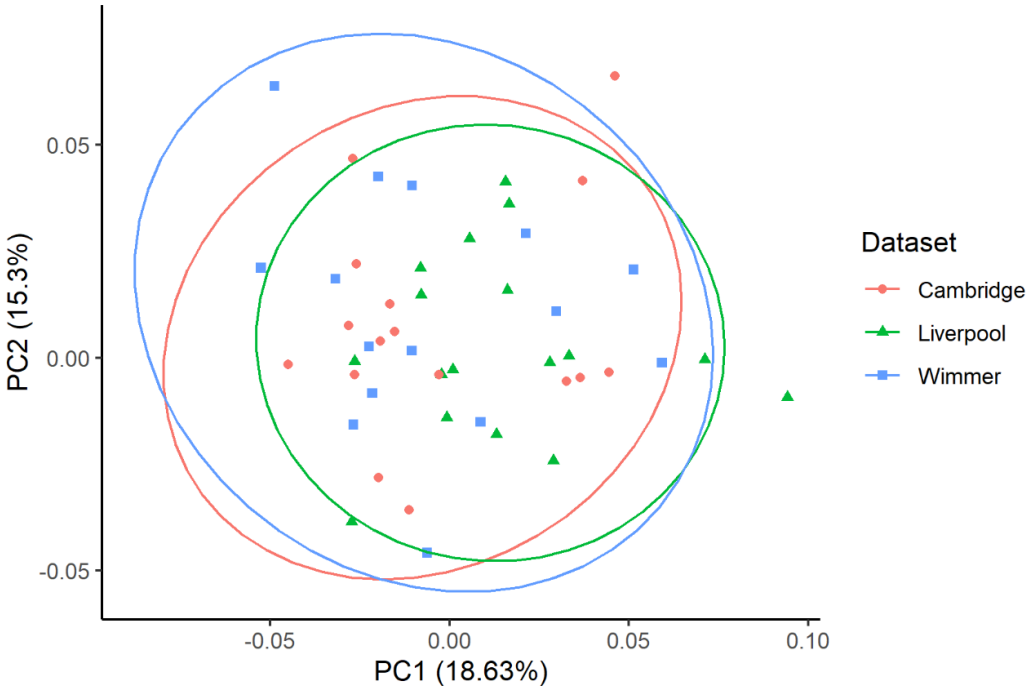

Figure A.1: Adult morphospace distribution along PC1 and PC2 by dataset coded for dataset. Ellipses represent 95% CI.

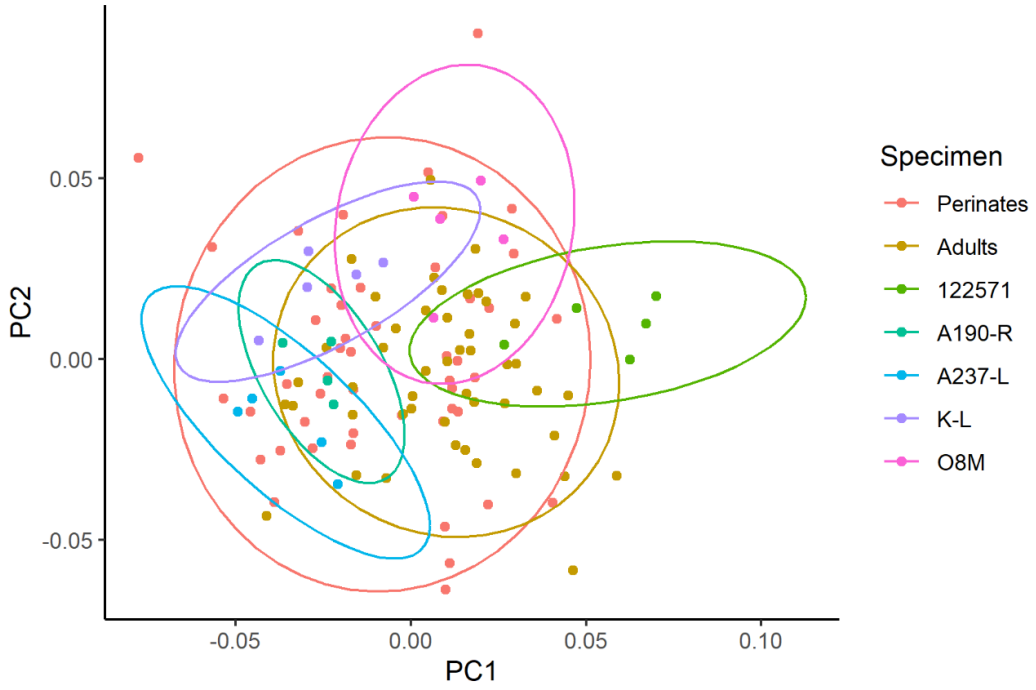

Figure A.2: PC1 and PC2 of configuration shapes with repeated specimens. Ellipses represent 95% CI.

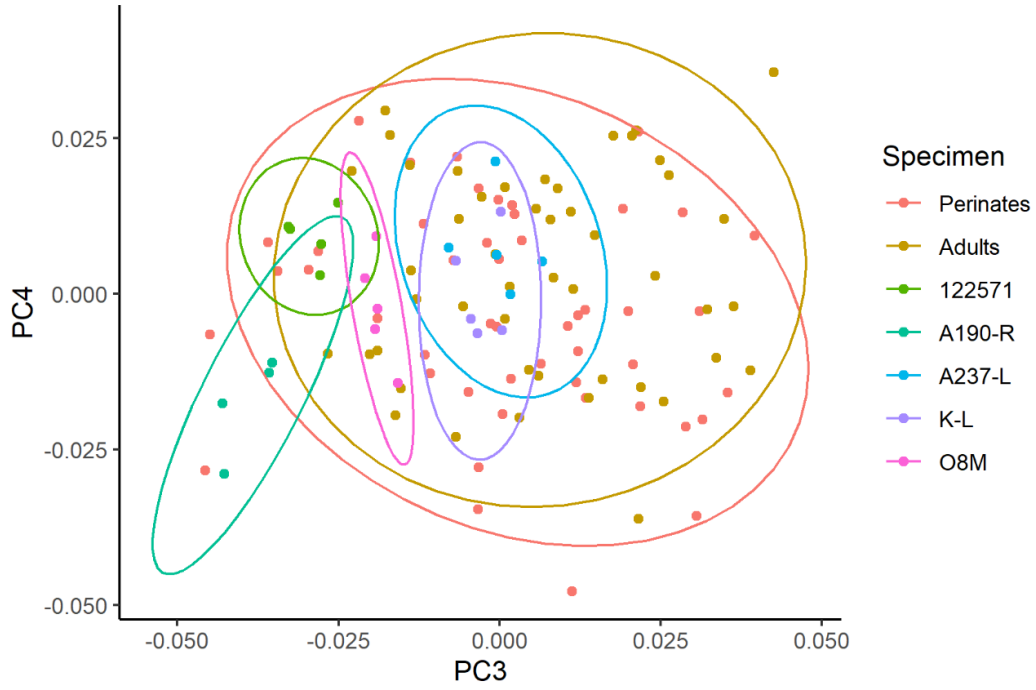

Figure A.3: PC3 and PC4 of configuration shapes with repeated specimens. Ellipses represent 95% CI.

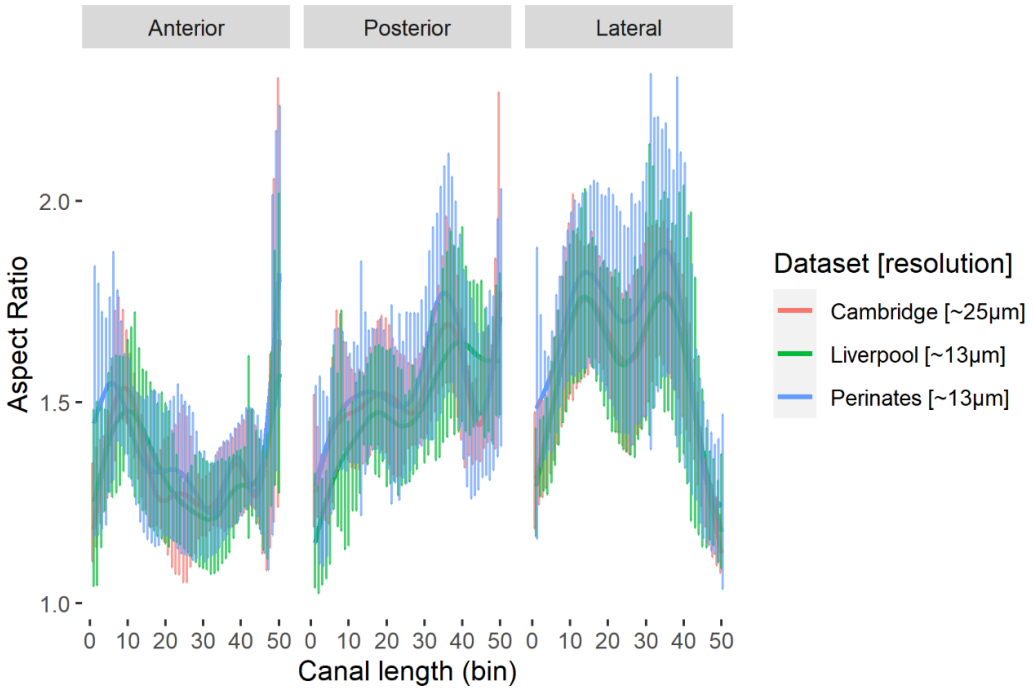

Figure A.4: Aspect ratio. Results are grouped by dataset.

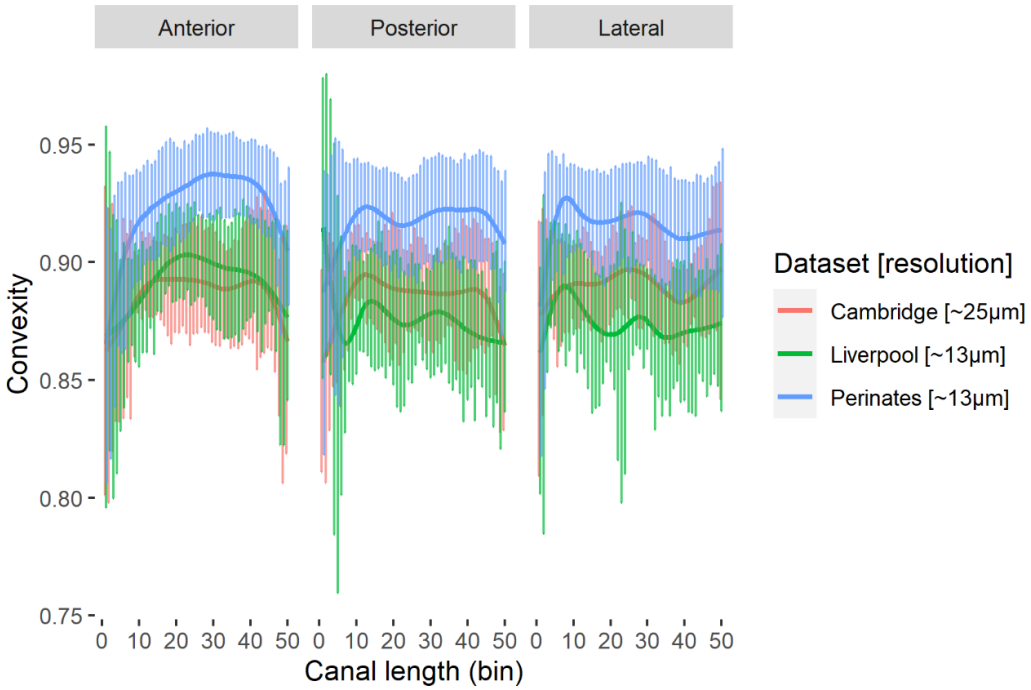

Figure A.5: Convexity. Results are grouped by dataset.

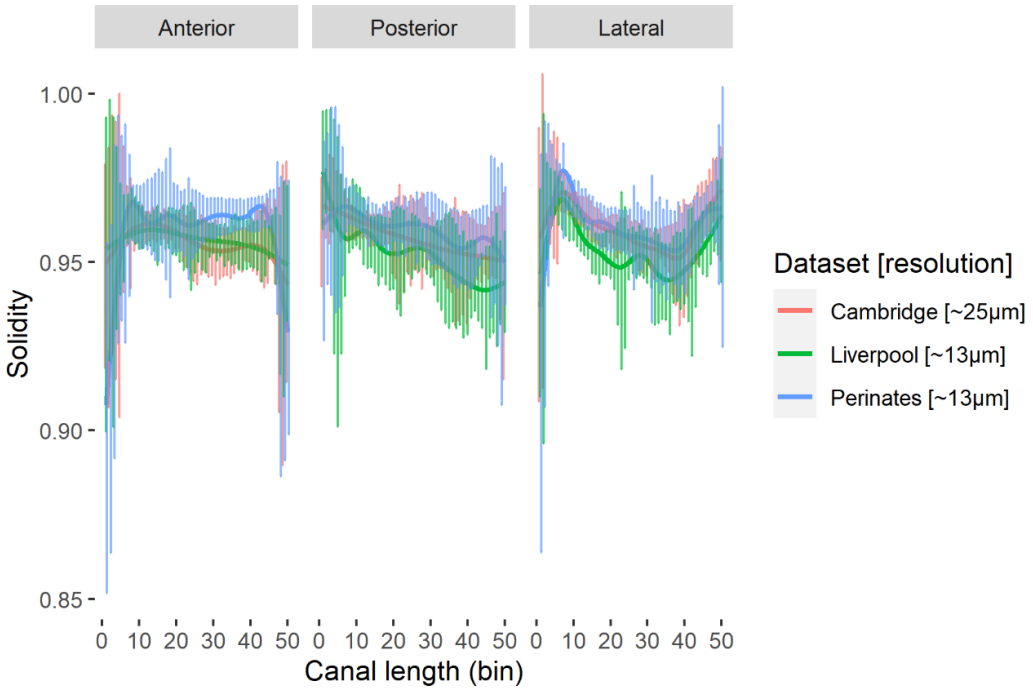

Figure A.6: Solidity. Results are grouped by dataset.

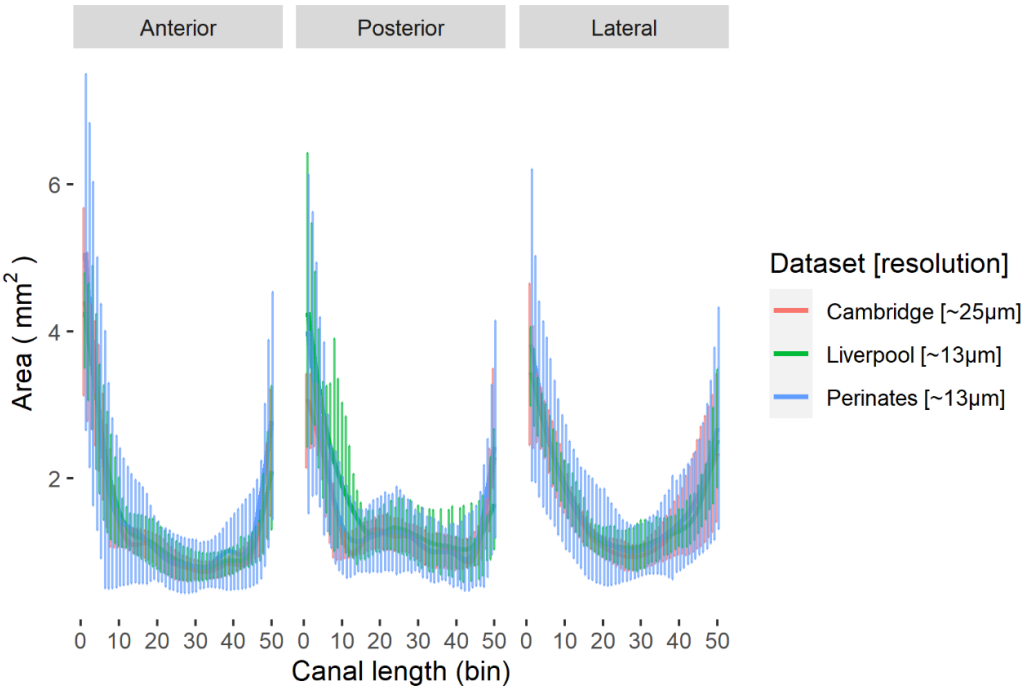

Figure A.7: Cross-sectional area. Results are grouped by dataset.

Appendix B

Supplementary material for chapter 4

Table B.1: Species and spatial resolution details for specimens used for skull measurement analysis. Data for perilymphatic group based on Gray [1].

Species for p. space data	Species measured	Spatial resolution (mm)			P group
		X	Y	Z	
Bradypus tridartylus	*Bradipus variegatus*	0.047	0.047	0.047	Medium
Camelus dromedarius		0.805	0.805	0.700	Medium
Canis familiaris		0.144	0.144	0.144	Small
Chlorocebus sabaeus		0.064	0.064	0.064	Large
Cercopithecus mona		0.188	0.188	0.188	Large
Cercopithecus nictitans		0.188	0.188	0.188	Large
Macaca nigra		0.064	0.064	0.064	Large
Dipus sagitta	*Jaculus Jaculus*	0.022	0.022	0.022	Small
Erinaceus eruopaeus		0.033	0.033	0.033	Medium
Felis catus		0.157	0.157	0.157	Small
Panthera tigris		0.430	0.430	0.300	Small
Gazella bennettii		0.085	0.085	0.085	Medium
Halichoerus grypus		0.448	0.448	0.300	Large
Callithrix jacchus		0.034	0.034	0.034	Large

continued on next page

Table B.1: (Continued)

Species for p. space data	Species measured	Spatial resolution (mm)			P group
		X	Y	Z	
Herpestes griseus	*Herpestes sanguineus*	0.033	0.033	0.073	Medium
Homo sapiens		0.320	0.320	0.320	Large
Hydrochoerus hydrochaeris	*Hydrochoerus hydrochaeris*	0.125	0.125	0.125	Small
Eulemur mongoz		0.059	0.059	0.059	Small
Oryctolagus cuniculus		0.041	0.041	0.041	Small
Lepus europaeus		0.069	0.069	0.069	Small
Lutra lutra		0.200	0.200	0.200	Small
Mus musculus		0.013	0.013	0.013	Small
Notoryctes typhlops		0.018	0.018	0.038	Small
Loris tardigradus	*Nycticebus bengalensis*	0.059	0.059	0.066	Small
Arctocephalus pusillus	*Otaria flavescens*	0.372	0.372	0.300	Small
Ovis aries		0.483	0.483	0.001	Small
Panthera leo		0.240	0.240	0.500	Small
Papio cynocephalus		0.142	0.142	0.142	Large
Isoodon obesulus		0.076	0.076	0.076	Small
Phoca vitulina		0.247	0.247	0.300	Large
Procyon cancrivorus	*Procyon lotor*	0.075	0.075	0.075	Small
Proteles cristata		0.082	0.082	0.181	Small

continued on next page

Table B.1: (Continued)

Species for p. space data	Species measured	Spatial resolution (mm)			P group
		X	Y	Z	
Pteropus medius		0.060	0.060	0.060	Small
Puma concolor		0.300	0.300	0.500	Small
Mustela putorius	*Mustela nivalis*	0.025	0.025	0.056	Small
Rattus norvegicus		0.058	0.058	0.058	Small
Sciurus vulgaris	*Sciurus carolinensis*	0.063	0.063	0.063	Small
Talpa europaea		0.046	0.046	0.046	Small
Tamandua tetradactyla		0.074	0.074	0.074	Small
Pipistrellus pipistrellus		*0.020*	0.020	0.020	Small

Table B.2: Species and spatial resolution details for specimens used for the cross-section analysis. P. group: Perilymphatic group.

Species measured	Spatial resolution (mm)			P. group
	X	Y	Z	
Bradypus tridactylus	0.047	0.047	0.047	Medium
Callithrix jacchus	0.034	0.034	0.034	Large
Canis lupus	0.144	0.144	0.144	None
Hydrochoerus hydrochaeris	0.125	0.125	0.125	Medium
Chlorocebus aethiops	0.038	0.038	0.038	Large
Diplobune	Mesh			NA
Equus caballus	0.015	0.015	0.015	Small
Erinaceus europaeus	0.033	0.033	0.033	Medium
Eulemur coronatus	0.029	0.029	0.029	Small
Felis catus	0.013	0.013	0.013	Small
Herpestes ichneumon	0.033	0.033	0.033	Medium
Homo sapiens	0.013	0.013	0.013	Large
Lepus europaeus	0.069	0.069	0.069	Small
Loxodonta africana	0.015	0.015	0.015	Large
Macaca nigra	0.064	0.064	0.064	Large
Megatherium	Mesh			NA
Mus musculus	0.012	0.012	0.012	Small
Mustela nivalis	0.025	0.025	0.056	Small
Nycticebus bengalensis	0.059	0.059	0.066	Small
Oryctoloagus	0.041	0.041	0.041	Small
Ovis aries	0.013	0.013	0.013	Small
Papio hamadryas	0.044	0.044	0.044	Large
Phoca vitulina	0.247	0.247	0.300	Large
Pipistrellus pipistrellus	0.020	0.020	0.020	Small
Procyon cancrivorus	0.075	0.075	0.075	Small
Pteropus giganteus	0.060	0.060	0.060	Small
Rattus norvegicus	0.030	0.030	0.030	Small
Sciurus vulgaris	0.063	0.063	0.063	Small
Talpa europaea	0.046	0.046	0.046	Small

Tamandua tetradactyla	0.074	0.074	0.074	Small

Appendix C

Supplementary material for chapter 5

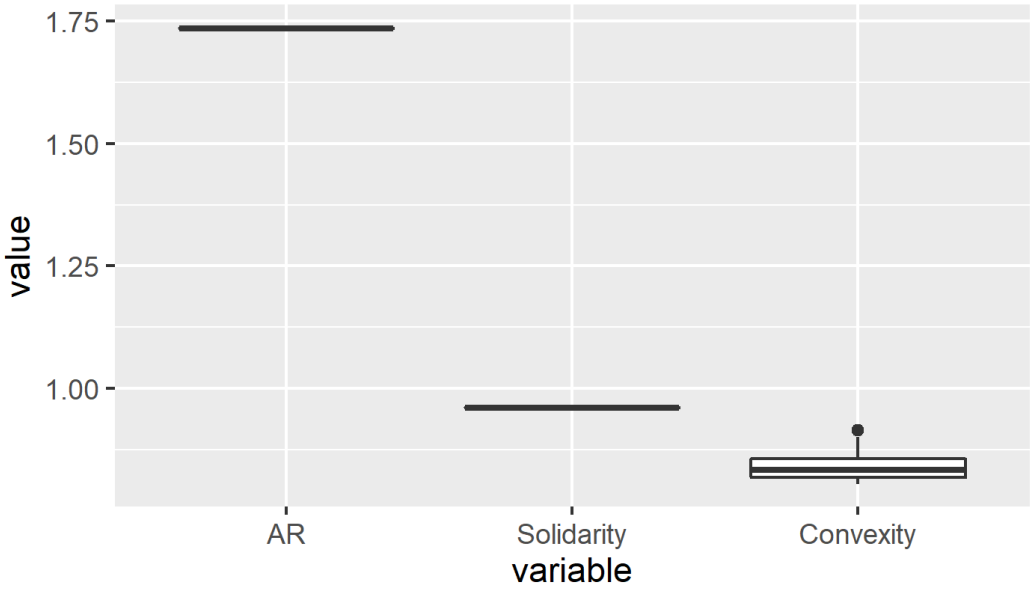

Figure C.1: A single slice slected at random from a random specimen and was rotated 1° at a time in ImageJ, thus generating 180 rotated slices. These rotated slices were then subjected to the same measuring techniques described in chapter 2. Values here are shown for rspect ratio (AR), solidity and convexity for the 180 rotated images.